The Role of eIF2B Localisation in Cell-Specific Stress Responses

Filipe Máguas da Silva Hanson

A thesis submitted in partial fulfilment of the requirements of
Sheffield Hallam University
for the degree of Doctor of Philosophy

March 2023

Candidate Declaration.

I hereby declare that:

1. I have not been enrolled for another award of the University, or other academic or professional organisation, whilst undertaking my research degree.
2. None of the material contained in the thesis has been used in any other submission for an academic award.
3. I am aware of and understand the University's policy on plagiarism and certify that this thesis is my own work. The use of all published or other sources of material consulted have been properly and fully acknowledged.
4. The work undertaken towards the thesis has been conducted in accordance with the SHU Principles of Integrity in Research and the SHU Research Ethics Policy.

The word count of the thesis is 44,629.

Name	Filipe Máguas da Silva Hanson
Award	Doctor of Philosophy (PhD)
Date of submission	31st March 2023
Faculty	Health and Wellbeing
Director of studies	Dr Susan G. Campbell

Acknowledgments.

I am extremely thankful to my Director of Studies, Dr Susan Campbell, for being the best supervisor I could have ever imagined (PhD newcomers are in great hands with you as their PGRT). I am very grateful for your guidance, wisdom, passion for research, for believing in me (even when I didn't), for being so caring of my well-being, our enthusiastic scientific conversations and support over these past years. To Dr Liz Allen for your kind words, insightful talks, and amazing advice. And to Dr Alison Cross for valuable advice throughout my PhD. I would like to thank Dr Nicola Woodroofe for helping me kickstart my project in the very first months of my PhD I also want to extend my gratitude for my lab's collaboration with Dr Truus Abbink for very fruitful Zoom meetings that led to key findings in my PhD. And to Dr Rachel Hodgson, whose wisdom made my PhD project possible and was an extraordinary help when I first started.

My PhD journey would not have been the same without the people that have accompanied me through this wild ride, and I feel so incredibly grateful to have so much love and friendship throughout these years at the BMRC, it truly always felt like a family.

Madalena, the Karen to my Brenda and eIF2B sister, for the endless laughs, the late-night dancing, our listening sessions but, most of all, the unconditional support. You could crack open a light in my darkest days in the lab, and sometimes all it took was our morning coreo (uhn!). Cristiana, for being a safe haven when my stress took the best of me and listening wholeheartedly to my (what always seemed trivial) problems. Muna, my Virgo partner-in-crime, who has never failed to make me smile for being one of the kindest people I've met. Sonia, for always caring effortlessly and I'm still waiting for our next gig together!

I would also like to thank Katie Kennedy, Paula, Katie Hudson, Oana, Alex Williamson and Lucy Dascombe, who made my days brighter filled with cherishing memories. A huge thanks to the rest of the BMRC PhD students for the chats, laughs, Pub Friday's and cheeky mid-week night outs.

I am also beyond grateful to other wonderful people that have blessed my PhD journey in Sheffield.

Nelma, my incredible science sister who has been there from the very start. Words cannot express how lucky I was to have you when I moved back to Sheffield. Your passion for science and brilliance shaped my own confidence as a scientist. It would have not been the same without our Eurovision sing-alongs, music video medleys and for you being so protective of me. Remiyah, who continuously inspires me and has been a symbol of bravery and warmth to me throughout these years. Maria Marcelino, aka Farmgirl Maria (I had to), the way we instantly connected still echoes as my fondest memories in Sheffield, and only makes me happier of how close we became.

To my dearest friends from back home in Portugal, who have supported me throughout so many phases of my life, both personally and professionally.

Melissa, whom I am proud to call my best friend (and bae) and has relentlessly been by my side and supported me, even from afar, through the ups and downs of this journey.

My angels Miguel (boozinho), Mariana and Maria Wilton-Ceregueiro, who were a beacon of joy and hope during lockdown; we may now all be in different countries but that has not stopped us from being together and supporting each other. My incredible friends and fellow biologists Ana Margarida, Alexandra, Brotas, Inês Oliveira, Inês Gonçalves, and Ana Rafael, who have great futures awaiting them and only makes me more grateful for witnessing it. And to my long-lasting friends Catarina, Cláudia, Patricia and Filipa, all the way back to 2005 in middle school and still going strong!

To Myles, for listening to my frustrations and not so good days in the lab, for understanding my concerns and helping me navigate through my anxiety. But above all, I am forever grateful for the love, passion, adventures, and resilience you have shown me over these past years.

And to my family to whom I owe my deepest gratitude. I would not be writing these words without your love and support. To my mom, my role model in science and in life. To my dad, the most supportive person I know. To my sister, who has looked after me effortlessly. To my grandmother, whose ability to love and care will always be inspiring. And to my dear grandfather Ferrer, to whom I dedicate this thesis.

Contents.

Summary.

Eukaryotic initiation factor 2B (eIF2B) is a guanine nucleotide exchange factor (GEF) and a master regulator of translation control. eIF2B recycles inactive eIF2-GDP to active eIF2-GTP. Under transient/acute cellular stress, a family of kinases phosphorylate the alpha subunit of eIF2 at serine 51 (eIF2α-P) activating the integrated stress response (ISR). This response pathway inhibits eIF2B activity resulting in overall translation attenuation and reprogramming of gene expression to overcome cellular stress. The duration of an ISR programme can dictate cell fate wherein chronic activation is adaptive to prologued stress but has pathological outcomes. Leukoencephalopathy with Vanishing White Matter Disease (VWMD) is a chronic ISR-related disorder linked to mutations in eIF2B. eIF2B is vital to all cell types, yet VWMD eIF2B mutations primarily affect astrocytes and oligodendrocytes suggesting cell-type specific functions of eIF2B. Regulation of the cytoplasmic localisation of eIF2B, also termed eIF2B bodies, has been implicated in the ISR. The work in this dissertation reveals that eIF2B localisation is cell-type specific in neuronal and glial cells. Each cell type possesses its own steady-state repertoire of eIF2B bodies with varying eIF2B subunit composition and GEF activity. This thesis also reports that neuronal and glial cells respond similarly to acute induction of the ISR whilst chronic ISR exerts cell-type specific differences. Herein, eIF2Bδ composition of eIF2B bodies is differentially modulated in a manner that correlates to the action of acute and chronic ISR. This dissertation also reports cell-type specific responses of the chemical inhibitor of the ISR (ISRIB) on eIF2Bδ composition and GEF activity of eIF2B bodies, providing evidence of a cell-specific action of ISRIB.

List of figures.

List of tables.

List of abbreviations.

By alphabetical order:

2ABct – eIF2B activator
4E-BP – eIF4E-binding protein
a.u. – Arbitrary units
AD – Alzheimer's disease
ALS – Amyotrophic lateral sclerosis
APS – Ammonium persulphate
AT – Acyl-transferase
ATF4 – Activating transcription factor 4
ATF6 – Activating transcription factor 6
AβO – Amyloid-β oligomer
BDNF – Brain-derived neurotrophic factor
BiP – Binding immunoglobulin protein
BSA – Bovine serum albumin
CACH - Childhood Ataxia Coupled with Central Nervous System hypomyelination
CHO – Chinese hamster ovary cell line
CHOP – C/EBP homologous protein
CML – Chronic myeloid leukaemia
CMT - Charcot-Marie-Tooth disease
CNS – Central nervous system
DAPI – 4,6-diamidino-2-phenylindole
DBA – Diamond–Blackfan anaemia
DBM – Dibenzoylmethane
ddH2O – Ultra-pure water
DMEM – Dulbecco's modified Eagle's medium
DMSO - Dimethyl sulfoxide
DNA – Deoxyribonucleic acid
DS – Down syndrome
dSMA-V – Distal spinal muscular atrophy type V
ECM – Extracellular matrix
eEF – Eukaryotic elongation factor
EF-T – Elongation factor-T
EF-Tu – Substrate of elongation factor-T
eIF – Eukaryotic initiation factor
eIF2 – Eukaryotic initiation factor 2
eIF2B – Eukaryotic initiation factor 2B
eIF2α – Alpha subunit of eIF2
eIF2α-P – Phosphorylated eIF2α
ER – Endoplasmic reticulum
eRF – Eukaryotic release factor
ERK – Extracellular signal-regulated kinase
FBS – Foetal bovine serum
FISH – Fluorescence in situ hybridization
FRAP – Fluorescence recovery after photobleaching
FRET – Fluorescence resonance energy transfer
FUS – Fused in sarcoma
G-418 – Geneticin
GADD34 – Growth arrest and DNA damage-inducible protein 34
GAP – GTPase-activating protein
Gcd – General control depressible
Gcn – General control nondepressible
GCN2 – General control nondepressible 2
GDI – GDP dissociation inhibitor
GDP – Guanosine diphosphate
GEF – Guanine exchange factor
GFAP – Glial fibrillary acidic protein
GFP – Green fluorescent protein
Gln1 – Glutamine synthetase
GTP – Guanosine triphosphate
h – Hours
HA – Primary human astrocytes
HCl – Hydrochloric acid
HD – Huntington's disease
HEAT – Huntingtin, elongation factor 3, protein phosphatase 2A and yeast kinase TOR1

HRI – Heme-regulated inhibitor
ICC – Immunocytochemistry
IF – Immunofluorescence
IMS – Industrial Methylated Spirit
IP – immunoprecipitation
iPSCs – Induced pluripotent stem cells
IRES – Internal ribosomal entry site
ISR – Integrated stress response
ISRIB – ISR Inhibitor
L180F – Leucine to phenylalanine mutation at residue 180
LB – Lysogeny broth
LLPS – Liquid-liquid phase separation
LTD – Long-term depression
LTP – Long-term potentiation
M – Molar
m^6A – N^6-methyladenosine
m^7G – Methylated guanosine
MBP – Myelin basic protein
MEDS - Microcephaly with simplified gyral pattern, epilepsy, and permanent neonatal diabetes Syndrome
MEHMO – Mental retardation, Epileptic seizures, Hypogenitalism, Microcephaly, Obesity Syndrome
MEM – Minimum Essential Medium Eagle
Met-tRNAi – Methionylated initiator transfer RNA
MFC – Multifactorial complex
mGFP – Monomeric green fluorescent protein
min – minutes
mM – Millimolar
MO3.13 – hybrid primary oligodendrocytic cell line
MRI – Mass Resonance Imaging
mRNA – Messenger RNA
ms – Milliseconds
mTOR - Mechanistic target of rapamycin
NaF – Sodium fluoride
NEAA – Nonessential amino acids
NeuN – Neuronal nuclei
nm – Nanometre
NPCs – Neural progenitor cells
ns – Non-significant
NT – Nucleotidyl-transferase
^oC – Celsius
OPCs – Oligodendrocyte progenitor cells
ORF – Open reading frame
p – P-value
P/S – Penicillin/streptomycin
PABP – Poly(A)-binding protein
PAPs – Perisynaptic astrocytic processes
P-bodies – Processing bodies
PBS - Phosphate buffered saline
PD – Parkinson's disease
PDCD4 – Programmed cell death 4
PEI – Polyethylenimine
PERK – PKR-like endoplasmic reticulum kinase
PERKi – PERK inhibitor
PERK-P – Phosphorylated PERK
PFA – Paraformaldehyde
PFKM – Phosphofructokinase
PGK1 – Phosphoglycerate kinase 1
PI3K – Phosphoinositide 3-kinase
PIC – Pre-initiation complex
PKR – Protein kinase R
PNDM – Permanent neonatal diabetes mellitus
PP1c - Protein phosphatase 1
PTMs – Post-translational modifications
PVOD – Pulmonary Veno-Occlusive Disease
RBP – RNA binding protein
RBPI - Ribose-1,5-bisphosphate isomerase
RFP – Red fluorescent protein
RGCs – Retinal ganglion cells
RNA – Ribonucleic acid
RNP – Ribonucleoprotein
ROI – Region of interest

ROS – Reactive oxygen species
rpm – rotations per minute
rRNA – ribosomal RNA
RSC – Regulatory sub-complex
RT – Room temperature
s – seconds
s.e.m. – standard error of mean
S51 – residue serine 51
S51A – serine to alanine mutation at residue 51
SA – Sodium arsenite
SDS – Sodium dodecyl sulfate
SDS-PAGE – SDS-polyacrylamide gel electrophoresis
SGs – stress granules
SH-SY5Y – adrenergic neuroblastoma cell line
SILAC – Stable isotope labelling of amino acids in cell culture
$t_{1/2}$ – Half-life
TBI – Traumatic brain injury
TBS – Tris buffered saline
TBST – TBS/Tween-20
TC – Ternary complex
TDP-43 – TAR DNA-binding protein 43
TEMED - *N,N,N′,N′*-Tetramethyl ethylenediamine.
Tg – Thapsigargin
tGFP – Turbo green fluorescent protein
TOP – Terminal oligopyrimidine
tRNA – transfer RNA
U373 – astrocytoma cell line
uORF – upstream open reading frame
UTR – untranslated region
v/v – Volume/volume
VWMD – Leukoencephalopathy with Vanishing White Matter Disease
w/v – Weight/volume
WRS – Wolcott–Rallison Syndrome
XBP1 – X-box binding protein 1
α – Alpha
β – Beta
γ – Gamma
δ – Delta
ε – Epsilon
μM – Micromolar

Chapter 1. General introduction.

1.1. Overview of eukaryotic translation.

All biological processes are intrinsically dependent upon the highly conserved and hierarchical process of translating thousands of messenger ribonucleic acids (mRNAs). mRNAs are first transcribed from genes and provide the blueprint to synthesize polypeptide chains complementary to specific DNA sequences. Once transcribed, post-transcriptional mechanisms mediate the stability and maturation of mRNAs (Corbett, 2018; Zhao *et al.*, 2016), hence regulating the control of gene expression at the RNA level. Fully matured mRNAs are assembled with ribosomes to translate its encoding polypeptide. Eukaryotic translation is segregated into three stages: initiation, elongation, and termination. Ribosomes consist of two subunits: a smaller 40S subunit and a larger 60S subunit, which jointly form the 80S eukaryotic ribosome. Assembly of the fully formed 80S ribosome occurs at initiation stage after the start codon of mRNA is scanned and recognised by several eukaryotic initiation factors (eIFs). Next, the elongation-competent 80S ribosome moves along the mRNA sequence and mediates transfer RNA (tRNA) codon base-pairing. tRNAs molecules are amino-acids carriers which are orderly loaded into the ribosome as it concomitantly synthesizes a polypeptide chain. At the termination stage, stop codon recognition releases the newly-made polypeptide chain and disassembles the ribosome for upcoming rounds of translation.

The translation initiation stage can be summed up as the process of start codon recognition and ribosomal assembly (Hinnebusch, 2014; Jackson *et al.,* 2010). A key protein integral to start codon recognition is eIF2, a heterotrimeric G protein bound to GTP as its active state. GTP-bound eIF2 initially attaches to methionylated initiator transfer RNA (Met-tRNAi), forming a ternary complex (TC) to be delivered to the 40S ribosomal subunit, ultimately establishing the 43S pre-initiation complex (PIC), in a reaction facilitated by other eIFs (Hinnebusch, 2014; Jackson *et al.,* 2010). The PIC scans the mRNA base-per-base until it reaches the first AUG start codon. Successful recognition triggers hydrolysis of eIF2-bound GTP to allow joining of the 60S subunit. A full 80S ribosome is then competent for the elongation phase of translation (Hinnebusch, 2014; Jackson *et al.,* 2010).

1.1.1. Post-transcriptional regulation of gene expression.

mRNAs (or pre-mRNAs) must be processed to produce mature mRNAs before departing the nucleus. mRNA processing includes modifications such as 5'-end capping, splicing of introns and 3'-end cleavage/polyadenylation to generate a mature, polyadenylated mRNA competent for the first stage of translation. These nuclear modifications are mediated by RNA-binding proteins (RBPs) and begin as the first nucleotides of the 5'-end of pre-mRNAs exit from RNA polymerase II (Singh *et al.,* 2015). 5'-end capping, or 7-methyguanosine (m^7G) cap, is the first modification made to pre-mRNAs and is required for cap-dependent translation (discussed in section 1.1.2.1.) and mRNA stability (Cheng *et al.*, 2006; Jackson *et al.*, 2010). Interestingly, the capping machinery is evolutionary diverse and may take in the cytoplasm to re-cap mRNAs (Ramanathan *et al.*, 2016). Next, the binding of the spliceosome scans and removes the introns of the coding sequence. Alternative RNA splicing can also occur where a combination of introns and exons are removed to create different mRNA variants of the same gene (Kelemen *et al.*, 2013). Splicing also dictates mRNA export to the cytoplasm by facilitating the binding of the Transcriptional Export (TREX) complex (Masuda *et al.*, 2005), a collective of RBPs (mainly export factors and helicases) that ultimately mediate the efficient RNA handover for translation. The poly-A-tail is a long chain of adenine nucleotides that promotes mRNA stability by preventing degradation, aids in mRNA export and enhances cap-dependent translation (Moqtaderi *et al.*, 2014).

Structurally, the coding sequence of mRNAs is flanked by untranslated regions (UTRs) at the 5'- and 3'-end. UTRs are key post-transcriptional control domains with a myriad of regulatory elements (notably secondary structures) and each UTR (5' or 3') have distinct functions in mRNA processing, stability, and translation. The length of 3'-UTRs controls the sub-cellular localisation of mRNAs (Berkovits & Mayr, 2015). Other *cis*-regulatory elements such as zip-code sequences also control mRNA localisation which is crucial for polarized cellular functions (Patel *et al.*, 2012). Most notably, the 3-'UTR can bind to the RNA-induced silencing complex (RISC). miRNAs, or microRNAs, are short RNA molecules (~21-24 nt) that bind to target sequences in mRNAs. When incorporated into the RISC, these complexes target 3'-UTR of target mRNAs, albeit not exclusively (*e.g.,* miR-103a-3p) (Zhou & Rigoutsos, 2014), and promote

their decay hence controlling mRNA stability (Peng & Croce, 2016). The 5'-UTR lodges the 5'-cap and contains specific sequences and motifs (*e.g.,* 5' terminal oligopyrimidine (5'TOP) motif, G-quadruplex structure, and cytosine-enriched regulator of translation (CERT)) which regulate different stages of translation (Schuster & Hsieh, 2019).

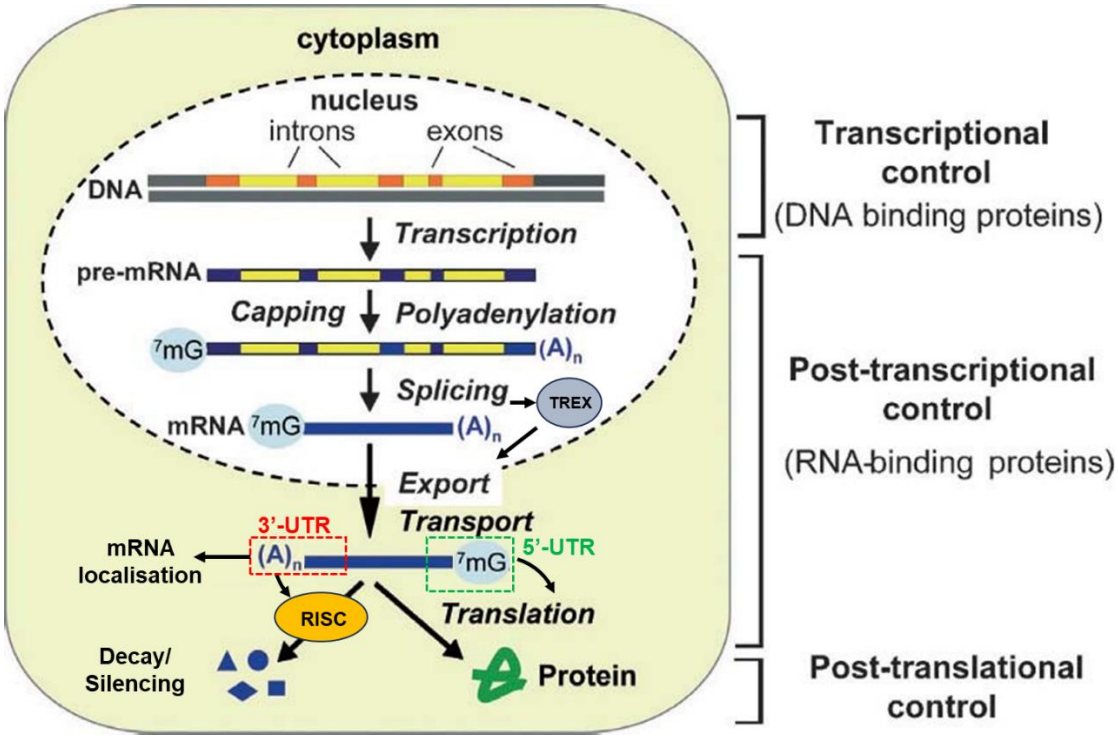

Figure 1.1. Mechanisms of post-transcriptional regulation of gene expression (modified from Halbeisen *et al.*, 2008).
Post-transcriptional regulation of gene expression is a multi-step program that starts at the nucleus by the recruitment of a cohort of RBPs to nascent pre-mRNA as it exists the RNA polymerase II. These RBPs (spliceosome, TREX, etc.) mediate 5′-end capping, splicing, editing, 3′-end cleavage and polyadenylation, which ultimately control mRNA fate by regulating its export and subsequent translation. The 3'-UTR regulate the mRNA localisation and is targeted by RISC to promote mRNA decay, hence the sub-cellular levels of mRNA availability. The 5'-UTR can be differently targeted at the three stages of translation.

1.1.2. Translation initiation.

1.1.2.1. Cap-dependent initiation.

The first stage of translation initiation relies on the availability Met-tRNAi. Met-tRNAi binds to its well-known carrier eIF2 which is regulated by the guanine exchange nucleotide factor (GEF), eIF2B (**Figure 1.1.**). The greater affinity of eIF2-GTP for Met-tRNAi than its GDP form allows TC assembly (Erickson & Hannig, 1996; Kapp & Lorsch, 2004) and further handover to the 40S ribosomal subunit. eIF2 comprises a core γ-subunit with major guanine binding sites for Met-tRNAi docking (Schmitt *et al.,* 2012) and two anchoring α- and β- subunits that stabilise eIF2-GTP:Met-tRNAi interactions (Naveau *et al.,* 2013). TC transfer to 40S subunits is then mediated by eIF1, -1A, -3 and -5. eIF1 and -1A cooperatively fine-tune 40S subunits into an open conformation for TC loading (Maag & Lorsch, 2003; Majumdar *et al.,* 2003). eIF3 is composed of 13 non-identical subunits (eIF3a-m) with varying functions in translation initiation. Initially shown to be associated with native 40S subunits to keep it apart from larger 60S subunits prior PIC assembly (Chaudhuri *et al.,* 1999; Thompson & Stone, 1977), some studies now show that each eIF3 subunit yield unique roles on maintaining PIC integrity (Erzberger *et al.,* 2014; Simonetti *et al.,* 2016). Additionally, eIF5 anchors eIF2:eIF3 interactions (Asano *et al.,* 2000). Interestingly, eIF1, 2, 3, and 5 initially form a multifactorial complex (MFC) conserved between yeast and mammalian cells prior to its delivery to TC to form the 43S PIC (Asano *et al.,* 2000; Sokabe *et al.,* 2012). More importantly, MFC is not rate-limiting for Met-tRNAi delivery to the 40S ribosome but is critical for the assembly of the 80S ribosome and eIF2 release (Sokabe *et al.,* 2012).

The PIC is recruited to the 5'end of mRNAs via cap recognition mediated by the eIF4F complex (eIF4F comprises eIF4E, -A and -G) (Gingras *et al.,* 1999). The cap-binding protein eIF4E stimulates eIF4A helicase activity onto 5'UTR of target mRNAs to remove secondary structures that prevent binding of PIC (Feoktistova *et al.,* 2013). eIF4G scaffolding activity enhances recruitment for stabilising the cap:eIF4E interaction whilst linking both ends of target mRNAs (5' and 3') into a circular-like conformation (closed loop) (Yanagiya *et al.,* 2009); previously suggested to be the most effective initiation model (Jackson *et al.,* 2010). Following cap recognition, the PIC scans along the 5'UTR in search for the start

codon. Additionally, 40S subunits may display direct recruitment to mRNAs in a cap-independent manner which is discussed further in section 1.1.1.2.

During scanning, the co-activity of eIF1 and eIF1A maintain an open RNA binding channel conformation of the 40S subunit (Passmore *et al.,* 2007). Upon start codon recognition eIF2-bound GTP is hydrolysed by GTPase-activating protein eIF5 (Huang *et al.,* 1997; Paulin *et al.,* 2001). This function is blocked by eIF1 in the absence of AUG codons (Cheung *et al.,* 2007). However, upon start codon recognition, eIF1 is dissociated from the 40S subunit to release Pi from eIF2:GDP:Pi, counterbalanced with a tighter eIF1A-40S interaction to stall further RNA scanning (Llácer *et al.,* 2018; Maag *et al.,* 2006; Passmore *et al.,* 2007). Then, eIF2-GDP complexed with eIF5 is recycled to eIF2-GTP by eIF2B for next rounds of TC assembly. At the final stage, eIF5B arbitrates 60S subunit joining accompanied by the release of the remaining eIFs (eIF1, -3, -1A) as it assembles into a fully formed 80S ribosome to commence elongation (Acker *et al.,* 2006; Acker *et al.,* 2009).

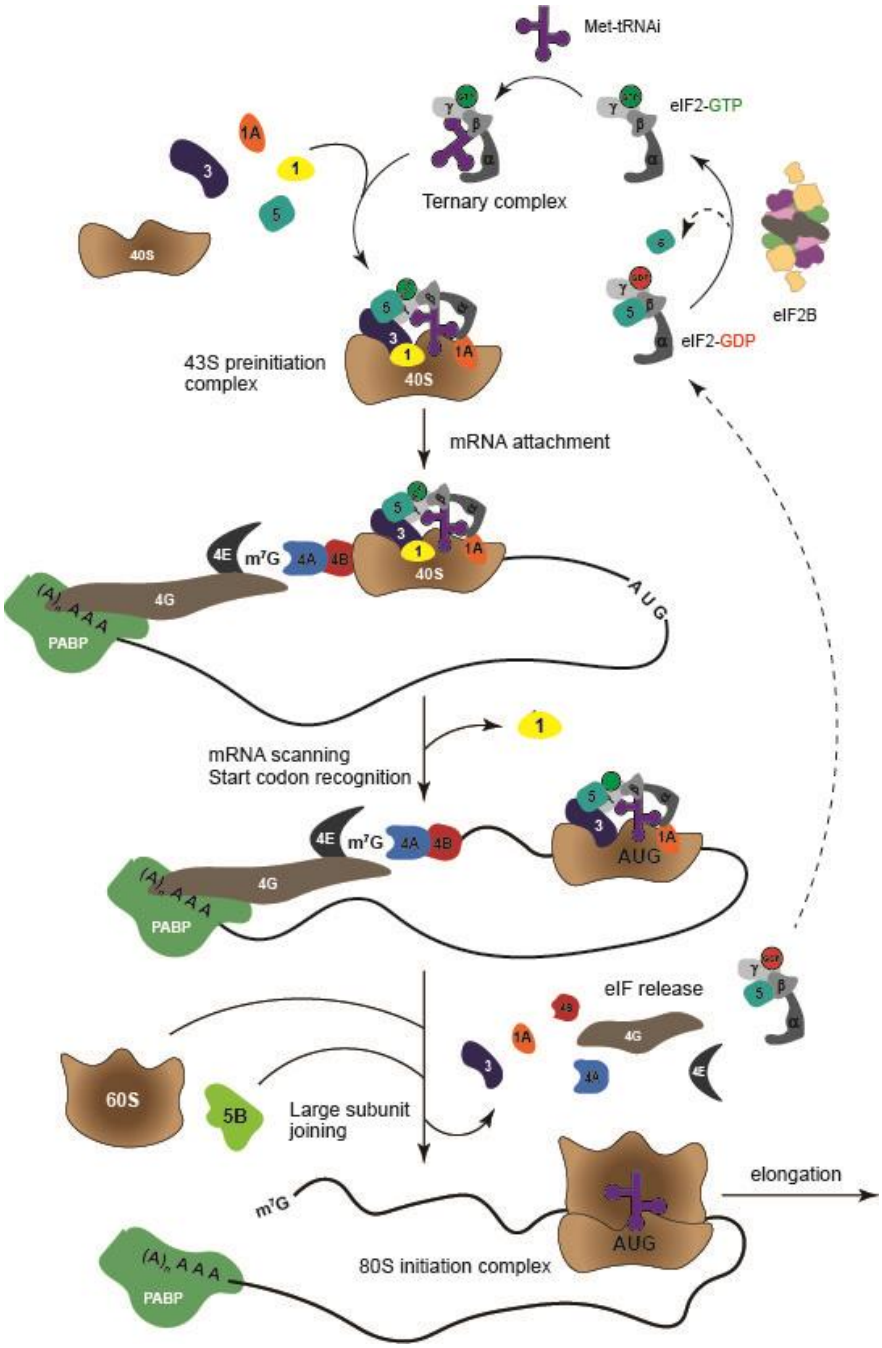

Figure 1.1. Cap-dependent translation initiation.
A ternary complex comprised of tRNA-bound eIF2 assembles on the small 40S ribosomal subunit, facilitated by eIF1, eIF1A, eIF3 and eIF5, to form the 43S preinitiation complex. This complex is loaded to target mRNA and subsequently starts scanning for the AUG start codon. After AUG recognition, eIF2-bound GTP is hydrolysed and dissociates together with other eIFs. eIF5B mediates large 60S ribosomal joining to form elongation-competent 80S ribosome. Guanine nucleotide exchange on eIF2, which is dissociated hand in hand with eIF5, is catalysed by eIF2B to allow upcoming runs of translation initiation.

1.1.2.2. Cap-independent initiation.

Although recognition of the m^7G cap structure of mRNAs is the most common mechanism of translation initiation, a smaller cohort of mRNAs are still translated without cap recognition (hence named “cap-independent”). Cap-independent translation predominantly involves recognition of internal ribosomal entry sites (IRES) located at 5′UTRs that directly binds the 40S ribosome to the mRNA sequence albeit still requiring a cohort of canonical eIFs (mostly the eIF4F complex) and recruits other IRES *trans*-acting factors (Lacerda *et al.,* 2017). First discovered by Pelletier and Sonenberg as the evading mechanism of poliovirus to translate its repertoire of viral proteins (Pelletier & Sonenberg, 1988), IRES-mediated translation is now appreciated as a eukaryotic mechanism of translation and may account for ~10% of mRNAs (Weingarten-Gabbay *et al.,* 2016). IRES-containing mRNAs predominantly encode for proteins required to be translated when canonical initiation is suppressed such as cellular stress responsive, pro-apoptotic, mitotic, and cellular differentiation-involved proteins (Liberman *et al.,* 2015; Shi *et al.,* 2016; Vaklavas *et al.,* 2016). More recently uncovered is a mechanism that is neither cap- nor IRES-dependent but instead is facilitated through the presence of N^6-methyladenosine (m^6A) in the mRNA 5′ UTRs (Meyer *et al.,* 2015). m^6A is a reversible base modification that can bind eIF3 which is sufficient to recruit the 40S ribosome (Meyer *et al.,* 2015). Interestingly, m^6A modifications occur more frequently under stress conditions (Zhou *et al.,* 2015) and are not eIF4F-dependent (Coots *et al.,* 2017), which may serve as a less regulatable pathway of translation initiation thus a more ubiquitous expression of selective mRNAs.

1.1.2.3. Novel and non-canonical functions of initiation factors.

Translation initiation factors yield specialised functions to support the process of initiating translation. A significant amount of the cell’s resources is allocated to generating and recruiting proteins that coordinate translation, aside from the energy demanded to synthesize the peptide chain itself. It is then perhaps unsurprising that translation factors may have alternative functions during protein synthesis. Recent evidence has furthered our understanding on these additional roles highlighting the functional versatility of translation factors as indicated in Table 1.1.

Table 1.1. Novel and other functions of translation initiation factors.

Gene/Protein	Canonical function(s)	Novel function(s)	References
EIF5/eIF5	• GTPase-activating protein: promotes hydrolysis of GTP from the TC • GDP dissociation inhibitor (GDI)	• Physically replaces eIF1 on the 40S ribosomal subunit to promote start-codon selection. • Stimulates a conformation of the 48S PIC compatible with eIF5B binding and 80S assembly. • Supports eIF5B recruitment to the PIC.	(Llácer *et al.,* 2018; Lin *et al.,* 2018)
EIF1/eIF1	• Blocks P_i release from eIF2-GTP complex until start-codon recognition.	• Key preventer of excessive uORF translation.	(Fijalkowska *et al.,* 2017; Zhou *et al.,* 2020)
EIF5B/eIF5B	• Promotes joining of the 40S and 60S ribosomal subunits and stabilizes Met-tRNAi binding.	• Mediates the delivery of Met-tRNAi and translation of IRES-dependent mRNAs. • Involved in uORF-mediated regulation of ATF4 translation by cooperating with eIF1A and eIF5: eIF5B depletion constitutively activates the ISR in an eIF2α-independent manner.	(Thakor *et al.,* 2012; Yamamoto *et al.,* 2014; Ross *et al.,* 2019)
EIF3D/eIF3d	• Subunit of eIF3 complex. • mRNA cap-binding protein that is required for specialized translation initiation.	• Directly interacts with viral IRESes and bridges PABP complex with poly(A)-end of specific mRNAs to enable RNA circularization and, subsequently, facilitating ribosome recruitment. • Functionally overlaps with eIF4E as an alternative cap recognition factor • Key regulator of protein synthesis during chronic ER stress.	(Guan *et al.,* 2017; Lee *et al.,* 2016; Thakor *et al.,* 2017)
EIF3A/eIF3a	• Subunit of eIF3 complex. • Scaffolding subunit for the primary eIF3 octamer.	• Interacts with p190A RhoGAP (which promotes GTP hydrolysis on a range of Rho GTPases involved in cell adhesion, cell migration, and cytokinesis): p190A●eIF3 complexes are suggested to direct eIF3 to sites of local translation and/or regulate levels of PIC formation.	(Parasuraman *et al.,* 2017)
EIF3K/eIF3k	• Non-essential eIF3 subunit. • Function in eIF3 complex remains undefined.	• Physically interacts with cyclin D3, a key component of the progression of G1 phase.	(Shen *et al.,* 2004)
EIF3F/eIF3f	• Subunit of eIF3 complex. • Function in eIF3 complex remains undefined.	• Positive regulator of the Notch pathway.	(Moretti *et al.,* 2010)

1.1.3. Translation elongation and termination.

The 80S initiation complex comprises of three tRNA-binding sites (A[aminoacyl]-site, P[peptidyl]-site and E[exit]-site) to allow proper docking and joining of free aminoacylated tRNAs to synthesize a nascent polypeptide chain, aided by the action of eukaryotic translation elongations factors (eEFs) (Dever *et al.,* 2018).

As translation initiation concludes with the formation of the 80S ribosome positioned with an aminoacyl-tRNA bound in the P-site, elongation commences. eEF1A in its active GTP-bound form generates an eEF1A•GTP•aminoacyl-tRNA ternary complex which binds to the ribosomal A-site. Complementary base-pairing induces GTP hydrolysis, eEF1A•GDP is released and the aminoacyl-tRNA is lodged in the A-site (Gromadski *et al.,* 2007). Structural studies support specialised roles for each subunit of the 80S ribosome for the decoding process. The 18S ribosomal RNA (rRNA), embedded in the 40S ribosomal subunit, performs a critical function in stabilising codon-anticodon interactions in the A-site (Demeshkina *et al.,* 2012; Loveland *et al.,* 2017) while the 60S ribosomal subunit promotes eEF1A hydrolysis (Shao *et al.,* 2016).

The peptidyltranferase activity of the ribosome forms a peptide bond which is catalysed between the aminoacyl-tRNA in the A-site and the aminoacyl-tRNA in the P-site. A new aminoacyl-tRNA can now occupy the empty A-site hence allowing subsequent rounds of elongation. This cycle is repeated until the elongating ribosome encounters a stop codon (UAA, UGA, or UAG) in the A site, which recruits eukaryotic release factors (eRF) eRF1 and eRF3 to promote mRNA and polypeptide release, and ribosome dissociation (Hellen, 2018).

1.1.4. Local translation in neural and glial cells.

It is well-established that protein synthesis is fine-tuned to meet the required energetic demand and proteome load of different cell types. Neurons are highly complex cells with specialised morphology and long cytoplasmic extensions to process brain information. Efficient neuronal activity requires dendritic signal collection, "decision-making" at the soma and signal transport through the axon, which releases neurotransmitters at synapses to neighbouring neurons; all within a short time course (~one-thousandth of a second) (Rangaraju *et al.,* 2017). To overcome this time constraint, neurons are particularly reliant on mRNA sorting and trafficking from the nucleus to be locally translated hence synthesising "ready-to-use" proteins, providing sets of local proteomes to each neuronal sub-compartment (Jung *et al.,* 2012). mRNAs are transported bi-directionally along microtubules to reach the far-end of axons and report back signalling from extrinsic cues (Sahoo *et al.,* 2018). mRNAs are packaged together with RNA-binding proteins (RBPs) - forming ribonucleoprotein (RNP) granules - which mediate their affinity to motor proteins and determine mRNA fate. For example, RBP zip-code protein 2 (ZBP2) interacts with 3'-UTR *cis*-acting sequences in β-actin mRNA to repress translation during transport to outgrowing axon terminals and is alleviated by post-translation modifications (PTMs) as it reaches its destination (Condeelis & Singer, 2005; Huttelmaier *et al.,* 2005). This action was found to be required for cytoskeleton-enriched deposition during axonal branching (Donnelly *et al.,* 2013; Turner-Bridger *et al.,* 2018; Wong *et al.,* 2017); whilst in mature dendrites it regulates synaptic plasticity (Eom *et al.,* 2003). Several other studies have pinpointed how local translation in axons support axonal growth, survival, and maintenance, as highlighted by local proteome changes of RhoA, ErbA2 and TC10 in developing sensory neurons (Gracias *et al.,* 2014; Walker *et al.,* 2012; Zivraj *et al.,* 2010).

Nonetheless, translation of mRNAs, even if spatially localised, requires the presence of eIFs at these sites. Although it may be generally assumed that eIFs are randomly dispersed throughout the cytoplasm, it remains poorly understood how neurons coordinate a concentrated stock of translation components to cellular regions. One hypothesis could be that the translation machinery may also be locally translated. Earlier studies have shown that RNPs house 40S and 60S ribosomal subunits, eIF2, and eIF4E (Krichevsky & Kosik, 2001; Smart *et al.,*

2003). Yeast studies detected RNP granules harbouring mixed combinations of translation factor mRNAs at polarizing growth edges (Pizzinga *et al.,* 2019). The Holt group has elegantly provided insights towards these unanswered questions by investigating the role of local translation in brain development. Brain development relies in proteome plasticity: cytoskeleton and adaptor proteins (*e.g*., β-actin, vimentin, fascin) are elevated during branching and wiring of axons, while upregulation of vesicle receptors and neurotransmission proteins occurs during maturation (Low & Cheng, 2006; Shigeoka *et al.,* 2016; Zivraj *et al.,* 2010). Interestingly, several eIFs are translated in a stage-specific manner during development (Shigeoka *et al.,* 2016). Wiring axons are enriched with active translation of various eIF3 complex subunits (eIF3c,d,f,I,k,m) and eIF1, and decreased upon adulthood. eIF4G-2 mRNA translation remains low during wiring processes, then enriched upon axonal pruning, only to be decreased again in adult mice (Shigeoka *et al.,* 2016). Whether this synthesis pattern is due to 5'-UTR elements (Thoma *et al.,* 2004) or spliced transcripts (Krichevsky & Kosik, 2001) it remains unknown.

However, this leads to the question of whether neurons rely on cell non-autonomous inputs to modulate their translation factory pool. Indeed, neurons require the interaction with glial cells to support on its function. Eyman *et al.* suggested that mRNAs are translocated from glial cells to axons to be translated (Eyman *et al.,* 2007). However, they failed to address the impact of each glial sub-type of the central nervous system (CNS). Broadly, astrocytes and oligodendrocytes are the main CNS glial cell types. Oligodendrocytes generate the insulating myelin-based sheath around axons to promote electrical conductivity (Ozgen *et al.,* 2016). An earlier study by Court *et al.* showed transfer of ribosomes from adjacent Schwann cells (myelin-forming glia of the peripheral nervous system (PNS)) to axons (Court *et al.,* 2008), which is quite surprising given the ribosome's macromolecular size. Astrocytes support neuronal metabolism, bridge the brain-blood barrier, and regulate ion and glutamate homeostasis in the synaptic cleft (amongst other functions). Astrocytes also regulate the activity of pre- and post-synaptic ends (also referred to as neuropil) by releasing its own repertoire of gliotransmitters (Harada *et al.,* 2016). Interestingly, astrocytic perisynaptic processes and neuropil comparative translatomes showed enrichment of different cohorts of eIFs for each cell type (Carney *et al.,* 2014) while the membrane-to-membrane proximity is suggested

to explain the presence of astrocyte-derived proteins in the neuropil (Chicurel *et al.,* 1993; Shavit *et al.,* 2011).

Apart from this possible link in regulating neuronal translation pool, astrocytes also rely heavily on local translation for cell-autonomous functions. A single astrocyte can contact (several) neurons as far as 300μm from the cell body (Sun & Jakobs, 2012), hence requiring rapid protein availability like neurons. Sakers *et al.* highlighted a set of mRNAs locally translated at astrocytic processes including Aqp4, responsible for modulating water homeostasis; Kif1c and Myo1D, associated with maintaining the cytoskeleton (Sakers *et al.,* 2017). In addition, the glial fibrillary acidic protein (GFAP), although known to be abundantly expressed in astrocytes, displayed unevenly concentrated pools at astrocytic processes (Bushong *et al.,* 2002). Indeed, later reports showed GFAP mRNA transport is mediated by a RBP implicated in schizophrenia (Aberg *et al.,* 2006) and brain cancers (Molenaar *et al.,* 2012), suggesting the concentration of GFAP at the astrocytic processes may be a controlled event.

1.2. Regulation of translation initiation.

Stress consists of any disturbing factor(s) that threaten cellular homeostasis which involves fine-tuning of protein synthesis to reset homeostasis or, under severe conditions, trigger cell death. Given that full rounds of protein synthesis require tremendous cellular energetic rates, the initiation phase is targeted with control mechanisms to promote early-on and energy-efficient translation reprogramming.

1.2.1. The integrated stress response (ISR) pathway.

eIF2 is a heterotrimeric complex composed of 3 subunits (α,β,γ) and a key target of translation control as the core inducer of the integrated stress response (ISR). eIF2 is phosphorylated at the α subunit (eIF2α-P) on serine 51 by eIF2α kinases in response to cellular stress. Once phosphorylated, eIF2α-P has a higher affinity to eIF2B and inhibits its GEF activity (further discussed in section 1.2.1.2.), preventing the replenishment of eIF2-GTP and therefore, TC formation. This results in a global inhibition of protein synthesis which is complemented with a paradoxical translation upregulation of stress-responsive mRNAs.

1.2.1.1. eIF2α kinases.

A plethora of cellular stresses induce the phosphorylation of the α subunit of eIF2 through eIF2α kinases. Thus, kinase activation is the first step of the ISR and occurs via autophosphorylation and/or dimerization (Donnelly *et al.,* 2013; Kashiwagi *et al.,* 2017; Rabouw *et al.,* 2020). Four well-described eIF2α kinases exist in mammalian cells: heme-regulated inhibitor (HRI), protein kinase R (PKR), PKR-like endoplasmic reticulum kinase (PERK), and general control nondepressible 2 (GCN2). The latter is the only eIF2α kinase present in *Saccharomyces cerevisiae* (Donnelly *et al.,* 2013). Each eIF2α kinase have been extensively reported to respond to a specific set of stresses. HRI was firstly discovered for downregulating protein synthesis in erythroid cells upon heme deficiency (Han *et al.,* 2001; Pal *et al.,* 1991). Further studies demonstrated that HRI can be activated in non-erythroid cells by non-heme-related mechanisms including arsenite-induced oxidative stress, heat shock and osmotic stress (Lu *et al.,* 2001; McEwen *et al.,* 2005). PKR is mainly activated by the presence of

double-strand RNA (dsRNA) generally from viral infection (Galluzzi *et al.,* 2008; García *et al.,* 2007). However, PKR is suggested to be the most versatile eIF2α kinase given that has been shown to be activated independently of dsRNA including ER stress (Onuki *et al.,* 2004), oxidative stress (Ruvolo *et al.,* 2001), bacterial surface proteins (Goh *et al.,* 2000) and cytokine signalling (Cheshire *et al.,* 1999; Goh *et al.,* 2000). PERK, as an ER transmembrane protein, is predominantly activated by ER stress usually caused by the accumulation of misfolded proteins in the ER lumen (Donnelly *et al.,* 2013). GCN2 is activated upon nutrient deficiency by sensing the availability of amino acid levels in yeast (Yang *et al.,* 2000) and mammals (Ye *et al.,* 2010). Activation of GCN2 has also been associated with viral infection (Berlanga *et al.,* 2006) and UV irradiation (Jiang & Wek, 2005). Recently, a fifth mammalian eIF2α kinase – microtubule affinity-regulating kinase 2 (MARK2) – has been reported to phosphorylate eIF2α in response to proteotoxic stress (Lu *et al.,* 2021). Moreover, while a single eIF2α kinase is activated at early stages of cellular stress, prolonged or extreme stress may activate multiple eIF2α kinases (Zhan *et al.,* 2004).

1.2.1.2. eIF2α phosphorylation and eIF2B inhibition.

eIF2α-P inhibits eIF2B activity, the hub event of the ISR. Cryo-EM structural studies have shed light on the interaction between eIF2α-P and eIF2B (Adomavicius *et al.,* 2019; Bogorad *et al.,* 2017; Gordiyenko *et al.,* 2019; Jennings *et al.,* 2017; Kashiwagi *et al.,* 2019; Kenner *et al.,* 2019; Schoof *et al.,* 2021) (**Figure 1.2.**). The structure and function of eIF2B is further discussed in section 1.3. Phosphorylation of eIF2α at S51 results in conformational changes to eIF2 which changes how eIF2 binds to eIF2B. eIF2α-P binding to eIF2B does not overlap with its unphosphorylated cognate binding interface (eIF2Bβ/δ), and rather contacts the eIF2Bα/δ surface of the regulatory sub-complex of eIF2B ($\alpha_2\beta_2\delta_2$) (also referred in literature as $eIF2B^{RSC}$). Structurally, S51-P refolds the S-loop of eIF2α in a manner that increases the hydrophobic attraction between eIF2α (residues I55, I58, and L61) and eIF2Bδ (residues L314, A315, A318, and F322) (Kenner *et al.,* 2019) (**Figure 1.2.**). Partial contact with eIF2Bβ facilitates the insertion of eIF2α-P to the eIF2Bα/δ surface (Adomavicius *et al.,* 2019). Refolding induced by eIF2α-P alters the localisation of eIF2γ (the GDP/GTP binding subunit of eIF2) towards an orientation that either loosely or transiently

interacts with eIF2Bε (and HEAT domain), and instead favours its anchoring onto eIF2Bγ (Adomavicius *et al.,* 2019; Jennings *et al.,* 2017; Kashiwagi *et al.,* 2019). Recent evidence by the Ron group suggests that this alternative eIF2γ:eIF2Bγ interaction stabilizes the eIF2α-P:eIF2B complex (Zyryanova *et al.,* 2021), although this remains to be performed experimentally. Hence, eIF2α-P-driven misplacement of eIF2γ prevents guanine nucleotide exchange activity (Adomavicius *et al.,* 2019; Kashiwagi *et al.,* 2019). In yeast, however, unphosphorylated eIF2α and eIF2α-P share the same eIF2Bα/δ binding surface, wherein the latter prompts a conformational shift of higher affinity to eIF2Bα and eIF2Bδ which displaces eIF2γ from proximity to the HEAT domain of eIF2Bε (Adomavicius *et al.,* 2019; Gordiyenko *et al.,* 2019). Moreover, in both yeast and mammals, two molecules of eIF2 (either unphosphorylated and/or phosphorylated) can anchor simultaneously at opposing tetrameric platforms of the eIF2B decamer. The eIF2α-P:eIF2B complex arrangement is referred to as 'unproductive state' (**Figure 1.2.**). Other terms have been considered such as 'I(inactive)-State' and 'wings-down' (Schoof *et al.,* 2021), the latter alluding to the conformational shape of eIF2B. Cellular levels of eIF2B are approximately 3- to 5-fold less than levels of eIF2 (Merrick & Pavitt, 2018), highlighting how even a minimal level of eIF2α-P can decrease eIF2B GEF activity and inhibit translation initiation.

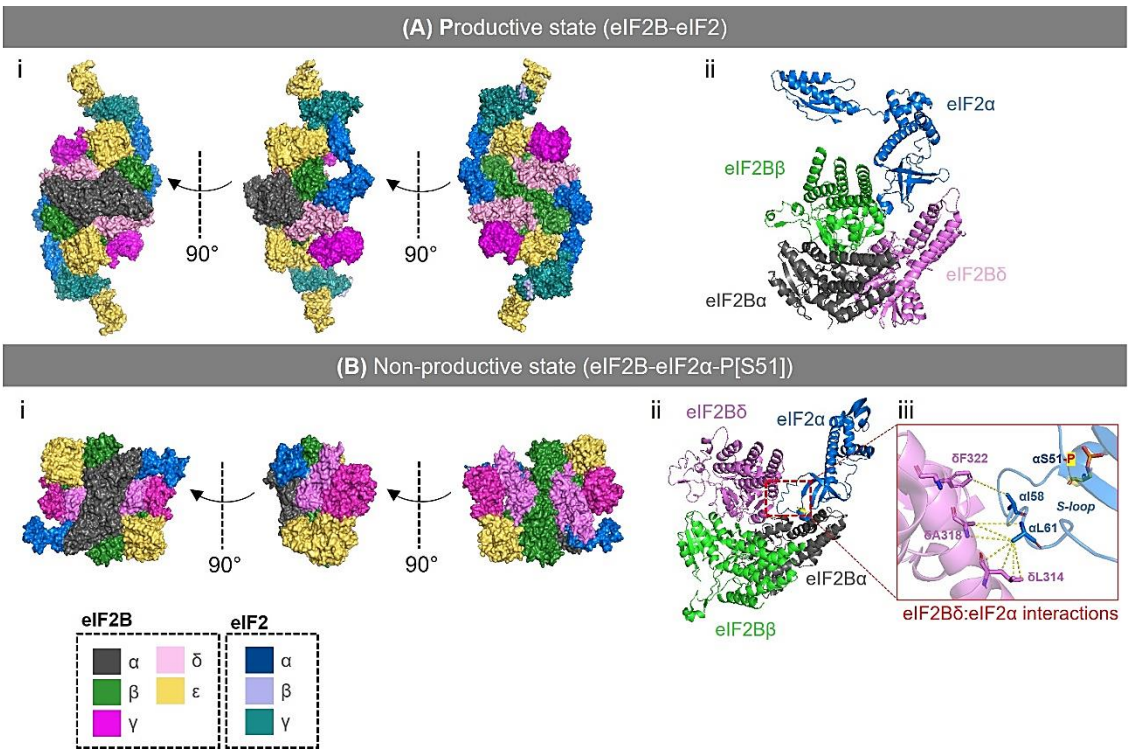

Figure 1.2. CryoEM structures of human eIF2B:eIF2 and eIF2B:eIF2α-P complexes.
(A) (i) Orthogonal surface views of human decameric eIF2B bound to two unphosphorylated human eIF2 heterotrimers (productive state). **(ii)** Cartoon representation of eIF2 binding to human eIF2B^{RSC} (α, β, δ subunits) (PBD: 6O81, resolution: 3.21 Å; drawn in PyMOL). **(B) (i)** Orthogonal surface views of human decameric eIF2B bound to two phosphorylated eIF2α subunits (non-productive state). **(ii)** Cartoon representation of phosphorylated eIF2α binding to human eIF2B^{RSC}. **(iii)** Hydrophobic interactions of eIF2Bδ and eIF2α residues upon phosphorylation of α51 based on Kenner *et al.,* 2019. Dashed yellow lines indicate distance between residues of <5 Å (PBD: 6O9Z, resolution: 3.03 Å; drawn in PyMOL).

1.2.1.3. Cellular signalling of the ISR.

Upon global suppression of protein synthesis, a number of stress-responsive proteins are upregulated to allow cellular recovery of homeostasis (~3% of total mRNAs; (Dang Do *et al.,* 2009)) (**Figure 1.3.**). The translation of such mRNAs is mostly regulated by the presence of upstream open reading frames (uORFs) in their 5'-UTR and, less commonly, by IRES mechanisms (Pakos-Zebrucka *et al.,* 2016). The most well-characterized uORF-containing transcript induced by eIF2α-P is the *ATF4* mRNA (and yeast equivalent GCN4) (**Figure 1.3.**). ATF4 mRNA is ubiquitously expressed and exists at low levels during steady-state conditions. This transcript contains two uORFs (Harding *et al.,* 2000; Vattem & Wek, 2004) with the second uORF (uORF2) overlapping the main ORF at a different reading frame. Following loading of the 43S PIC at the 5'-cap, the ribosome scans towards the 3'-end until AUG recognition of the first ORF (uORF1). Because levels of TCs are abundant at normal conditions, the scanning ribosome can re-charge Met-tRNAi^{Met} at the subsequent AUG sites of uORF1. Because uORF2 overlaps out-of-frame with the main ORF of *ATF4*, the ATF4 protein is not expressed. In the presence of cellular stress, eIF2α-P reduces the abundance of TCs. Hence, the scanning ribosome is less likely to be re-charged with Met-tRNAi^{Met} in a timely manner to translate uORF2. Instead, this delay in re-initiation bypasses the scanning ribosome from uORF2 and continues to scan the transcript until it reaches the main ORF of *ATF4*.

The translated ATF4 protein can dictate two different cellular outcomes, either inducing pro-survival or pro-apoptotic pathways. ATF4-mediated dephosphorylation of eIF2α is crucial for a pro-survival ISR (Kojima *et al.,* 2003). ATF4 protein is a transcription factor of the ATF/CREB sub-family. ATF4 forms homodimers and can heterodimerize with various other transcription factors and binding partners (*e.g.*, C/EBPβ) to act as a trans-activator (Pakos-Zebruscka *et al.,* 2016) or, although less well-known, as a repressor (Bartsch *et al.,* 1995; Karpinski *et al.,* 1992). ATF4 activates the expression of transcription factor C/EBP homologous protein (CHOP) and growth arrest and DNA damage-inducible protein 34 (GADD34) (**Figure 1.3.**). Although ATF4 itself induces GADD34 activation, ATF4/CHOP heterodimers have been shown to facilitate GADD34 expression (Han *et al.,* 2013); hence CHOP expression is suggested to precede GADD34. GADD34 recruits protein phosphatase 1 (PP1c) which

together act as a stress-induced eIF2α phosphatase. CReP (or PPP1R15B) is a GADD34 paralogue, also able to interact with PP1c, but is constitutively expressed to sustain baseline levels of eIF2α dephosphorylation (Jousse *et al.,* 2003). Hence, GADD34 acts as a negative feedback loop to restore translation after cellular stress is resolved. If a pro-survival ISR cannot replenish homeostasis, the ISR shifts towards an apoptotic regiment (**Figure 1.3.**). One of the most well-studied mechanism of ISR-driven cell death is due to a second output of ATF4:CHOP interaction (Kaspar *et al.,* 2021; Marciniak *et al.,* 2004; McCullough *et al.,* 2001; Teske *et al.,* 2013; Yamaguchi & Wang, 2004) (**Figure 1.3.**). CHOP has been extensively implicated as pro-apoptotic through a variety of mechanisms. CHOP up-regulates the expression of death receptors DR5 (Zou *et al.,* 2008). Interestingly, CHOP's interaction with ATF4 contributes to the survival/death balance of the ISR by regulating ATF4's binding affinity to promoters of autophagy genes (B'Chir *et al.,* 2013). Furthermore, CHOP leads to ATF5-mediated transcription of various cell death genes (Teske *et al.,* 2013). Nonetheless, an earlier study shows that cells can partially avoid cell death upon CHOP depletion (Oyadomari *et al.,* 2001), suggesting that additional factors are at play in mediating the apoptotic arm of the ISR.

1.2.1.4. Length of ISR signalling and cell fate.

It has been commonly reported that transient activation of the ISR induces phosphorylation of eIF2α which represses global levels of translation ('acute ISR') and induces expression of genes involved in supporting cellular recovery to regain homeostasis. In contrast, transition to a chronically activated ISR ('chronic ISR') is widely reported as adaptive to prolonged stress, ultimately pro-apoptotic when cells are unable to overcome sustained stress with pathological consequences such as neurodegeneration and cancer (Bond *et al.,* 2020; Ghaddar *et al.,* 2021; Rutkowski *et al.,* 2006) (**Figure 1.3.**). This duality of the ISR (protective and pro-apoptotic) is intrinsically time-dependent but remains poorly defined as to what mediates this switch.

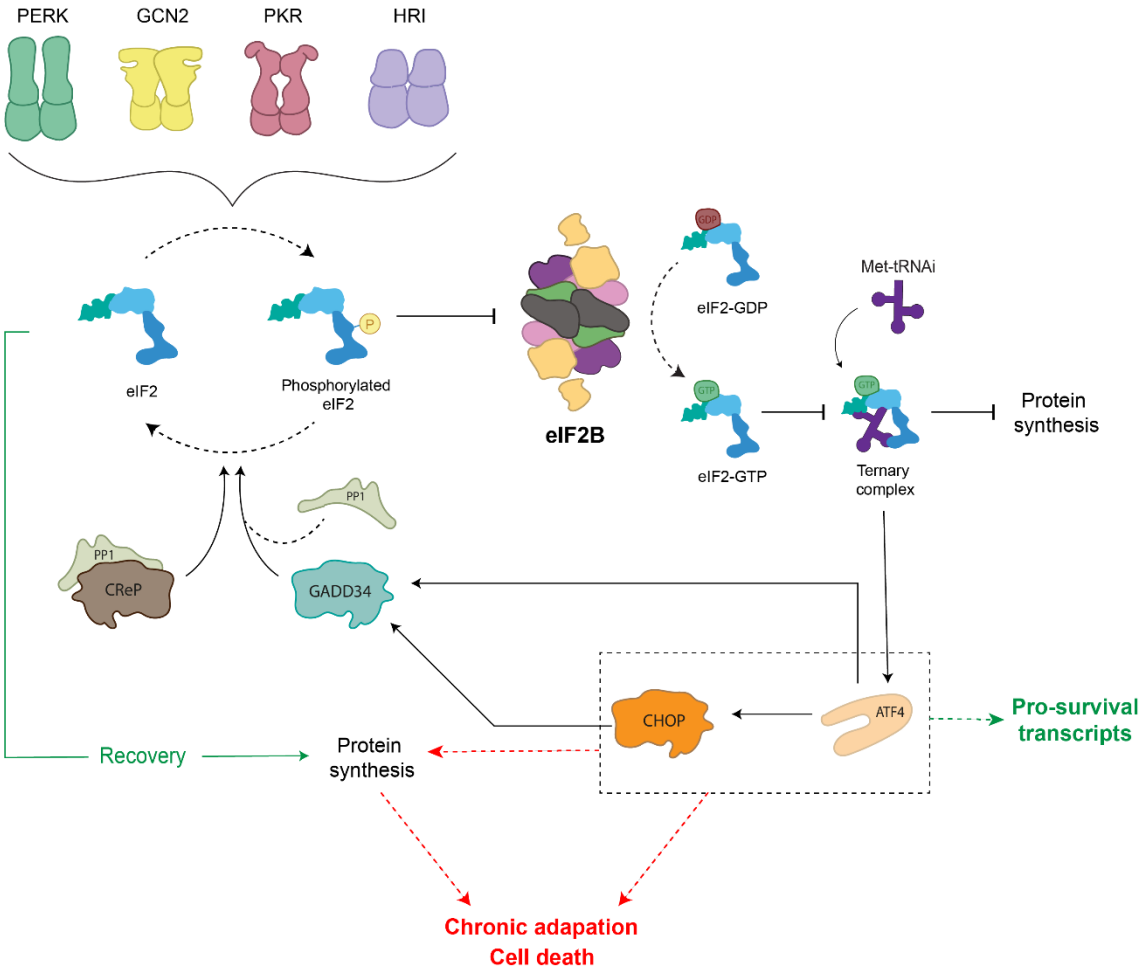

Figure 1.3. Activation of the ISR pathway.
In response to various cellular stress stimuli eIF2α kinase molecules are activated through dimerization. eIF2α kinases phosphorylate the α subunit of eIF2. In its phosphorylated form, eIF2 is a competitive inhibitor of eIF2B activity preventing replenishment of eIF2-GTP within the cell. This leads to inhibition of global protein synthesis while the translation of specific stress response mRNAs, including ATF4, is upregulated. During episodes of acute ISR, ISR effectors are able to restore homeostasis and ATF4-mediated activation of CHOP induces the transcription of GADD34 to promote dephosphorylation of eIF2α. In cases where ISR effectors are unable to restore homeostasis, the cell transitions into a chronically activated ISR. Protein synthesis is restored via an eIF2B independent mechanism and ATF4-mediated activation of CHOP promotes proapoptotic gene expression.

1.2.2. The mTOR pathway.

Another major pathway that regulates translation initiation is through the mammalian target of rapamycin (mTOR). mTOR exists as two distinct complexes: mTORC1, which is crucial in the control of translation initiation; and mTORC2, with additional roles in cytoskeleton reorganisation. mTORC1 is a serine/threonine kinase that is activated in response to growth factors by phosphoinositide 3-kinase (PI3K) and extracellular signal-regulated kinase (ERK) pathways. Upon mTORC1 activation, a subset of eIFs is phosphorylated to enhance global translation as well as promoting privileged expression of mRNAs harbouring terminal oligopyrimidine (TOP) at their 5'-end (Thoreen, 2017). Phosphorylation of eIF4G, which promotes assembly of eIF4E and eIF4A to form the eIF4F complex, enhances its scaffolding activity. Similarly, phosphorylation of eIF4B allows the required cooperative interaction with eIF4A to promote eIF4A's helicase activity of unwinding secondary structures of target mRNAs (Andreou *et al.,* 2017). Another key target of mTOR are eIF4E-binding proteins (4E-BPs). 4E-BPs directly bind to eIF4E and compete with eIF4G which prevent formation of the eIF4F complex. During steady-state, mTORC1 activation phosphorylates 4E-BPs which hinders their binding affinity for eIF4E, allowing eIF4F-depedent translation initiation (Pelletier *et al.,* 2015; Sonenberg & Hinnebusch, 2009). Additionally, mTORC1 phosphorylates programmed cell death 4 (PDCD4) which prevents eIF4A binding and relieves eIF4A inhibitory activity (Dennis *et al.,* 2012).

1.2.3. Alternative signalling.

During stress the translation apparatus remains necessary to support selective cap-dependent gene expression, (notably stress-responsive genes), despite the deficiency of canonical eIF2 activity and TC formation. Alternative signalling of translation initiation exists to overcome this limitation such as eIF3d-, eIF2A- and eIF2D-dependent mechanisms.

1.2.3.1. eIF3d.

The multi-subunit eIF3 complex is critical in recruiting mRNA to the 40S ribosome (Hinnebusch, 2014). However, some evidence highlights specialised roles for the eIF3d subunit in mediating translation initiation. PAR-CLIP experiments performed to identify binding sites of RBPs highlighted ~500 mRNAs involved in cell proliferation that are translationally regulated by eIF3d due to internal stem loops located at the 5'-UTR (Lee *et al.,* 2015). Further investigation by the same group resolved the eIF3d cap-binding domain at atomic resolution and elegantly reported that eIF3d mediates cap recognition alternatively to the eIF4F complex (Lee *et al.,* 2016). It was therefore proposed an eIF3-specialised mode of translation initiation may occur for a subset of mRNAs involving the 5' cap and/or 5'-UTR-specific secondary structures (Lee *et al.,* 2015; Lee *et al.,* 2016). Recent work also suggests eIF3d-specialised translation under conditions of chronic ISR (Guan *et al.,* 2017). This study showed that translation recovery during chronic ER stress occurs independently of eIF4F cap recognition and restoration of eIF2B activity, and instead requires eIF3d in a PERK-dependent manner (Guan *et al.,* 2017). eIF3d-RNA co-IP experiments displayed increased binding affinity of transcriptionally induced mRNAs such as ATF4, GADD34 and BiP (Guan *et al.,* 2017), implying eIF3d as a key mediator of ISR responsive transcripts hence avoiding repression mechanisms reliant upon the eIF4F complex. eIF3d-dependent translation has been recently shown to be harnessed for HCMV-infected cell protein synthesis (Thompson *et al.,* 2022) in a manner that mimics the ISR translational reprogramming observed by (Guan *et al.,* 2017).

1.2.3.2. eIF2A and eIF2D.

eIF2A is an initiator tRNA carrier that functionally replaces eIF2, the canonical carrier of Met-tRNAi^{Met}, when its activity is compromised during cellular stress (Kim *et al.,* 2011; Kwon *et al.,* 2017). The same group later reported that eIF5B, harbouring ribosome-binding and GTPase activities, releases eIF2A from the 40S ribosome hence facilitating the handover of Met-tRNAi^{Met} as eIF2A lacks a GTPase domain (Kim *et al.,* 2018). Hence, eIF2A:eIF5B cooperative interaction allows baseline translation in the absence of active eIF2. Similarly, eIF2D can also interact with the 40S ribosomal subunit to deliver the Met-tRNAi yet in a GTP-independent manner (Dmitriev *et al.,* 2010). This shift towards eIF2A/eIF2D upon

eIF2α-P is apparent given that a few studies in both yeast and mammalian models highlight that viability and steady-state global translation is insensitive to eIF2A and eIF2D depletion (Dmitriev *et al.,* 2010; Golovko *et al.,* 2016; Sanz *et al.,* 2017; Zoll *et al.,* 2002); while the Walter group demonstrated that uORF translation of BiP mRNA cannot be translated in the absence of eIF2A (Starck *et al.,* 2016). Another recent study highlighted that ATF4 translation requires eIF2D to resolve ER stress in *Drosophila* and human cell lineages (Vasudevan *et al.,* 2020), suggesting that eIF2D-driven control of ATF4 translation is an evolutionarily conserved control mechanism. The authors postulate that eIF2D alongside other identified factors (DENR, MCTS-1) act as eIF2α-independent deliverers of Met-tRNAi^{Met} to the scanning ribosome to re-initiate ORF translation.

1.3. eIF2B.

1.3.1. eIF2B structure and sub-complexes.

eIF2B is composed of five non-identical proteins named eIF2Bα-ε based on their increasing size. eIF2Bγ and eIF2Bε subunits are responsible for the GEF activity of eIF2B. While eIF2Bε can carry out GEF by itself, eIF2Bγ can stimulate eIF2 binding to eIF2Bε (Gomez & Pavitt, 2000). In contrast, the regulatory subunits (eIF2Bα, eIF2Bβ, eIF2Bδ) are not required to provide basal GEF activity, however their presence boosts the full GEF capacity of eIF2B. Moreover, eIF2B regulatory subunits are pivotal to inhibiting the GEF activity of eIF2B by sensing eIF2α-P (Pavitt, 2005). Interestingly, yeast eIF2Bα is the only non-essential gene of eIF2B but is particularly important in eIF2α-P sensing (Dever *et al.,* 1993; Elsby *et al.,* 2011; Hannig & Hinnebusch, 1988).

Before the crystal structure of the full eIF2B complex was resolved, eIF2B was believed to be a heteropentamer composed of one copy of each subunit (Webb & Proud, 1997). In 2014, several publications identified an eIF2B complex yielding twice the expected mass of the putative pentamer, hence existing instead as a decamer containing two copies of each subunit (Bogorad *et al.,* 2014; Gordiyenko *et al.,* 2014; Wortham *et al.,* 2014) (**Figure 1.4.**). At the time these reports sparked some debate as one study anticipated that eIF2B assembled through a catalytic core ($\gamma_2\varepsilon_2$) bound to adjacent regulatory complexes (αβδ) at opposite sides (Gordiyenko *et al.,* 2014); while others proposed an hexameric regulatory core $(\alpha\beta\delta)_2$ flanked by opposing catalytic heterodimers (γε) (Wortham *et al.*, 2014; Bogorad *et al*., 2014). The latter model was validated by Kashiwagi and colleagues after successfully resolving the crystal structural of the *S.pombe* eIF2B decamer (Kashiwagi *et al.,* 2016).

By combining high-collision energy, mass spectrometry and pulldown assays, Wortham and colleagues elegantly proposed a model for eIF2B decamer assembly through precursors of eIF2B sub-complexes (Wortham *et al.,* 2016). Because eIF2Bε expression is regulated by levels of eIF2Bγ and both can dimerize, eIF2Bγε heterodimers are initially formed. eIF2Bβ and δ can also form heterodimers and bind to eIF2Bγε to assemble an intermediate eIF2Bβδγε tetramer. Unlike the remaining subunits, eIF2Bα can form homodimers and act at the final stage of eIF2B assembly by stapling two opposing tetramers to generate the full $eIF2B(\alpha\beta\delta\gamma\varepsilon)_2$ holocomplex (Wortham *et al.,* 2016). eIF2B sub-complexes

are sufficiently stable to exist in its (supposedly) intermediate state. It is proposed that eIF2B(βδγε) and eIF2B(γε) sub-complexes are present in mammalian cells and yield increasingly lower GEF activity compared to the full holocomplex (~50% and ~20%, respectively) (Liu *et al.,* 2011; Wortham *et al.,* 2014). It remains to be understood if eIF2B sub-complexes hold intrinsic functions as stand-alone complexes beyond transient precursors of eIF2B decamers. In mammalian cells, it has been recently proposed that eIF2B sub-complexes, which have different binding affinity to eIF2α-P, reside at eIF2B bodies and provide two distinct sub-populations of GEF hotspots that are differently targeted during cellular stress (Hodgson *et al.,* 2019). This model is discussed in detail in section 1.3.4.2.

Catalytic subunits eIF2Bε and γ share homologous regions with each other. Both contain a nucleotidyl-transferase (NT) domain and an acyl-transferase (AT) domain that secures interaction between ε- and γ- subunits, as well as the interactions with other subunits (Wang *et al.,* 2012). The HEAT domain of eIF2Bε is the most critical motif for GEF activity and resides at the distal edge of the C'-terminus. The HEAT remains structurally unresolved (Kashiwagi *et al.,* 2016) due to its intrinsically disordered nature. Regulatory subunits share a higher degree of homologous regions, mostly differing at their *N*-terminal, and are more well conserved than its catalytic partners (Price *et al.,* 1996). More impressively is how closely related the hexameric regulatory core eIF2B$(\alpha\beta\delta)_2$ is to the hexameric core of archaeal ribose-1,5-bisphosphate isomerase (RBPI) (Kuhle *et al.,* 2015; Nakamura *et al.,* 2012) which implies that, in an evolutionary sense, eIF2B(αβδ) may have existed as an ancient sugar phometabolite-sensing enzyme which later evolved to serve as the core of eIF2B as a GEF protein. This model is supported by earlier observations that glucose-6-phosphate regulates eIF2B activity (Gross *et al.,* 1988) and, more recently, an activity-based screening identifying various sugar phosphate metabolites that bind to conserved regions of eIF2Bα and enhance decamer formation (Hao *et al.,* 2021).

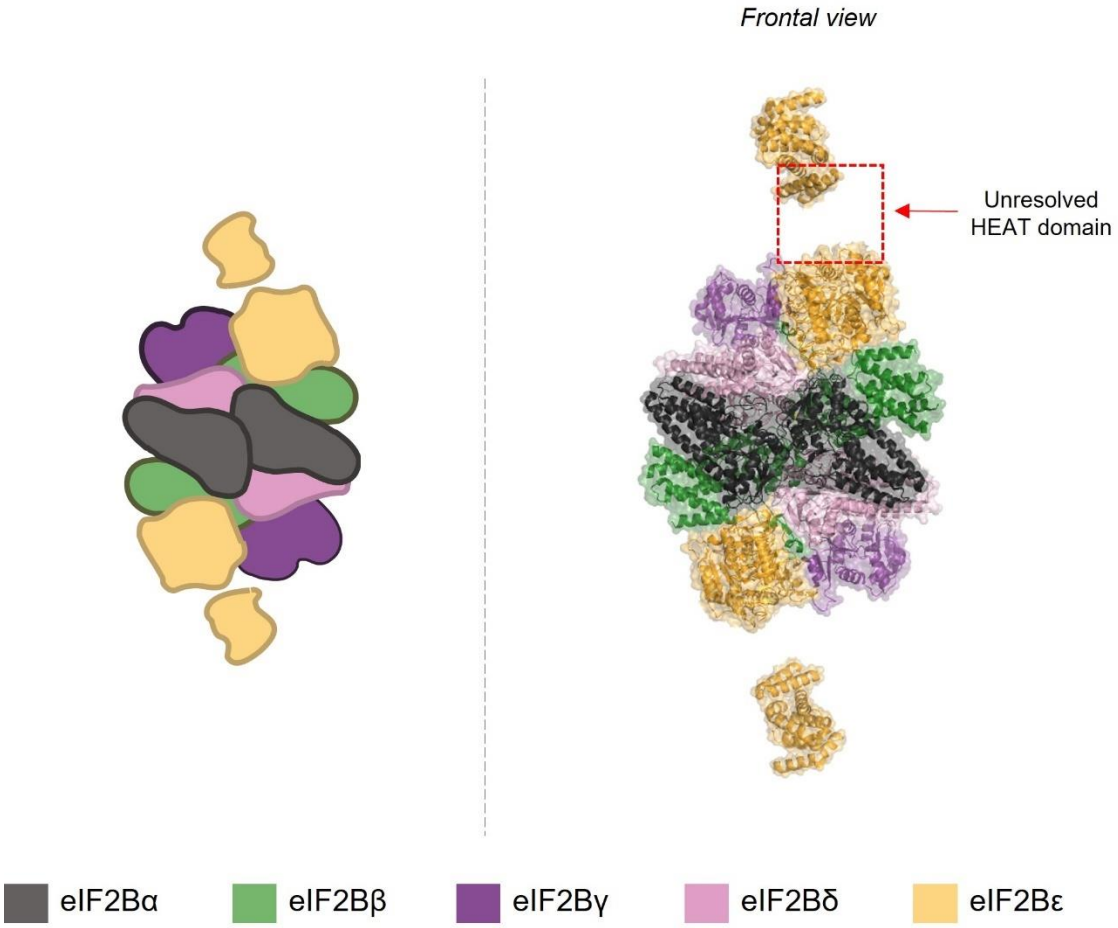

Figure 1.4. Structure of mammalian eIF2B.
eIF2B is composed of two copies of each of its five subunits. The regulatory subunits (eIF2Bα, eIF2Bβ, and eIF2Bδ) reside in the centre of the decamer, forming a hexameric regulatory core. This core is bordered on either side by a heterodimer of the catalytic subunits. The image of the left is the resolved crystal structure of mammalian eIF2B (PBD: 6O81, drawn in PyMOL), highlighting the unresolved region at the HEAT domain due to its high flexibility. The image on the right is the cartoon representation of the crystal structure of mammalian eIF2B.

1.3.2. Guanine nucleotide exchange activity.

The main function of eIF2B is to catalyse the GDP:GTP exchange of eIF2 thus acting as a rate-limiting factor for levels of TCs (eIF2-GTP●Met-tRNAi). eIF2B blunts the binding of Mg^{2+} ion and GDP from eIF2 which favours GDP release and a transient complex of nucleotide-free eIF2 (*apo*-eIF2). However, eIF2B poses as an atypical GEF protein. Initially it was anticipated that eIF2B behaved similarly to tRNA-binding elongation factor-T (EF-T), a bacterial GEF protein for EF-Tu with conserved domains to eIF2 (Schmitt *et al.,* 2010). EF-T has a higher affinity to nucleotide-free EF-Tu than its GDP/GTP-bound cognate, which facilitates the anchoring of EF-Tu to EF-T while promoting nucleotide exchange (Gromadski *et al.,* 2002). This binding mode is recapitulated by many other GEF proteins and respective G protein partners (Bos *et al.,* 2007). However, nucleotide binding does not influence the affinity of eIF2 with eIF2B as both yeast *apo*-eIF2 and nucleotide-bound (GDP or GTP) bind similarly to eIF2B (Jennings *et al.,* 2017). Strikingly, eIF2B serve as an antagonist for Met-tRNAi binding to eIF2-GTP (Jennings *et al.,* 2017), which can be viewed as contradictory to eIF2B's function in forming TCs. Instead, the catalytic core of eIF2B (eIF2Bγ,ε) firstly dissociates eIF2 from the eIF2-GDP●eIF5 complex, then nucleotide exchange takes place and Met-tRNAi competes with eIF2B for eIF2-GTP binding which is facilitated by eIF2B's lack of binding specificity as described previously (Jennings *et al.,* 2017; Jennings & Pavitt, 2010; Jennings *et al.,* 2013). Upon TC formation, eIF5 is recruited back to generate a quaternary complex of eIF2-GTP, Met-tRNAi and eIF5 (eIF2-GTP●Met-tRNAi●eIF5) that prevents eIF2B from re-joining (Jennings *et al.,* 2017). This sequential mechanism of eIF2B GEF activity provides different checkpoints for regulation (Jennings *et al.,* 2017) and may be seen as an evolutionary tunning given that bacterial GEF protein EF-T is included in an intermediate quaternary complex EF-Tu-GDP/GTP●tRNA●EF-T that is used as a template for EF-Tu TC formation during optimal conditions or EF-Tu TC decline when confronted with cellular stress (Burnett *et al.,* 2014; Burnett *et al.,* 2013).

A key question that remains is how GTP is transferred from eIF2B to eIF2. It has been shown that GTP transfer occurs from eIF2Bγ to eIF2γ as the only subunits with GDP/GTP-binding domains (Gordiyenko *et al.,* 2014; Hannig *et al.,* 1993; Kershaw *et al.,* 2021). It was recently proposed that GTP availability regulates

the GEF activity of eIF2B (Kershaw *et al.,* 2021). GTP only binds to eIF2Bγ when complexed to eIF2Bε (eIF2Bγε) which in return encourages GDP release from eIF2 (Kershaw *et al.,* 2021). This falls in agreement with earlier findings that eIF2Bγε subcomplexes have increased GEF activity than eIF2Bε (Fabian *et al.,* 1997; Gomez & Pavitt, 2000; Pavitt *et al.,* 1998; Williams *et al.,* 2001). Although recent biochemical reports revealed these GTP-binding surfaces in eIF2B-eIF2 complexes are placed in adjacent to each other, they are not in proximity (Adomavicius *et al.,* 2019; Gordiyenko *et al.,* 2019; Kashiwagi *et al.,* 2019; Kenner *et al.,* 2019). Kershaw *at. al* provide the attractive suggestion that GTP binding to eIF2Bγ promotes moderate conformational changes that decrease this gap with eIF2γ (Kershaw *et al.,* 2021), which would strikingly resemble the local arrangements adopted by eIF2 to perform its functional roles (Beilsten-Edmands *et al.,* 2015).

1.3.3. Other intrinsic roles of eIF2B subunits.

Martin *et al.* showed that expression of an alternative isoform of eIF2Bδ correlates to the magnitude of ISR activation in a cell-type manner (Martin *et al.,* 2010). These isoforms derive from alternative splicing of eIF2Bδ mRNA and produces a long-variant and short-variant of eIF2Bδ, which differ in their N-terminal sequence. Cell lines with an attenuated induction of classical ISR markers (eIF2α-P, ATF4, CHOP) upon cellular stress treatments showed high expression of the long-variant eIF2Bδ protein (Martin *et al.,* 2010). In contrast, overexpressing the short-variant of eIF2Bδ in a shRNA-knockdown cell line for endogenous eIF2Bδ (hence initially depleted of all isoforms) caused an increased upregulation of ISR markers (Martin *et al.,* 2010). Moreover, cells exclusively expressing the short-variant eIF2Bδ protein showed similar inhibition of protein synthesis upon ER stress to control cells, while protein synthesis levels in cells expressing the long-variant protein were unchanged by cellular stress (Martin *et al.,* 2010). While both variants of eIF2Bδ do not affect the integrity of eIF2B complex, the long-variant protein has impaired binding to eIF2α-P (Martin *et al.,* 2010). Although these observations were performed in cancer-derived cell lines, which have inherently defective rates of protein synthesis (Dolfi *et al.,* 2013), these data show that eIF2Bδ isoforms have divergent intrinsic roles in activating the ISR.

More recently, an intronically polyadenylated mRNA isoform of eIF2Bγ was identified (Circir *et al.,* 2022). Alternative polyadenylation sites produces either truncated proteins (isoforms) or encode the same protein but with different 3'-UTR lengths (Di Giammartino *et al.,* 2011). In the study conducted by Circir *et al.,* the C'-terminus truncated isoform of eIF2Bγ is constitutively expressed across different tissues and co-regulated with full-length eIF2Bγ in a ~1:9 ratio (truncated : full-length). Structural modelling revealed significant electrostatic changes that antagonize the eIF2Bγ:eIF2γ interaction hence likely to loosen or completely abrogate eIF2 binding to eIF2B (Circir *et al.,* 2022). How the expression of truncated eIF2Bγ is impacted upon cellular stress or if the phosphorylation state of eIF2α alters an already unstable eIF2B:eIF2 complex was not investigated. Altogether, it is plausible to speculate that eIF2B subunit isoform expression may play a key role in regulating the equilibrium between active (eIF2B:eIF2) and inactive (eIF2B:eIF2α-P), this requires further investigation specially in the context of disease (Keefe *et al.,* 2020; Slynko *et al.,* 2021). Other isoforms of eIF2B subunits are reported in the NCBI database but remain to be explored.

1.3.4. eIF2B localisation: the 'eIF2B body'.

1.3.4.1. eIF2B bodies in yeast.

The spatial re-localisation of cytoplasmic proteins into large assemblies has been extensively reported as an adaptive energetic strategy. These assemblies inherently protect, store, and regulate the activity of proteins (Franzmann *et al.,* 2018). Notably in yeast models, specific eIFs have been observed to localise to cytoplasmic assemblies upon glucose starvation as a response to downregulate protein synthesis. Poly(A) binding protein Pab1p localise to P-bodies alongside poly(A)+ mRNA and translation initiation factors eIF4E and eIF4G2 during conditions of translation inhibition (Brengues & Parker, 2007). Similarly, Hoyle *et al.* observed the same mRNP complex containing Pab1p, eIF4E and eIF4G2 to localise to functionally distinct granules known as yeast stress granules (SGs) (Hoyle *et al.,* 2007). Additionally, under certain stresses, these yeast SGs harbour eIF3 and 40S subunits (Grousl *et al.,* 2009), further emphasizing the selective targeting of translation factors to cytoplasmic granules. Despite the ongoing debate between the compositional crossover between P-bodies and SGs (Kedersha *et al.,* 2005; Wilczynska *et al.,* 2005), the co-localisation of RNA-

binding proteins and translation factors is ultimately induced upon suppression of translation initiation.

In 2005, eIF2B joined this repertoire of translation factors able to localise to cytoplasmic granules and termed as “eIF2B bodies” (Campbell *et al.,* 2005). eIF2B bodies did not co-localise with Met-tRNAi hence not active site of TC formation (Campbell *et al.,* 2005). eIF2 (eIF2B’s substrate) dynamically shuttles through eIF2B bodies at a rate that mirrored cellular levels of eIF2B GEF, hence eIF2B bodies are sites of active GEF activity (Campbell *et al.,* 2005). Interestingly, yeast eIF2B bodies are shaped as a filamentous structure. A screening of GFP-tagged yeast strains showed that additional proteins can form filamentous structures (Noree *et al.,* 2010). Extended screening in budding yeast identified many more metabolic enzymes with filament-forming capability (Shen *et al.,* 2016). Filament formation has been recently reviewed for its variety of physiological functions including metabolic control, protein stabilisation and intracellular transport (Park & Horton, 2019). More significantly, filamentation can either promote or inversely inhibit enzymatic activity. These divergent functionalities of filament formation may be due to the accessibility of substrate’s binding sites and the stacking-like architecture of filamentation. For example, the active conformation of SgrAI, a bacterial allosteric type II restriction endonuclease, is more stable when polymerized into a filament (Polley *et al.,* 2019). Glutamine synthetase (Gln1), which converts glutamate into glutamine, form starved-induced inactive filaments which is reversed upon filament dissolution to allow efficient recovery of translation (Petrovska *et al.,* 2014). In contrast, Acetyl CoA carboxylase, a component of the fatty acid biogenesis, possess the ability to form both active and inactive filaments (Hunkeler *et al.,* 2018). eIF2B bodies are suggested to follow this latter mode of enzymatic regulation.

Norris *et al.* showed that *GCN3* (eIF2Bα) mutations that evokes loss of eIF2B body formation (Gcn-) sustains GEF activity even in the presence of eIF2α-P, while mutations that decrease eIF2B’s catalytic activity (Gcd-) breaks down eIF2B bodies into smaller building blocks (‘micro’ eIF2B bodies) (Norris *et al.,* 2021). These data imply that yeast eIF2B bodies enhance eIF2B activity and are necessary for normal regulation of eIF2B activity, which falls in agreement with eIF2Bα-depleted complexes harbouring decreased activity (Wortham *et al.,* 2014). Nonetheless, the functional relevance of eIF2B body formation is a

debatable issue. Conflicting reports in yeast models either observe formation of eIF2B bodies exclusively upon cellular stress (Moon & Parker, 2018a; Nüske *et al.,* 2020), while others have observed the steady-state presence of eIF2B bodies which is further stimulated during stress (Campbell *et al.,* 2005; Noree *et al.,* 2010; Norris *et al.,* 2021), and remains to be fully agreed on.

1.3.4.2. eIF2B bodies in mammalian cells.

In mammalian cells, eIF2B localisation forms under normal conditions but with a more complex morphology. Unlike in yeast where a single eIF2B body exists, Hodgson *et al.* proposed that mammalian eIF2B bodies exist as two major sub-populations based on its size and eIF2B subunit composition: small eIF2B bodies and medium/large eIF2B bodies (Hodgson *et al.,* 2019) (**Figure 1.5.**). The large/medium bodies contain all five subunits of eIF2B while small bodies predominantly contain the γ- and ε- subunits of eIF2B. eIF2 is a mobile component of both types of eIF2B bodies and the movement or shuttling of eIF2 within these bodies correlates with cellular eIF2B GEF activity. Expectedly, upon induction of the acute ISR, eIF2α-P co-localised to large/medium bodies and showed decreased eIF2 shuttling (Hodgson *et al.,* 2019). Smaller bodies, being depleted of regulatory subunits, did not co-localise with eIF2α-P but increased the shuttling of eIF2. This was accompanied by an increased degree of co-localisation with eIF2Bδ, suggesting that novel eIF2B(γδε) subcomplexes potential form following ISR activation (Hodgson *et al.,* 2019). Hodgson *et al.* interpret these results with the compelling idea that different eIF2B sub-complexes reside at eIF2B bodies which may facilitate cellular stress responses.

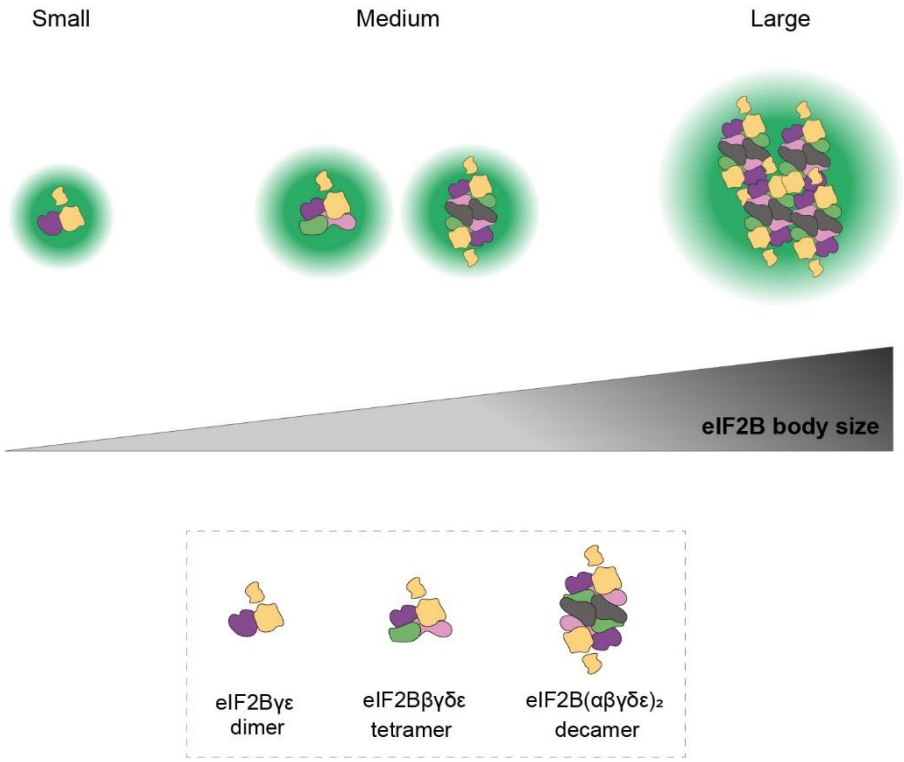

Figure 1.5. eIF2B subcomplexes localise to different sized eIF2B bodies (model proposed by Hodgson *et al.*, 2019).
eIF2B exists as different eIF2B sub-complexes. Small eIF2B bodies are mainly composed of catalytic subunits (eIF2Bγ and eIF2Bε), which suggests that eIF2B(γε) heterodimers reside at these sites. Medium contained modest levels of regulatory subunits (eIF2Bα, eIF2Bβ, eIF2Bδ) and large eIF2B bodies contained all subunits of eIF2B, which suggests that eIF2B(βδγε) tetrameric and eIF2B$(\alpha\beta\delta\gamma\varepsilon)_2$ decameric complexes reside at these bodies.

1.4. ISRIB.

1.4.1. Mechanism of action of ISRIB.

ISRIB was first published as a memory-enhancing small molecule capable of binding to eIF2B and reversing the inhibitory effects of eIF2α-P by restoring translation (Sekine *et al.,* 2015; Sidrauski *et al.,* 2013; C. Sidrauski *et al.,* 2015a; Sidrauski *et al.,* 2015b). It was later shown by size-exclusion chromatography that ISRIB's mechanism of action centred on its ability to stabilize eIF2B decamer observed in lysates of HEK293 cells (Sidrauski *et al.,* 2015b). In 2018, the crystal structure of human eIF2B and ISRIB appeared in the literature by two independent groups and showed that ISRIB binds to β- and the δ- subunits of eIF2B (Tsai *et al.,* 2018; Zyryanova *et al.,* 2018). Given ISRIB's own symmetry as a small molecule, it was expected that ISRIB lodged in a symmetrical interface pocket, which was confirmed as it engages with the same residues of opposing eIF2Bβδ dimers (Tsai *et al.,* 2018; Zyryanova *et al.,* 2018). This way ISRIB dimerizes two eIF2Bβδγε tetramers to form eIF2B$(βδγε)_2$ octamers which facilitates the joining of eIF2B$α_2$ dimers to generate eIF2B decamers (Tsai *et al.,* 2018; Zyryanova *et al.,* 2018) (**Figure 1.6.**). It is still not clear whether ISRIB directly binds to eIF2B tetramers to form a 'stapled' octamer with direct effect on GEF activity and/or whether it induces conformational changes that alter eIF2B's binding mode to favour nucleotide exchange and discourage eIF2α-P interaction. This confusion is mostly attributed to the fact that ISRIB did not enhance the *in vitro* GEF activity of a fully assembled human eIF2B complex but promoted eIF2B$(βγδε)_2$ octamers with higher GEF activity in cell lysates (Tsai *et al.,* 2018; Zyryanova *et al.,* 2018); which favours a direct mode of ISRIB binding. In contrast, two eIF2Bδ mutations that are seemingly distal from ISRIB's binding pocket are ISRIB resistant (Sekine *et al.,* 2015) which warrants that ISRIB evokes modest allosteric changes as it binds two opposing tetramers.

ISRIB's mode of action depends however on evoking allosteric outputs to eIF2B (Zyryanova *et al.,* 2021). Taking into account that two eIF2 (either both unphospho-, both phospho- or one of each) substrates can bind at opposing sides of eIF2B decamer, once ISRIB is bound to pre-existing eIF2B decamers it prevents formation of the strongly inhibited complex of eIF2α-P:eIF2B:eIF2α-P (Zyryanova *et al.,* 2021). This strongly inhibited complex has a deformed ISRIB-binding pocket, hence addition of ISRIB discourages eIF2B complexed with two

eIF2α-P substrates and favours all other remaining states, which inherently hold either partial or full catalytic activity (Zyryanova *et al.,* 2021). The same study also showed that high levels of eIF2α-P blunted this ISRIB-induced balance of eIF2:eIF2B (Zyryanova *et al.,* 2021), arguably by depleting the majority of free eIF2B and preventing binding of ISRIB. This is consistent with other studies showing that ISRIB rescues protein synthesis within modest levels of eIF2α-P but not upon high(er) levels (Hodgson *et al.,* 2019; Rabouw *et al.,* 2019).

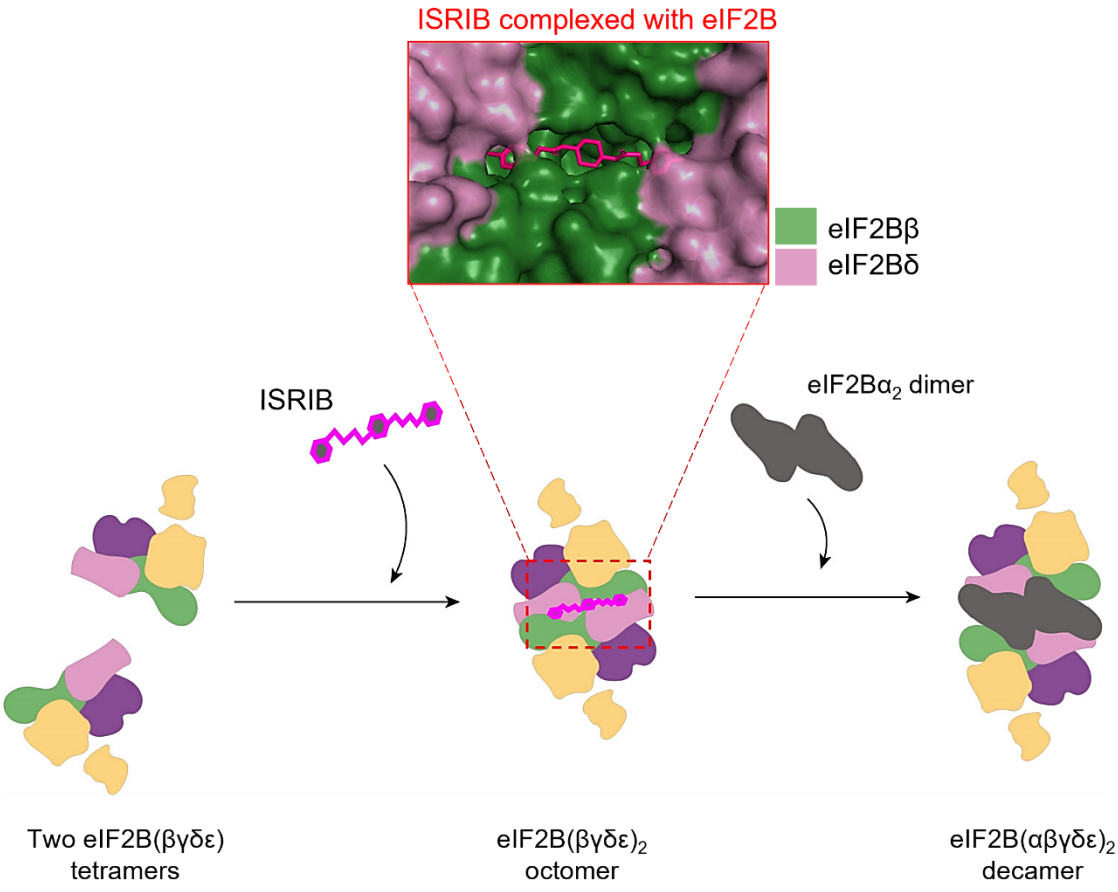

Figure 1.6. ISRIB stabilizes decameric eIF2B.
ISRIB binds at a symmetrical interface of eIF2Bβ/δ of two eIF2B tetramers (PBD: 6EZO, drawn in PyMOL) and joins into an eIF2B octomer, which encourages joining of a eIF2Bα$_2$ dimer to form the eIF2B decamer.

1.4.2. Therapeutical value of ISRIB.

The therapeutic effects of ISRIB have gained momentum over the past years. ISR impairment is a common hallmark of multiple human pathologies (Pakos-Zebrucka *et al.,* 2016) and since the publication of Halliday *et al.* which showed that ISRIB counteracts prion-causing phenotypes without immediate toxic effects akin to other compounds (GSK2606414, a PERK inhibitor, caused pancreatic toxicity despite its restorative properties) (Halliday *et al.,* 2015), it has placed eIF2B activation as a promising "fine-tuner" of the ISR. Another small molecule that targets eIF2B is 2BAct which activates eIF2B similarly to ISRIB although its unknown if it shares a similar binding pocket (Wong *et al.,* 2019). Like ISRIB, 2BAct reversed neuropathology signs in VWMD mice models harbouring an eIF2B$\varepsilon^{R191H/R191H}$ mutation (Wong *et al.,* 2019). ISRIB has also proven effective in ameliorating disease models of Alzheimer's disease (Hu *et al.,* 2022; Oliveira *et al.,* 2021), Down syndrome (Zhu *et al.,* 2019), Huntington's disease (Xu *et al.,* 2022), amyotrophic lateral sclerosis (Bugallo *et al.,* 2020), traumatic brain injury (Chou *et al.,* 2017), intellectual disability (Young-Baird *et al.,* 2020), lung fibrosis (Watanabe *et al.,* 2021; Dobrinskikh *et al.,* 2022) and various types of cancer (Dudka *et al.,* 2022; Jewer *et al.,* 2020; Palam *et al.,* 2015; Varone *et al.,* 2022) (**Table 1.2.**). The fact that ISR modulators such as ISRIB can be applied to such a variety of human pathologies showcases the unsurprising interest in unveiling eIF2B's function and its regulation in the context of disease.

Table 1.2. ISRIB is effective in various disease models.

Disease	Model used	Diseased phenotype	Effect of ISRIB	References
Alzheimer's disease (AD)	• Synthetic-Aβ-injected mice model	• Brain accumulation of the amyloid-β peptide (Aβ) as the main culprit for deregulation in AD brains and manifested symptoms of memory loss. • ISR markers are elevated in AD brains.	• Restored synapse function and memory. • Prevents Aβ-induced synaptic loss.	(Oliveira *et al.,* 2021; Hu *et al.,* 2022)
Down syndrome (DS)	• Ts65Dn mice, DS post-mortem tissue and iPSC from DS patients	• Increased (PKR-)eIF2α-P levels in DS mouse brain, DS human brain and DS iPSC cells. • Severe loss of long-term memory and synaptic plasticity.	• Full restoration of synaptic transmission, long-term memory and protein synthesis rates in Ts65Dn mice.	(Zhu *et al.,* 2019)
Huntington's disease (HD)	• Primary cortical/striatal neuronal cultures. • Striatal cell line derived from HD knock-in mice	• Caused by expanded polyglutamine repeat in the huntingtin (Htt) protein. • Protein synthesis recovery after cellular stress is impaired and increases vulnerability to neuronal death.	• Restored protein synthesis upregulation during post-stress recovery in HD cells.	(Xu *et al.,* 2021)
Traumatic brain injury (TBI)	• Mice with focal contusion injury in the hippocampus	• Increased eIF2α-P levels persisting up to 4 weeks post-TBI. • Spatial learning and memory severely impaired.	• Single dose of ISRIB reversed long-term TBI-induced cognitive deficits.	(Chou *et al.,* 2017)
Amyotrophic Lateral Sclerosis (ALS)	• G93A SOD1 (ALS mutant)-expressing primary cortical neurons	• Increased neuronal cell death linked to upregulated ISR and UPR markers.	• Improved the survival of ALS-SOD1-expressing neurons. • Attenuated PERK-mediated inhibition of translation.	(Bugallo *et al.,* 2020)
MEHMO syndrome	• MEHMO-mutant iPSC	• X-linked intellectual disability associated to mutations in eIF2γ; • Chronic activation of the ISR, shorten neurites and less dendrite projections.	• Rescued the cell growth, translation, and neuronal differentiation defects associated with the *EIF2S3* mutation	(Young-Baird *et al.,* 2020)
Leukoencephalopathy with Vanishing White Matter disease (VWMD)	• VWMD transgenic mice	• see section 1.5.1.	• see section 1.5.1.	(Abbink *et al.,* 2019; Wong *et al.,* 2018)
Breast cancer	• 2D and 3D cultures of T47D, MCF7, and MDA-MB-231 cells	• Hypoxia-induced stem-cell-like phenotypes that encourages tumorigenesis and is resistant to chemotherapy drugs.	• Prevents expression of stem-cell-like key transcripts that are regulated by the ISR. • Increased action of paclitaxel, a canonical chemotherapy	(Jewer *et al.,* 2020; Varone *et al.,* 2022)

Chronic Myeloid Leukaemia (CML)	• Mice models injected with peripheral blood mononuclear cells isolated from CML patients	• Exaggerated activation of PERK-eIF2α axis of the ISR promotes oncogenic JAK/STAT5 signalling.	• ISRIB combined with imatinib increases sensitivity to imatinib. • Decreased leukaemia tumour engraftment.	(Dudka *et al.,* 2022)
Lung Fibrosis	• *SFTPC*-Muc5b transgenic mice.	• Muc5b overexpression is the strongest risk factor for idiopathic pulmonary fibrosis. • Muc5b enhances ER stress markers in lung epithelial cells upon exposure to damaging substances.	• Single injection of ISRIB diminished *Atf4* translation in Muc5b-overexpressing mice; • Accelerated epithelial repair	(Dobrinskikh *et al.,* 2023; Watanabe *et al.,* 2021)
Pancreatic ductal adenocarcinoma	• PANC-1 cells	• Upregulation of ISR-driven antiapoptotic signalling which provides chemoresistance.	• Improved chemosensitivity to gemcitabine.	Palam *et al.,* 2015)

1.5. Translation dysregulation and disease.

Translation is intrinsically dysregulated in a variety of human diseases which include, amongst the most reported ones, cancer (Bhat *et al.,* 2015), viral infection (Stern-Ginossar *et al.,* 2019), immunodeficiency (Piccirillo *et al.,* 2014), 2014), metabolic disorders (Morita *et al.,* 2013), and neurological disorders (Buffington *et al.,* 2014). The aetiology of these diseases is assigned into three groups of disease-causing mutations (Scheper *et al.,* 2007; Tahmasebi *et al.,* 2018). (1) Mutations that alter the structure of specific mRNAs which impairs its processing and expression of the encoded proteins; (2) mutations in translation factors hence affecting global mRNA translation and the steps that regulate them; and (3) mutations in components of the translation machinery such as ribosomal proteins, tRNAs and amino-acyl-tRNA synthetases.

Given the essential role of translation and its control in all cell types, there is a surprising pattern of tissue-specificity of the diseases associated with deficiencies in protein synthesis. Tissues such as the brain and pancreas are more reliant on a tight regulation of its proteome and by proxy more vulnerable to defects in the translation machinery (Scheper *et al.,* 2007; Tahmasebi *et al.,* 2018).

Mutations in *EIF2S3*, encoding the γ subunit of eIF2 (eIF2γ), are linked to Mental retardation, Epileptic seizures, Hypogenitalism, Microcephaly, Obesity (MEHMO) Syndrome, a rare X-linked intellectual disability (Skopkova *et al.,* 2017). MEHMO mutations impair eIF2 function by compromising the integrity of eIF2 heterotrimeric complex and ability to form TCs (Borck *et al.,* 2012, Young-Baird *et al.,* 2019; Young-Baird *et al.,* 2020). Consistent with lowered eIF2 function, MEHMO mutations constitutively activate the ISR (Skopkova *et al.,* 2017). Like MEHMO, Leukoencephalopathy with Vanishing White Matter Disease (VWMD) is caused by mutations in any of the five subunits of eIF2B which is mostly linked to a hypersensitive ISR (Hanson *et al.,* 2022; Kantor *et al.,* 2005). In contrast to MEHMO, VWMD is a more localised disorder as it predominantly affects the white matter of the brain. VWMD and impact of eIF2B mutations are discussed in more depth in section 1.5.1.

However, insufficient activation of the ISR is also linked to similar pancreatic and neurological symptoms. Autosomal recessive mutations in the gene encoding eIF2α kinase PERK (*EIF2AK3*) cause Wolcott–Rallison Syndrome (WRS). WRS manifests mostly as early onset diabetes, although intellectual deficits and

microcephaly have also been reported in some cases (Delépine *et al.,* 2000; Scheper *et al.,* 2007; Zhang *et al.,* 2006). At the hub of WRS pathogenesis is a deficiency in insulin-secreting β-cells. WRS mutations either impair or fully abrogate PERK activity, which is selectively detrimental to these cells by not being able to fine-tune their easily overloaded ER which triggers excessive apoptotic signalling (Zhang *et al.,* 2002; Zhang *et al.,* 2006).

Apart from PERK mutations, other mutations that threaten ER homeostasis have been observed in syndromes with overlapping clinical features to WRS. Mutations in *PPP1R15B*, encoding the steady state eIF2α phosphatase CReP, cause multiple failures including diabetes, severe microcephaly, growth retardation, developmental delay, and intellectual disability (Abdulkarim *et al.,* 2015; Kernohan *et al.,* 2015). CReP has been recently shown to promote local translation at ER sites (Kastan *et al.,* 2020), although the impact of the reported mutational landscape in this novel function remains unknown. Moreover, mutations in genes encoding ER components have also been implicated in other disorders by preventing clearance of misfolded proteins. Mutations in *DNAJC3* (Ladiges *et al.,* 2005; Synofzik *et al.,* 2014), *SIL1* (Chung *et al.,* 2002; Senderek *et al.,* 2005) and *IER3IP1*(Abdel-Salam *et al.,* 2012; Arlt & Schäfer, 2011; Poulton *et al.,* 2011), which encode for ER chaperones and regulatory factors have been linked to pancreatic β-cell failure and neural tissue degeneration.

Homozygous and compound-heterozygous mutations in *EIF2AK4*, which encode eIF2α kinase GCN2, are associated with Pulmonary Veno-Occlusive Disease (PVOD). Histological studies show a consensus of obstructive changes in pulmonary veins due to capillary dilation and proliferation (Longchamp *et al.,* 2018; Montani *et al.,* 2017; Pietra *et al.,* 2004). Given the role of GCN2 in the ISR it remains remarkable why ISR-sensitive tissues (brain and pancreas) are unaffected by GCN2-PVOD mutations. However, mutations in GCN1, which activate GCN2, are observed in cases of intellectual disability (Hu *et al.,* 2019) suggesting non-canonical roles of GCN2 activity in CNS health.

Notably, these disease-causing mutations represent a fraction of the landscape of known disorders of translation malfunction (Tahmasebi *et al.,* 2018). Yet a clear overlapping of affected tissues and phenotypes exists despite the vast array of impaired functions in protein synthesis. A table which summarises the normal functions of key mutated genes, how they dysregulate translation and associated disorders is provided in **Table 1.3**.

Table 1.3. Dysregulation of translation in disease.

Gene/Protein	Function/mechanism	Disease phenotype	Disorder(s)	References
EIF2AK3/PERK	• Stress-responsive eIF2α kinase.	• Impaired or abolished PERK activity. • Exaggerated UPR activation and β-cell apoptosis.	Wolcott-Rallison syndrome (WRS).	(Delépine *et al.,* 2000; Scheper *et al.,* 2007; Zhang *et al.,* 2006)
EIF2AK4 (GCN2)	• Stress-responsive eIF2α kinase.	• Impairs proangiogenic function of the GCN2/ATF4 signalling pathway during amino acid starvation.	Pulmonary Veno-occlusive Disease (PVOD).	(Pietra *et al.,* 2004; Montani *et al.,* 2017; Longchamp *et al.,* 2018)
EIF2S3/eIF2γ	• GTP-binding subunit of the eIF2 complex. • Promotes ribosomal scanning and selection of the AUG start codon.	• Loss of eIF2 complex integrity. • Increased ATF4 mRNA levels. • Dysregulated rates of Met-tRNAi^{Met} formation.	MEHMO syndrome (X-linked intellectual disability).	(Skopkova *et al.,* 2017; Young-Baird *et al.,* 2020)
EIF2B1-5/ eIF2Bα-ε*	• Guanine nucleotide exchange factor of eIF2.	• Attenuation of translation. • Inappropriate ATF4-CHOP induction	Leukoencephalopathy with vanishing white matter (VWMD); permanent neonatal diabetes mellitus (PNDM).	(Hanson *et al.,* 2022)
PPP1R15B/ CReP	• eIF2α phosphatase: constitutively expressed PP1c-binding regulatory subunit that dephosphorylates eIF2α-P[S51]. • Promotes local translation initiation at the ER unregulable by cellular stress.	• Decreased affinity to PP1c and eIF2α dephosphorylation. • Increased β-cell apoptosis.	Severe microcephaly; intellectual disability; diabetes.	(Abdulkarim *et al.,* 2015; Kastan *et al.,* 2020; Kernohan *et al.,* 2015)
DNAJC3/p58^{IPK}	• ER chaperone that facilitates protein folding and protein homeostasis. • Component of the UPR-mediated negative feedback loop of PERK activity during recovery phase.	• Pancreatic β cell failure.	Diabetes mellitus; multisystemic neurodegeneration.	(Ladiges *et al.,* 2005; Synofzik *et al.,* 2014)
SIL1	• Nucleotide exchange factor (ATP-ADP exchange) for ER chaperone BiP.	• SIL1 loss-of-function mediated through aggregation of mutant SIL1. • Clinical features include cell type sensitivity: cerebellum and	Marinesco-Sjögren syndrome.	(Chung *et al.,* 2002; Senderek *et al.,* 2005)

		cerebellar Purkinje cells are more vulnerable to loss of SIL1 function.		
IER3IP1	• ER-stress induced protein that mediates cell differentiation. • Component of DNA damage and p53-mediated apoptosis pathway.	• Elevated apoptosis of the cerebral cortex and pancreatic β cells.	Microcephaly with simplified gyral pattern, epilepsy, and permanent neonatal diabetes syndrome (MEDS).	(Poulton *et al.,* 2011; Arlt and Schäfer, 2011; Abdel-Salam *et al.,* 2012)
GARS, KARS, AARS, YARS, HARS, MARS	• tRNA synthetases.	• Loss-of-function and mislocalisation to cytosolic granules.	Charcot-Marie-Tooth (CMT) disease; distal spinal muscular atrophy type V (dSMA-V).	(Antonellis *et al.,* 2003; Tahmasebi *et al.,* 2018)
RPS19	• Required for the maturation of 40S ribosomal subunits.	• p53 activation which promotes erythroid deficits	Diamond–Blackfan anaemia (DBA).	(Draptchinskaia *et al.,* 1999)

***** The author refers the reader to section 1.5.1. for a comprehensive review of eIF2B mutations and VWMD.

1.5.1. Leukoencephalopathy with Vanishing White Matter disease.

Mutations in any of the five subunits of eIF2B lead to the fatal neurological disorder Leukoencephalopathy with Vanishing White Matter Disease (VWMD) (Leegwater *et al.,* 2001; van der Knaap *et al.,* 2002). VWMD is amongst the most prevalent inherited leukodystrophies (white matter disorders), also referred to as childhood ataxia coupled with central nervous system hypomyelination (CACH) (Schiffmann *et al.,* 1994; van der Knaap *et al.,* 1999). VWMD is a progressive disorder where patients experience worsened neurological decline following episodes of acute physiological distress such as head trauma, acute fright, infections, and fever (Bugiani *et al.,* 2010; van der Knaap *et al.,* 2006; Vermeulen *et al.,* 2005). Given that eIF2B is at the hub of the ISR, most of the research has focused on eIF2B's function in the regulation of protein synthesis and ability to respond to cellular stress of brain tissue. Despite the well-known role of eIF2B in general translation (Hanson *et al.,* 2022; Pakos-Zebrucka *et al.,* 2016), the tissue specificity observed in VWMD remains poorly understood. Moreover, the genotype-phenotype correlation in VWMD is imperfect (Liu *et al.,* 2011; van der Lei *et al.,* 2010) which implies that eIF2B holds unknown functional features. There is no current cure for VWMD, and treatment is limited to symptomatic care (van der Knaap *et al.,* 2022).

1.5.1.1. Clinical diagnosis and neuropathology of VWMD.

A large-scale study partially decoded VWMD's clinical variability by inversely correlating age of onset to disease severity (Hamilton *et al.,* 2018). Congenital and early infantile forms often present extreme neurologic symptoms (severe encephalopathy, strong seizures) with short lifespan, whilst adult onset are mostly associated to behavioural and cognitive impairments with slow disease progression (Hamilton *et al.,* 2018; van der Knaap *et al.,* 2003). Although there are similar numbers of cases in males and females, females tend to develop milder pathology than males (van der Lei *et al.,* 2010), and some VWMD mutations can cause ovarian failure (Boltshauser *et al.,* 2002). Diagnosis of VWMD is currently limited to Mass Resonance Imaging (MRI) and then later confirmed through genotyping potential VWMD patients to determine the presence of eIF2B mutations. MRI findings show progressive white matter rarefaction lacking reactive glial scarring concomitant with cerebrospinal fluid

replacement and accumulation, leading to cystic degeneration and tissue cavitated lesions without any signs of improvement (Patay, 2005; Stellingwerff *et al.,* 2021; van der Knaap *et al.,* 1997; van der Knaap *et al.,* 1998). However, certain brain areas yielding lower myelin content show signs of mild repair over time (Stellingwerff *et al.,* 2022). Although the brain white matter is selectively vulnerable in VWMD, a recent report now shows that cortical structures (grey matter) are not spared from VWMD mutations (Man *et al.,* 2022) which failed to be originally identified in *post-mortem* VWMD tissues (Bugiani *et al.,* 2010; Bugiani *et al.,* 2018; Rodriguez *et al.,* 1999).

Immunohistochemical examinations indicate atypical myelin features ranging from thin/dispersed sheaths to complete myelin loss (Bruck *et al.,* 2001). Ultimately, myelin abnormalities lead to axonal atrophy and numeral density decrease at sites of relatively undamaged white matter, whereas complete loss of axons is appreciated in cavitated lesions (Fogli *et al.,* 2002; Klok *et al.,* 2018). However, the histopathologic hallmark features of VWMD are restricted to macroglial cells - astrocytes and oligodendrocytes. VWMD-affected oligodendroglial cells display an aberrant finely vacuolar-like cytoplasmic morphology, often referred in literature as "foamy" oligodendrocytes (Rodriguez *et al.,* 1999; Wong *et al.,* 2000; Bugiani *et al.,* 2018). Increased pro-apoptotic markers in oligodendrocytes of infants and young children with VWMD could explain the higher degree of oligodendrocytic loss (Francalanci *et al.,* 2001), whereas older patients with prolonged clinical course show a somewhat reverse-like phenotype of anti-apoptotic and pro-proliferative profile concomitant with increased oligodrondroglial density (Van Haren *et al.,* 2004; Wong *et al.,* 2000). Astrocytes in human VWMD are dysmorphic with large blunt processes alongside reduced efficiency of astrogliosis (Dooves *et al.,* 2016; Zhou *et al.,* 2019). Additionally, Bergmann glia - a subclass of astrocytes - show translocation to outer brain layers coupled with aberrant processes with distinctive cytoskeleton features (Dooves *et al.,* 2018).

1.5.1.2. Astrocyte-driven pathology of VWMD.

Initially, oligodendrocyte pathology was the focus of VWMD pathology due to the reduced myelination in VWMD patients. However, the current view has shifted towards deficiency in astrocytic maturation and function driving oligodendrocyte pathology and axonal abnormalities (Bugiani *et al.,* 2018; Dooves *et al.,* 2016). In the affected white matter areas, VWMD astrocytes show an untypical splicing of the intermediate filament GFAP isoform GFAPδ, which favours condensed filament networks associated with blunt cell processes (Huyghe *et al.,* 2012; Perng *et al.,* 2008). Unlike control brains, where GFAPα is predominantly expressed and induces astrocytic differentiation at stages of human cortex development, increased GFAPδ/GFAPα ratio were observed in VWMD suggesting arrested immaturity (Bugiani *et al.,* 2011; Huyghe *et al.,* 2012; Kamphuis *et al.,* 2012). Several approaches have consistently shown higher levels of astrocyte precursor cells, which results in pathological consequences prior to clinical disease onset (Bugiani *et al.,* 2018; Liu *et al.,* 2004). In fact, co-culture models of VWMD astrocytes and control oligodendrocyte progenitor cells (OPCs) have shown stalled oligodendroglia maturation into myelin-forming cells potentially linked to exaggerated secretion of glucosaminoglycan hyaluronan, a major component of the brain ECM profile, later confirmed in *post-mortem* VWMD tissues (Bugiani *et al.,* 2013; Dooves *et al.,* 2016). A recent secretomics profiling of VWMD astrocytes demonstrates impairment of classic OPC maturation markers (Deng *et al.,* 2023). Others have shown that stem cell-derived and iPSC-derived neurons and oligodendrocytes from VWMD patients grown normally in culture while astrocytes exhibit classic VWMD impairments (Dietrich *et al.,* 2005; Zhou *et al.,* 2019). Moreover, VWMD astrocytes promote axonal de-myelination and increased axon density while VWMD forebrain cells co-cultured with control astrocytes show no differences (Klok *et al.,* 2018). VWMD cortical astrocytes have been recently reported to show similar pathologic traits, albeit less severe, than VWMD white matter astrocytes (Man *et al.,* 2022) which implies the involvement of grey matter astrocytes in VWMD. Additionally, VWMD mutant OPCs also display mitochondrial dysfunction in a cell autonomous manner (Herrero *et al.,* 2019) thus also underlining an intrinsic role of oligodendrocytes in VWMD pathology. These previous findings indicate that astrocyte dysfunction is central in VWMD, which falls under the astrocytopathies (van der Knaap &

Bugiani, 2017), by primarily driving immature oligodendrocytes and ultimately disrupting axonal structures.

1.5.1.3. Genotype-phenotype correlation of VWMD.

VWMD is an autosomal recessive disorder caused by mutations in any of the genes *EIF2B1-5*, encoding the five subunits (α-ε) of eIF2B. Thus far, around 200 mutations have been identified predominantly missense mutations. Nonsense and frameshift mutations have also been reported albeit less common (Shimada *et al.,* 2015). VWMD is an extremely complex disease given that no clear relationship exists between the eIF2B mutational landscape and disease severity (Liu *et al.,* 2011; van der Knaap *et al.,* 1998). Biochemically, eIF2B mutations have been shown to (1) disrupt GEF activity of eIF2B, (2) destabilise complex integrity by affecting the core structure or binding of subunit interfaces, and (3) affect the binding of eIF2B to eIF2 (de Almeida *et al.,* 2013; Kashiwagi *et al.,* 2016; Li *et al.,* 2004; Slynko *et al.,* 2021). Intriguingly, mutations associated with some of the most ultra-severe cases have little to no impact on eIF2B function and stability (Liu *et al.,* 2011; Wortham & Proud, 2015) but may alternatively affect mRNA processing and expression of eIF2B subunits (Slynko et a., 2021), although the latter suggestions remain to be performed experimentally. This possibility is consistent with another study that identified truncated *EIF2B5* transcripts with divergent functions to full-length *EIF2B5* in VWMD zebrafish models (Keefe *et al.,* 2020). Adult-onset mutations have a milder decrease of GEF activity of eIF2B complexes (~20-40%) than mutations reported in childhood-onset VWMD cases (~30-80%) (Li *et al.,* 2004; Matsukawa *et al.,* 2011), potentially suggesting that robust decrease of eIF2B activity may be linked to earlier ages of VWMD onset.

1.5.1.4. Cellular pathogenesis of VWMD.

The ISR is chronically dysregulated in VWMD (Abbink *et al.,* 2019; van Kollenburg *et al.,* 2006). The basis of this dysregulation in VWMD is linked to hypersensitivity upon stress-induced activation. Under normal conditions, VWMD mutations that decrease eIF2B activity do not impact basal global translation which falls in line with the initial viability of VWMD patients. However, under acute stress treatments, *in vitro* models of VWMD have shown a stronger repression of translation coupled with exaggerated ISR activation compared to controls (Kantor *et al.,* 2005; Moon & Parker, 2018b; Sekine *et al.,* 2016; Wong *et al.,* 2018). VWMD patient-derived lymphoblasts showed increased levels of phosphorylated eIF2α persisting over a longer time span, which was linked to a delayed induction of the GADD34-mediate negative feedback to allow recovery (Moon & Parker, 2018b). In contrast, VWMD mice brains unexpectedly showed reduced levels of eIF2α-P, although an increased GADD34 signature is suggested to explain this feature (Abbink *et al.,* 2019; Wong *et al.,* 2019). GADD34 expression seems to be progressively enhanced as evidenced at three different time points of VWMD mice (2.5, 5 and 7 months) (Wong *et al.,* 2019). Despite these conflicting results, it suggests that VWMD cells can respond to acute stress episodes, eventually normalising eIF2α levels, but develop a gradually higher threshold of ISR-inducible GADD34. Therefore, all these data imply that VWMD features a pathological prolonged ISR that worsens upon stress, albeit through mechanisms still not fully known. In a clinical perspective it follows in agreement with disease progression, wherein stress-related episodes like febrile infections exacerbate neurological deterioration.

A prolonged ISR activation is expected to maintain lower levels of ternary complexes, hence favouring ATF4 expression (Harding *et al.,* 2000). In agreement, two *in vivo* studies have shown increased ATF4-regulated transcriptomes and proteomes specifically to astrocytes in mutant-harbouring mice (Abbink *et al.,* 2019; Wong *et al.,* 2019). Wong *et al.* dissected the differential enrichment of ISR targets between CNS cell types of mutant VWMD mice in comparison to control mice and identified that wild-type astrocyte clusters exclusively showed an enriched basal ISR signature, and VWMD mutant mice showed further exacerbation (Wong *et al.,* 2019). This provided the first *in vivo* evidence of the ISR hypersensitivity of VWMD (Moon & Parker, 2018b; Sekine *et*

al., 2016; Wong *et al.,* 2018). In contrast, VWMD neurons and myelinating oligodendrocytes clusters showed little differences in comparison to their control equivalents (Wong *et al.,* 2019). It is noteworthy that blocking the ISR entirely by introducing an eIF2α^{S51A} mutation (hence unable to phosphorylate eIF2α at serine 51) in VWMD mutant cells worsened VWMD pathology (Sekine *et al.,* 2016). This puzzling reliance on a faulty ISR remains poorly understood; however several papers provide strong evidence that downregulation of this crippled ISR (rather than a full blockage) by eIF2B activation via small molecules that stabilise the eIF2B holocomplex (ISRIB, 2Bact) ameliorates VWMD pathology (Tsai *et al.,* 2018; Zyryanova *et al.,* 2018; Wong *et al.,* 2018; Wong *et al.,* 2019; Abbink *et al.,* 2019; Schoof *et al.,* 2021; Zyryanova *et al.,* 2021) as discussed in section 4. These data centres the ISR activity as the main target for therapeutic intervention in VWMD pathophysiology.

However, additional cellular mechanisms beyond a dysregulated ISR are at play in VWMD (Wisse *et al.,* 2017). Defective mitochondrial activity is particularly detrimental to VWMD glial cells (Herrero *et al.,* 2021; Herrero *et al.,* 2019), despite evidence of the same abnormalities in VWMD primary fibroblasts (Gat-Viks *et al.,* 2015; Raini *et al.,* 2017) albeit not manifested in VWMD patients. eIF2B physically interacts with a wide scope of proteins involved in cellular transport, immune response, and differentiation (among others) (Hanson *et al.,* 2022) which may contribute to the complexity of VWMD. eIF2B mutations commonly affect functions of amino acids biosynthesis and transport of serine, glycine, and cysteine (Abbink *et al.,* 2019). These amino acids alongside glutamate are involved in glutathione synthesis, an antioxidant that carefully modulates the redox potential of the brain (Banerjee, 2012); wherein deregulated glutathione is prone to imbalance this state. Altered redox potential has been previously linked to myelin maturation impairment (Alameda *et al.,* 2018; Monin *et al.,* 2016). Strikingly, Foster *et al.* listed a set of proteins that are locally translated at presynaptic astrocytic processes which included components of the glycolysis metabolism such as ATP-dependent 6-phosphofructokinase (PFKM) and phosphoglycerate kinase 1 (PGK1) (Foster *et al.,* 2018). PFKM and PGK mediate intermediate steps of glucose conversion to pyruvate that overlap with the biosynthesis machinery of serine and cysteine (Li *et al.,* 2015). These reports highlight that VWMD mutations may affect local translation - which is pivotal to brain cells - and may contribute to the tissue specificity observed in VWMD.

1.5.1.5. eIF2B bodies and VWMD.

It has been shown that VWMD mutations can impact the integrity and functionality of eIF2B bodies in yeast model systems (Moon & Parker, 2018a; Norris *et al.,* 2021). Deletion of eIF2Bα causes complete loss of eIF2B bodies and different VWMD eIF2Bα mutations alter localisation and activity phenotypes of eIF2B bodies (Norris *et al.,* 2021), highlighting the likely involvement of localised pools of eIF2B in VWMD pathology. More importantly, eIF2B bodies are targeted for regulation during cellular stress in both yeast and mammalian models (Campbell *et al.,* 2005; Hodgson *et al.,* 2019; Taylor *et al.,* 2010). Exclusive to mammalian cells, different sub-populations of eIF2B bodies exist and are differently regulated in their subunit composition and rate of shuttling eIF2 upon activation of the acute ISR (Hodgson *et al.,* 2019), as described in section 3.4.2. Given the role of the ISR in VWMD (Abbink *et al.,* 2019), the impact of this tiered regulation of eIF2B localisation may contribute to the pathology of VWMD which remains to be addressed.

1.5.2. Other eIF2B-related disorders.

1.5.2.1. Permanent neonatal diabetes mellitus.

Heterozygous *de novo* missense mutations in the *EIF2B1* gene (eIF2Bα) have been reported in patients with permanent neonatal diabetes mellitus (PNDM), a disorder that causes early-onset diabetes (De Franco *et al.,* 2020). PNDM mutations predominantly affect the binding surface of eIF2α-P which may hinder eIF2B's regulation upon cellular stress (Pavitt *et al.,* 1997; Taylor *et al.,* 2014). Unlike VWMD, PNDM mutations are prevalent in the *N*-terminal of eIF2Bα while the former mostly occur at the *C*-terminal (De Franco *et al.,* 2020; Slynko *et al.,* 2021). eIF2B activity is fine-tuned via insulin-stimulated phosphorylation of eIF2Bε for pancreatic β-cell function (Gilligan *et al.,* 1996; McManus *et al.,* 2005; Welsh *et al.,* 1998). It is currently suggested that PNDM mutations may intrinsically disrupt pancreatic β-cell health due to inadequate regulation of eIF2B (Hanson *et al.,* 2022). Although PNDM patients do not exhibit severe neurological features, two reported cases displayed mild learning disability or attention deficit disorder (Alamri *et al.,* 2016) highlighting a link between cognition and eIF2B.

1.5.2.2. Cognitive decline.

eIF2B and the regulation of protein synthesis plays a key role in synaptic plasticity and cognitive function (Costa-Mattioli *et al.,* 2005; Huber *et al.,* 2000; Sutton & Schuman, 2006). Synaptic plasticity can be defined by the activity of synaptic connections which ultimately coordinates the basis of learning and memory storage. High activity strengthens synapses prompting long-term potentiation (LTP), while low activity weakens it resulting in long-term depression (LTD) (Neves *et al.,* 2008). Interestingly, the phosphorylation status of eIF2α, and therefore eIF2B activity, can dictate the fate of a given synapse either facilitating LTP or LTD. Synapses undergoing local reductions of eIF2α-P are predicted to be potentiated. Upon eIF2α-P, mRNA translation of ATF4 suppresses CREB, a major transcription factor of plasticity-relevant proteins (Jiang *et al.,* 2010; Kida, 2012). In support of this, mutant eIF2α heterozygous mice ($eIF2\alpha^{+/S51A}$) displayed improved LTP and long-term memory consolidation (Costa-Mattioli *et al.,* 2005). In contrast, LTD relies on increased levels of eIF2α-P. Prisco *et al.* elegantly reported that uORF-driven translation remodels expression of cell surface receptors at synapses required for mGluR-LTD (Di Prisco *et al.,* 2014). It is the current view that this modulation of the eIF2α phosphorylation status can be adjusted to support a given learning task. LTP-dependent paradigms, such as contextual fear conditioning, shifts synapses to repress eIF2α-P, while LTD learning programs, such as object-in-place learning, demands the regulated translation of transcripts containing uORFs (Costa-Mattioli *et al.,* 2007; Di Prisco *et al.,* 2014).

As the hub of adaptability to learning and long-term memory storage, eIF2α-P, and thus modulation of eIF2B activity, has been studied in detail for cognition improvement. ISRIB, the eIF2B GEF activity enhancer, has been shown to attenuate eIF2α-P-dependent translational control without changes to eIF2α phosphorylation status per se (Guthrie *et al.,* 2016; Rabouw *et al.,* 2019; Zhu *et al.,* 2019). Indeed, eIF2B activation strengthens synaptic plasticity and memory consolidation in healthy rodents (Sidrauski *et al.,* 2013). ISRIB also proved beneficial to counteract abnormally elevated levels of eIF2α-P and LTP-impairment in models of PD, DS and TBI (see Introduction section 1.4.2.) as well as alcohol addiction (Izumi & Zorumski, 2020) and drug abuse (Placzek *et al.,* 2016). However, less is known of the impact of eIF2B activity modulation on LTD

synapses which require eIF2α-P. Conflicting studies in AD models have shed some light on the involvement of eIF2B activation in LTD. Amyloid-β oligomer (AβO) accumulation is an age-related pathological hallmark of AD triggering ATF4-dependent neuronal cell death, resulting in progressive cognitive decline (Oliveira & Klann, 2021). ISRIB ameliorated AβO-induced cognitive deficiency in rodents, which the authors attribute to the loss of eIF2B content observed in *post-mortem* AD brain (Oliveira *et al.,* 2021). Surprisingly, two other studies failed to recapitulate the beneficial cognitive effects of eIF2B activation in AD mice models (Briggs *et al.,* 2017; Johnson & Kang, 2016). Although the authors suggest different administration regimens and absence of ISR markers as plausible reasoning for these unexpected results, AβO accumulation has been previously reported to selectively elevate LTD (Shankar *et al.,* 2008), favouring the eIF2α-P-dependent axis of synaptic plasticity. In support of this, eIF2B activation prevented proper object-placing learning of healthy rodents, which requires eIF2α-P-dependent translation (Di Prisco *et al.,* 2014). Accordingly, augmenting eIF2α-P corrected deficient LTD in dystonia mice models (Rittiner *et al.,* 2016). Therefore, tailoring eIF2B function depending on the level of dependence eIF2α-P could offer new avenues of therapeutic interventions.

Potential roles of eIF2B PTM modulation in cognition also warrants further investigation. A recent report has shown a novel role for eIF2B modulation during axonal wiring (Cagnetta *et al.,* 2019). Rapid protein synthesis in growing axons overloads the ER, alleviated by eIF2α-P which paradoxically prevents key bursts of global translation. Guidance-cue Sema3A signalling overcomes this constraint by transiently supressing GSK-3β-mediated phosphorylation of eIF2Bε (Ser535), enhancing eIF2B activity to rescue global translation over specific time courses (Cagnetta *et al.,* 2019). Additionally, lithium treatment in Down syndrome rodent models has been shown to inhibit GSK-3β activity (Bertsch *et al.,* 2011), and thereby increase eIF2B activity, and improve synaptic strength (Contestabile *et al.,* 2013).

1.5.2.3. Cancer.

Translation dysregulation is critical for cancer cell survival and proliferation (Bhat *et al.,* 2015). Cancer cells hijack the translation machinery to promote high levels of protein synthesis while being able to tolerate lethal stresses such as hypoxia and nutrient deprivation (Robichaud *et al.,* 2019). The role of the ISR has been extensively implicated in cancer however remains somewhat controversial. Induction of eIF2α-P has been shown to prevent tumorigenesis in some cancer types (Schewe & Aguirre-Ghiso, 2009) while being beneficial to the survival of others (Guo *et al.,* 2017). However, whether eIF2B has intrinsic roles in cancer growth is also not fully understood. Earlier studies suggested eIF2Bε may act as an oncogene. *EIF2B5* mRNA is upregulated in a range of different cancer types, but not the remaining eIF2B subunits (Balachandran & Barber, 2004). More strikingly, the same study reported that increased eIF2B activity caused the observed doubling of cell growth rate in cancer-transformed mouse embryonic fibroblasts. A follow-up study showed that knockdown of eIF2Bε expression ameliorated tumorigenesis in the same cell line (Gallagher *et al.,* 2008) showcasing the potential role of eIF2Bε in cancer.

1.6. Project rationale.

eIF2B plays a key role in regulating protein synthesis by being the main event of the ISR. Our group has previously shown that cellular eIF2B localisation is regulated during the ISR and may act as an additional regulatory mechanism of the ISR itself. Mutations in eIF2B leads to VWMD which is an incurable and complex disease with a poor correlation between eIF2B mutations, genotype impairment and disease severity. The paradoxical knowledge that eIF2B is an essential translation factor and VWMD is an ISR-driven neurological disorder mainly caused by astrocytic dysfunction implies the compelling idea that eIF2B has cell-specific functions. Hence, this thesis aims to address the following overall hypothesis:

eIF2B localisation and/or regulation during the ISR is cell-type specific.

This hypothesis was addressed via a detailed analysis of the following aims:

(1) Examine whether cell-specific patterns of eIF2B bodies exist between neuronal and glial cell lines.
(2) Investigate the regulation of eIF2B bodies during the acute and chronic stages of the ISR between cell types.
(3) Assess the impact of the ISR and ISR modulators in the cell-specific GEF activity of eIF2B bodies.

Chapter 2. Material and methods.

2.1. Cell culture.

2.1.1. List of reagents and materials.

Table 2.1. List of reagents and materials used in cell culture.

Reagents	Supplier	Catalog number	Other information
Minimum Essential Medium (MEM)	Gibco	11095-080	500mL
Heat-inactivated fetal bovine serum (FBS)	Gibco	10082-147	500mL
MEM non-essential amino acids (NEAA)	Gibco	11140-035	100x
Sodium pyruvate	Gibco	11360-070	100mM
L-Glutamine	Gibco	25030-081	200mM
Penicillin/streptomycin (P/S)	Gibco	15140-122	10000 U/mL
Dulbecco's modified Eagle's medium:F-12 (1:1) (DMEM:F-12)	Lonza	F151272	25mM HEPES; discontinued
Astrocyte Medium (AM)	ScienCell	1801	500mL
AM-FBS	ScienCell	0010	10mL
Astrocyte Growth Supplement (AGS)	ScienCell	1852	10mL
AM-P/S	ScienCell	0503	10mL
HyClone (Ham's Nutrient Mixture) F-12	Fisher Scientific	10235122	500mL
Trypsin-EDTA solution	Gibco	25300-062	0.05%
Trypan Blue solution	Gibco	15250-061	0.4%
Phosphate-buffered saline (PBS)	Gibco	14190-094	500mL
Dimethyl sulfoxide (DMSO)	VWR	BKC-17	50mL
ISRIB	Sigma-Aldrich	SML0843	5mg
Thapsigargin (Tg)	Sigma-Aldrich	T9033	1mg
Sodium arsenite (SA)	Sigma-Aldrich	S7400	100g
GSK2606414	Tocris	5107	50mg
Materials	**Supplier**	**Catalog number**	**Other information**
Countess™ Cell Counting Chamber Slides	Invitrogen	C10228	
MycoAlert™ Mycoplasma Detection Kit	Lonza	LT07-318	
Nalgene® Mr. Frosty	Thermo Scientific	5100-0001	H × diam. 86 mm × 117 mm

2.1.2. Cell lines and maintenance.

Human Glioblastoma Astrocytoma (U373) cell line (purchased from ATCC, #08061901) were cultured in MEM supplemented with 10% (v/v) FBS, 1% (v/v) NEAA, 1% (v/v) sodium pyruvate, 1% (v/v) L-glutamine and 1% (v/v) penicillin/streptomycin (P/S). Human neuroblastoma (SH-SY5Y) cell line (purchased from ATCC, CRL-2266) were cultured in DMEM:F-12 supplemented with 10% (v/v) FBS, 1% (v/v) L-glutamine and 1% (v/v) P/S. Human Glial Oligodendrocytic Hybrid Cell Line (MO3.13) cell line (kindly gifted by Prof Nicola Woodroofe, originally derived from Cedarlane #CLU301) were cultured in DMEM supplemented with 10% (v/v) FBS, 1% (v/v) L-glutamine and 1% (v/v) P/S. Human primary astrocytes (HA) were cultured in AM supplemented with 2% (v/v) AM-FBS, 1% (v/v) AGS and 1% (v/v) AM-P/S. All previous cell lines were validated with antibodies against lineage-specific markers. Wild-type CHO-C30 cells and CHO-C30 cells harbouring the L180F mutation within the *EIF2B4* gene (Sekine *et al.,* 2015) were a kind gift from Professor David Ron (Cambridge Institute for Medical Research) and cultured in F-12 Ham supplemented with 10% (v/v) FBS, 1% (v/v) L-glutamine and 1% (v/v) P/S. All cell lines were maintained at 37°C under 5% CO_2 and were routinely tested by the technical team for contamination with MycoAlert™ Mycoplasma Detection Kit (Lonza, #LT07-318).

2.1.3. Cell passage.

Cells were all grown in T75 or T175 flasks and sub-cultured when 70%-80% confluent. All cell lines were sub-cultured no further than passage 25. After discarding the media, cells were washed once with PBS. The flasks were then incubated with 2 mL of trypsin-EDTA at 37ºC for a maximum of 5 min. To de-activate trypsin, the cells were resuspended in 9 mL of growing media and the suspensions were transferred into 50 mL tubes. The cells were then spun at 1000 rpm for 5 min. After spinning the supernatant was discarded and the pelleted cells were re-suspended in fresh media. The cells were counted by resuspending 10 µL of the suspension with 10 µL of Trypan Blue and loaded into a CountesS™ Cell Counting Chamber. The cell suspension was then aliquoted into T75 or T175 flasks containing fresh complete medium, depending on the split ratio intended. SH-SY5Y and U373 were normally split in a ratio between 1:3-1:6; while MO3.13, primary astrocytes and CHO cells were usually split between 1:8-1:10.

2.1.4. Thawing and freezing vials.

Cell vials stored in liquid nitrogen were thawed in water bath at 37 ºC until defrostED (usually ~2-3 minutes). The suspended cells were then pipetted into T75 flasks containing 15 mL of the corresponding growth medium. Media was discarded the following day and replaced with fresh media to remove traces of DMSO. To freeze cells, after trypsinisation and spinning, the pelleted cells were resuspended in FBS containing 10% DMSO. The tubes were maintained for 24h in a Mr. Frosty™ Freezing Container (Thermo Fischer Scientific) at -80ºC and moved to liquid nitrogen the following day for long-term storage or maintained at -80ºC for short-term usage.

2.1.5. Cell treatments.

For acute/transient induction of the ISR, cells were treated with 1µM Tg (stock solution: 1 mg/mL diluted in DMSO stored at -20°C) for 1h at 37°C; 125 µM or 500 µM SA (stock solution: 50mM diluted in ddH_2O stored at 4°C) for 30 minutes at 37°C.

For chronic induction of the ISR, cells were treated with 300nM Tg for 24h at 37°C. For acute/transient cellular stress previously challenged with a chronic induction of the ISR, cells were treated with 300nM Tg for 24h at 37°C where 1µM Tg or 125µM SA were added in the last 60 and 30 minutes at 37°C, respectively. For ISRIB treatment, 200nM ISRIB was added to cells for either 1h or 24h at 37°C. For PERK inhibition treatment, cells were treated with 500nM GSK2606414 for 1h at 37°C.

As control, cells were treated with vehicle solution (DMSO) with the highest volume and treatment duration at 37°C depending on its respective drug experimental setup.

2.2. DNA plasmids.

2.2.1. List of reagents, plasmids, and materials.

Table 2.2. List of reagents, DNA plasmids and materials used.

Reagents	Supplier	Catalog number	Other information
LB broth	Sigma-Aldrich	L3022	1kg
LB agar	Sigma-Aldrich	L2897	1kg
Carbenicillin disodium salt	Merck	C1389	250mg
Glycerol	Fischer Scientific	G/0600/17	2.5L
JM109 Competent Cells	Promega	L2005	*Escherichia coli* (*E. coli*)
G-418 solution	Merck	G418-RO	50mg/mL
Branched 25-kDa polyethylenimine (PEI)	Sigma-Aldrich	408727	100mL
Plasmids	**Supplier**	**Catalog number**	**Other information**
EIF2B5 (pCMV6-AC-tGFP)	Origene	RG202322	10µg
EIF2S1 (pCMV6-AC-tGFP)	Origene	RG200368	10µg
pCMV6-AC-mGFP	Origene	PS100040	10µg
pCMV6-AC-RFP	Origene	PS100034	10µg
Materials	**Supplier**	**Catalog number**	**Other information**
GeneJET™ plasmid Miniprep kit	Thermo Scientific	K0503	
NanoDrop 1000 spectrophotometer	Thermo Scientific	ND-1000	
Lipofectamine™ 3000 kit	Invitrogen	L3000001	

2.2.2. Plasmid preparation.

On arrival, all plasmids were centrifuged at 5000 *g* for 5min, added with 100ul of sterile water to dissolve the DNA (final concentration of 0.1µg/µL) and incubated for 10 minutes at RT. Plasmid solutions were briefly vortexed followed by quick spin (<5000 *g*) and stored at -20˚C.

2.2.3. Constructs.

pCMV6-AC-tGFP plasmid vector encoding *EIF2B5* (eIF2Bε) and pCMV6-AC-tGFP plasmid vector encoding *EIF2S1* (eIF2α) were purchased from Origene (Rockville, Maryland, USA). The coding ORF of *EIF2B5* from the pCMV6-AC-tGFP vector was sub-cloned into a pCMV6-AC-mGFP and pCMV6-AC-RFP vector (performed by Dr Rachel Hodgson, SHU). The constructs were verified by sequencing.

2.2.4. Bacterial transformation.

50µL of JM109 competent cells were mixed with 0.1µg of DNA plasmid and incubated on ice for 60 minutes. A 42°C heat-shock for 90s was performed, followed by immediate incubation on ice for 2 minutes. Resuspended bacteria:plasmid mixture was plated out on LB agar plates with carbenicillin (50 µg/mL) and incubated overnight at 37°C. Single colonies were selected and cultured in LB broth with 50 µg/mL carbenicillin, followed by overnight incubation at 37°C.

The previous solutions were made as follows:

(1) *Carbenicillin (1mg/mL stock solution)*: 10mg of carbenicillin disodium salt (Thermo Fischer Scientific) were dissolved in 10mL ddH_2O.The solution was aliquoted and stored at 4ºC.

(2) *LB-agar:* 17.5g of LB agar were dissolved in 500 mL ddH_2O. The solution was autoclaved and kept at RT.

(3) *Carbenicillin agar plates:* LB-agar was melted in the microwave. The solution was left to cool down for about 30 min at RT. Next, carbenicillin stock solution was added to a final concentration of 50µg/mL. The agar+carbenicillin was then poured into 10cm^3 dishes and left to solidify at RT. The plates were stored at 4ºC.

2.2.5. Glycerol stocks.

For long-term storage, 500 µL of an overnight liquid bacterial culture was mixed with 500 µL of 50% glycerol (v/v), gently mixed, transferred to cryovials and stored at -80ºC.

2.2.6. DNA purification.

The glycerol stock was used to inoculate into 10mL of LB broth containing 50 µg/mL carbenicillin and grown overnight at 37ºC with constant shaking (no more than 250 rpm). To make up LB broth solution, 10g of LB broth powder was dissolved in 500mL ddH2O. The solution was autoclaved and kept at RT. After 16-18h, cultures were centrifuged at 8000 rpm at RT for 2min and the DNA plasmid was isolated using a GeneJET plasmid Miniprep kit (Fisher Scientific, Loughborough, UK) according to the manufacturer's instructions. Plasmid DNA was eluted in 50µL elution buffer and quantified using a NanoDrop 1000 spectrophotometer (ND-1000) (Thermo Fischer Scientific).

2.2.7. Transient transfection procedures.

U373, SH-SY5Y and MO3.13 cells were seeded at a density of $3x10^5$, $5x10^5$ and $2.5x10^5$ cells/well, respectively, in a 6-well plate and incubated at 37ºC for at least 24h before transfection to ensure sub-culturing recovery and optimal physiological condition for transfection. Preparation of transfection complexes were performed in appropriate medium without serum for each cell line as indicated below.

2.2.7.1. PEI transfection.

Transient transfection for U373 cells was performed with transfection reagent 25-kDa polyethylenimine, branched (PEI) (Sigma-Aldrich, #408727). Transient transfection was obtained by using PEI (stock: 1mg/mL, sterile-filtered) at a molar concentration of 4:1 [PEI(µg) : DNA(µg)]. For each well of a 6-well plate, 4µg PEI and 1µg plasmid DNA was diluted in 100µL of FBS-free and P/S-free MEM and incubated at RT for 10 minutes. 600µL of FBS-containing and P/S-free MEM was added to the transfection mixture, and full 700µL mixture was transferred to cover cells and incubated for 2h at 37°C. 2mL of P/S-free MEM was added after 2h and incubated overnight at 37°C. Cell culture media was fully changed to complete MEM and incubated for 24-48h at 37°C prior to confocal imaging.

2.2.7.2. Lipofectamine 3000 transfection.

Transient transfection for SH-SY5Y and MO3.13 was performed with Lipofectamine-3000 following manufacturer's instructions. Briefly, transfection complexes were prepared in appropriate FBS-free medium of each cell line (DMEM:F12 for SH-SY5Y cell line and DMEM for MO3.13 cell line) at a molar ratio of 1.5:1:2 (Lipofectamine [µL] : DNA [µg] : P3000 [µL]) and incubated at RT for 15 minutes. The transfection complex was added to cells, and they were then incubated for 24-48h at 37°C.

2.2.7.3. Stable transfection.

To prepare stable cell lines the transient transfection protocol was initially followed. U373 cells were transfected with 1µg of DNA plasmid and incubated for 48 hours at 37°C. Prior to beginning the stable cell line a kill curve assay was performed to assess minimal selective antibiotic concentration for total cell death after 10 days of incubation at 37°C for untransfected cells. Once the kill curve was completed and the appropriate concentration of G-418 (stock: 50mg/mL) (Roche) was identified (600µg/mL) this was added to the media after 48 hours of transfection and changed every 2 days for 10 days of incubation at 37°C to promote the formation of stable cell lines.

Drug-resistant colonies were trypsinized and centrifuged at 1000 *g* for 5 minutes, and the resulting pellet was resuspended in G-418-containing media and expanded in T75 to generate a polyclonal cell line.

2.3. Immunoblotting.

2.3.1. List of reagents and materials.

Table 2.3. List of reagents and materials used in immunoblotting.

Reagents	Supplier	Catalog number	Other information
Phosphate-buffered saline (PBS)	Gibco	14190-094	500mL
CelLytic M	Sigma-Aldrich	C2978	250mL
Sodium fluoride (NaF)	Sigma-Aldrich	201154	5g
Phenylmethylsulfonyl fluoride (PMSF)	Sigma-Aldrich	P7626	1g
β-Glycerophosphate disodium salt hydrate	Sigma-Aldrich	G9422	50g
Phosphatase inhibitor cocktail 2	Sigma-Aldrich	P5726	1mL
Phosphatase inhibitor cocktail 3	Sigma-Aldrich	P0044	1mL
Protease inhibitor cocktail	Sigma-Aldrich	P8340	1mL
4x Laemmli sample buffer	BioRad	1610747	10mL
2-mercaptoethanol	VWR	BC98	100mL
Chameleon® Duo Pre-stained Protein Ladder	LiCor	928-60000	500µL
Revert™ Total Protein Stain	LiCor	926-11011	100mL
Marvel Original Dried Skimmed Milk	Tesco	n/a	n/a
Bovine serum albumin (BSA)	Merck	A7906	100g
Tris	Fisher Scientific	T/3710/60	1kg
Tween-20	Sigma-Aldrich	P1379	500mL
Sodium dodecyl sulfate (SDS)	VWR	L5750	500g
Ammonium persulphate (APS)	Sigma-Aldrich	A3678	100g
N,N,N′,N′-Tetramethyl ethylenediamine (TEMED)	Sigma-Aldrich	T9281	25mL
Puromycin dihydrochloride	Gibco	A1113803	10x1mL
Cycloheximide	Sigma-Aldrich	203350	25mg
Antibodies	**Supplier**	**Catalog number**	**Dilution factor**
Rabbit anti-eIF2Bα	Proteintech	18010-1-AP	1:500
Rabbit anti-eIF2Bβ	Proteintech	11034-1-AP	1:500
Mouse anti-eIF2Bγ	Santa Cruz	sc-137248	1:500
Rabbit anti-eIF2Bδ	Proteintech	11332-1-AP	1:500
Rabbit anti-eIF2Bε	Abcam	ab32713	1:500
Mouse anti-eIF2α	Abcam	ab5369	1:500
Rabbit anti-phosho-eIF2α[ser51] [E90]	Abcam	ab32157	1:500
Rabbit anti-PERK	Proteintech	20582-1-AP	1:1000
Rabbit anti-GADD34	Proteintech	10449-1-AP	1:500
Rabbit anti-CHOP	Proteintech	15204-1-AP	1:1000
Rabbit anti-ATF4	Abcam	ab184909	1:750
Rabbit anti-GAPDH	Cell Signalling	#2118	1:5000
Mouse anti-puromycin (clone 12D10)	Merck	MABE343	1:500
Goat anti-rabbit IRDye 680RD	LiCor	925-68071	1:10000
Goat anti-mouse IRDye 800CW	LiCor	925-32210	1:10000
Materials	**Supplier**	**Catalog number**	**Other information**
Qubit™ Protein Assay kit	Invitrogen	Q33212	
4-20% Precast Gels Mini-PROTEAN® TGX™	BioRad	4561096	
MiniPROTEAN® Handcast System	BioRad	1658000FC	
Trans-Blot® Turbo™ RTA Mini 0.2 µm Nitrocellulose Transfer Kit	BioRad	1704270	
Trans-Blot® Turbo™ Transfer System	BioRad	1704150	
Odyssey Scanner	LiCor	Model 9120	

2.3.2. Protein extraction.

In order to prepare protein extracts, media was discarded, and cells were washed once in PBS. Cells were lysed in CelLytic M freshly supplemented for each use with 10mM NaF, 1mM PMSF, 17.5mM β-glycerophosphatase, 1% (v/v) phosphatase inhibitor cocktail 2, 1% (v/v) phosphatase inhibitor cocktail 3 and 1% (v/v) protease inhibitor cocktail; for 30 min in ice with regular agitation. Cell lysates were centrifuged at 12,000 *g* for 10 min at 4°C and tested for protein quantification. Lysates were stored at – 80°C if needed.

2.3.3. Protein quantification.

Protein extracts were quantified using the Qubit™ Fluorometric Quantification assay. Qubit™ Working solution buffer was made up by diluting the Qubit™ Reagent in Qubit™ Buffer at a ratio of 1:200 (Reagent:Buffer). 200µL of Working solution was prepared for each sample and standard. 10µL of each of the three Qubit™ Standards was diluted in 190µL of Qubit™ Working solution in Qubit™ Assay Tubes for 15 min at RT. 1µL of each extract sample was diluted in 199µL of Qubit™ Working solution in Qubit™ Assay Tubes for 15 min at RT. The fluorescence intensity of the standards was firstly determined to calibrate the Qubit™ Fluorometer (automatic standard curve) followed by the readings of each sample (units = µg/mL).

2.3.4. Western blot analysis.

Samples were boiled in 4x Laemmli sample buffer (supplemented with fresh 10% (v/v) 2-mercaptoethanol) at 100°C for 5 minutes. 15-30µg of whole-protein lysate were loaded on a 5% stacking gel and resolved on either 10% or 7.5% polyacrylamide gels (**Table 2.1**). Alternatively, 4-20% Precast Gels were also used. Gel electrophoresis was performed on the MiniPROTEAN® Handcast System in 1x running buffer (25 mM Tris pH 8.3, 250 mM glycine, 0.1% w/v SDS) at 120 V for ~60-75 minutes. 1-2 µL of Chameleon® Duo Pre-stained Protein Ladder was used as a molecular weight marker. Polyacrylamide gels were semi-dried transferred onto nitrocellulose membrane using Trans-Blot Turbo Transfer System at 1.3A and 15V for 30 minutes, following manufacturer's instructions. When necessary, membranes were subjected to Revert™ Total Protein Stain for normalization, imaged and washed out following manufacturer's instructions. Membranes were blocked in Tris-buffered saline (TBS) supplemented with 5%

(w/v) milk or 5% (w/v) BSA for 1h at RT or overnight at 4°C. Blocked membranes were probed with primary antibodies diluted in TBS supplemented with 0.1 % (v/v) Tween-20 (TBST) and 5% (w/v) milk or 5% (w/v) BSA, overnight at 4°C. Membranes were then washed 3 times for 5 min/each in TBST, followed by probing with secondary antibodies diluted in 5% milk or 5% BSA in TBST for 1h at RT and washed 3 times for 5 min/each in TBST. Membranes were visualised and quantified on a LiCor Odyssey Scanner with Image Studio Lite software.

Table 2.4. List of reagents/solutions and respective quantities to hand cast SDS-PAGE gels used in this study.

	10% resolving gel (Bottom)	7.5% resolving gel (Bottom)	5% stacking gel (Top)
ddH_2O	4.0 mL	4.85 mL	2.7 mL
30% Acrylamide/bis-acrylamide	3.3 mL	2.5 mL	670 µL
1 M Tris base pH 6.8			500 µL
1.5 M Tris base pH 8.8	2.5 mL	2.5 mL	
10% SDS	100 µL	50 µL	40 µL
10% APS	100 µL	100 µL	40 µL
TEMED	4 µL	15 µL	4 µL

2.3.5. Puromycin incorporation assay.

For puromycin integration, 2.5µL of puromycin dihydrochloride solution was added per 1mL of medium (final concentration: 91µM) to cells incubated at 37°C for 5min and immediately harvested. Cells were washed twice with ice-cold PBS supplemented with 355µM cycloheximide, lysed and immunoblotted as described previously in sections 6.3.4. Primary puromycin-specific antibody was used to detect puromycinylated proteins. GAPDH immunoblotting was used as a loading control.

2.4. Immunocytochemistry.

2.4.1. List of reagents and materials.

Table 2.5. List of reagents and materials used in immunocytochemistry.

Reagents	Supplier	Catalog number	Other information
Industrial Methylated Spirit (IMS)	Fisher Scientific	M/4470/17	2.5L
Methanol	Fisher Scientific	M/3950/17	2.5L
4% Paraformaldehyde in PBS (PFA)	Alfa Aesar	J61899	250mL
Phosphate-buffered saline (PBS)	Gibco	14190-094	500mL
Tween-20	Sigma-Aldrich	P1379	500mL
Triton X-100	BDH Laboratories	306324N	500mL
Bovine serum albumin (BSA)	Merck	A7906	100g
ProLong™ Gold Antifade Mountant with DAPI	Invitrogen	P36935	5x2mL
Antibodies	**Supplier**	**Catalog number**	**Dilution factor**
Rabbit anti-eIF2Bα	Proteintech	18010-1-AP	1:25
Rabbit anti-eIF2Bβ	Proteintech	11034-1-AP	1:25
Mouse anti-eIF2Bγ	Santa Cruz	sc-137248	1:50
Mouse anti-eIF2Bδ	Santa Cruz	sc-271332	1:50
Goat anti-Rabbit AlexaFluor-594®	Invitrogen	A-11012	1:500
Goat anti-Mouse AlexaFluor-594®	Invitrogen	A-11032	1:500
Materials	**Supplier**	**Catalog number**	**Other information**
Academy squared glass coverslips	Smith Scientific	NPS13/2222	22x22mm

2.4.2. Immunofluorescence assay.

Squared glass coverslips were rinsed with 70% IMS, added to 6-well plates and left to completely dry out. Cells were seeded and transfected as described previously (section 6.2.7.). U373 and SH-SY5Y cell lines were fixed in ice-cold 100% methanol at -20°C for 15 min. MO3.13 cell line was fixed in 4% (w/v) paraformaldehyde (PFA) in PBS at RT for 20 min. For methanol fixation, cells were washed with PBS supplemented with 0.05% (v/v) Tween-20 (PBST) for 3 times for 3 minutes, then blocked in 1% (w/v) BSA diluted in PBST for 1h at RT or overnight at 4°C, under gentle shaker. For PFA fixation, cells were washed 3 times with PBST for 3 minutes, permeabilized with 0.1% (v/v) Triton X-100 diluted in PBS for 5 minutes at RT, washed 3 times with PBST for 3 minutes, and then blocked in 1 % (w/v) BSA in PBST for 1h at RT or overnight at 4°C, under gentle shaker. Cells were probed with primary antibodies diluted in 1 % (w/v) BSA in PBST, overnight at 4°C under gentle shaker. Cells were then washed 3 times with PBST for 5 minutes, followed by probing with the appropriate host species AlexaFluor-594® conjugated secondary antibody diluted in 1% (w/v) BSA in PBS, for 60 minutes at RT. Following secondary antibody incubation, cells were washed with PBST, three times for 5 minutes, and mounted with ProLong™ Gold Antifade Mountant with DAPI and left to dry out for 24 hours at RT. Cells were visualised on a Zeiss LSM 800 confocal microscope.

2.5. Confocal imaging and analysis.

Imaging was performed using a Zeiss LSM 800 confocal microscope combined with Zeiss ZEN 2.3 (blue edition) software for data processing and analysis. 63x or 40x plan-apochromat oil objectives and a 488 nm diode laser with maximum output of 1.0 % laser transmission were used for excitatory imaging at 488 nm. Additionally, a 561 nm laser with maximum output of 5.0% laser transmission was used for excitatory imaging at 594 nm. A 63x plan-apochromat oil objective, diode lasers with maximum output of at 0.2 % laser transmission and a maximal 0.8x zoom input was used for Airyscan imaging. Image acquisition was performed by maximum intensity orthogonal projection of a Z-stack of automatically calculated increments for complete single cell imaging and 3D projection. Live cell imaging was performed by pre-heating the incubation chamber to 37°C and regulate CO_2 levels of stage area sealed box to 5%.

2.5.1. Fluorescence recovery after photobleaching (FRAP) analysis.

FRAP analysis was performed to quantify the shuttling rate of eIF2 through eIF2B bodies as in the methodology described for mammalian cells by (Hodgson *et al.,* 2019). FRAP experiments were carried out by live cell imaging on the LSM 800 confocal microscope. Specific areas containing cytoplasmic eIF2α-mGFP foci were targeted for bleaching using 23 iterations at 100 % laser transmission (488 nm diode laser). Pre-bleaching image and intensity of targeted foci (ROI – region of interest) was captured followed by 44 images captured every 151ms for a total of 7.088s. In-cell fluorescence intensity was captured to normalise against ROI. Out-of-cell fluorescence, or background intensity (B), was measured and subtracted from ROI and T values to provide corrected measurements. Normalised data was fitted to a one-phase association curve using GraphPad Prism to quantify rate of recovery and half-time of recovery. The relative percentage of eIF2 recovery was determined as the plateau of the normalised FRAP curve.

2.5.2. Analysis of eIF2B bodies.

eIF2B body analysis was carried out using Zeiss ZEN 2.3 (blue edition) software. eIF2B bodies were categorised by size and sub-divided to small bodies (<1μm^2) and large bodies (≥1μm^2). Single-cell images were captured and processed for automatic detection of 488nm fluorescence foci (eIF2B bodies) prior manual setup of intensity threshold to include all eIF2B bodies on a cell-by-cell basis. A singular threshold setup for all images was not possible due to fluctuations of fluorescence between different captured cells. mGFP-positive cells were counted blindly until desired number was reached and details on total counted bodies and independent biological replicates is provided in **Table 2.6**. Risk of cell counting bias was reduced by applying the same counting direction pattern throughout all imaging experiments (**Figure 2.1.**).

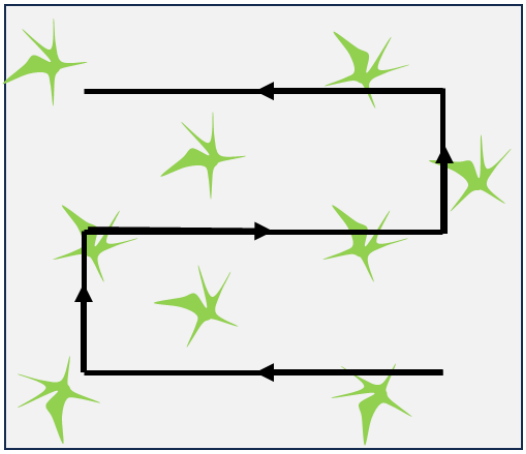

Figure 2.1. Schematic of the cell counting direction.

Table 2.6. Descriptive statistics of cell counting. Additional information on total number of GFP-positive cells analysed per experiment (and respective Figure numbering), number of technical replicates and number of independent biological repeats (*N*). *ICC*, immunocytochemistry.

ICC			
Experiment (Figure)	Cells counted	Technical replicates	*N*
3.2.	100	1	4
3.3.	50	1	3
3.4.	50	1	3
3.5.	30	1	3
3.7.	50	1	1
4.7.	30	1	3
4.8.	30	1	3
4.9.	30	1	3
4.10.	30	1	3
5.1.	30	1	3

2.5.3. Relative percentage of eIF2B body sub-populations.

The relative percentage of each size category of eIF2B bodies was performed with the average of each biological repeat: the number of small bodies and large bodies was divided by the total number of bodies per cell and converted into percentages (% small bodies = [number of bodies with area <1μ^2/total number of bodies] x 100; (% large bodies = [number of bodies with area ≥1μ^2/total number of bodies] x 100).

2.5.4. Manual analysis of co-localisation.

Co-localisation was performed by eye and assessed on a body-by-body basis of all detected eIF2B bodies per cell. A positive co-localisation was observed when a secondary antibody (Alexa-Fluor-594®) signal full overlapped with a GFP-tagged eIF2Bε foci (**Figure 2.2. A**). In contrast, co-localisation was classified as negative upon partial or no overlapping of secondary antibody signal with eIF2Bε-mGFP (**Figure 2.2. B**).

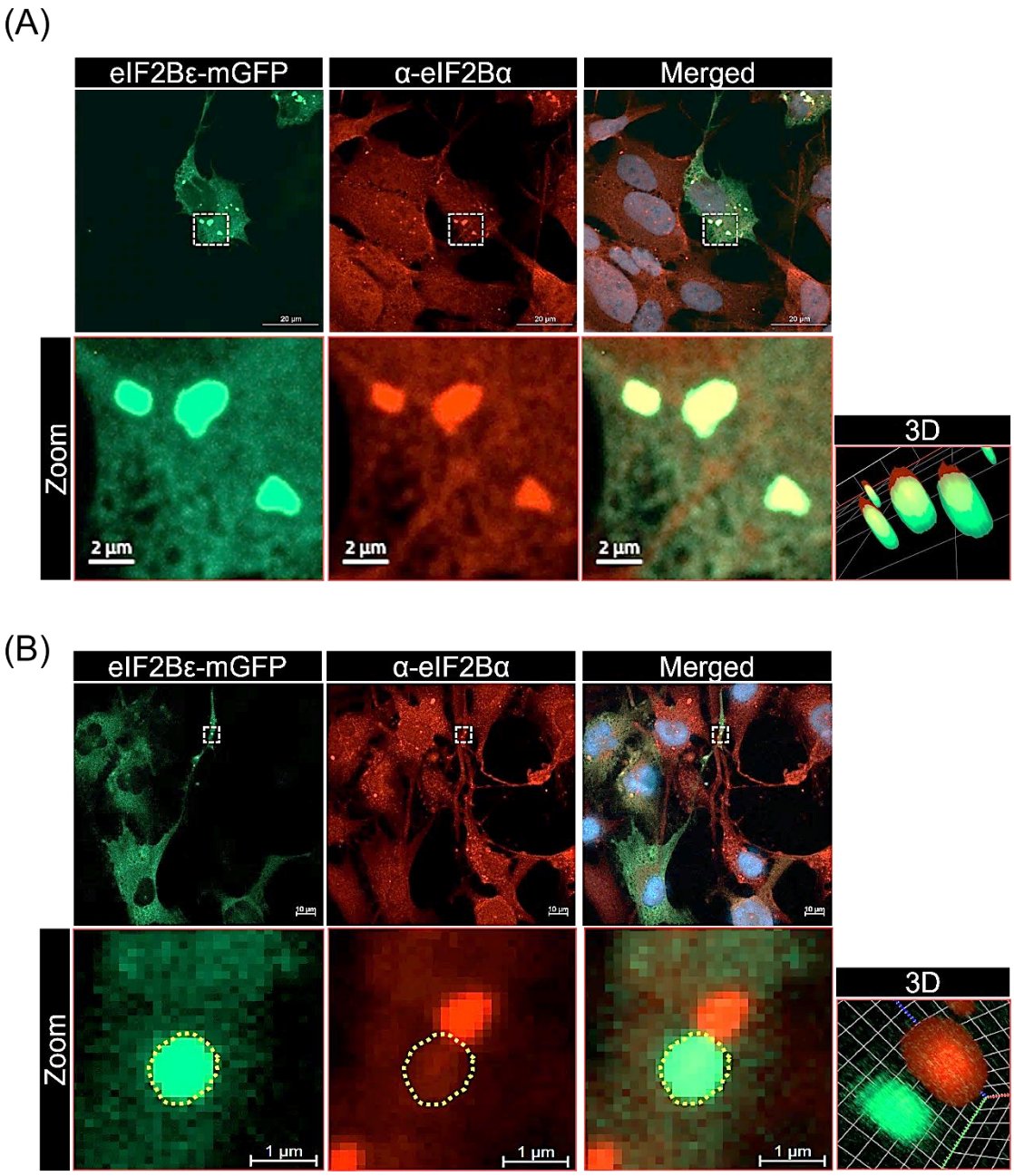

Figure 2.2. Co-localisation with eIF2B bodies.
Representative image of a **(A)** positive and **(B)** negative colocalization of an eIF2B body (488nm channel) with secondary antibody signal foci (561 nm channel)**.** 3D modelling of co-localisation of 488nm signal and 561 nm signal captured on a Zeiss LSM 800 Confocal.

2.6. Illustration tool and statistical analysis.

All diagrams, expected when referencing the source publication, were drawn in Adobe Illustrator (v26). All statistical assessments were made in GraphPad Prism 7 software, with a significance at $p<0.05$. All data is presented as means ± standard errors of the mean (s.e.m.). Due to discrepancies between cell line batches and technical variation between experiments, the data of each experiment was normalized to vehicle samples when appropriate, which were assigned the mean value of 1. Data was subjected to Shapiro-Wilk normality test. If parametric, data was analysed by one-way ANOVA test for comparison of three of more groups followed by Tukey's correction *post-hoc* test. If non-parametric, data was analysed by Kruskal-Wallis test for comparison of three of more groups followed by Dunn's correction *post-hoc* test. Asterisks indicate respective statistical significance as follows: *$p<0.05$; **$p<0.01$ and ***$p<0.001$. Detailed *p*-values are included in the caption of each figure.

Chapter 3. Characterisation of eIF2B localisation in neuronal and glial cells during steady-state conditions.

3.1. Introduction.

A key protein complex involved in ensuring efficient translation initiation takes place is eIF2. eIF2 is a heterotrimeric G-protein (Naveau *et al.,* 2013; Schmitt *et al.,* 2012). In its active GTP-bound state, eIF2 is complexed with methionylated initiator transfer RNA (eIF2-GTP-Met-RNAi) forming a TC to locate the first start codon to the ribosome (Hinnebusch & Lorsch, 2012). Following codon recognition, eIF2-GTP is hydrolysed to eIF2-GDP through the action of the canonical GTPase-activating protein eIF5 (Paulin *et al.,* 2001). eIF5 hinders GDP release (GDP dissociation inhibitor, GDI) from eIF2 (Jennings & Pavitt, 2010). Crucial for successive rounds of translation is the regeneration of GTP-bound eIF2 catalysed by eIF2B. Prior to its GEF function, eIF2B acts as a GDI displacement factor (Jennings *et al.,* 2013) removing eIF5, followed by GDP release from eIF2 (Williams *et al.,* 2001); all in all, posing as a powerful control checkpoint for the availability of TCs. In its native form, eIF2B is a heterodecameric complex composed of two copies of 5 non-identical subunits (termed eIF2Bα-ε). The γ and ε subunits catalyse the GEF activity, whereas the α, β and δ subunits regulate this activity in response to different cellular stress insults (Bogorad *et al.,* 2014; Kimball *et al.,* 1998; Pavitt *et al.,* 1998; Pavitt *et al.,* 1997). Structurally, eIF2B decameric conformation is comprised of an eIF2B$(\alpha\beta\delta)_2$ hexameric regulatory core laid between two opposing eIF2Bγε catalytic heterodimers (Tsai *et al.,* 2018; Zyryanova *et al.,* 2018). In mammalian cells, eIF2B has been reported to exist in different sub-complexes arrangements with varying subunit composition (Wortham *et al.,* 2014).

In yeast cells, eIF2B localises to stable cytoplasmic foci termed ‘eIF2B bodies’ where GEF activity takes place and are targeted for eIF2B regulation (Campbell *et al.,* 2005; Moon & Parker, 2018a; Norris *et al.,* 2021; Nüske *et al.,* 2020; Taylor *et al.,* 2010). These studies were further extended in human astrocytic cells and showed that heterogeneous populations of different-sized bodies correlated to its eIF2B subunit makeup (Hodgson *et al.,* 2019). Larger bodies contained all eIF2B

subunits, whilst small bodies predominantly consisted of the γ and ε catalytic subunits.

Despite its essential role in the ISR across all cell types (Pakos-Zebrucka *et al.,* 2016), mutations in any of the five subunits of eIF2B result in the neurological disorder VWMD (van der Knaap *et al.,* 2006). VWMD mutations are selectively detrimental to astrocytes, triggering immature oligodendrocytes and, ultimately, cause neuronal death due to axonal de-myelination (Bugiani *et al.,* 2011; Dooves *et al.,* 2016; Dooves *et al.,* 2018; Klok *et al.,* 2018; Leferink *et al.,* 2018). Nonetheless, studies have shown that cultured neurons are surprisingly unaffected by eIF2B mutations (Klok *et al.*, 2018), collectively implying cell-type specific features of eIF2B function and regulation at least to brain cell types, which remains to be understood.

3.2. Hypothesis and rationale.

eIF2B localisation has been reported in yeast models (Campbell *et al.,* 2005) and, more recently, in mammalian cells (Hodgson *et al.,* 2019). However, the latter has shown a higher degree of diversity and complexity. VWMD is directly linked to eIF2B mutations (Leegwater *et al.,* 2001). The understanding of VWMD pathology has shifted towards astrocyte dysfunction being the central cell type to be primarily drive white matter loss (Dooves et al., 2016). Oligodendrocytes have been implicated with maturation abnormalities and mitochondrial decay (Herrero *et al.,* 2019) while neurons remain directly resilient to VWMD mutations (Klok *et al.,* 2018). Because of this cell type vulnerability of eIF2B mutations, the main scientific aim of this chapter is to investigate the cellular localisation of eIF2B in neuronal, astrocytic and oligodendrocytic cell types. To test this hypothesis, the following experimental objectives were employed:

- Analyse the prevalence and distribution of the different sub-populations of eIF2B bodies by transient transfection, immunocytochemistry, and confocal imaging.
- Assess the composition make-up of the different sub-populations of eIF2B bodies by co-localisation imaging and analysis.
- Perform FRAP to quantify the substrate shuttling of the different sub-populations of eIF2B bodies.

3.3. Results.

3.3.1. eIF2B localises to heterogenous cytoplasmic foci ('eIF2B bodies') in a cell-type specific manner.

To analyse eIF2B localisation, transient transfection using the catalytic ε subunit of eIF2B tagged with monomeric Green Fluorescent Protein (eIF2Bε-mGFP) were performed in neuroblastoma (SH-SY5Y), astrocytoma (U373) and hybrid primary oligodendrocytes (MO3.13) cell lines. Given the main goal of this study was to address potential distinct localisation patterns between cell types, the cell lineage of each cell line was validated through immunostaining with selective markers anti-NeuN, anti-GFAP and anti-MBP antibodies in SH-SY5Y, U373 and MO3.13, respectively (**Figure 3.1.**). Next, a PEI transfection protocol as described in (Hodgson *et al.,* 2019) resulted in increasing cytotoxicity in a dose-dependent manner of PEI(µg):DNA(µg) ratios in MO3.13 cells; and low GFP+ transfection efficiency (<10%) in SH-SY5Y cells (data not shown). These technical impediments were solved by transfecting SH-SY5Y and MO3.13 cells using the Lipofectamine 3000 protocol.

All cell types unanimously displayed either dispersed expression of eIF2Bε-mGFP throughout the cytoplasm or localised to cytoplasmic foci (termed 'eIF2B bodies') (**Figure 3.2. A**). Analysis of the percentage of transfected cells displaying eIF2B bodies showed that U373 cells have the highest % of cells containing eIF2B bodies (53.50% ± 2.18) followed by MO3.13 cells (33.25% ± 1.65) and SH-SY5Y cells exhibiting the lowest % (19.25% ± 2.06) (**Figure 3.2. B**).

The size and abundance of eIF2B bodies per cell also varied across the cell types. eIF2Bε-mGFP localisation was categorised into two groups based on size ranges: small eIF2Bε-mGFP bodies (<1µ^2) and large eIF2Bε-mGFP bodies (≥1µ^2) (**Figure 3.3.A**). Small eIF2Bε-mGFP bodies were the predominant subpopulation across cell types ranging from ~ 10-30 bodies per cell (SH-SY5Y: 10.33 ± 2.48; U373: 30.83 ± 6.59; MO3.13: 28.65 ± 3.59) (**Figure 3.3. B**). In contrast, all cell types displayed a minority of ~ 1-3 large eIF2Bε-mGFP bodies per cell (SH-SY5Y: 1.73 ± 0.36; U373: 2.53 ± 0.28; MO3.13: 1.79 ± 0.33) (**Figure 3.3. B**). For cross-comparison between cell types, the raw counting data was transformed into the % of the number of bodies of each size category normalised against the total number of detected bodies per cell. U373 and MO3.13 cells

exhibited no significant differences in the % of small bodies per cell (U373: 88.19% ± 1.55; MO3.13: 89.34% ± 0.81), while SH-SY5Y cells showed a significantly decreased % of small bodies (71.46% ± 2.83) compared to the glial cells (**Figure 3.3. B**). SH-SY5Y cells displayed a significant increase % of large eIF2Bε-mGFP bodies per cell (30.54% ± 2.83) in comparison to U373 and MO3.13 cells (U373: 13.81% ± 1.55; MO3.13: 12.66% ± 0.81) (**Figure 3.3. B**). Furthermore, small eIF2B bodies across the cell types have similar average size (SH-SY5Y: 0.222 μm^2 ± 0.015; U373: 0.243 μm^2 ± 0.013; MO3.13: 0.247 μm^2 ± 0.005), while neuronal cells display bigger large eIF2B bodies (SH-SY5Y: 5.154 μm^2 ± 0.844; U373: 2.556 μm^2 ± 0.239; MO3.13: 2.010 μm^2 ± 0.039) (**Figure 3.3. C**).

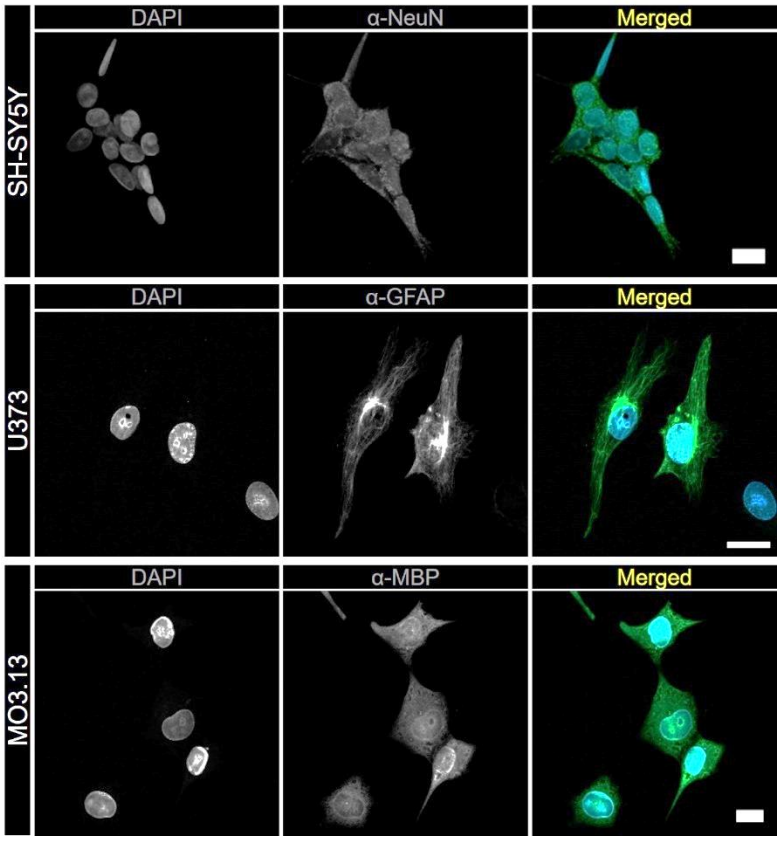

Figure 3.1. Antibodies against selective markers for neuronal and glial cells were used to validate cellular lineage.
Representative confocal images of neuroblastoma (SH-SY5Y), astrocytoma (U373) and hybrid primary oligodendrocytes (MO3.13) immunostained for neural marker neuronal nuclei (NeuN), astrocytic marker glial fibrillary acidic protein (GFAP), and oligodendrocytic marker myelin basic protein (MBP), respectively. DAPI shows nuclei. Scale bar: 50μm.

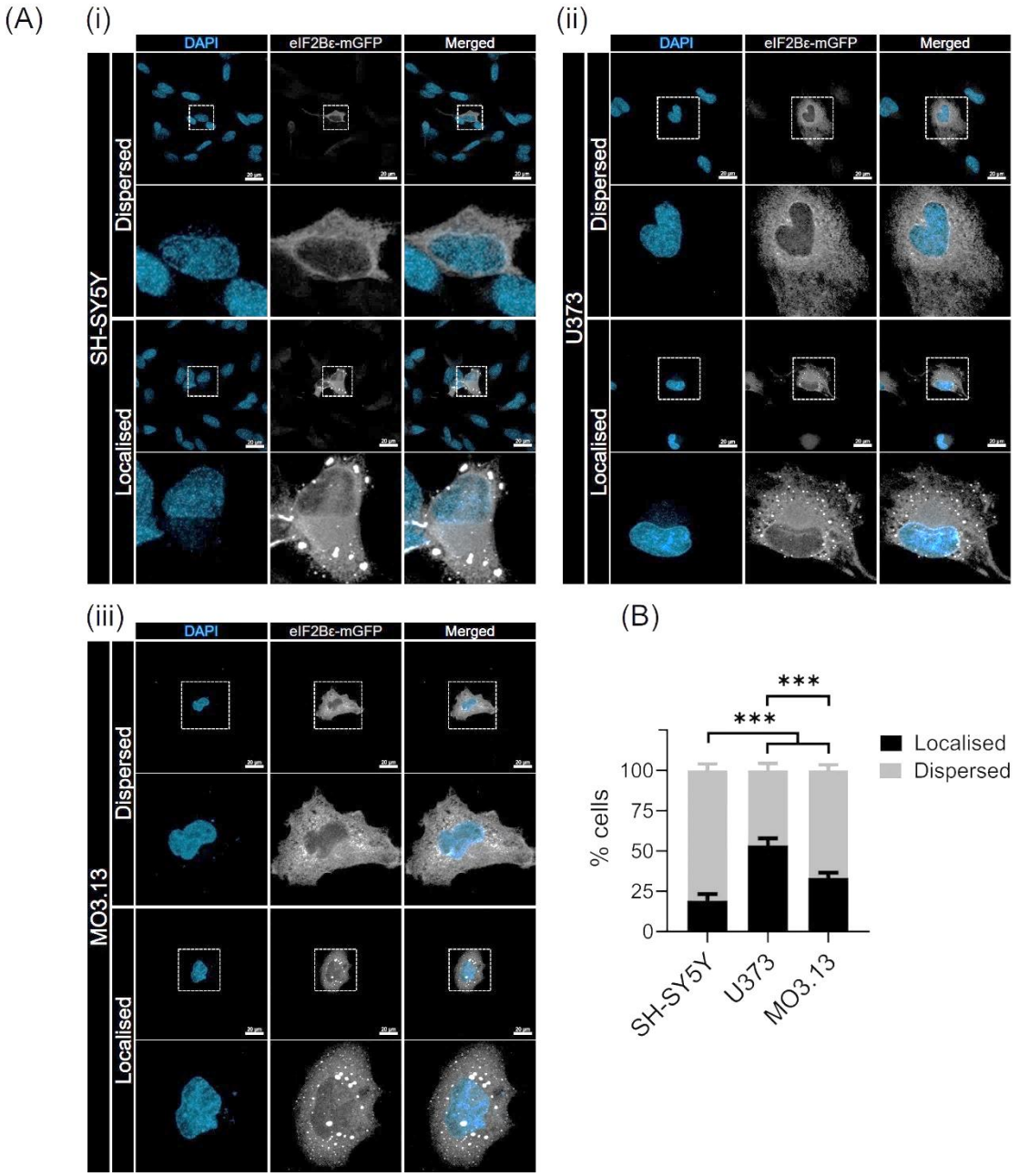

Figure 3.2. eIF2B localisation is higher in astrocytic cells.
(A) Representative confocal images of (i) SH-SY5Y, (ii) U373 and (iii) MO3.13 cells transiently transfected with eIF2Bε-mGFP displaying exclusively dispersed throughout the cytoplasm or co-exhibiting localised foci (termed 'eIF2B bodies'). DAPI stains nuclei.
(B) Mean percentage of cells displaying dispersed cytoplasmic and eIF2Bε-mGFP bodies in a population of 100 transfected cells was quantified manually and analysed using two-way ANOVA followed by *post-hoc* Tukey's test for multiple comparisons. Error bars: ± s.e.m. (*N*=4). ***p<0.0001 (SH-SY5Y vs. U373/MO3.13); ***p=0.0003 (U373 vs. MO3.13).

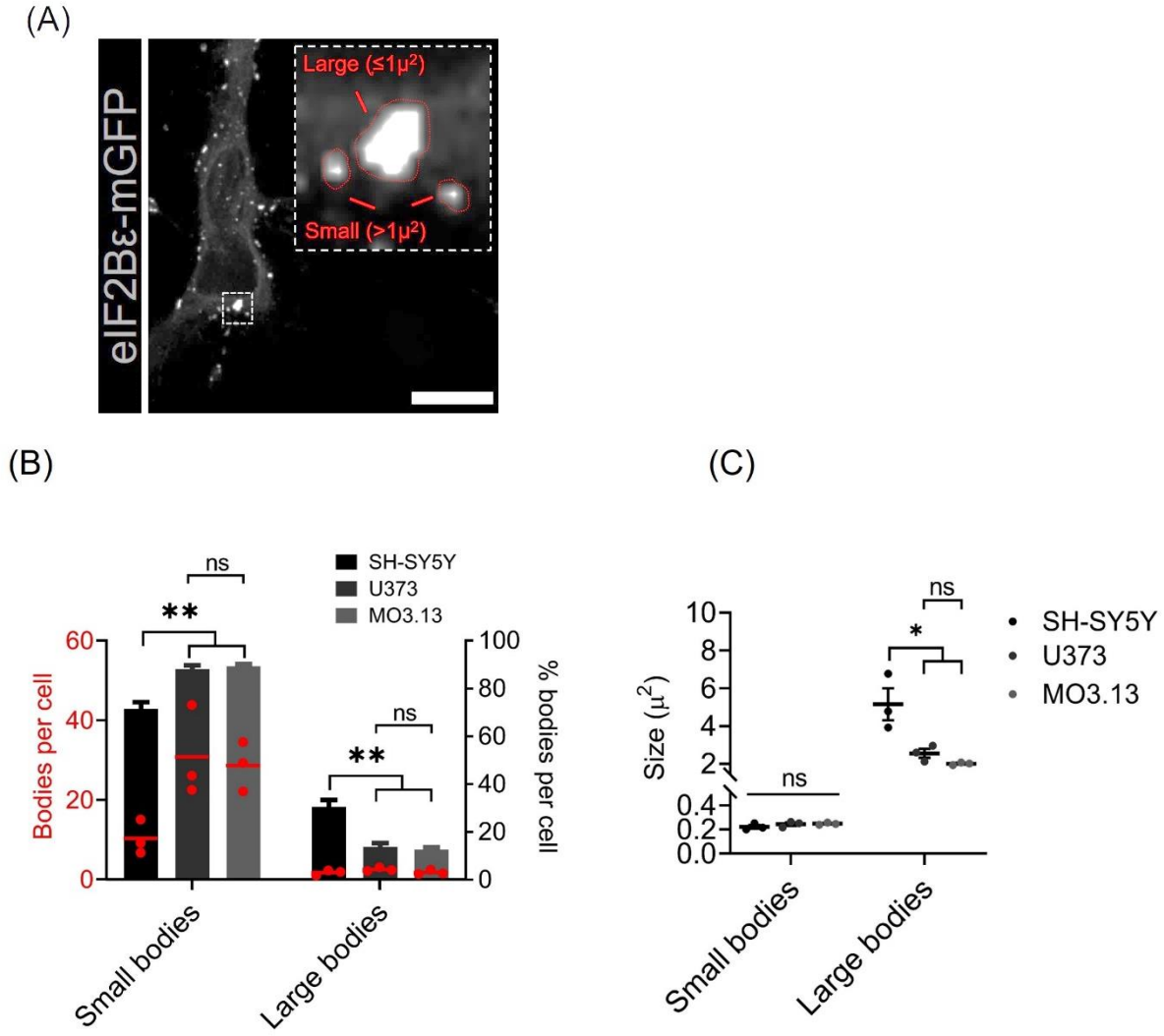

Figure 3.3. Astrocytic and oligodendrocytic cells share size distribution of eIF2B localisation.
(A) Representative confocal image of U373 cells transiently transfected with eIF2Bε-mGFP and displaying the two sized categories of eIF2B localisation: small eIF2Bε-mGFP bodies (<1μm^2) and large eIF2Bε-mGFP bodies (≥1μm^2). Scale bar: 50 μm.
(B) Mean number of small eIF2Bε-mGFP bodies and large eIF2Bε-mGFP bodies in a population of 50 transfected cells per replicate was quantified manually and is graphed in red (*N*=3). The mean percentage of eIF2Bε-mGFP bodies was quantified for small ([number of small bodies/total bodies] x 100) and large ([number of large bodies/total bodies] x 100 and analysed using one-way ANOVA followed by *post-hoc* Tukey's test for multiple comparisons. Error bars: ± s.e.m. (*N*=3). ***p*=0.0020 (SH-SY5Y vs. U373); ***p*=0.0014 (SH-SY5Y vs. MO3.13); ns: non-significant.
(C) The mean size average (μ^2) of eIF2Bε-mGFP bodies was quantified and analysed using one-way ANOVA followed by *post-hoc* Tukey's test for multiple comparisons. Error bars: ± s.e.m. (*N*=3). **p*=0.0258 (SH-SY5Y vs. U373); **p*=0.0110 (SH-SY5Y vs. MO3.13); ns: non-significant.

3.3.2. Stable expression of tGFP-tagged eIF2Bε shows similar localisation patterns to transient expression of mGFP-tagged eIF2Bε.

Transient transfection yields temporary overexpression of a given protein-construct of interest. To confirm that this technical feature did not impact on eIF2B localisation, stable cell line expressing tGFP-tagged eIF2Bε in U373 cells were generated (**Figure 3.4. A**). tGFP (or TurboGFP) is a dimeric version of the mGFP tag. Transient transfection with eIF2Bε-tGFP showed a similar size distribution of eIF2B bodies in SH-SY5Y, U373 and MO3.13 cells when compared to the data presented in section 3.2.1.

Western blot analysis confirmed the co-expression of endogenous eIF2Bε and tGFP-tagged eIF2Bε at a ratio of 1:0.11 (eIF2Bε:eIF2Bε-tGFP) in stably transfected U373 cells (**Figure 3.4. B**). Immunofluorescence analysis exhibited cells displaying either dispersed expression of eIF2Bε-tGFP throughout the cytoplasm or containing eIF2Bε-tGFP bodies (**Figure 3.4. C**). Next, the same cut off for body size as in section 3.2.1 to classify small bodies ($<1\mu^2$) and large bodies ($\geq1\mu^2$) was carried out. Similarly to transiently transfected cells, small bodies were the predominant sub-population of eIF2B bodies of ~ 19 bodies per cell (18.76 ± 5.51), representing 92.89% ± 2.57 of total bodies per cell (**Figure 3.4. D**). Large eIF2B bodies represented a minority of ~ 1 bodies per cell (1.16 ± 0.29), thus the remaining 7.11% ± 2.57 of total bodies (**Figure 3.4. D**).

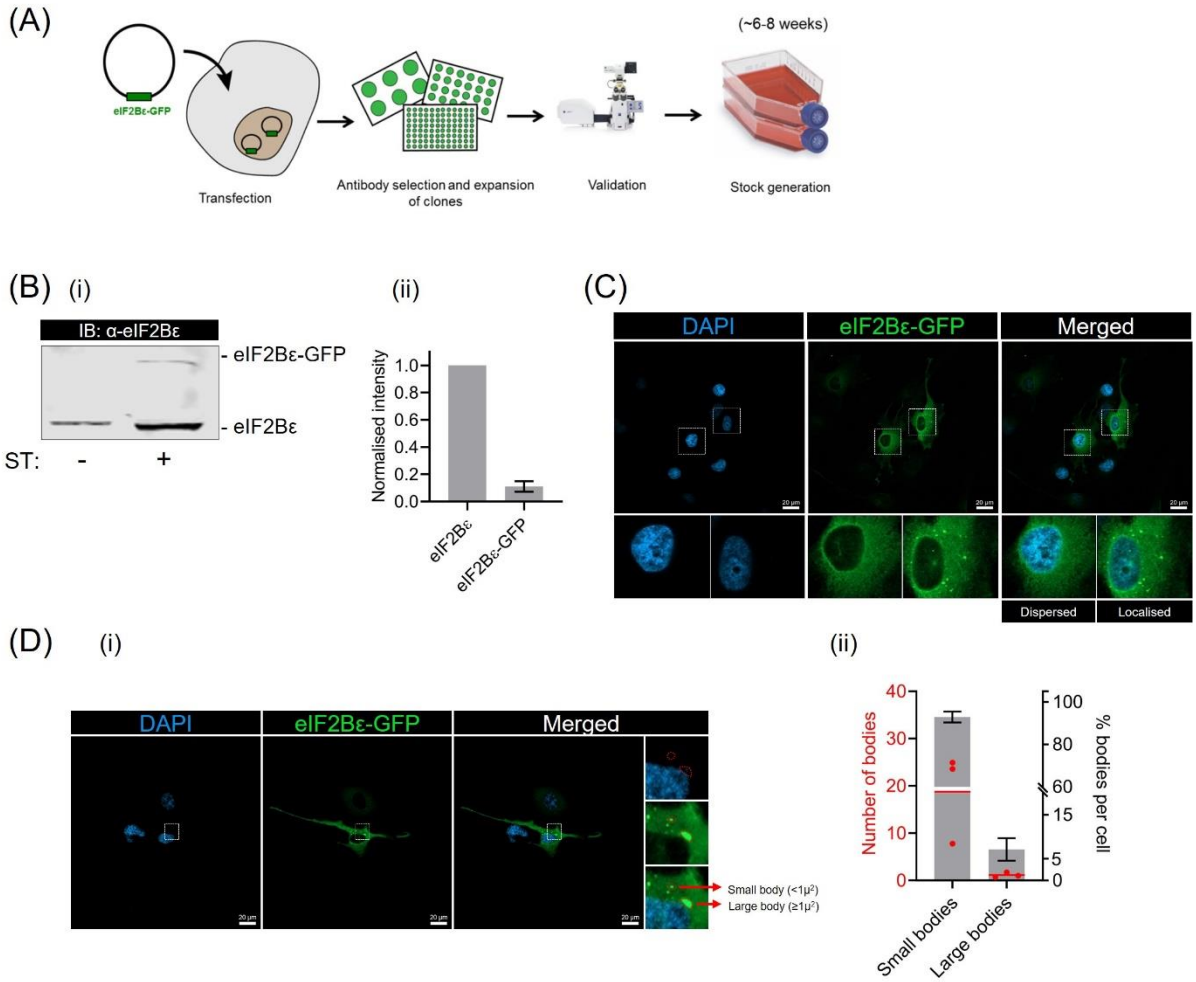

Figure 3.4. Stable expression of eIF2Bε-tGFP shows similar localisation patterns to transient expression.

(A) Schematic representation outlining the protocol to generate a stable cell line expressing eIF2Bε-GFP (see Methods section for detailed description).

(B) (i) Western blotting analysis of U373 cells on the expression levels of eIF2Bε. Cells are either unstransfected (lane 1) or stably expressing eIF2Bε-tGFP. 'eIF2Bε' denotes endogenous eIF2Bε and 'eIF2Bε-tGFP' denotes GFP-tagged eIF2Bε. *ST*, stable transfection. **(ii)** Quantification of the intensity levels of endogenous eIF2Bε and eIF2Bε-GFP in stably transfected U373 cells. Fold-change of eIF2Bε-tGFP is relative to endogenous eIF2Bε. Error bars: ± s.e.m. (*N*=3).

(C) Representative confocal images of U373 stably transfected with eIF2Bε-tGFP displaying exclusively dispersed throughout the cytoplasm or co-exhibiting localised foci (termed 'eIF2B bodies'). Scale bar: 20μm. DAPI shows nuclei.

(D) (i) Representative confocal image of U373 cells stably transfected with eIF2Bε-tGFP and displaying the two sized categories of eIF2B localisation: small eIF2Bε-GFP bodies (<1μ^2) and large eIF2Bε-tGFP bodies (≥1μ^2). Scale bar: 20μm. DAPI shows nuclei. **(ii)** The mean number of small eIF2Bε-tGFP bodies and large eIF2Bε-tGFP bodies in a population of 50 cells per replicate was quantified manually and is graphed in red (*N*=3). The mean percentage of eIF2Bε-tGFP bodies was quantified for small ([number of small bodies/total bodies] x 100) and large ([number of large bodies/total bodies] x 100 and analysed using one-way ANOVA followed by post-hoc Tukey's test for multiple comparisons. Error bars: ± s.e.m. (*N*=3).

3.3.3. eIF2B subunit make-up of eIF2B bodies is cell-type specific.

A relationship between eIF2B body size and subunit composition in U373 cells has been previously shown, where larger eIF2B bodies contains all five subunits and smaller eIF2B bodies are largely composed of catalytic make-up (Hodgson et al., 2019). Having demonstrated that eIF2B localisation harbours cell-type specific features regarding size and abundance (**Section 3.2.1**), the next aim was to investigate whether this size:subunit relationship was conserved between different cell types.

To analyse the subunit composition of eIF2B bodies, SH-SY5Y, U373 and MO3.13 cells transiently expressing eIF2Bε-mGFP were immunostained with antibodies against regulatory (anti-eIF2Bα, anti-eIF2Bβ, anti-eIF2Bδ) and catalytic (anti-eIF2Bγ) subunits of eIF2B (**Figure 3.5. A**). During the immunocytochemistry protocol, all three cell lines were firstly fixed in methanol, which led to drastic morphology changes and poor staining in MO3.13 cells (data not shown). Methanol dehydrates cells, removing lipids from membranes and precipitate proteins (Troiano *et al.,* 2009). Oligodendrocytes have sensitive protein-protein and lipid-protein interactions prior and post-myelination processes (Ozgen *et al.,* 2016), hence a methanol-driven disruption of these interactions could interfere with cellular architecture and antibody access to subcellular compartments. A PFA approach overcame this limitation as PFA crosslinks proteins and lipids, whilst maintaining cell structures and membranes are kept intact (Mason & O'Leary, 1991).

eIF2Bγ co-localisation showed the highest mean percentage in small eIF2B bodies across all cell types (SH-SY5Y: 51.99% ± 1.52; U373: 31.86% ± 1.46; MO3.13: 31.63% ± 8.57) (**Figure 3.5. B**). Also for small bodies, SH-SY5Y cells displayed a higher percentage of co-localisation of regulatory subunits eIF2Bα (SH-SY5Y: 27.58% ± 3.67; U373: 7.72% ± 2.72; MO3.13: 8.13% ± 2.00), eIF2Bβ (SH-SY5Y: 17.33% ± 9.35; U373: 5.94% ± 0.55; MO3.13: 0.68% ± 0.38) and eIF2Bδ (SH-SY5Y: 20.83% ± 2.05; U373: 10.63% ± 2.75; MO3.13: 9.03% ± 2.38).

In large eIF2B bodies, eIF2Bγ co-localisation was dominant across all cell types (SH-SY5Y: 91.23% ± 8.78; U373: 93.22% ± 1.54; MO3.13: 77.02% ± 12.43) (**Figure 3.5. B**). MO3.13 cells displayed lower eIF2Bα co-localisation albeit with no statistical significance compared to other cell types (SH-SY5Y: 60.26% ± 7.78;

U373: 59.02% ± 5.18; MO3.13: 38.25% ± 2.78) and near absence of eIF2Bβ co-localisation (SH-SY5Y: 38.38% ± 9.74; U373: 41.13% ± 9.09; MO3.13: 0.62% ± 0.32). eIF2Bδ co-localisation to large eIF2B bodies was overall similar across cell types (SH-SY5Y: 62.39% ± 12.80; U373: 67.48% ± 3.68; MO3.13: 65.00% ± 5.75).

(A)

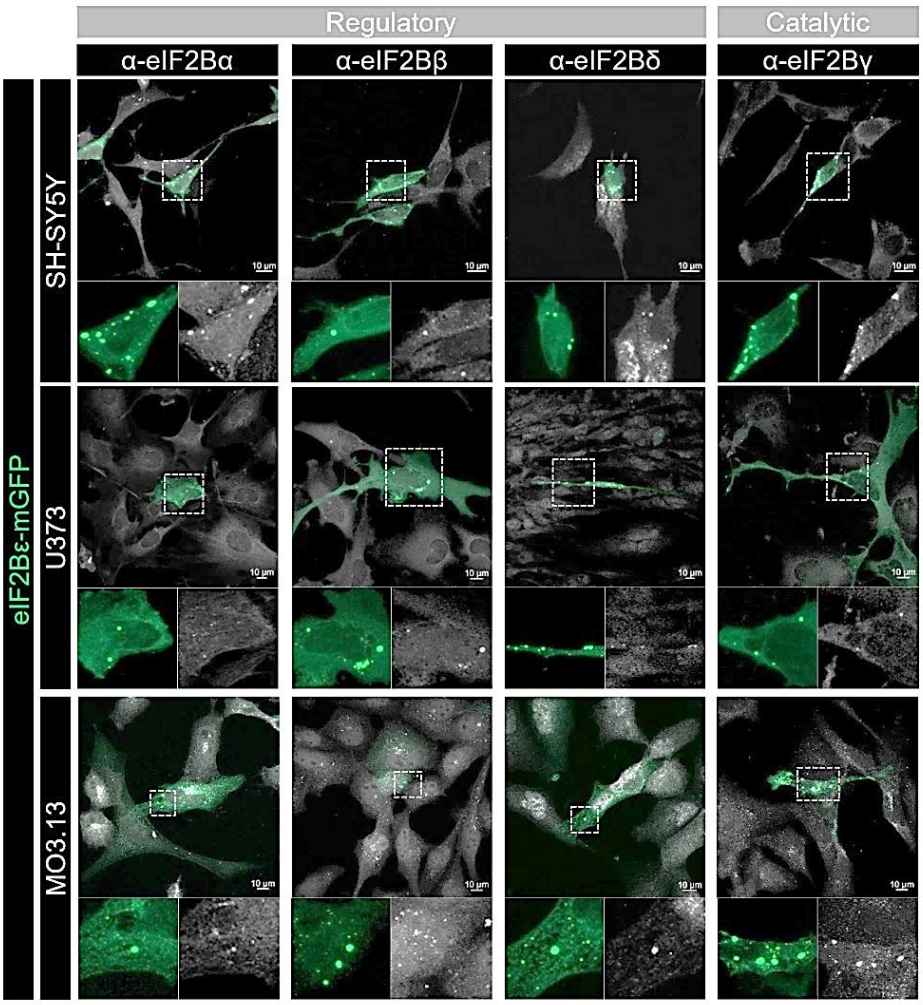
Regulatory
Catalytic
α-eIF2Bα
α-eIF2Bβ
α-eIF2Bδ
α-eIF2Bγ
eIF2Bε-mGFP
SH-SY5Y
U373
MO3.13
10 μm

(B)

(i)

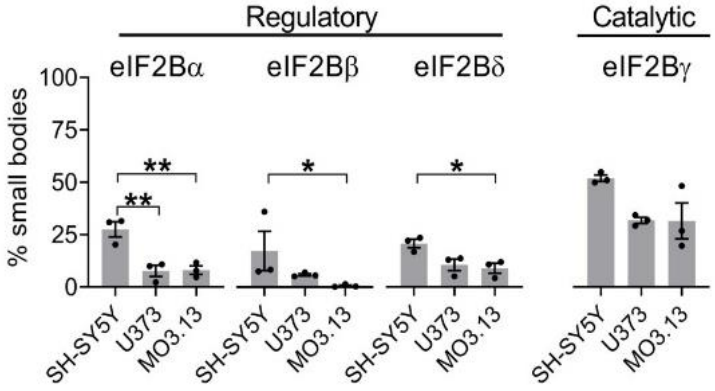
Regulatory
Catalytic
eIF2Bα
eIF2Bβ
eIF2Bδ
eIF2Bγ
% small bodies
100
75
50
25
0
**
**
*
*
SH-SY5Y
U373
MO3.13

(ii)

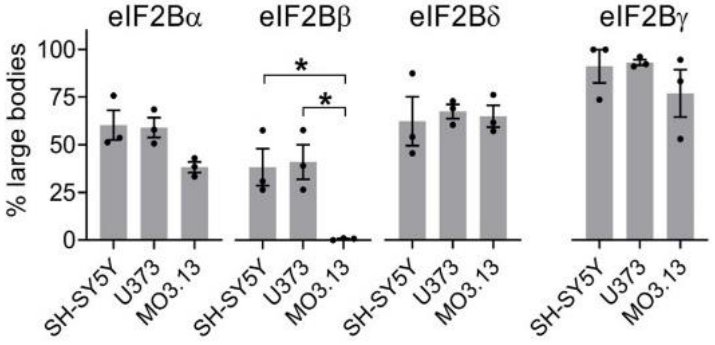
eIF2Bα
eIF2Bβ
eIF2Bδ
eIF2Bγ
% large bodies
100
75
50
25
0
*
*
SH-SY5Y
U373
MO3.13

Figure 3.5. Regulatory subunit composition (eIF2Bα, β, δ) is increased in neuronal small eIF2B bodies and decreased in oligodendrocytic large eIF2B bodies.
(A) Representative images of SH-SY5Y, U373 and MO3.13 cells transiently transfected with eIF2Bε-mGFP and immunostained with primary antibodies against α-eIF2Bα, α-eIF2Bβ, α-eIF2Bδ and α-eIF2Bγ. Scale bar: 10μm.
(B) (i) Mean percentage of small eIF2Bε-mGFP bodies displaying co-localisation with α-eIF2B(α-γ) cytoplasmic foci was quantified manually and analysed in a population of at least 30 cells per replicate using one-way ANOVA followed by *post-hoc* Tukey's test for multiple comparisons for parametric data (error bars: ± s.e.m.; *N*=3). ***p*=0.0066 (eIF2Bα: SH-SY5Y vs. U373); ***p*=0.0073 (eIF2Bα: SH-SY5Y vs. MO3.13); **p*=0.0311 (eIF2Bδ: SH-SY5Y vs. MO3.13) Kruskal-Wallis followed by Dunn's test for multiple comparisons as used for non-parametric data (error bars: ± s.e.m.; *N*=3). **p*=0.0219 (eIF2Bβ: SH-SY5Y vs. MO3.13). **(ii)** Mean percentage of large eIF2Bε-mGFP bodies displaying co-localisation with α-eIF2B(α-γ) cytoplasmic foci was quantified manually and analysed in a population of at least 30 cells per replicate using one-way ANOVA followed by *post-hoc* Tukey's test for multiple comparisons (error bars: ± s.e.m.; *N*=3). **p*=0.0308 (eIF2Bβ: SH-SY5Y vs. MO3.13); **p*=0.0229 (eIF2Bβ: U373 vs. MO3.13).

3.3.4. Expression levels of eIF2B subunits are similar across cell types.

Endogenous expression of eIF2B subunits is tightly regulated to ensure stoichiometric assembly of eIF2B sub-complexes and decameric eIF2B. eIF2Bε expression is guided by the co-expression of eIF2Bγ, and eIF2Bβ expression levels mediates ubiquitin-controlled expression of eIF2Bδ (Wortham *et al.,* 2016). Cell-type disparities of eIF2Bα levels are suggested to dictate the cellular proportions of eIF2B(βγδε):eIF2B(αβγδε)$_2$ complexes (Wortham *et al.,* 2014). In line with this, it was next determined whether cell-type specific expression of eIF2B subunits in the cell lines used in this study correlated with the observed differential eIF2Bα-γ composition of eIF2Bε-containing bodies.

Western blotting analysis of SH-SY5Y, U373 and MO3.13 cells revealed that all three cell types follow the same expression trend (**Figure 3.6. A**). eIF2Bγ levels showed the lowest expressions levels followed by eIF2Bδ levels. eIF2Bα and eIF2Bβ remained at similar levels across the cell types. eIF2Bε levels were the highest expressed subunit (**Figure 3.6. B**). Hence, these data show that the cell-type specific subunit composition of eIF2B bodies are independent of its expression levels.

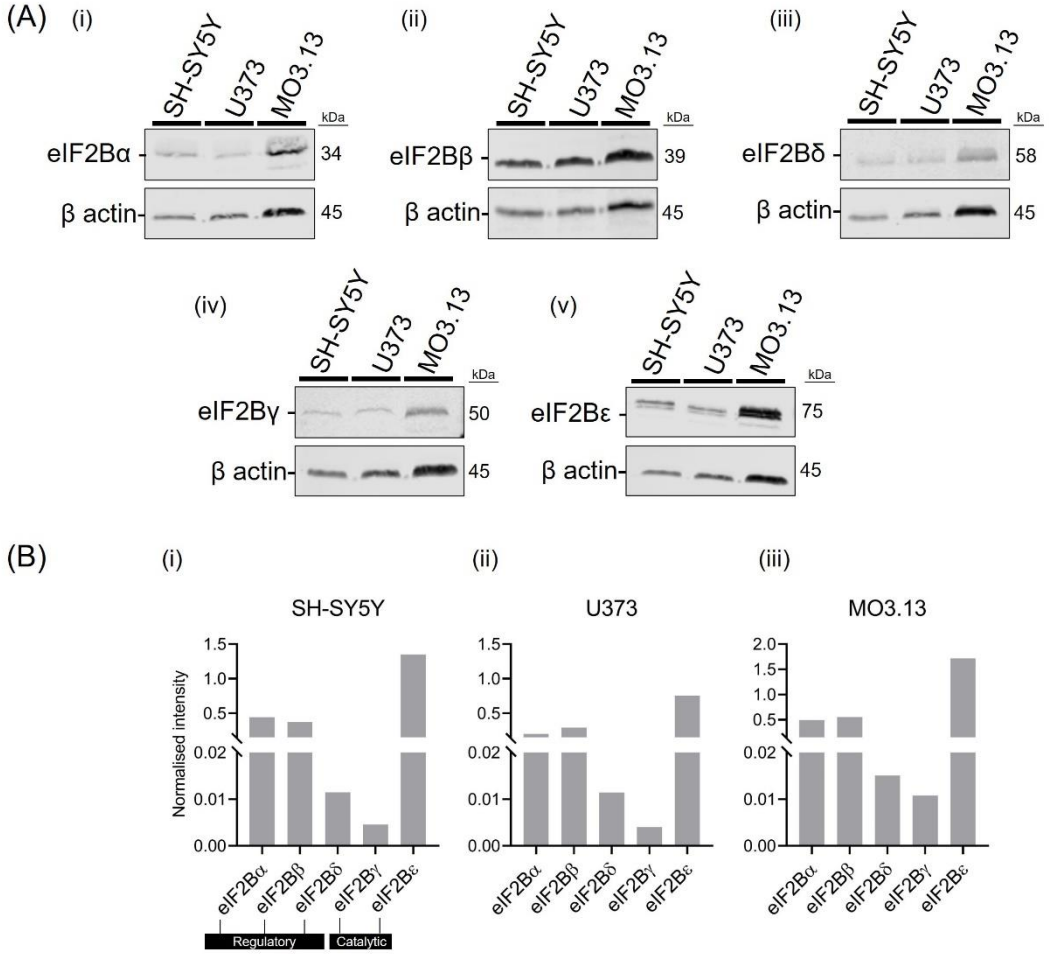

Figure 3.6. Endogenous expression levels of eIF2B subunits (α-ε) follows the same trend across cell types.
(A) Western blotting analysis of SH-SY5Y, U373 and MO3.13 cells on the expression levels of eIF2Bα, eIF2Bβ, eIF2Bδ, eIF2Bγ and eIF2Bε. β-actin expression levels were used as loading control.
(B) Quantification of the intensity levels of eIF2Bα-ε normalised against the loading control (β-actin) (*N*=1).

3.3.5. eIF2B subunits co-localise to stably expressed eIF2Bε-tGFP bodies.

To discard the possibility that temporary overexpression of eIF2Bε could interfere with the co-localisation of endogenous subunits to discrete eIF2Bε-containg bodies observed in section 3.3.3., immunofluorescence assays were carried out in U373 cells stably expressing eIF2Bε-GFP to analyse the co-localisation of eIF2Bα-γ subunits. All four subunits (α-γ) showed co-localisation to eIF2Bε-GFP bodies (**Figure 3.7 A**). In a population of 50 cells (*N*=1), 9.67% of small eIF2Bε-tGFP bodies (<1μm^2) co-localised with the α-eIF2Bα signal while large eIF2Bε-tGFP bodies (≥1μm^2) showed a predominant 94.29% of co-localisation with α-eIF2Bα (**Figure 3.7 B**). In contrast, 57.06% of small eIF2Bε-GFP bodies co-localised with α-eIF2Bγ antibody signal while all large eIF2Bε-GFP bodies (100.00%) co-localised with α-eIF2Bγ (**Figure 3.7 B**). These data demonstrate that, like the transient transfection, stably expressed small eIF2B bodies have a predominantly catalytic composition, while larger bodies display a higher degree of regulatory and catalytic make-up.

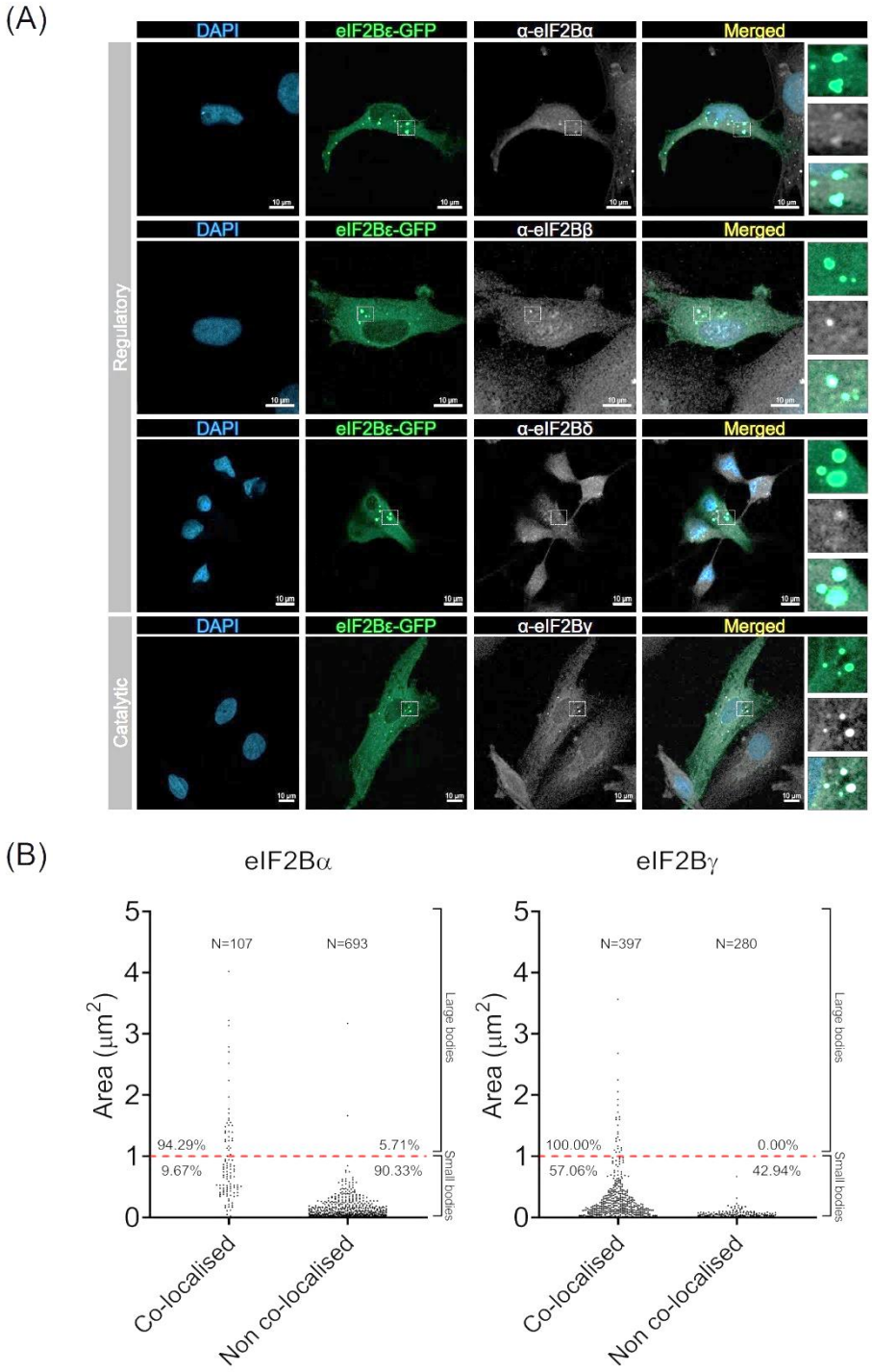

Figure 3.7. eIF2B subunits (α-γ) co-localise to stably expressed eIF2Bε-tGFP.
(A) Representative images of U373 cells stably transfected with eIF2Bε-tGFP and immunostained with primary antibodies against α-eIF2Bα, α-eIF2Bβ, α-eIF2Bδ and α-eIF2Bγ. DAPI stains nuclei. Scale bar: 10μm.
(B) Scatter dot plot showing the number of eIF2Bε-tGFP bodies that displayed co-localisation with α-eIF2Bα (left panel) and α-eIF2Bγ (right panel) cytoplasmic foci in a population of 50 cells from 1 biological experiment. Dotted red line indicates the size threshold of small (<1μm^2) and large (≥1μm^2) eIF2Bε-tGFP bodies. Percentage values below red line indicate percentage of small bodies co-localised with antibody signal (left side) or showing no co-localisation (right side).

3.3.6. The eIF2 shuttling through eIF2B bodies is cell-type specific.

eIF2B controls the availability of TCs by its guanine exchange activity in converting inactive GDP-bound eIF2 to active GTP-bound cognate (Jennings *et al.,* 2017). Previous studies have shown that the shuttling rate of the alpha subunit of eIF2 (eIF2α) through eIF2B bodies directly measures the activity of an individual eIF2B body (Campbell *et al.,* 2005; Hodgson *et al.,* 2019; Norris *et al.,* 2021). Based on the protocol established by (Campbell & Ashe, 2006), fluorescence recovery after photobleaching (FRAP) was performed to quantify the movement of eIF2 through eIF2B bodies. This technique relies on the irreversibility of photobleaching hence photon-induced loss of fluorescence in a given region of interest can only be recovered through movement of neighbouring fluorophore-bound constructs.

SH-SY5Y, U373 and MO3.13 were transiently co-transfected with eIF2α-tGFP and eIF2Bε-RFP. Live cell imaging confirmed the co-localisation of eIF2α-tGFP foci and eIF2Bε-RFP foci (**Figure 3.8. A**). FRAP analysis was performed by quantifying the rate of recovery of fluorescence intensity of an individual region of interest containing an eIF2α-tGFP foci (**Figure 3.8. B**) which is directly correlated to an eIF2Bε-RFP body of the same size category and plotted as a FRAP recovery curve. FRAP analysis revealed that eIF2α-tGFP recovery of small eIF2B bodies was relatively similar across cell types, although slightly higher for U373 cells despite not being statistically significant (SH-SY5Y: 34.21% ± 1.92; U373: 42.32% ± 3.61; MO3.13, 34.16% ± 2.64) (**Figure 3.8. C**). Overall, eIF2 recovery was rapid – measured in seconds (s) – with a similar $t_{1/2}$ across cell types (SH-SY5Y: 0.86 s ± 0.03; U373: 0.68 s ± 0.12; MO3.13: 0.67 s ± 0.16). Large eIF2B bodies showed drastic discrepancies. SH-SY5Y and U373 cells exhibited similar eIF2α-tGFP recovery (SH-SY5Y: 36.13% ± 2.61; U373: 37.08% ± 0.40) whilst MO3.13 cells have significantly lower recovery (22.51% ± 3.76) (**Figure 3.8. D**). Furthermore, eIF2 recovery was significantly faster in U373 cells when compared to MO3.13 cells (SH-SY5Y: 1.13 s ± 0.08; U373: 0.90 s ± 0.05; MO3.13: 1.23 s ± 0.03).

(A)

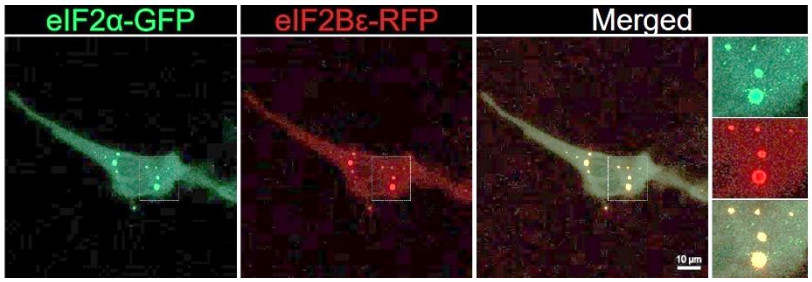

(B)

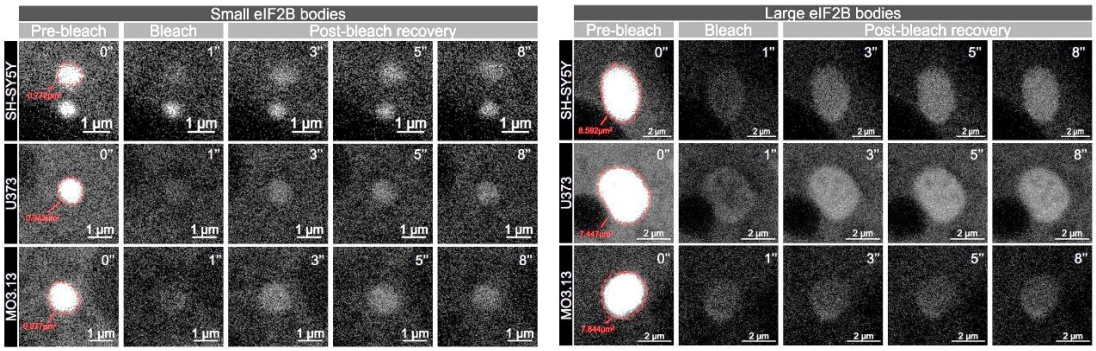

(C) *Small bodies*

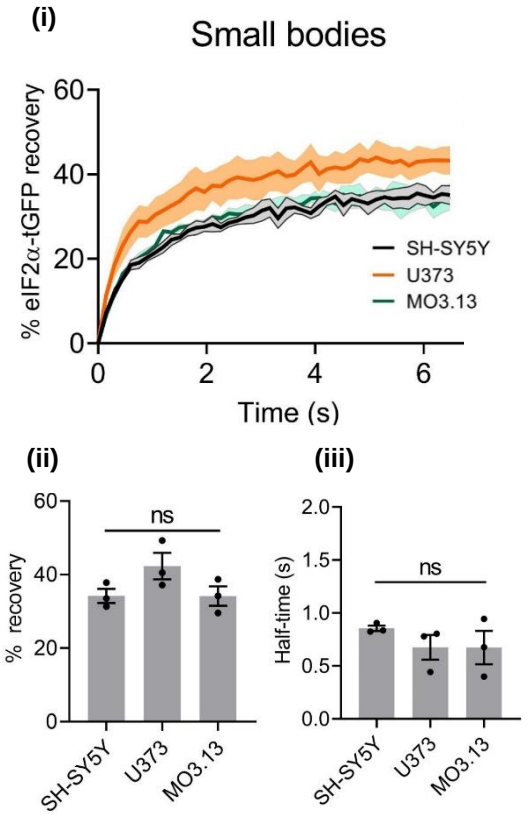

(D) *Large bodies*

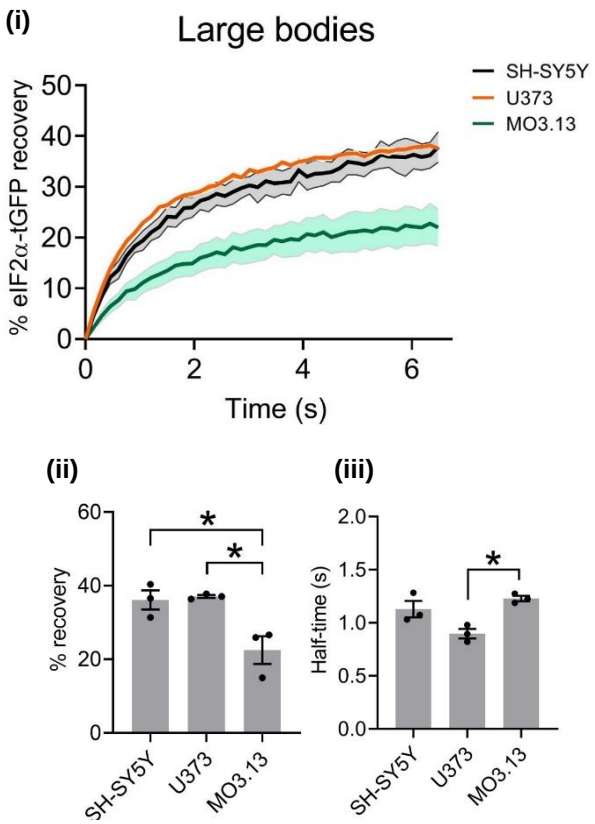

Figure 3.8. Shuttling of eIF2α-tGFP through large eIF2Bε-RFP bodies is decreased in oligodendrocytic cells.
SH-SY5Y, U373 and MO3.13 cells transiently co-transfected with eIF2α-tGFP and eIF2Bε-RFP. eIF2α-tGFP foci fluorescence was quantified to carry out fluorescence recovery after photobleaching (FRAP). eIF2Bε-RFP foci mark the eIF2B body.
(A) Representative live cell imaging of a U373 cell co-expressing eIF2α-tGFP and eIF2Bε-RFP.
(B) FRAP was performed in single small (<1μm^2) and large (≥1μm^2) eI2FB bodies.
(C) (i) Quantification of normalised FRAP curves for eIF2α-tGFP of 10-15 small eIF2Bε-RFP (<1μm^2) bodies of SH-SY5Y, U373 and MO3.13 cells. The data were graphed and shown as the mean and s.e.m. bands (*N*=*3*). **(ii)** Mean percentage of eIF2α-tGFP recovery determined from normalised FRAP curves replicate using one-way ANOVA followed by *post-hoc* Tukey's test for multiple comparisons. **(iii)** Quantification of the half time need for post-bleach full recovery of eIF2α-tGFP. Error bars: ± s.e.m. (*N*=3). ns: non-significant.
(D) (i) Quantification of normalised FRAP curves for eIF2α-tGFP of 10-15 large eIF2Bε-RFP (≥1μm^2) bodies of SH-SY5Y, U373 and MO3.13 cells. The data were graphed and shown as the mean and s.e.m. bands (*N*=*3*). **(ii)** Mean percentage of eIF2α-tGFP recovery determined from normalised FRAP curves replicate using one-way ANOVA followed by *post-hoc* Tukey's test for multiple comparisons. Error bars: ± s.e.m. (*N*=3). **p*=0.0256 (SH-SY5Y vs. MO3.13); **p*=0.0191 (U373 vs. MO3.13). **(iii)** Quantification of the half time need for post-bleach full recovery of eIF2α-tGFP. Error bars: ± s.e.m. (*N*=3). **p*=0.0116 (U373 vs. MO3.13).

3.4. Discussion.

eIF2B localisation has gained attention over the past years. First discovered by Campbell and Ashe and colleagues in the yeast *S. cerevisiae* where all five subunits of eIF2B were observed to localise to a single cytoplasmic focus, earning its term as 'eIF2B bodies' (Campbell *et al.,* 2005). Further studies have shown eIF2B localisation is a cellular feature not only in other yeast strains (Noree *et al.,* 2010; Taylor *et al.,* 2010; Moon & Parker, 2018a; Norris *et al.,* 2021) but also present in mammalian cells (Hodgson *et al.,* 2019). However, the latter has shown a higher level of diversity and functional complexity. Despite the ubiquitous role of eIF2B in the control of protein synthesis in all cell types, mutations in any of the five subunits of eIF2B are causative of the neurological disorder VWMD. The pathobiology of VWMD is mainly characterized by astrocytic dysfunction and abnormal maturation of oligodendrocytes, suggesting cell-type specific functions of eIF2B. Thus, the aim of this chapter was to address potential cell-type specific features of basal eIF2B localisation of brain cells which special focus to VWMD-sensitive cell types (astrocytic and oligodendrocytic cells).

3.4.1. Insights into the cell-type specific functional relevance of eIF2B localisation.

The characterisation of cellular eIF2B localisation in neuronal, astrocytic and oligodendrocytic cells was undertaken based on the protocol and categorising approach of (Hodgson *et al.,* 2019). The three cell types were transiently transfected with mGFP-tagged eIF2Bε to analyse the localisation and functionality of eIF2B bodies. Transient expression of GFP-tagged eIF2Bε in U373 cells (**Figures 3.2.**, **3.3.** and **3.5**) showed similar eIF2B body distribution and subunit composition compared to stable transfection (**Figures 3.4.** and **3.7.**). These experiments were of upmost importance to discard whether transient overexpression of eIF2Bε affects eIF2B localisation patterns. Importantly, stable transfection was also performed in SH-SY5Y and MO3.13 cells however due to low efficiency of GFP expression verified by western blot analysis and ICC (data not shown), transient transfection was carried out throughout this thesis.

eIF2B bodies pose as steady-state clusters of eIF2B complexes and sites of local GEF activity (Campbell *et al.,* 2005; Hodgson *et al.,* 2019; Norris *et al.,* 2021;

Taylor *et al.,* 2010). The data presented in this chapter now demonstrates that the prevalence of eIF2B bodies is modulated in a cell-type specific manner (**Figure 3.2.**). Amongst the cell types used in this study, astrocytic cells exhibited increased number of cells harbouring eIF2B bodies (~54%) in comparison to oligodendrocytic (~33%) and neuronal (~19%) cells (**Figure 3.2. B**). Because eIF2B bodies accounts for only a certain portion of total eIF2B, with the remaining GEF exchange occurring elsewhere in the cytoplasm, it is hypothesized that the degree of eIF2B localisation differs depending on the cellular requirement for regulated GEF activity, both for steady state purposes and ability to respond to stress. It is quite established that the rate of global protein synthesis varies to accommodate cell-type specific cellular needs. Accordingly, astrocytes rely on speedy induction of growth factors, chemokines, and cytokines; whilst also manifesting shorter half-lives of proteins in comparison to neurons (Dörrbaum *et al.,* 2018; Toyama *et al.,* 2013) which indicates that cell identity determines protein turnover. Protein turnover is crucial for the maintenance of the cellular proteome and to dynamically fine-tune the abundance of individual proteins when confronted with internal or external cues. In agreement with the above, synaptic plasticity is inherently dependent on specific rates of protein turnover (Rosenberg *et al.,* 2014; Schanzenbächer *et al.,* 2016). Oligodendrocytes face similar demands when, during differentiation to fully matured myelinating oligodendrocytes, undergo production of high contents of proteins and lipids to produce myelin sheaths. It is therefore plausible that the localisation of eIF2B mirrors this dependency on cell-type specific protein turnover, which is further supported by aberrant astrogliosis upon robust stimulation of gene expression in VWMD eIF2B5$^{R132H/\ R132H}$ mutant mice (Cabilly *et al.,* 2012). Although reduced eIF2B activity does not affect the total proteome of the brain nor translation rates under basal conditions (Cabilly *et al.,* 2012; Gat-Viks *et al.,* 2015; Geva *et al.,* 2010; Raini *et al.,* 2017) it would be worthy to investigate how disruption of eIF2B localisation, for instance with VWMD mutations that abolishes eIF2B bodies (Norris *et al.,* 2021), impacts on protein turnover on a cell type-basis by quantitative methods of amino acid labelling like SILAC (Stable Isotope Labelling of Amino acids in Cell culture), in which proteome abundance differences in unlabelled and fully labelled samples are compared (Ong *et al.,* 2002).

Other GEF proteins also show a localised phenotype and may thus be a general feature to allow proper GEF activity. Cdc42, a Rho GTPase involved in endothelial barrier control, is activated by Rho GEFs (Gef1 and Scd1) where specific cellular localisation may facilitate its function (Fritz & Pertz, 2016; Reinhard *et al.,* 2016). Rab proteins, involved in the spatiotemporal regulation of vesicular transport, require physical interaction with intracellular compartments which is partially mediated by local recruitment of its cognate Rab GEFs (Blümer *et al.,* 2013). The reliance on local GEFs is particularly prominent in key neuronal functions such as spine remodelling and synaptic signalling (Evans *et al.,* 2015; Komiyama *et al.,* 2002; Wilkinson *et al.,* 2017). Interestingly, local pools of Cdc42, the substrate of GEFs Gef1 and Scd1, controls cellular polarization to promote cell cycle progression in budding yeast and migrating astrocytes (Nern & Arkowitz, 2000; Osmani *et al.,* 2010). In budding yeast, eIF2B body formation are mainly observed in the mother cell (Campbell *et al.,* 2005), which have a different cell cycle identity to the daughter cell (Thomas *et al.,* 2018) hence eIF2B bodies could play role in cell division like other GEFs (David *et al.,* 2012). Another recent study showed that knockout of GEF protein Vav3, a mediator of intracellular reorganizations of the cytoskeleton, in astrocytes altered its secretory repertoire of neurotrophic factors which led to exaggerated outgrowth of dendrite processes in co-cultured hippocampal neurons (Wegrzyn *et al.,* 2022). In addition, Vav3 also aids in oligodendrocyte maturation and remyelination which are key dysfunctional characteristics observed with VWMD eIF2B mutations (Ulc *et al.,* 2017). Akin to the GEFs mentioned previously, Vav3 function requires specific membrane localisation (Charvet *et al.,* 2005). It is therefore not surprising that GEFs have been appreciated for their multi-layered role in neurodegeneration, as reviewed in detail by (Droppelmann *et al.,* 2014).

It is noteworthy to point out that the data in this chapter furthers our understanding in the functional relevance of GEFs. Herein, a cell-type specific pattern of eIF2B bodies, a highly conserved GEF protein involved in translation initiation, is presented. It is quite surprising that only a portion of cells harbour eIF2B bodies as opposed to all cells, given this apparent functional role that cellular localisation has on GEFs. Others have argued that the subcellular localisation of GEFs acts as a guidance cue to direct its substrate localisation (Blümer *et al.,* 2013), however eIF2B localisation is somewhat more robust; wherein eIF2B bodies,

apart from being sites of shuttling of its substrate eIF2 (Campbell *et al.,* 2005), can display high area sizes (≥1μm^2) (**Figure 3.3. A**) and exhibit a rather randomised distribution throughout the cytoplasm (**Figure 3.2. A**). However, the movement of eIF2B bodies may not be random and may also display cell-specific features given its link to eIF2B regulation (Taylor *et al.,* 2010). Fusel alcohols, which inhibits translation in budding yeast, tethers eIF2B bodies to specific sites hence slowing its movement across the cell which is observed in tandem with decreased shuttling of eIF2 (Taylor *et al.,* 2010), however whether this mechanism is conserved in mammalian cells is not known.

By default, given that different cell types harbour distinct eIF2B localisation patterns (**Figure 3.2. B**), implies that the presence of eIF2B bodies is, albeit not mutually exclusively, a dynamic phenomenon with cell-type specific rates of eIF2B body dissolution and assembly. Given these emerging roles of GEFs in the brain (and other cell types but beyond the scope of this thesis), it would be interesting to investigate potential cell-type specific patterns in the localisation of other GEFs.

3.4.2. The relationship between eIF2B body size and eIF2B subunit composition is cell-type specific.

Hodgson *et al.* demonstrated that, in astrocytic cells, all five 5 subunits localise to large eIF2B bodies, suggesting that decameric eIF2B resides at these sites, whilst small eIF2B bodies harbour mainly eIF2Bγε heterodimers given its predominant catalytic make-up (Hodgson *et al.,* 2019). The data in this chapter expanded these studies by showing that this relationship between eIF2B subunit composition and eIF2B body size is cell type dependent (**Figure 3.5.**).

Firstly, neuronal cells harboured increased levels of regulatory subunits (eIF2Bα-δ) in small bodies in comparison to both types of glial cells. Secondly, in the larger eIF2B bodies, neuronal and astrocytic cells followed the size:subunit relationship described by (Hodgson et al., 2019), wherein all four subunits (eIF2Bα-γ) showed a higher degree of co-localisation to eIF2Bε compared to its cognate small bodies; while oligodendrocytes exhibited the surprising absence of eIF2Bβ (**Figure 3.5. B**).

It was previously argued that the co-localisation of eIF2B subunits to eIF2Bε-containing bodies correlates to the presence of different eIF2B sub-complexes (Hodgson *et al.,* 2019; Wortham *et al.,* 2014). Thus, the data in this chapter demonstrates small eIF2B bodies of astrocytic and oligodendrocytic cells mainly contain eIF2Bγε heterodimers, while in neuronal cells these small bodies may contain tetrameric and decameric complexes. Furthermore, the full eIF2B decameric is suggested to reside in large eIF2B bodies of neuronal and astrocytic cells, whilst in oligodendrocytes the lack of eIF2Bβ is somewhat intriguing.

eIF2B body formation in yeast is highly debated to this date. Numerous studies have observed the exclusive presence of eIF2B bodies during stress conditions such as acidic cytoplasm, glucose depletion and amino acid deprivation (Marini *et al.,* 2020); whilst others have shown steady-state localisation of eIF2B, further stimulated by cellular stress (Norris *et al.,* 2021). The role of cellular stress in the cell-type specific localisation of eIF2B is further discussed in Chapter 4. Nonetheless, these studies provided pivotal evidence to the organizational structure of eIF2B bodies and its enzymatic regulation. It is the current view that multiple dimerization of eIF2B decamers are bundled together to form the membraneless filament-like eIF2B body (Marini *et al.,* 2020; Nüske *et al.,* 2020).

These body-forming interactions are somewhat more dependent on some eIF2B subunits than others. Structural evidence supports the notion of eIF2B dimerization via eIF2Bα (Gcn3p in yeast) (Bogorad *et al.,* 2014; Wortham *et al.,* 2014; Kashiwagi *et al.,* 2016; Norris *et al.,* 2021) although others have proposed an additional dimerization of eIF2B through the Gcd1p (eIF2Bγ) and Gcd6p (eIF2Bε) subunits (Gordiyenko *et al.,* 2014). Further cryo-EM studies of eIF2B pinpoints a predominant interaction of opposing Gcd6p/eIF2Bε subunits to drive the dimerization of eIF2B decamers (Marini *et al.,* 2020). Interestingly, Gcn3p (eIF2Bα) deletion fully abrogates eIF2B body formation in yeast while Gcn3p mutants that affects the catalytic activity (Gcd^-) of eIF2B still displays localisation phenotype albeit as “microfoci” bodies with decreased GEF activity (Norris *et al.,* 2021). Altogether, these reports support that eIF2B body formation is due to a versatile interaction of eIF2B subunits when assembled as decamers while heterodimeric and tetrameric eIF2B sub-complexes fail to drive body formation.

It is however noteworthy that regulatory mutations of eIF2Bα/Gcn3p (Gcn^-) mimic the dispersed phenotype of eIF2Bα/Gcn3p null strains (which supports the role of eIF2Bα in body formation), but are also viable mutations (Norris *et al.,* 2021); suggesting that eIF2B sub-complexes may be present in a dispersed manner. In mammalian cells, the data presented in this chapter demonstrates that catalytic heterodimeric eIF2B (eIF2Bγε) can localise to eIF2B bodies, here termed small eIF2B bodies, irrespective of the observed cell type (**Figure 3.5. B**). Hence, decameric eIF2B is not required for eIF2B body formation in mammalian cells. Nonetheless, it cannot be ruled out that the presence of the eIF2B decamer may play a role in the integrity of eIF2B bodies. In this chapter, neuronal cells displayed small eIF2B bodies which have increased regulatory composition accompanied by a higher proportion of large eIF2B (which includes all five subunits) (**Figure 3.5. B**). In yeast, eIF2B bodies are suggested to arise from the stacking of smaller filament-like bodies (Nüske *et al.,* 2020; Marini *et al.,* 2020). It is therefore plausible that an increased presence of decameric eIF2B in small eIF2B bodies (as seen in neuronal cells) prompts the fusion of small bodies and is responsible for the shift towards large eIF2B bodies. This is further strengthened by the fact that large eIF2B bodies in neuronal cells have increased average size (**Figure 3.3. C**).

However, this begs the question why are eIF2B sub-complexes able to localise to discrete bodies in mammalian cells but not in yeast? Given the essential role of eIF2B in translation, it is unsurprising that eIF2B subunits are conserved between yeast and mammals (Price *et al.,* 1996). It is therefore plausible that PTMs participate in this higher complexity on eIF2B body formation in mammalian cells. In line with this, acetylation sites have been identified in eIF2B. Acetylation has linked to the regulation of phosphorylation susceptibility of large protein complexes (Choudhary *et al.,* 2009). Interestingly, eIF2Bε are largely absent of acetylation sites, whereas all eIF2B regulatory subunits have *N*-terminal acetylation sites (Beilsten-Edmands *et al.,* 2015). Such sites may have a role in stabilising complex formation as *N*-terminal acetylation can either prevent or redirect degradation (Arnesen, 2011). Moreover, recent evidence highlights the existence of PTM variability in a cell-type manner (Carpenter *et al.,* 2022). Given that PTMs regulate protein localisation (*e.g.,* GAPDH (Ventura *et al.,* 2010)), a further understanding of the significance of these PTMs sites could uncover new regulation layers in the context of cell-type specific eIF2B localisation.

3.4.3. eIF2B bodies are heterogeneous sites of eIF2B complexes.

In MO3.13 cells, co-localisation of eIF2Bα and eIF2Bδ to eIF2Bε-containing bodies increases proportionally to body size (**Figure 3.5. B**). Given that eIF2Bβ remains largely depleted in all eIF2B bodies (including large bodies), it suggests that in oligodendrocytes the decameric eIF2B does not localise to eIF2B bodies. This is an almost contradictory feature given the high demand of translation machinery to generate myelin sheaths (Ozgen *et al.,* 2016). The lack of decameric eIF2B to large eIF2B bodies may allow consistently stable levels of GEF activity, even when confronted with cellular stress, providing a continuous source of eIF2B activity rather than a complete shutdown. Surprisingly, eIF2Bβ can form eIF2B bodies in MO3.13 cells but do not co-localise with eIF2Bε-mGFP (**Figure 3.5. A**). It would be important to confirm if these eIF2Bβ-containing bodies in MO3.13 cells are functionally active by FRAP analysis. For instance, activation of PKR coalescences a portion of cellular PKR to non-active clusters to buffer eIF2α-P (Zappa *et al.,* 2022). In agreement, pharmacological dissolution of these clusters caused an exaggerated ISR (Zappa *et al.,* 2022). It is possible that eIF2Bβ localises to discrete foci in a PKR fashion, in this case to control its

localisation from eIF2Bε-containing bodies thus preventing the presence of decameric eIF2B.

The presence of eIF2Bα (in the absence of eIF2Bβ) to large eIF2B bodies in MO3.13 cells is itself surprising. Decameric eIF2B is assembled from two intermediate eIF2B(βδγε) subcomplexes stapled together by an eIF2Bα$_2$ dimer. Hence, the data presented in this chapter supports the presence of eIF2Bγε dimer; however, localisation of eIF2Bα without eIF2Bβ is suggested to be somewhat biochemically inconceivable (Wortham *et al.,* 2014). While the expression levels of eIF2Bβ are relatively similar across cell types (**Figure 3.7.**). PTMs may take place and might disrupt its interface contacts with eIF2Bδ to form eIF2Bβδ heterodimer precursors (Bogorad *et al.,* 2014; Kuhle *et al.,* 2015). Moreover, collision-induced dissociation releases eIF2Bβ from eIF2B(βδγε) tetramers (Wortham *et al.*, 2014), hence its assembly to the eIF2B sub-complex may be flexible which would make its localisation to eIF2B bodies more easily controlled. Understanding this cell type ability of eIF2Bβ depletion from eIF2B bodies (given that other cell types do not show this) warrants further investigation.

Yeast models have shown that all five subunits localise to eIF2B bodies and eIF2Bα mutants fully disrupt body formation (Norris *et al.,* 2021), supporting a homogenous composition of eIF2B decamers to eIF2B bodies (**Figure 3.9.**). However, the unexpected lack of eIF2Bβ, but not remaining subunits, to large eIF2B bodies in MO3.13 cells (**Figure 3.5.**) implies the heterogeneous presence of sub-complexes to these bodies (**Figure 3.9.**). Moreover, although the % of eIF2Bγ co-localisation to small eIF2B is paramount in all cell types (hence mainly sites of catalytic sub-complexes), the fact that regulatory eIF2Bα, β, and δ show a lower but not absent % of co-localisation implies by default the existence of a cell-specific threshold of regulatory composition to small bodies, thus suggesting the presence of other sub-complexes rather than solely eIF2Bγε dimers. In accordance, the absence of colocalization of eIF2Bβ to eIF2B bodies in MO3.13 cells (ranging from 0.62-0.68%) but not in SH-SY5Y and U373 cells (ranging from 5.94-41.13%) (**Figure 3.5. B**) corroborates the sensitivity of our immunocytochemistry and co-localisation assays to support our hypothesis of a cell-specific heterogeneous presence of eIF2B sub-complexes to eIF2B bodies. This hypothesis on the aetiology of eIF2B bodies is further strengthened by the FRAP analysis of small versus large bodies (**Figure 3.8.**). Small eIF2B bodies,

despite slight increased regulatory composition in neuronal cells, are functionally similar across the cell types; suggesting that the predominantly catalytic composition is responsible for a cell type-independent rate of eIF2α shuttling (and therefore GEF activity) during steady-state conditions. However, cell type disparities are observed in the activity of large eIF2B bodies, where the regulatory make-up in oligodendrocytic cells is drastically distinct. Biochemical assays have shown sub-complexes of eIF2B have reduced activity when compared to the full holocomplex containing all five subunits (Liu *et al.,* 2011). In line with these findings, the absence of decameric eIF2B in large eIF2B bodies agrees with the observed lessened rate of eIF2α shuttling in oligodendrocytes (**Figure 3.8. C**).

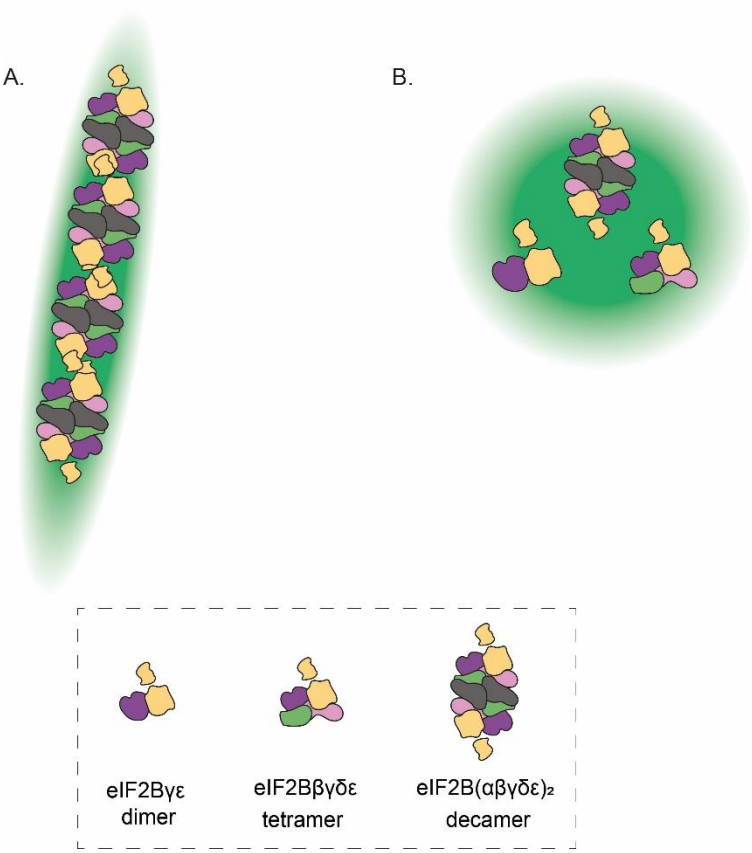

Figure 3.9. The homogenous *versus* heterogenous composition of eIF2B bodies hypothesis.
(A) In yeast, eIF2B bodies are composed of eIF2B decamers (eIF2B$(\alpha\beta\gamma\delta\varepsilon)_2$ holocomplex) stacked together in a filamentous structure (also called eIF2B filaments). (B) In mammalian cells, the data in chapter proposes that eIF2B bodies are sites of heterogeneous composition of eIF2B complexes (both sub-complexes and decamers) in a size and cell-type manner.

3.4.4. The localisation of eIF2B is cell-type specific: implications of a tailored regulation of translation initiation in brain cell types.

The existence of two functionally distinct sizes of eIF2B bodies is suggestive to allow a level of plasticity of translation control with: (1) predominantly catalytic-containing bodies, hence unregulatable by stress; (2) and bodies that when they surpass a certain threshold of regulatory composition provides both increased basal activity (Liu *et al.,* 2011) and be tightly modulated in the presence of cellular stress (Elsby *et al.,* 2011; Fabian *et al.,* 1997; Krishnamoorthy *et al.,* 2001; Pavitt *et al.,* 1998). The presence of different eIF2B subcomplexes localised to cytoplasmic foci could facilitate the local availability of TCs in comparison to a scattered pool accomplished by dispersed eIF2B (both decameric and other subcomplexes). It provides flexible availability of eIF2B subcomplexes of specific eIF2B activity and regulatable sensitivity that can accommodate translational needs on a cell type manner upon cellular stress. Interestingly, spatial distribution and local translation of mRNAs is paramount to allow efficient synaptic transmission (Holt *et al.,* 2019; Jung *et al.,* 2012) and functional polarization of astrocytes (Boulay *et al.,* 2017; Mazaré *et al.,* 2021). Another study highlighted newly translated ribosomal proteins in axons of primary cultured neurons to allow local protein synthesis (Shigeoka *et al.,* 2019). Furthermore, perisynaptic astrocytic processes (PAPs), known to regulate synaptic transmission by the release of its repertoire of gliotransmitters (Harada *et al.,* 2016), have shown alterations to its local proteome after fear conditioning (Mazaré *et al.,* 2021). Contextual fear-based memory acquisition requires local reductions of eIF2α-P to increase synaptic strength (Costa-Mattioli *et al.,* 2007). Hence, it is an attractive possibility that the cell type specificity of eIF2B localisation contributes to synaptic plasticity, which warrants further investigation.

eIF2B has been extensively studied for its pivotal roles in general initiation of translation (Hanson *et al.,* 2022), however in this chapter, cell-type specific localisation and activity of eIF2B is presented which further supports specialised functions of the translational machinery in brain cells. In line with this, eIF3g mediates translation of mRNAs involved in neuronal activity in a 5'-UTR-depedent manner (Blazie *et al.,* 2021). eIF3 complex and the helicase eIF4A are selectively required during dendrite pruning in *Drosophila* sensory neurons (Rode *et al.,* 2018). Strikingly, several initiation factors are translated in a development-

stage-specific manner (Shigeoka *et al.,* 2016) as opposed to an expected constitutive translation. Taken together, emerging evidence support that certain translation initiation complexes (such as eIF3) are tailored to fine-tune the production of relevant proteins in a cell-type manner. It is therefore plausible to hypothesise that the cell-type specific patterns of eIF2B localisation mirrors specialised functions in these cells to sustain a tailored demand of TCs. Indeed, astrocytes and oligodendrocytes are observed to harbour similar distribution of small eIF2B bodies (**Figure 3.3. B**), which during steady-state conditions are suggested to be functionally similar (**Figure 3.8. B**) and may be accommodate the high levels of translation required by these cells. In contrast, neuronal cells contain a higher abundance of large bodies (**Figure 3.3. B**), which contain all subunits, which might make translation more efficient and/or more easily regulated.

3.4.5. Final observations.

The results in this chapter demonstrate that eIF2B localises to spatially discrete cytoplasmic foci of varying size (small and large eIF2B bodies) in a cell-type specific manner amongst brain cells. Each cell type has its own repertoire of eIF2B bodies regarding abundance, composition, and basal GEF activity. These data provide attractive insights to whether the localisation of other GEF proteins could contribute to cell-type specific rates of translation and other biological processes. Similarly, the existence of cell-type specific patterns of eIF2B bodies may contribute to a tailored initiation of translation, which may facilitate the challenging demands of local translation in brain cells.

Taken together, the size variability of eIF2B bodies correlates to the presence of eIF2B sub-complexes in a cell-type manner (**Figure 3.10.**). Distinct eIF2B sub-complexes have different affinity to cellular stress (Liu *et al.,* 2011), which grants different stress sensitivities to eIF2B bodies (Hodgson *et al.,* 2019). Therefore, the next chapter of this thesis will focus on how cell-type specific induction of cellular stress impacts eIF2B localisation.

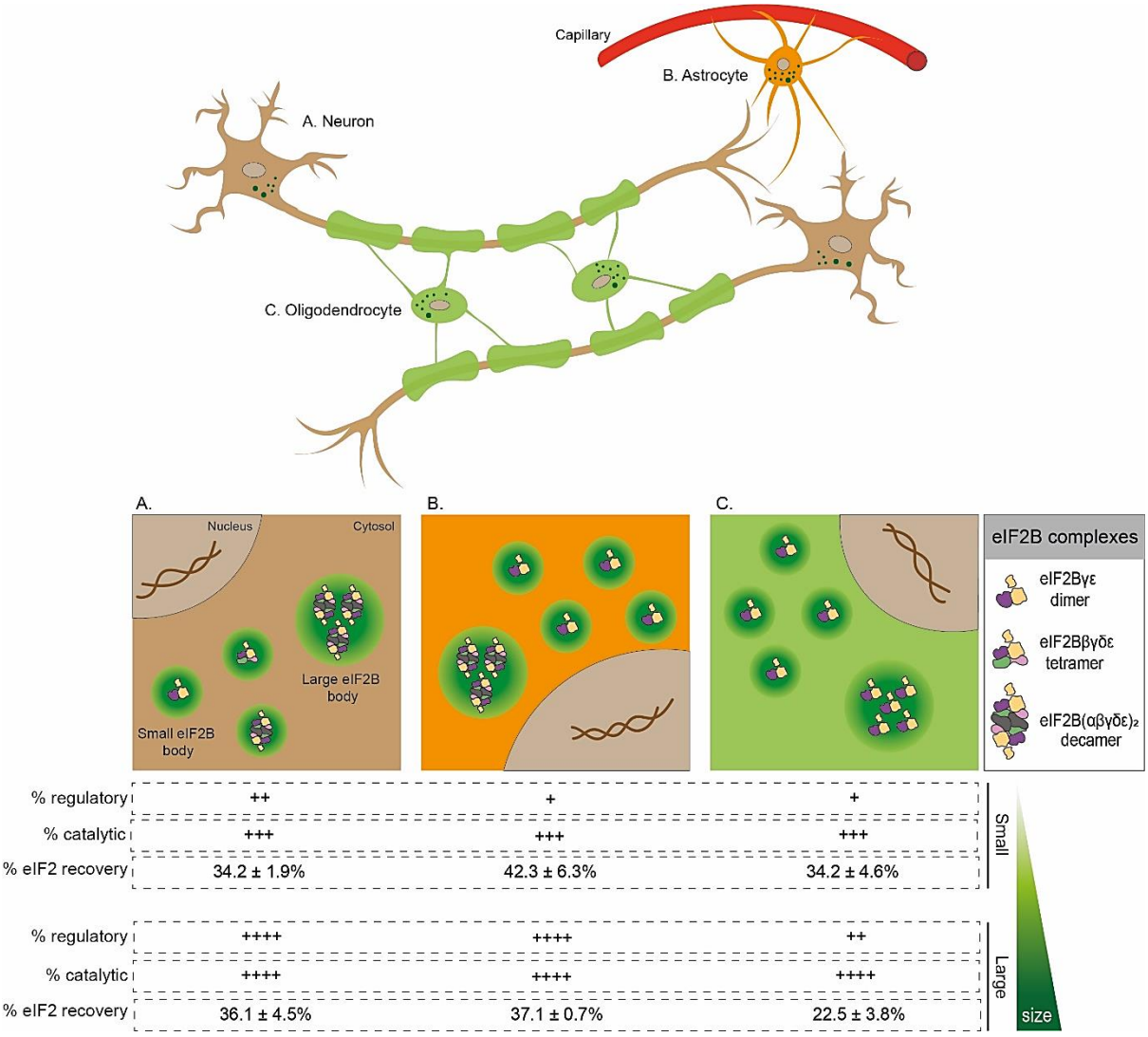

Figure 3.10. eIF2B bodies are modulated in a cell-type specific manner during basal conditions.
eIF2B localises to cytoplasmic foci (eIF2B bodies) of specific subunit composition and eIF2B activity, the latter being measured as the shuttling rate of substrate eIF2. Small eIF2B bodies is the predominant sub-population of total eIF2B bodies amongst all cell types, however the small:large ratio is cell-type specific. **(A)** Neurons harbour a higher proportion of large eIF2B bodies compared to glial cell types. Small eIF2B bodies contain increased regulatory make-up, suggesting variability of eIF2B complexes (heterodimer, tetramer, decamer) residing in these foci. Large eIF2B bodies contain a high degree of all subunits, implying a predominantly composition of decameric eIF2B. **(B)** In astrocytes, small eIF2B bodies are mainly composed of catalytic heterodimers, whilst large eIF2B bodies, for containing all subunits, are made-up of decameric eIF2B. **(C)** Oligodendrocytes harbour a somewhat more uniform composition between small and large eIF2B bodies. Both size categories contain a predominantly catalytic make-up, and large eIF2B bodies are partially depleted of regulatory composition. Amongst the sub-complexes validated by native MS (Wortham *et al.,* 2014), co-localisation data presented here suggests small and large bodies mainly contain catalytic heterodimers and not other sub-complexes. Accordingly, large eIF2B bodies show a reduced basal activity (quantified by FRAP analysis as the shuttling rate of eIF2) in comparison to other cell types, which is in line with previous findings that subcomplexes of eIF2B have reduced activity when compared to the full holocomplex (Liu *et al.,* 2011).

Chapter 4. Cellular stress responses regulate eIF2B localisation in a cell-type manner.

4.1. Introduction.

At the hub of translation control is the regulation of eIF2B activity by the ISR (Pakos-Zebrucka *et al.,* 2016). During acute or transient activation of the ISR pathway, stress-sensing kinases (PERK, PKR, GCN2, HRI) activate the phosphorylation of the α subunit of eIF2 at serine 51 (eIF2α-P). Phosphorylated eIF2α acts as a competitive inhibitor to its unphosphorylated cognate, blocking GEF activity of the decameric eIF2B by inhibiting the interaction of eIF2γ with the eIF2Bε subunit (Adomavicius *et al.,* 2019; Kashiwagi *et al.,* 2017; Kashiwagi *et al.,* 2019; Kashiwagi *et al.,* 2016). Attenuated eIF2B activity limits TC levels and overall reduces global protein synthesis. Concomitantly, a specific subset of mRNAs harbouring uORFs bypass this translation attenuation including ATF4 and CHOP (Harding *et al.,* 2000). ATF4 reprogrammes the translation landscape by activating privileged gene expression to promote homeostasis (Pakos-Zebrucka *et al.,* 2016). If the stress is prologued or unresolved, transition to a chronically activated ISR is widely reported as adaptive and ultimately pro-apoptotic when cells are unable to overcome it with pathological consequences (Bond *et al.,* 2020).

Previous work from our lab demonstrated that upon transient ER and oxidative stress, the acute ISR differentially modulates eIF2B body subpopulations, decreasing the GEF activity of larger bodies and inversely increasing GEF activity within small bodies in a manner dependent of levels of eIF2α-P (Hodgson *et al.,* 2019). This increase in GEF activity was concomitant with a redistribution of eIF2Bδ to small bodies, suggesting the existence of a previously unidentified eIF2Bγδε heterotrimeric sub-complex. ISR-targeting drugs (*e.g*. ISRIB) which boost translation, recapitulated this eIF2Bδ redistribution to small bodies in unstressed cells (Hodgson *et al.,* 2019), thus implying this action might be an innate response to the ISR to allow low baseline levels of translation to cope with cellular stress. The functional relevance of eIF2Bδ redistribution is still unknown. Furthermore, the impact of chronic ISR programme on eIF2B localisation remains to be addressed.

4.2. Hypothesis and rationale.

The main scientific aim of this chapter is to characterise the cellular stress responses of neuronal, astrocytic and oligodendrocytic cells during acute (or transient) and chronic induction of the ISR and its correlation with changes in eIF2B localisation. It is hypothesized that the ISR is upregulated in a cell-type specific manner which triggers cell-type specific changes to patterns of eIF2B localisation. To test this hypothesis, the following experimental objectives were employed:

- Quantify the induction magnitude of the acute and chronic ISR programmes across the cell types by western blot.
- Utilize a devised VWMD-mimicking stress protocol to determine different stress responses across cell types.
- Analyse the changes in abundance and eIF2Bδ composition upon different stress treatments by transient transfection, immunocytochemistry, and confocal imaging.

4.3. Results.

4.3.1. The acute ISR is heightened in neuronal cells compared to glial cells.

Upon various cellular stress stimuli, acute ISR is activated where eIF2α is phosphorylated at serine 51 (eIF2α-P[S51]), inhibiting eIF2B activity thus attenuating global protein synthesis (Pakos-Zebrucka *et al.,* 2016). Firstly, an acute ISR was activated in SH-SY5Y, U373 and MO3.13 cells using thapsigargin (Tg) and sodium arsenite (SA) as stress inducers. To quantify this response western blot analysis with antibodies against phosphorylated eIF2α and total eIF2α was carried out (**Figure 4.1. A**). Tg and SA are canonical ISR inducers, triggering ER stress and oxidative stress, respectively. Tg disrupts calcium levels from the ER triggering PERK-mediated phosphorylation of eIF2α, whilst SA induces reactive oxygen species (ROS) generation and activates HRI-mediated phosphorylation (see Introduction section 1.2.1.1.).

In the absence of stress, baseline levels of phosphorylated eIF2α are similarly low across all cell types (SH-SY5Y: 0.23 a.u ± 0.04, U373: 0.40 a.u ± 0.11, MO3.13: 0.25 a.u ± 0.03) (**Figure 4.1. B**). Upon treatment with Tg (1µM) for 1 h, SH-SY5Y exhibited a higher upregulation of eIF2α-P in comparison to U373 and MO3.13 cells (SH-SY5Y: 1.87 a.u ± 0.05, U373: 1.24 a.u ± 0.23, MO3.13: 1.16 a.u ± 0.05). Next, cells were treated with two different concentrations of SA for 30 minutes to induce mild (125µM) and high (500µM) oxidative stress. A mild SA exposure similarly upregulated eIF2α-P levels across cell types (SH-SY5Y: 1.75 a.u ± 0.66, U373: 1.23 a.u ± 0.51, MO3.13: 0.95 a.u ± 0.33), whilst a higher exposure to SA led to a statistically significant upregulated phosphorylation of eIF2α in SH-SY5Y cells in comparison to U373 and MO3.13 cells (SH-SY5Y: 4.72 a.u ± 0.91, U373: 1.63 a.u ± 0.26, MO3.13: 1.60 a.u ± 0.30). Taken together, these data indicate that neuronal cells have an upregulated acute ISR in comparison to astrocytes and oligodendrocytes, hence showing higher sensitivity to cellular stress.

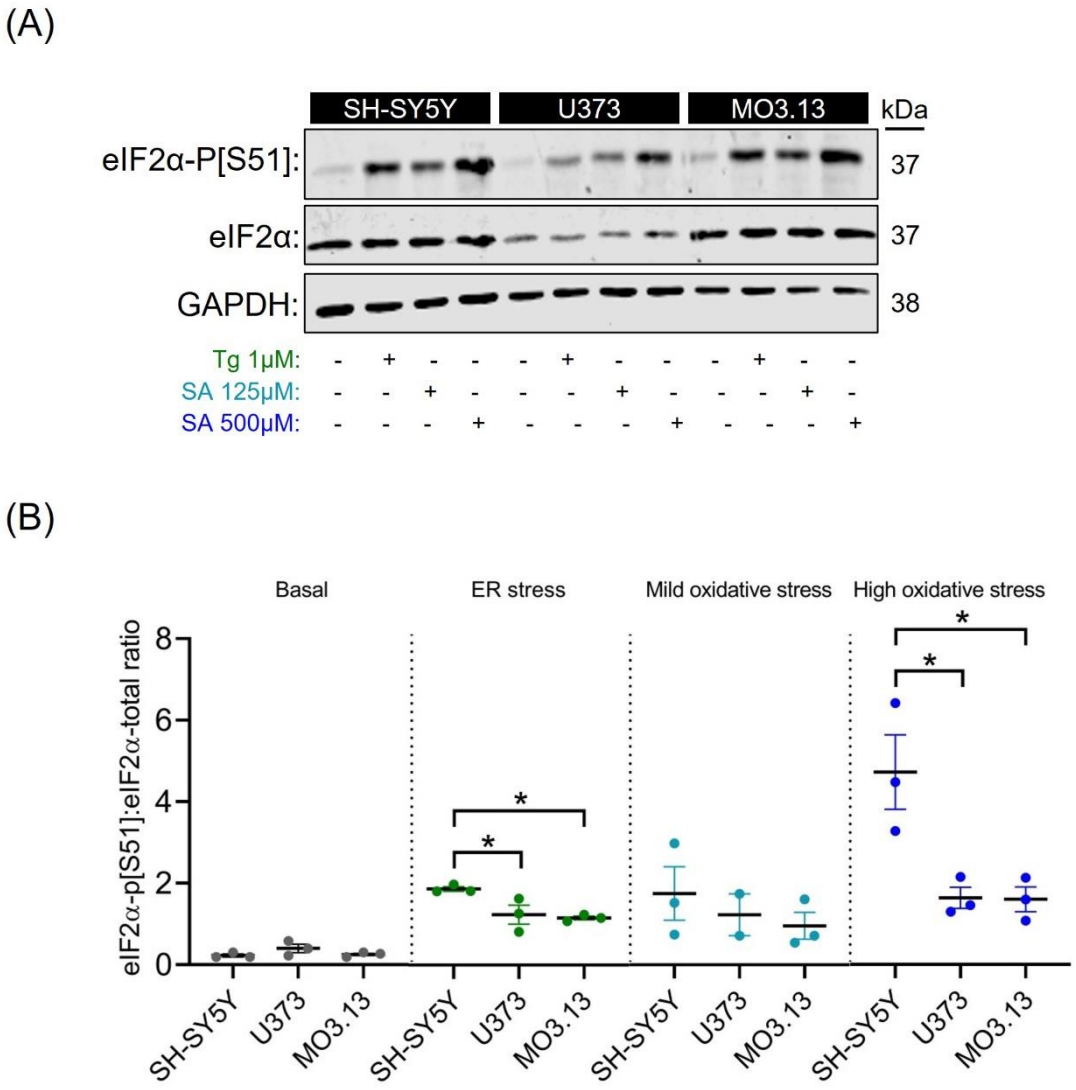

Figure 4.1.Neuronal cells have an upregulated ISR induction upon acute cellular stress.
(A) Western blot analysis of SH-SY5Y, U373 and MO3.13 cells after treatment with thapsigargin (Tg) (1 μM, 1h), mild sodium arsenite (SA) (125 μM, 0.5h) or high sodium arsenite (500 μM, 0.5h) and immunoblotted against phosphorylated eIF2α at serine 51 (eIF2α-p[S51]) and total eIF2α. GAPDH was used as loading control.
(B) Quantification of intensity levels of eIF2α-p[S51] normalised against total levels of eIF2α and analysed using one-way ANOVA followed by *post-hoc* Tukey's test. Error bars: ± s.e.m. (*N*=2-3). *ER stress:* Tg 1 μM 1h; *Mild oxidative stress:* 125 μM 0.5h; *High oxidative stress:* 500 μM 0.5h. **p*=0.0451 (ER stress, SH-SY5Y vs. U373); **p*=0.0281 (ER stress, SH-SY5Y vs. MO3.13); **p*=0.0213 (High oxidative stress, SH-SY5Y vs. U373); **p*=0.0203 (High oxidative stress, SH-SY5Y vs. MO3.13).

4.3.2. Chronic ER stress is protective against further ER stress insults.

Sustained exposure to unresolved cellular stress transitions the acute ISR program into a chronically activated ISR. This chronic ISR stimulates ATF4-mediated transcriptional reprogramming to allow cellular adaptation to sustained stress leading to: (a) dephosphorylation of eIF2α, and (b) recovery of protein synthesis. However, a chronic ISR can be tipped towards the expression of pro-apoptotic genes when cells are unable to overcome sustained stress with pathological consequences (Rutkowski *et al.,* 2006; Bond *et al.,* 2020; Ghaddar *et al.,* 2021). VWMD is associated with a chronically activated ISR mainly in astrocytes and myelinating oligodendrocytes (Dooves *et al.,* 2017; Abbink *et al.,* 2019; Wong *et al.,* 2019) wherein neurological deterioration occurs upon episodes of acute stress (*e.g.* head trauma, infections) (van der Knaap *et al.,* 2006). Taken together, this suggests that exposure of acute cellular stress, and therefore activation of the acute ISR program, are potentially detrimental to astrocytes and oligodendrocytes undergoing chronic ISR.

To test this hypothesis, a VWMD-mimicking environment was devised whereby cells exposed to chronic ER stress are subsequently challenged with an acute insult. To do that, cells were treated for 24h with Tg 300nM followed by a treatment with Tg 1µM in the last 1 h (Tg 24h + Tg last 1h). To properly assess the impact of an additional stress treatment on chronically preconditioned cells, the cells were also treated solely with either Tg 1µM for 1h (Tg 1h) or with Tg 300nM for 24h (Tg 24h) (**Figure 4.2.1. i**). Importantly, the terms of “acute” and “chronic” used throughout this thesis do not intend to fully recapitulate clinical timespans (**Figure 4.2.1. ii**).

(i)

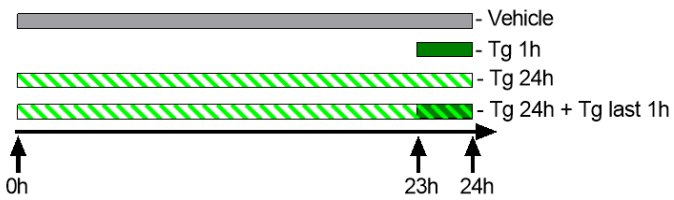

(ii)

	Acute	Chronic
Cell-based model	0.5-1h	24h
VWMD	Days/weeks	Months/years

Figure 4.2.1. VWMD-mimicking experimental setup: repeated stresses.
(i) Timeline indicates time of first Tg treatment (0h), second treatment (23h) and time of harvest (24h). **(ii)** Timespan of drug-induced stress treatment used in cell models in this thesis and clinical acute episodes (infections, fever) and chronic stress reported in VWMD.

Then, cells were subjected to (a) western blot analysis against phosphorylated eIF2α and total eIF2α (**Figure 4.2.2. A**), to quantify the induction of the ISR programme, and (b) puromycin incorporation assay (**Figure 4.2.2. B**), to quantify levels of global protein synthesis. Basal levels of eIF2α-P were similar across cell types (as also shown in **Figure 4.1.**) while MO3.13 cells showed higher basal global translation (Figure **4.2.2. C i**), hence the data was normalised to its respective vehicle sample given these cell-specific variations. Overall, all cell types displayed a similar trend of levels of eIF2α-P upon the aforementioned Tg treatments, although the significance of these changes was cell type specific (**Figure 4.2.2. C ii**). Tg for 1h robustly upregulated eIF2α-P in SH-SY5Y and MO3.13 cells, and a more modest upregulation in U373 cells in comparison their respective vehicle levels (SH-SY5Y: 3.67-fold ± 0.49; U373: 2.60-fold ± 0.86; MO3.13: 4.42-fold ± 0.59), confirming the induction of the acute ISR by ER stress. Next, levels of eIF2α-P significantly dropped at Tg 24h in SH-SY5Y and MO3.13 cells and more modestly in U373 cells (SH-SY5Y: 2.08-fold ± 0.28; U373: 2.07-fold ± 0.50; MO3.13: 2.71-fold ± 0.34), which is in line with the notion that dephosphorylation of eIF2α is observed upon chronic ISR (Pakos-Zebrucka *et al.,* 2016). Interestingly, an additional (acute) Tg treatment in the last 1h of a Tg 24h treatment did not significantly alter the levels of eIF2α-P (SH-SY5Y: 2.33-fold ± 0.33; U373: 2.14-fold ± 0.58; MO3.13: 2.89-fold ± 0.36). These data suggest that chronic ISR prevents further phosphorylation of eIF2α when confronted with a similar stressor.

Western blot analysis of puromycin incorporation with the same Tg treatments revealed a stronger trend between cell types regarding inhibition and recovery of translation (**Figure 4.2.2. C iii**). Tg for 1h significantly decreased translation in comparison to vehicle levels (SH-SY5Y: 0.14-fold ± 0.05; U373: 0.20-fold ± 0.06; MO3.13: 0.16-fold ± 0.09). When Tg was treated for 24h, translation levels showed significant recovery of translation as expected (SH-SY5Y: 0.68-fold ± 0.10; U373: 0.42-fold ± 0.05; MO3.13: 0.56-fold ± 0.11). However, an additional Tg treatment in the last 1h did not further alter levels of translation (SH-SY5Y: 0.58-fold ± 0.07; U373: 0.42-fold ± 0.06; MO3.13: 0.46-fold ± 0.12). Thus, chronic ISR primes cells to be unresponsive to additional similar cellular stress.

Altogether, these data conclude that chronic ISR may play a ubiquitous protective role against a repeated stress insult.

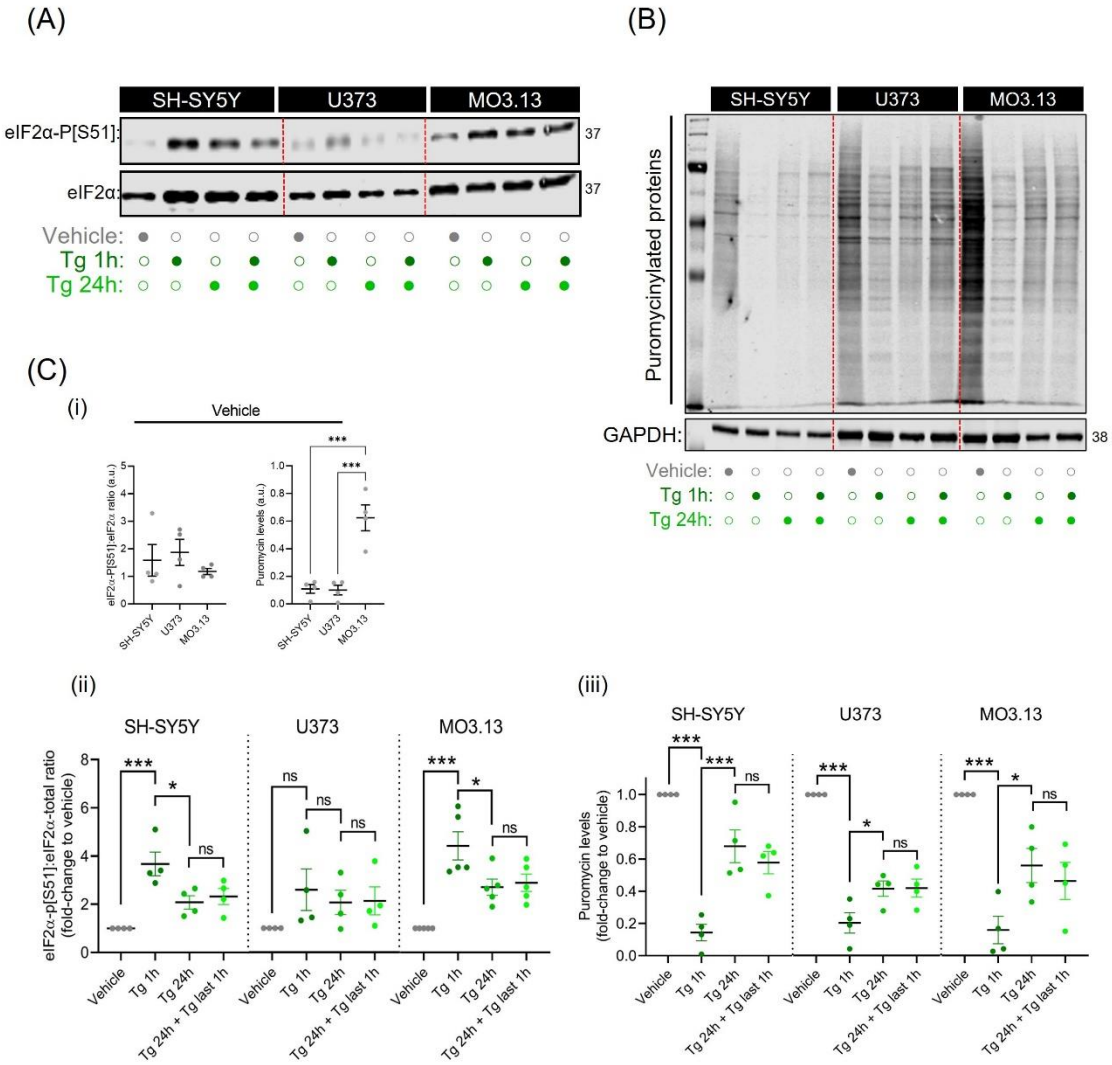

Figure 4.2.2. Protein synthesis levels shows recovery upon chronic ER stress and remains unchanged when challenged with a subsequent acute ER stress treatment.
SH-SY5Y, U373 and MO3.13 cells were treated with acute thapsigargin (Tg) for 1h (1 μM), mild Tg for 24h (300 nM) or with mild Tg for 24h with an additional acute Tg in the last 1 hour (300 nM 24h + 1 μM last 1h). DMSO for 24h was used as vehicle control.
(A) Western blot analysis of SH-SY5Y, U373 and MO3.13 cells immunoblotted against eIF2α-p[S51] and total eIF2α.
(B) Western blot analysis of SH-SY5Y, U373 and MO3.13 cells subjected to puromycin incorporation assay. GAPDH levels were used as loading control. **(C) (i)** Quantification of intensity levels of eIF2α-p[S51] normalised against total levels of eIF2α and analysed using one-way ANOVA followed by *post-hoc* Tukey's. Data is presented as fold-change levels of eIF2α-p[S51]:total-eIF2α ratio in comparison to vehicle levels. Error bars: ± s.e.m. (*N*=4-5).SH-SY5Y: ***p=0.0004, *p=0.0222; MO3.13: ***p<0.0001; *p=0.0273; *ns*, non-significant. **(ii)** Quantification of intensity levels of puromycinylated proteins normalised against GAPDH levels and analysed using one-way ANOVA followed by *post-hoc* Tukey's test. Data is presented as fold-change levels of puromycin:GAPDH ratio in comparison to vehicle levels. Error bars: ± s.e.m. (*N*=4). SH-SY5Y: ***p<0.0001 (Vehicle vs. Tg 1h), ***p=0.0005 (Tg 1h vs. Tg 24h); U373: ***p<0.0001, *p=0.0404; MO3.13: ***p=0.0001; *p=0.0348; *ns*, non-significant.

4.3.3. Differential GADD34-mediated recovery within neuronal and glial cells.

A chronic ISR induction is characterized by ATF4-mediated expression of GADD34, which dephosphorylates eIF2α-P and promotes expression of downstream ISR effectors such as CHOP (see Introduction section 1.2.1.3.).

To confirm that ATF4 expression took place before the 24h time point of cell harvest, ATF4 levels in SH-SY5Y, U373 and MO3.13 cells were monitored over time. Cells were treated with Tg (300nM) for 1h, 4h, 8h and 24h and western blot analysis of ATF4 was carried out (**Figure 4.3**). ATF4 levels peaked at 4h, 1h and 8h after Tg treatment for SH-SY5Y, U373 and MO3.13 cells, respectively, and was undetected after 24h treatment.

Expression of GADD34 and CHOP across the three cell types were next examined (**Figure 4.3**). SH-SY5Y cells showed a heightened expression of GADD34 at 8h following and decreased at 24h, which correlated to a decrease of eIF2α-P and was also proportional to CHOP induction. Interestingly, GADD34 levels remained elevated at 24h in U373 cells which correlated to the absence of eIF2α dephosphorylation. In MO3.13 cells, GADD34 also remained elevated at 24h, although eIF2α dephosphorylation took place ~4h of Tg treatment, yet it correlated with increased CHOP expression.

Taken together, these findings may indicate that GADD34 feedback loop is faster in neuronal cells, and controls eIF2α dephosphorylation and CHOP expression in a cell-type manner.

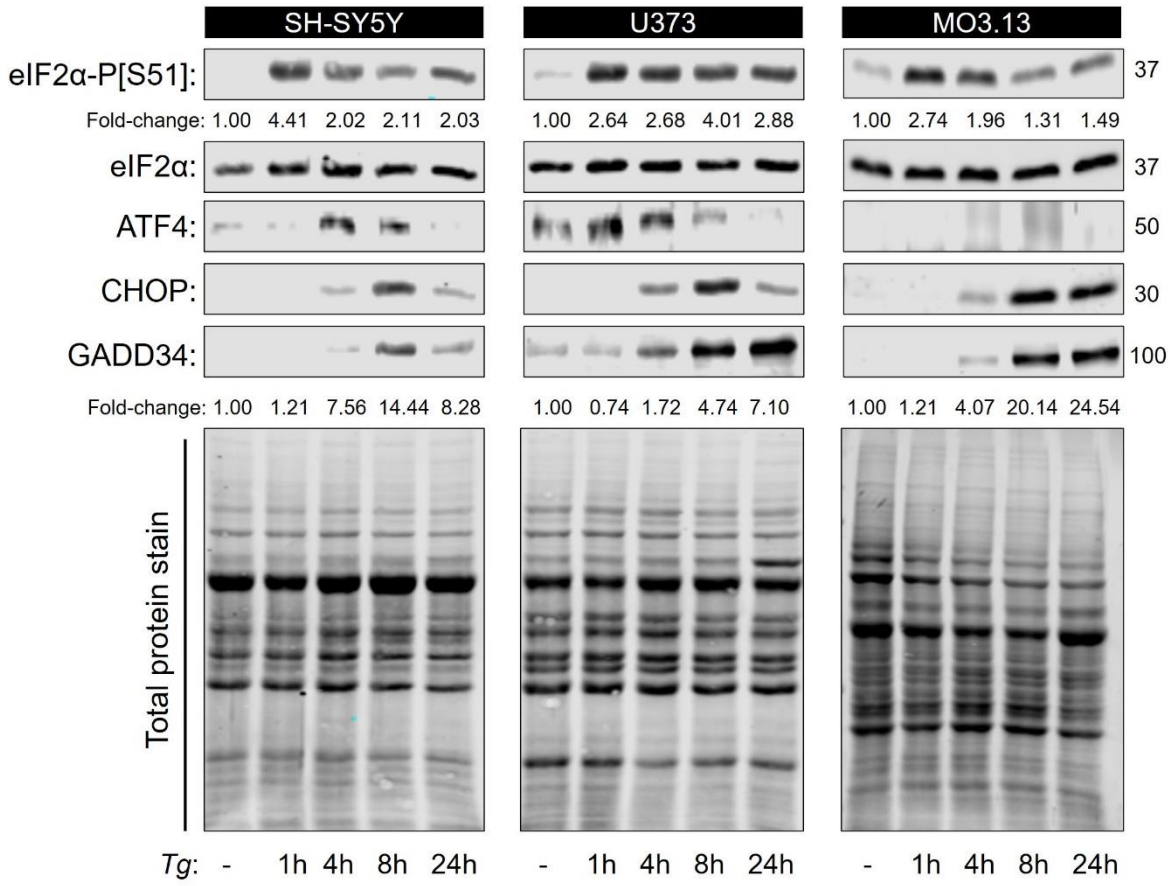

Figure 4.3. GADD34 feedback loop during chronic ER stress is faster in neuronal cells. Western blot analysis of SH-SY5Y, U373 and MO3.13 cells after treatment with Tg (300 nM) for 0h (untreated; "-"), 1h, 4h, 8h and 24h and immunoblotted against eIF2α-P[S51], total eIF2α, and ISR markers ATF4, CHOP and GADD34. Fold-enrichment of eIF2α-P[S51]:total-eIF2α and GADD34:total protein ratios in comparison to untreated levels are labelled below respective blots.

4.3.4. Primary human astrocytes exhibit a similar ISR profile pattern to U373 cells.

U373 cells exhibited a somewhat weak upregulation of eIF2α-P after treatment with Tg 1h and non-significant differences when further exposed to prologued ER stress treatment (Tg 1h *vs.* Tg 24h) (**Figure 4.2. C i**). To confirm that these findings are specific to astrocytes, given that SH-SY5Y and MO3.13 cells exhibited significant differences amongst the different Tg conditions (**Figure 4.2. C i**), primary human astrocytes (HA) were subjected to the Tg treatments as described in section 4.2. Western blot analysis against phosphorylated eIF2α and total eIF2α, and puromycin incorporation assay was then carried out (**Figure 4.4. A**).

Following the treatments, HA cells displayed a significantly upregulation of eIF2α-P when treated with Tg 1h alone in comparison to vehicle levels (8.884-fold ± 0.999) (**Figure 4.4. B i**). Upon treatment with Tg 24h, levels of eIF2α-P remained elevated (11.950-fold ± 0.827) while an additional Tg treatment in the last 1h of a 24h pre-treatment displayed non-significant changes to both Tg 1h and Tg 24h alone (13.940-fold ± 2.822) (**Figure 4.4. B i**). Puromycin incorporation assay revealed that an acute Tg 1h treatment significantly suppressed levels of protein synthesis when compared to vehicle levels (0.199-fold ± 0.062) (**Figure 4.4. B ii**) while protein synthesis levels upon Tg 24h treatment displayed slight recovery (0.430-fold ± 0.072) albeit without statistically significance (p=0.1239). When the cells were treated with an additional Tg treatment for the last 1 h of the 24h chronic treatment similar translation levels to Tg 24h alone were observed (**Figure 4.4. B i**).

Taken together, despite a more robust upregulation of the acute ISR in primary astrocytes in comparison to U373 cells (**Figure 4.2. C i**), astrocytes do not exhibit significant dephosphorylation of eIF2α when transitioning to a chronic ISR although recovery of translation is observed.

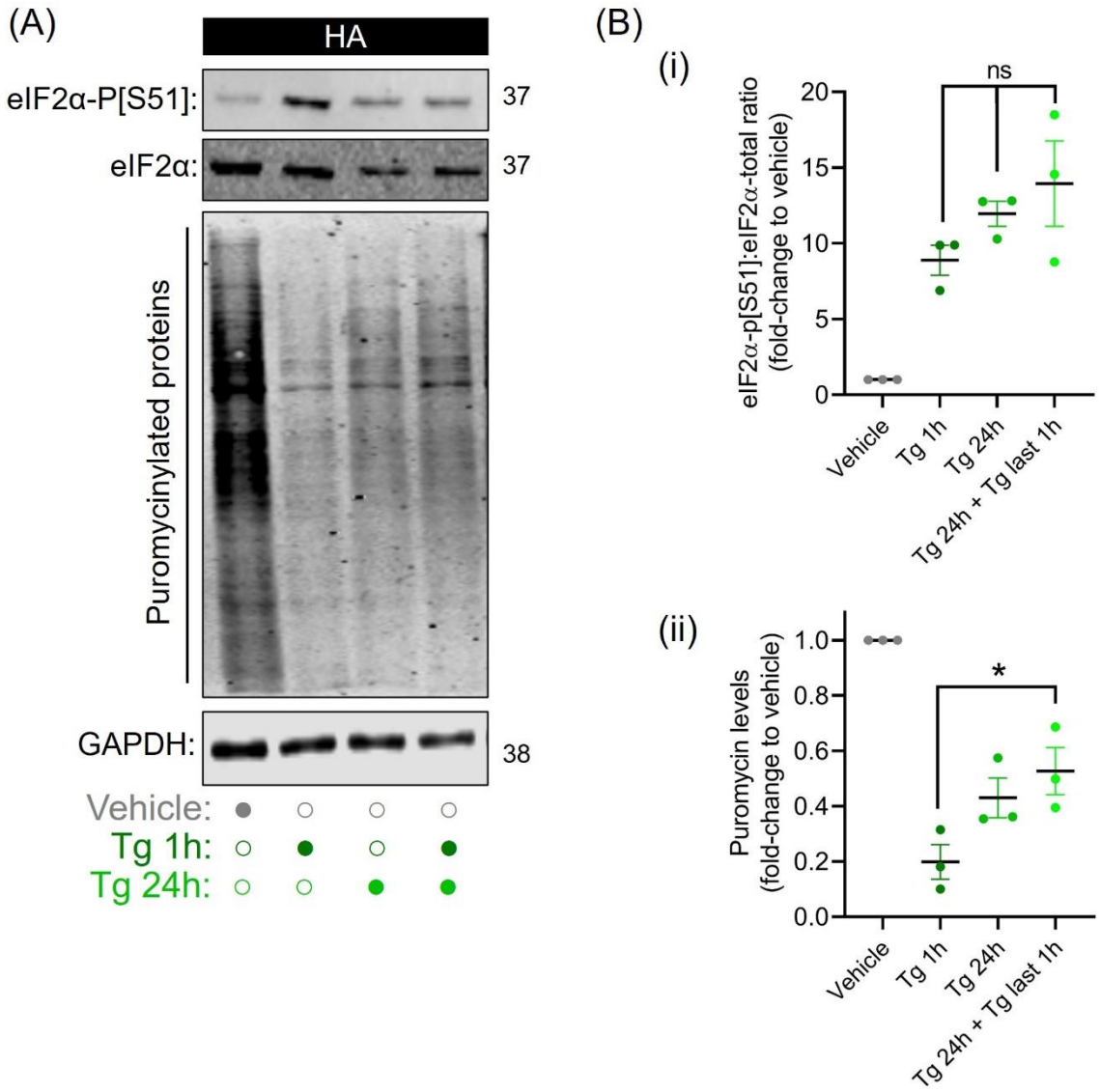

Figure 4.4. Protein synthesis levels shows recovery upon chronic ER stress and remains unchanged when challenged with a subsequent acute ER stress treatment in human primary astrocytes.
Human primary astrocytes (HA) cells were treated with acute thapsigargin (Tg) for 1h (1 μM), mild Tg for 24h (300 nM) or with mild Tg for 24h with an additional acute Tg in the last 1 hour (300 nM 24h + 1 μM last 1h). DMSO for 24h was used as vehicle control. **(A)** Western blot analysis of HA cells immunoblotted against eIF2α-p[S51] and total eIF2α. **(B)** Western blot analysis of HA cells subjected to puromycin incorporation assay. GAPDH levels were used as loading control. **(C**) **(i)** Quantification of intensity levels of eIF2α-p[S51] normalised against total levels of eIF2α and analysed using one-way ANOVA followed by *post-hoc* Tukey's test. Data is presented as fold-change levels of eIF2α-p[S51]:total-eIF2α ratio in comparison to vehicle levels. Error bars: ± s.e.m. (*N*=3). *ns*, non-significant. **(ii)** Quantification of intensity levels of puromycinylated proteins normalised against GAPDH levels and analysed using one-way ANOVA followed by *post-hoc* Tukey's test. Data is presented as fold-change levels of puromycin:GAPDH ratio in comparison to vehicle levels. Error bars: ± s.e.m. (*N*=3). **p*=0.0278.

4.3.5. The acute ISR is reset upon a different stressor during chronic ISR in a cell-type specific manner.

Having shown that a chronic ISR induction can protect cells from repeated stress insult (**Figure 4.2.2.**), it was questioned whether this preconditioning remains protective with a different ISR stressor as the second insult. To test this hypothesis, SH-SY5Y, U373 and MO3.13 were treated with Tg (300nM) for 24 h and then treated with SA (125µM) for the last 30 minutes (Tg 24h + SA last 0.5h). As control, cells were also treated solely with either 125µM SA for 30 minutes (SA 0.5h) or with 300nM Tg for 24h (Tg 24h) (**Figure 4.5.1.**).

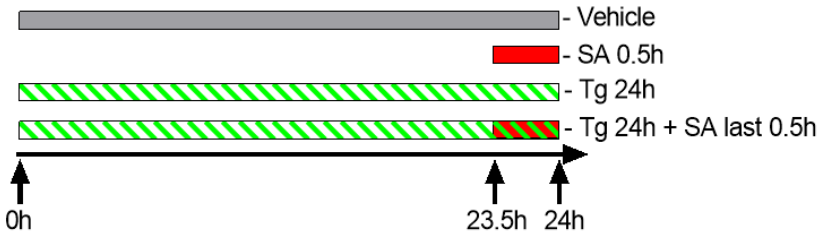

Figure 4.5.1. VWMD-mimicking experimental setup: alternative stresses. Timeline indicates time of first Tg treatment (0h), second treatment (23h) and time of harvest (24h).

Cell extracts were then subjected to (a) western blot analysis against phosphorylated eIF2α and total eIF2α (**Figure 4.5.2. A**), to quantify the induction degree of the ISR programme; and (b) puromycin incorporation assay (**Figure 4.5.2. B**), to quantify levels of global protein synthesis.

Overall, SA alone for 30min significantly increased eIF2α-P in comparison to vehicle levels (SH-SY5Y: 7.713-fold ± 1.212; U373: 8.311-fold ± 1.553; MO3.13: 5.382-fold ± 0.544) (**Figure 4.5.2. C i**), which marked the acute ISR induced by oxidative stress as expected (Pakos-Zebrucka *et al.,* 2016). Surprisingly, preconditioning cells to Tg showed cell-specific disparities in levels of eIF2α-P (**Figure 4.5.2. C i**). In SH-SY5Y cells, an additional SA treatment did not significantly upregulated eIF2α-P when compared to the Tg 24h alone (Tg 24h: 4.098-fold ± 0.354; Tg + SA: 4.392-fold ± 0.435). However, a significant increase of eIF2α-P was observed in U373 (Tg 24h: 3.767-fold ± 0.328; Tg + SA: 8.311-fold ± 1.553) and MO3.13 cells (Tg 24h: 3.360-fold ± 0.503; Tg + SA: 5.382-fold

± 0.544). Thus, chronic ISR primes cells to be unresponsive in the presence of a different stressor in a cell-specific manner.

Interestingly, analysis of puromycin incorporation assays did not reveal cell-specific differences in levels of translation (**Figure 4.5.2. C ii**). An initial SA treatment robustly suppressed translation in all cell types (SH-SY5Y: 0.294-fold ± 0.101; U373: 0.317-fold ± 0.057; MO3.13: 0.197-fold ± 0.038) and this decrease was similarly observed in cells pre-conditioned with Tg (SH-SY5Y: 0.294-fold ± 0.101; U373: 0.2331-fold ± 0.033; MO3.13: 0.180 ± 0.064).

These data imply that suppression of protein synthesis during chronic ISR is uncoupled from eIF2α-P when confronted with an alternative stressor in neuronal cells. In contrast, astrocytes and oligodendrocytes reset an acute-like ISR by being able to upregulate eIF2α-P and inhibiting translation in the presence of chronic ISR.

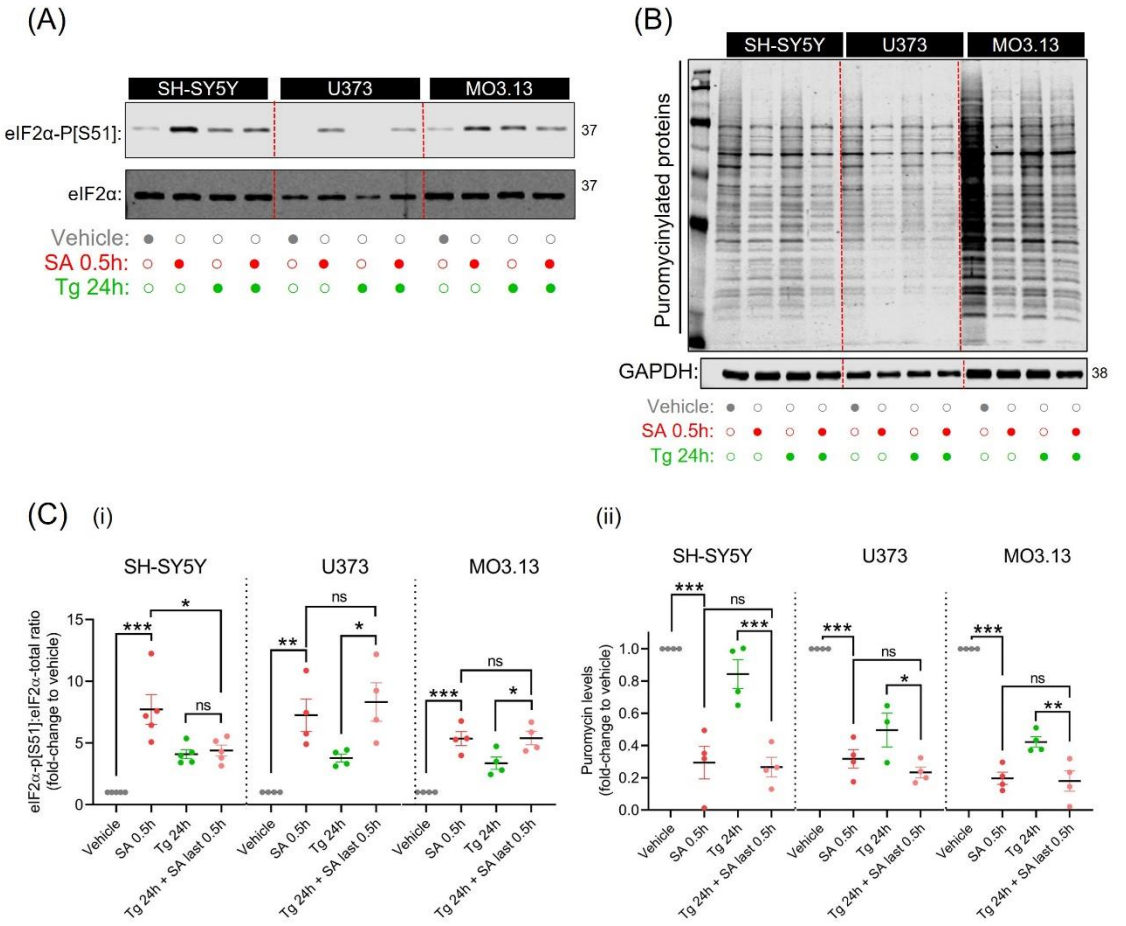

Figure 4.5.2. A subsequent mild oxidative stress treatment to chronically ER stressed cells further increase eIF2α-P in a cell-type manner and suppresses protein synthesis.
SH-SY5Y, U373 and MO3.13 cells were treated with mild oxidative stress (SA) for 0.5h (125μM), mild Tg for 24h (300nM) or with mild Tg for 24h with an additional mild oxidative stress in the last 0.5 hour (300nM 24h + 125μM last 0.5h). DMSO for 24h was used as vehicle control.
(A) Western blot analysis of SH-SY5Y, U373 and MO3.13 cells immunoblotted against eIF2α-p[S51] and total eIF2α.
(B) Western blot analysis of SH-SY5Y, U373 and MO3.13 cells subjected to puromycin incorporation assay. GAPDH levels were used as loading control.
(C) (i) Quantification of intensity levels of eIF2α-p[S51] normalised against total levels of eIF2α and analysed using one-way ANOVA followed by *post-hoc* Tukey's test. Data is presented as fold-change levels of eIF2α-p[S51]:total-eIF2α ratio in comparison to vehicle levels. Error bars: ± s.e.m. (*N*=4-5). SH-SY5Y: ***p<0.0001, *p=0.0137; U373: **p=0.0051, *p=0.0388; MO3.13: ***p=0.0001; *p=0.0425; ns, non-significant. **(ii)** Quantification of intensity levels of puromycinylated proteins normalised against GAPDH levels and analysed using one-way ANOVA followed by *post-hoc* Tukey's test. Data is presented as fold-change levels of puromycin:GAPDH ratio in comparison to vehicle levels. Error bars: ± s.e.m. (*N*=3-4).SH-SY5Y: ***p<0.0001 (Vehicle vs. SA), ***p=0.0007 (Tg vs. Tg + SA); U373: ***p<0.0001, *p=0.0305; MO3.13: ***p<0.0001, **p=0.0054; *ns*, non-significant.

4.3.6. Inhibition of translation by the ISR is partially eIF2α-independent in a cell-type manner.

In the previous section, strong suppression of translation despite a significant absence of elevated eIF2α-P was observed in SH-SY5Y cells (**Figure 4.5. C**). These data imply that inhibition of protein synthesis under this specific stress environment (chronic ER stress + oxidative stress) may be independent from eIF2α. To test this hypothesis, cells were treated with ISR inhibitor ISRIB (**Figure 4.6. A**). ISRIB stabilizes the eIF2B decamer and reverses the inhibitory effects downstream of eIF2α-P (Sidrauksi *et al.,* 2013). Hence, upon ISRIB treatment an expected restoration of protein synthesis should be observed if cells are dependent on the eIF2α-axis of translation control.

Western blotting against eIF2α-P and total eIF2α was performed on SH-SY5Y, U373 and MO3.13 and showed that ISRIB did not alter stress-induced induction of phosphorylated eIF2α (**Figure 4.6. B**). Cells were also subjected to puromycin incorporation assay to investigate rates of translation (**Figure 4.6. B**). Western blot analysis of puromycinylated proteins of SH-SY5Y cells revealed that ISRIB was unable to fully restore translation to control levels (p=0.0116) in SH-SY5Y cells. In contrast to SH-SY5Y cells, ISRIB treatment fully recovered translation in U373 and MO3.13 cells to control levels (U373: 1.003-fold ± 0.119; MO3.13: 1.037-fold ± 0.190).

Taken together, translation control upon chronic ISR (chronic ER stress) in neuronal cells further challenged with an oxidative stress is partially eIF2α-independent, while glial cells remain eIF2α-dependent.

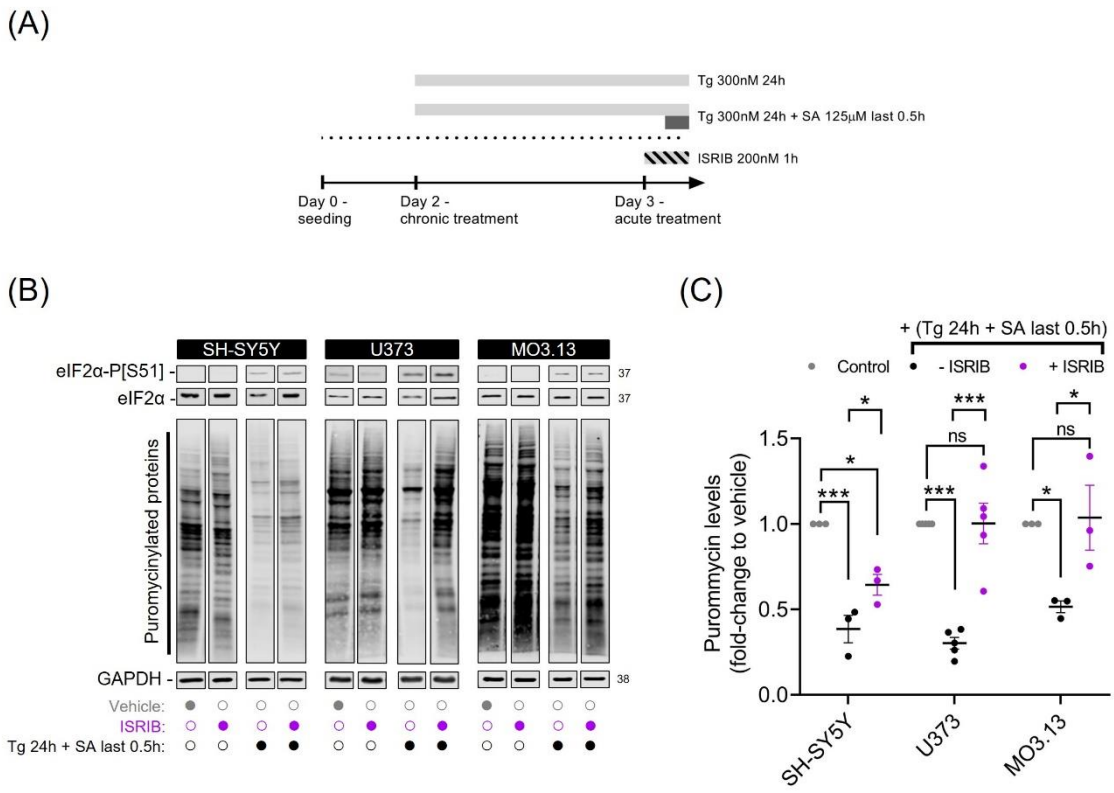

Figure 4.6. Inhibition of protein synthesis of chronically ER stressed neuronal cells challenged with an additional mild oxidative stress treatment is partially eIF2α-independent.
(A) SH-SY5Y, U373 and MO3.13 cells were treated with mild Tg for 24h with an additional mild oxidative stress in the last 0.5 hour (300 nM 24h + 125 μM last 0.5h). Cells were additionally treated with or without ISRIB (200 nM) in the last 1h of treatment. DMSO for 24h was used as vehicle control.
(B) Western blot analysis of SH-SY5Y, U373 and MO3.13 cells immunoblotted against eIF2α-p[S51] and total eIF2α. Cells were also subjected to puromycin incorporation assay. GAPDH levels were used as loading control. **(C)** Quantification of intensity levels of puromycinylated proteins normalised against GAPDH levels and analysed using one-way ANOVA followed by post-hoc Tukey's test. Data is presented as fold-change levels of puromycin:GAPDH ratio in comparison to vehicle levels. Error bars: ± s.e.m. (*N*=3-4).; SH-SY5Y: ***p=0.0007, *p=0.0116 (control vs. +ISRIB); *p=0.0452 (-ISRIB vs. +ISRIB); U373: ***p<0.0001; MO3.13: *p=0.0491 (control vs. -ISRIB), *p=0.0370 (-ISRIB vs. +ISRIB); *ns*, non-significant.

4.3.7. eIF2B localisation increases upon induction of the ISR in a cell-type manner.

Efficient eIF2B activity is at the core of the ISR by dictating the fate of the acute ISR: decreased eIF2B activity initiates the acute ISR and is terminated upon restoration of eIF2B activity, allowing recovery of protein synthesis (Pakos-Zebrucka *et al.,* 2016). In yeast models, eIF2B localisation is suggested to play a role during acute cellular stress albeit with conflicting results. While some studies show that eIF2B bodies are not present during unstressed conditions but are rather stress-induced entities (Moon & Parker, 2018a; Nüske *et al.,* 2020), others demonstrate eIF2B bodies as a steady-state feature further stimulated upon cellular stress (Norris *et al.,* 2021). Our lab has previously shown that mammalian cells also display eIF2B bodies and the abundance and composition of eIF2B bodies are modulated upon induction of the acute ISR (Hodgson *et al.,* 2019). The role of eIF2B localisation during chronic ISR remains to be addressed.

The impact of acute and chronic ISR on eIF2B localisation therefore next examined. Treatments as described in sections **4.3.2.** and **4.3.5.** were used to induce the acute ISR (Tg 1h, SA 0.5h) and chronic ISR (Tg 24h, Tg 24h + Tg last 1h, Tg 24h + SA last 0.5h). To observe eIF2B bodies, SH-SY5Y, U373 and MO3.13 cells were transiently transfected with eIF2Bε-mGFP, treated with the above-mentioned conditions, and subjected to immunofluorescence analysis to quantify the % of cells displaying localised eIF2B (**Figure 4.7.**).

In SH-SY5Y cells, acute induction of the ISR showed no significant differences in eIF2B localisation upon acute Tg and SA treatment (Tg 1h: 23.67% ± 4.70; SA 0.5h: 26.33% ± 1.76). However, Tg 24h + SA last 0.5h treatment, SH-SY5Y cells displayed a significant increase of cells harbouring eIF2B bodies (46.00% ± 6.81) in comparison to the vehicle % (22.00% ± 2.08).

U373 cells displayed an overall higher sensitivity in stimulating eIF2B localisation upon cellular stress. Induction of the acute ISR significantly increased % cells harbouring eIF2B bodies via oxidative stress (SA 0.5h: 68.67% ± 1.86) as did ER stress (Tg 1h: 59.67% ± 3.84), despite the latter showed statistical non significance. Similar increases in the % cells containing eIF2B bodies were also observed during chronic treatments (Tg 24h: 66.67% ± 1.86; Tg 24h+ Tg last 1h:

66.00% ± 0.58; Tg 24h + SA last 0.5h: 79.33% ± 2.19) in comparison to vehicle levels (48.33% ± 5.78).

MO3.13 cells showed a general increase of % cells containing eIF2B bodies across both acute and chronic treatments (Tg 1h: 29.00% ± 1.53; SA 0.5h: 32.00% ± 1.53; Tg 24h: 30.33% ± 3.48; Tg 24h + Tg last 1h: 33.00% ± 4.51; Tg 24h + SA last 0.5h: 35.00% ± 4.73) in comparison to vehicle % (20.33% ± 1.45), despite only the combinational condition of Tg 24h + SA last 0.5h exhibited statistical significance.

Taken together, these findings indicate that cellular eIF2B localisation is enhanced predominantly upon chronic ISR in neuronal and oligodendrocytic cells, while astrocytic cells exhibited a higher degree of eIF2B localisation in both acute and chronic ISR.

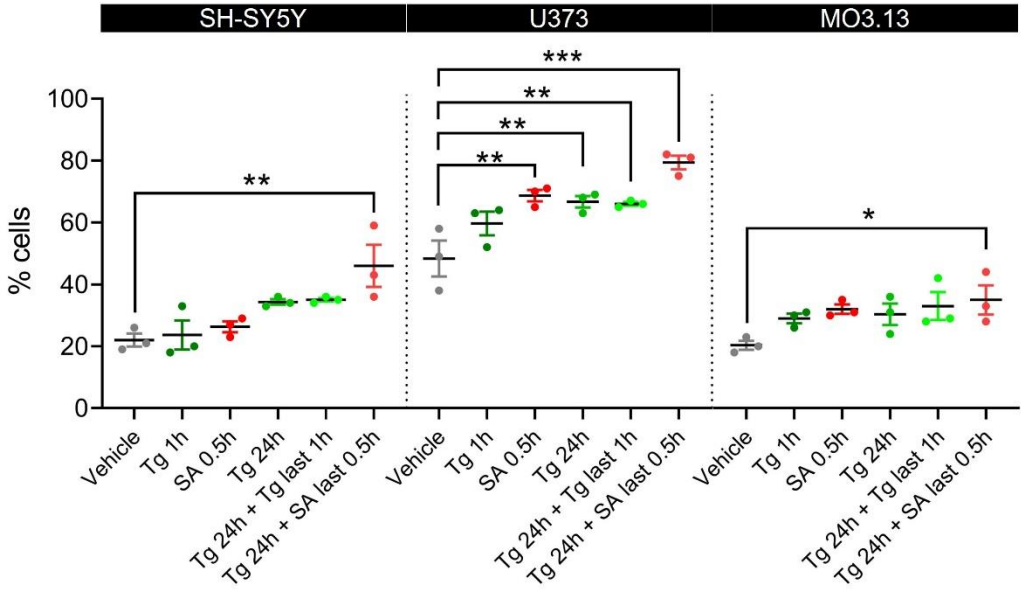

Figure 4.7. eIF2B localisation increases during cellular stress in a cell-type manner. SH-SY5Y, U373 and MO3.13 cells after treatment with acute cellular stress (Tg 1 μM 1h; SA 125 μM 0.5h), chronic cellular stress (Tg 300 nM 24h) or chronic cellular stress followed by a subsequent acute treatment (Tg 300 nM 24h + Tg 1 μM last 1h/SA 125 μM last 0.5h). DMSO for 24h was used as vehicle control. Percentage (%) of cells transiently transfected with eIF2Bε-mGFP and expressing eIF2B bodies and analysed using one-way ANOVA followed by *post-hoc* Tukey's test. Error bars: ± s.e.m. (*N*=3). SH-SY5Y: ***p*=0.0020; U373: **p=0.0028 (SA 0.5h), ***p*= 0.0061 (Tg 24h), ***p*= 0.0079 (Tg 24h + Tg last 1h), ****p*<0.0001; MO3.13: **p*=0.0276.

4.3.8. The sub-population profile of eIF2B bodies changes during cellular stress in a cell-type manner.

eIF2B bodies are divided into two sub-populations based on size termed small and large bodies, with different compositional make-up and sensitivity to stress (Hodgson *et al.,* 2019). Here, the number of small and large eIF2B bodies during different stress conditions was investigated. During acute Tg and SA treatment, SH-SY5Y cells displayed an increase of the number of small eIF2B bodies in comparison to vehicle (Tg 1h: 1.279-fold; SA 0.5h: 1.943-fold), albeit only statistically significant for the latter stress (**Figure 4.8. A**). Upon the chronic ISR stress treatments (Tg 24h, Tg 24h + Tg last 1h, Tg 24h + SA last 0.5h), the number of small eIF2B bodies were similar to vehicle levels (**Figure 4.8. A**). Surprisingly, U373 and MO3.13 cells showed only minor changes to the number of small eIF2B bodies with no statistical significance (**Figure 4.8. A**). Moreover, large eIF2B bodies in all cell types showed either minor (and nonsignificant) or highly variable changes in their abundance upon acute and chronic cellular stress (**Figure 4.8. B**).

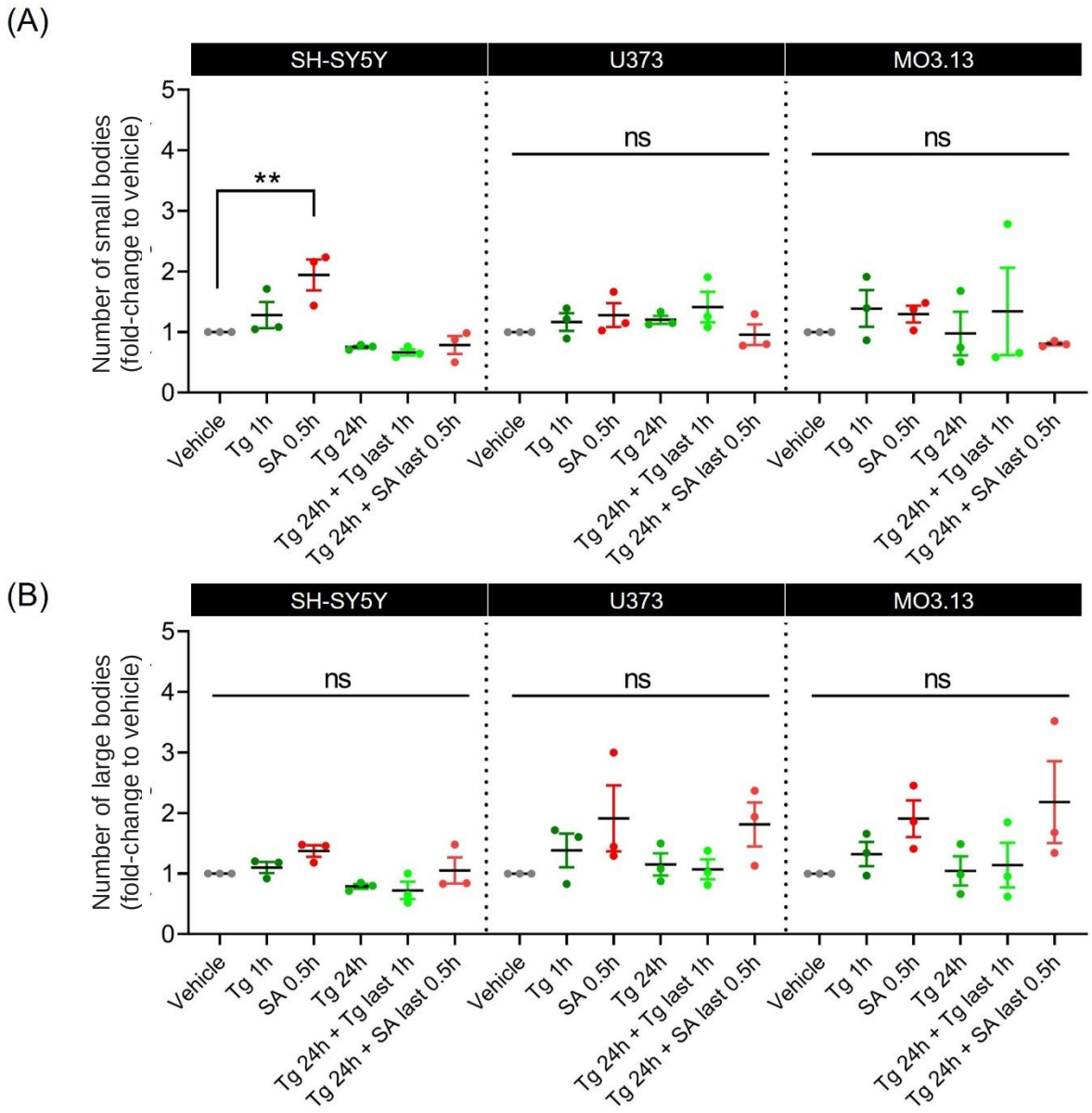

Figure 4.8. The abundance of eIF2B bodies is impacted during cellular stress in a cell-type manner.
SH-SY5Y, U373 and MO3.13 cells were transiently transfected with eIF2Bε-mGP and treated with acute cellular stress (Tg 1 μM 1h; SA 125 μM 0.5h), chronic cellular stress (Tg 300 nM 24h) or chronic cellular stress followed by a subsequent acute stress treatment (Tg 300 nM 24h + Tg 1 μM last 1h/SA 125 μM last 0.5h). DMSO for 24h was used as vehicle control. Number of **(A)** small eIF2B bodies and **(B)** large eIF2B bodies were quantified manually and analysed using one-way ANOVA followed by *post-hoc* Tukey's test. Error bars: ± s.e.m. (*N*=3). ***p*=0.0034; *ns*, non-significant.

4.3.9. Remodelling of eIF2Bδ composition of small eIF2B bodies is a general cellular feature during the acute ISR.

The regulatory composition of small eIF2B bodies is remodelled upon induction of the first ISR programme in astrocytes (Hodgson *et al.,* 2019). More specifically, eIF2Bδ localisation is increased in small eIF2B bodies whilst large eIF2B bodies remain unchanged. These previous findings suggest that eIF2Bδ redistribution of eIF2B bodies plays a role in the acute ISR although its functional relevance is still elusive. Whether this feature is recapitulated in other mammalian cell types also remains unknown. Furthermore, whether this compositional remodelling is maintained upon transition to a chronic ISR programme is unknown.

To address these aims, SH-SY5Y, U373 and MO3.13 cells were transiently transfected with eIF2Bε-mGFP and subjected to stress conditions as previously outlined. Immunofluorescence analysis with a specific eIF2Bδ antibody (**Figure 4.9. A**) showed a significant fold-change increase of % small eIF2B bodies co-localising with α-eIF2Bδ upon Tg 1h treatment across all cell types in comparison to the vehicle control (SH-SY5Y: 1.863-fold ± 0.206; U373: 1.680-fold ± 0.207; MO3.13: 1.808-fold ± 0.296) (**Figure 4.9. B i**). This implies that eIF2Bδ redistribution upon induction of the acute ISR is a general cellular feature.

Upon chronic stress, no significant differences to vehicle levels of % small bodies co-localising with α-eIF2Bδ was observed for all cell lines (SH-SY5Y: 0.808-fold ± 0.111; U373: 1.129-fold ± 0.068; MO3.13: 0.993-fold ± 0.160) (**Figure 4.9. B i**), suggesting the acute-induced redistribution of eIF2Bδ localisation to small bodies is reversed upon transition to a chronic ISR. Furthermore, a subsequent acute Tg treatment (Tg last 1h) to preconditioned cells did not impact the % small bodies co-localising with α-eIF2Bδ (SH-SY5Y: 0.838-fold ± 0.208; U373: 0.824-fold ± 0.139; MO3.13: 0.814-fold ± 0.067) (**Figure 4.9. B i**), suggesting that an ongoing chronic ISR buffers the acute-induced redistribution of eIF2Bδ upon repeated stress.

Overall, the % of large eIF2B bodies co-localising with α-eIF2Bδ remained unchanged upon all stress treatments (**Figure 4.9. B ii**), implying that small bodies are selectively targeted for regulatory remodelling upon acute induction of the ISR.

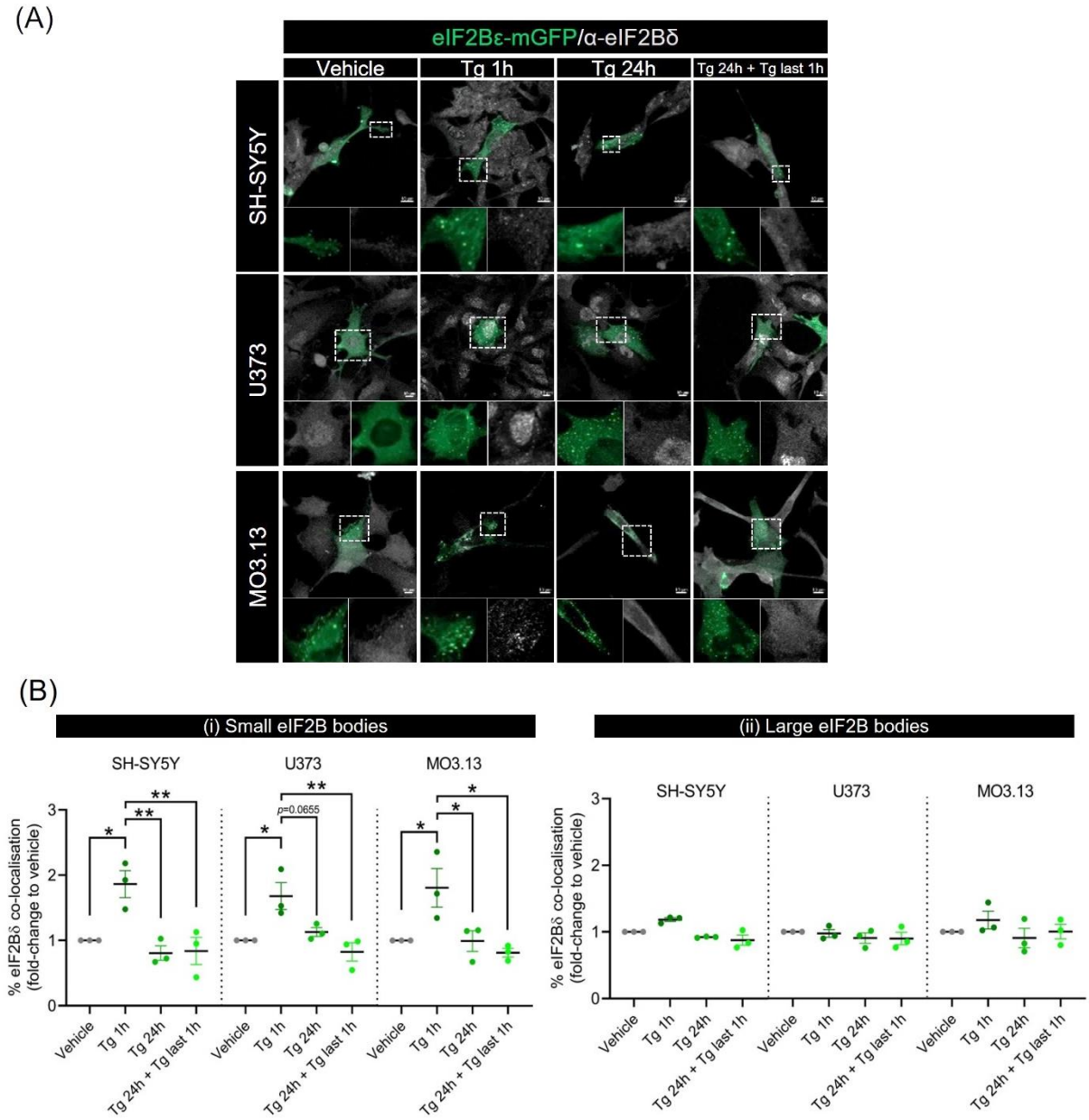

Figure 4.9. Remodelling of eIF2Bδ localisation of small eIF2B bodies is transient during ER stress and unchanged when challenged with a subsequent acute ER stress treatment. **(A)** Representative images of SH-SY5Y, U373 and MO3.13 cells transiently transfected with eIF2Bε-mGFP and immunostained with an antibody against α-eIF2Bδ. Cells were treated with acute thapsigargin (Tg) for 1h (1 μM), mild Tg for 24h (300 nM) or with mild Tg for 24h with an additional acute Tg in the last 1 hour (300 nM 24h + 1 μM last 1h). DMSO for 24h was used as vehicle control. Scale bar: 10μm.
(B) Mean percentage of **(i)** small and **(ii)** large eIF2Bε-mGFP bodies displaying co-localisation with α-eIF2Bδ cytoplasmic foci was quantified manually and analysed in a population of 30 cells per replicate using one-way ANOVA followed by *post-hoc* Tukey's test for multiple comparisons. Data is presented as the fold-change relative to vehicle-treated cells. SH-SY5Y: ***p*=0.0061 (Tg 1h vs. Tg 24h), ***p*=0.0072 (Tg 1h vs. Tg 24h+Tg last 1h), **p*=0.0189; U373: ***p*=0.0069, **p*=0.0245; MO3.13: **p*=0.0419 (vehicle vs. Tg 1h), **p*=0.0401 (Tg 1h vs. Tg 24h), **p*=0.0147 (Tg 1h vs. Tg 24h+Tg last 1h).

4.3.10. eIF2Bδ composition of small eIF2B bodies is increased during chronic ISR in a cell-type manner.

eIF2Bδ remodelling of small eIF2B bodies is suggested to be a ubiquitous feature of the acute ISR, whilst transition to a chronic ISR reverses this redistribution to unstressed levels and further insults with similar stresses did not redistribute eIF2Bδ. However, chronically stressed cells exposed to an alternative acute stress triggered cell-type specific induction of eIF2α-P. Therefore, it was tested whether this would also mirror cell-type specific eIF2Bδ remodelling of small eIF2B bodies.

SH-SY5Y, U373 and MO3.13 cells were transiently transfected with eIF2Bε-mGFP and subjected to SA treatment alone for 30 minutes (SA 0.5h), inducing the acute ISR, or added at the last 30 minutes of a 24h treatment of Tg (Tg 24h + SA last 0.5h). Immunofluorescence analysis with a specific eIF2Bδ antibody (**Figure 4.10. A**) showed that SA 0.5h treatment led to a fold-change increase of % small bodies co-localising with α-eIF2Bδ in comparison to vehicle % in all cell types (**Figure 4.10. B i**). Interesting for SH-SY5Y cells treated with Tg 24h + SA last 0.5h, no significant increase in the % of small bodies co-localising with α-eIF2Bδ. In contrast, U373 and MO3.13 cells treated with Tg 24h + SA last 0.5h exhibited similar fold-change increase of % small bodies co-localising with α-eIF2Bδ to levels of SA-only treatment. Finally, the % of large eIF2B bodies co-localising with α-eIF2Bδ showed no significant fold-change differences to vehicle %, for any stress treatment (**Figure 4.10. B ii**).

Taken together, chronic ER stress impairs the neuronal response of remodelling the regulatory composition of small eIF2B bodies upon exposure to transient oxidative stress. In parallel, chronically ER stressed glial cells retain the ability of inducing eIF2Bδ redistribution when confronted with oxidative stress.

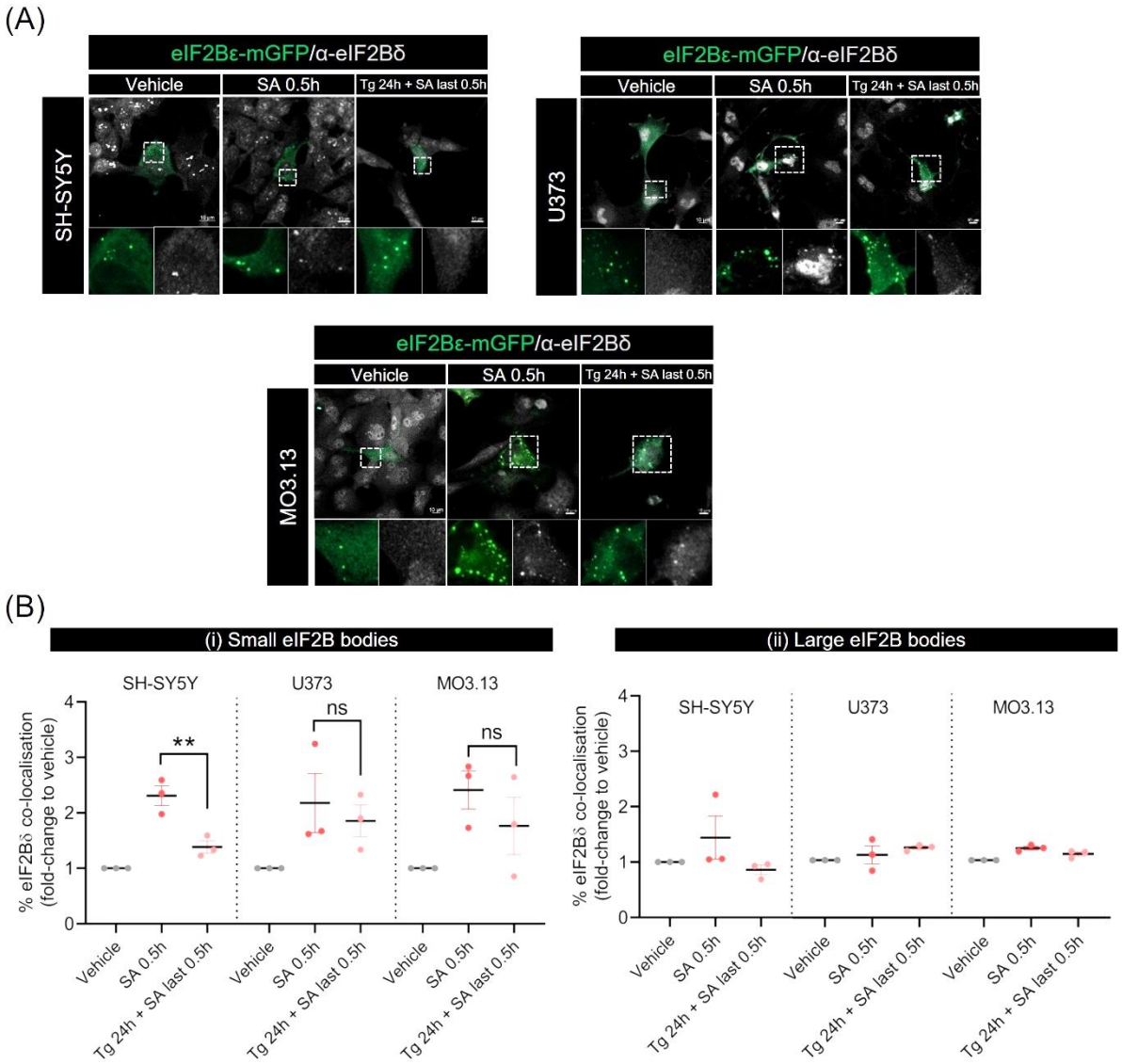

Figure 4.10. A subsequent oxidative stress on chronically ER stressed cells remodel eIF2Bδ localisation of small eIF2B bodies in a cell-type manner.
(A) Representative images of SH-SY5Y, U373 and MO3.13 cells transiently transfected with eIF2Bε-mGFP and immunostained with an antibody against α-eIF2Bδ. Cells were treated with acute sodium arsenite (SA) for 0.5h (125μM), mild Tg for 24h (300nM) or with mild Tg for 24h with an additional acute SA in the last 0.5 hour (300nM 24h + 125μM last 0.5h). DMSO for 24h was used as vehicle control. Scale bar: 10μm. **(B)** Mean percentage of **(i)** small and **(ii)** large eIF2Bε-mGFP bodies displaying co-localisation with α-eIF2Bδ cytoplasmic foci was quantified manually and analysed in a population of 30 cells per replicate using one-way ANOVA followed by *post-hoc* Tukey's test for multiple comparisons. Data is presented as the fold-change relative to vehicle-treated cells. ***p*=0.0039; ns, non-significant.

4.3.11. Regulatory remodelling of small eIF2B bodies is partially dictated by eIF2α-P.

Induction of the acute ISR selectively targets the eIF2Bδ composition of small eIF2B bodies. However, it remains unknown what directly triggers this movement of eIF2Bδ into small eIF2B bodies. eIF2α-P acts as the initial ISR signal. Thus, eIF2α-P could play an additional role of regulating the composition of eIF2B bodies. To test this hypothesis, cells were treated with Tg for 1h in the presence or absence of GSK2606414, a potent inhibitor of eIF2α kinase PERK (PERKi), thus blocking eIF2α-P in the presence of ER stress.

Western blot analysis of the eIF2α-P levels and puromycin incorporation assay of SH-SY5Y, U373 and MO3.13 cells confirmed the inhibitory effects of PERKi in the presence of Tg (**Figure 4.11. A**). Tg alone elevated levels of eIF2α-P and inhibited translation. Co-treatment of Tg and PERKi completely blocked eIF2 phosphorylation and protein synthesis rates remained at control levels. Next, immunofluorescence analysis was carried out using an eIF2Bδ antibody in cells transiently expressing eIF2Bε-mGFP under the previously described Tg and PERKi conditions (**Figure 4.11. B**).

While Tg treatment showed an increase of small bodies co-localising with α-eIF2Bδ compared to vehicle, the presence of PERKi diminished the effect of Tg in SH-SY5Y and U373 cells (**Figure 4.11. C**). However, this effect did not normalise eIF2Bδ localisation to vehicle levels. Furthermore, the effect of PERKi was modest in Tg-treated MO3.13 cells and showed no statistical significance (**Figure 4.11. C**). In contrast, eIF2Bδ localisation in large eIF2B bodies were unchanged in all described conditions (**Figure 4.11. C**).

Taken together, these data indicate that eIF2Bδ localisation to small eIF2B bodies is partially dictated by eIF2α-P in a cell-type specific manner.

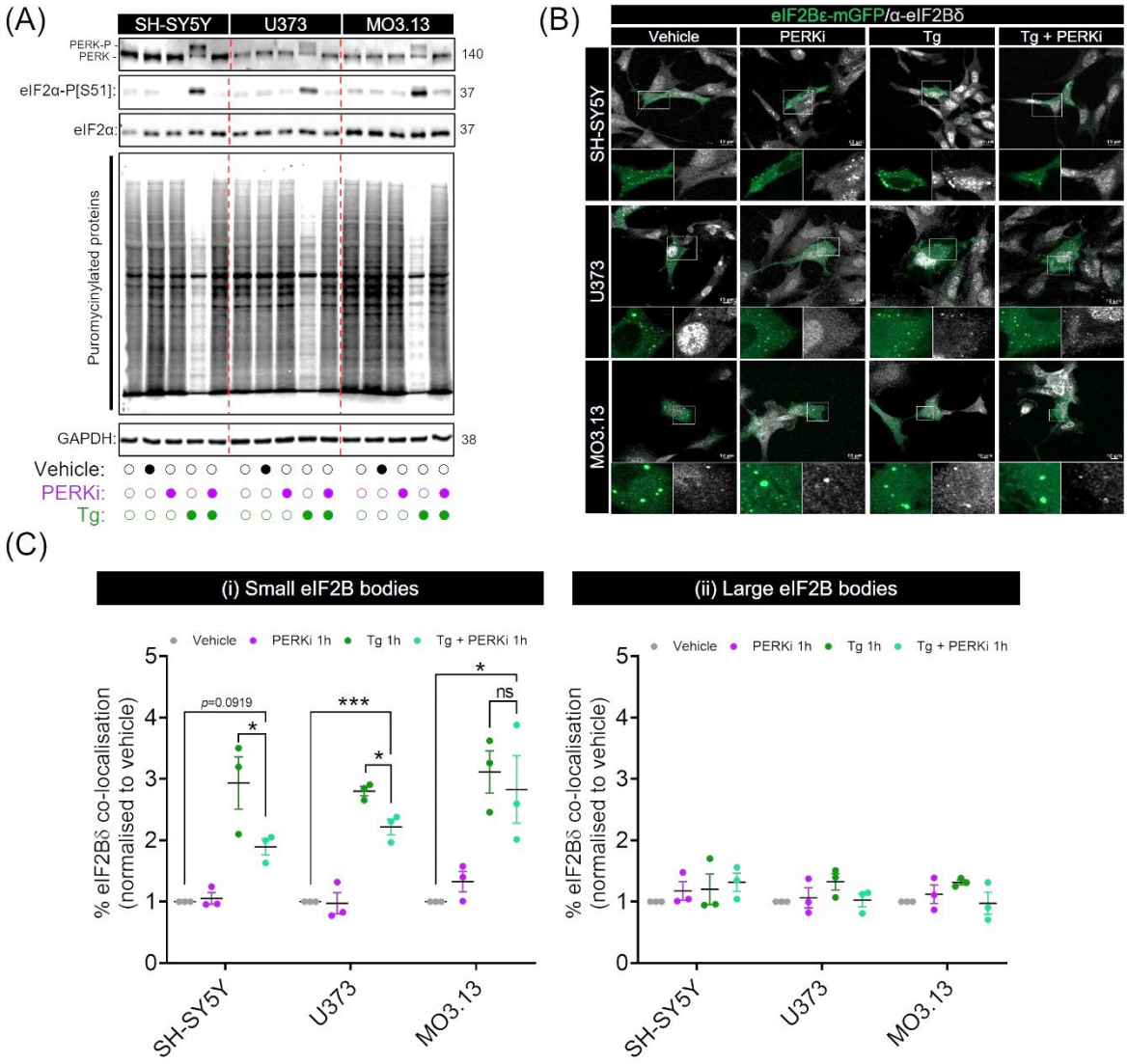

Figure 4.11. eIF2Bδ remodelling of small eIF2B bodies is partially dictated by levels of eIF2α-P in a cell-type manner.
SH-SY5Y, U373 and MO3.13 cells were treated with GSK2606414 (PERKi) (500 nM), Tg (1 μM) or co-treated with PERKi and Tg for 1 h. DMSO for 1h was used as vehicle control.
(A) Western blot analysis of cells immunoblotted against total PERK (phospho-PERK and pan-PERK), eIF2α-p[S51] and total eIF2α (top panels). Western blot analysis of cells subjected to puromycin incorporation assay (bottom panels). GAPDH levels were used as loading control.
(B) Confocal images of cells transiently expressing eIF2Bε-mGFP and immunolabelled with primary anti-eIF2Bδ subjected to treatment conditions as described previously. Scale bar: 10μm.
(C) Mean % of **(i)** small eIF2B bodies and **(ii)** large eIF2B bodies displaying co-localisation with α-eIF2Bδ antibody signal was quantified manually in 30 cells per biological repeat and analysed using one-way ANOVA followed by *post-hoc* Tukey's test. Data is presented as fold-enrichment of % eIF2Bδ co-localisation in comparison to vehicle levels. Error bars: ± s.e.m. (*N*=3). ***p=0.0003; *p=0.0484 (SH-SY5Y); *p=0.0277 (U373); *p=0.0201 (MO3.13); *ns*, non-significant.

4.4. Discussion.

eIF2B localisation has been implicated during the activation of the acute ISR (Hodgson *et al.,* 2019). It was demonstrated that eIF2Bδ composition is selectively increased in small eIF2B bodies in astrocytes, however the functional relevance of this cellular feature is vastly unknown. The role of eIF2B GEF activity during acute translation inhibition is well-known (Pakos-Zebrucka *et al.,* 2016), however the role of eIF2B during a chronic action of the ISR is still poorly understood. Deciphering these mechanisms would provide insights into the novel roles of eIF2B during cellular stress scenarios relevant to ISR-related diseases. In Chapter 3, a cell-type specific pattern of eIF2B localisation during unstressed conditions was reported. For this chapter, the impact of acute and chronic ISR programmes on eIF2B localisation will be investigated in neuronal, astrocytic and oligodendrocytic cells.

4.4.1. Insights into cell-type specific induction of the acute ISR.

The acute ISR was firstly characterised to further investigate its impact on eIF2B localisation. The data in this chapter exhibited the expected increased phosphorylation of eIF2α when treated with canonical ISR stressors (Tg, SA), indeed confirming the induction of the acute ISR (**Figure 4.1.**); however, neuronal cells have an upregulated acute ISR when compared to astrocytic and oligodendrocytic cells (**Figure 4.1.**). Hodgson *et al.* demonstrated that the activity of eIF2B bodies is regulated in a manner dependent of levels of eIF2α-P wherein the shuttling of eIF2 is enhanced in small eIF2B bodies upon a narrow range of eIF2α-P but can be inversely reduced upon robust induction of the acute ISR (Hodgson *et al.,* 2019). This impact of cellular stress on the activity of eIF2B bodies is further discussed in Chapter 5. However, it brings an important question about what is the functional relevance of a cell-type specific induction of acute ISR programmes? Surprisingly, despite an enhanced acute ISR in neuronal cells, protein synthesis levels are observed to be similarly suppressed across the cell types (**Figure 4.2.2.** and **Figure 4.5.2.**), which implies that this neuronal-specific magnitude of ISR induction could play additional roles in stress coping beyond inhibition of bulk translation. It is plausible to speculate that an upregulated ISR programme serves as a cue for neuron-specific proteins regulated by eIF2α-P. A

detailed list of such proteins has been reviewed elsewhere (Chesnokova *et al.,* 2017), wherein only a minority have been examined for their role during cellular stress (e.g., BACE1 (O'Connor *et al.,* 2008)() while eIF2α-P-dependent mRNA translation of proteins involved in synaptic plasticity is more well-known (Di Prisco *et al.,* 2014; Ma *et al.,* 2013; Ramos-Fernández *et al.,* 2016).

4.4.2. The acute ISR is dynamically 'switched on' during chronic ISR.

A sustained induction of the ISR has been extensively implicated with pathological consequences. The data presented here shows the ability of cells to re-fire the acute ISR following chronic ISR depending on whether cells are faced with repeated stresses or treated with a different stressor. An initial chronic ER stress was protective towards a second ER stress treatment (**Figure 4.2.2.**). This has been shown by others where preconditioning cells to mild eIF2α-P, either through inhibition of PP1c (Yadav *et al.,* 2017) or stress-inducing agents (Lu *et al.,* 2004), has been shown to be cytoprotective. Strikingly, replacing the second insult with an oxidative stress reset the ISR and elevated eIF2α-P in glial cells whilst neuronal cells showed little impact (**Figure 4.5.2.**). Our observations were additionally strengthened by the fact that ISRIB (which reverses inhibitory effects of eIF2α-P) was unable to restore translation under these stress conditions (chronic Tg + acute SA), but not when treated with Tg alone for 24h, in neuronal cells (**Figure 4.6.**). This provides supporting evidence that chronically ER stressed neurons redirect towards an eIF2α-independent mechanism only when exposed to oxidative stress. These results are quite unexpected given that GADD34 expression levels are still elevated in these cells (**Figure 4.3.**), as GADD34 mRNA levels are known to serve as a molecular memory damper to subsequent stresses (Batjargal *et al.,* 2022; Klein *et al.,* 2022; Shelkovnikova *et al.,* 2017). This apparent ability of (at least) glial cells to 'reset' the ISR in the presence of GADD34 while neuronal cells seem to "forget" how to respond brings an important question: was it even meant to be remembered? Given this lack of a subsequent ISR induction in neuronal cells four possible reasons are considered albeit not mutually exclusive:

(1) The transition to a chronic ISR signals neurons to its inability to trigger adaptation through the ISR solely, hence shifting towards alternative and/or

parallel signalling pathways (e.g., mTOR (Guan *et al.,* 2014; Terenzio *et al.,* 2018), eIF2A (Kim *et al.,* 2011), eIF3d (Guan *et al.,* 2017), or eEF1A2 (Mendoza *et al.,* 2021)). Indeed, this notion of translational control plasticity in neurons is strikingly evident by the ability to ensure ER stress resolution even upon PERK deficiency (Wolzak *et al.,* 2022).

(2) Secondly, acute ISR in neurons may be triggered by cell non-autonomous mechanisms, supported by recent work where targeting PERK-eIF2α axis of astrocytes rescues prion-causing neuronal dysfunction (Smith *et al.,* 2020).

(3) Thirdly, neuronal cells may not require continuous rounds of ISR programs to resolve stress damage to some extent (Kole *et al.,* 2013), so it could be that a single activation of the ISR, even if sustained into a chronic state, is sufficient for adaptive homeostasis.

(4) Finally, multiple eIF2α kinases might be activated during neuronal chronic ER stress, thus less susceptible to fire an acute ISR when subsequently challenged with a different stressor, whereas in glial cells activation of eIF2α kinases is limited to a specific stimulus. This notion of 'kinase redundancy' was first reported in *S. pombe* by Zhan *et al.* where prolonged exposure to oxidative stress triggered both Hri2p (HRI) and Gcn2p (GCN2) (Zhan *et al.,* 2004). Indeed, ER stress resolution through the canonical PERK-eIF2α axis can be shifted to a secondary HRI-eIF2α mechanism coupled with tRNA modulation to inhibit translation in neurons, while astrocytes are exclusively dependent on PERK activity (Wolzak *et al.,* 2022). Moreover, despite the well-studied role of GCN2 in amino acid depletion and proteasomal stress (Pakos-Zebrucka, 2016), neurons preferentially inhibit translation upon proteasome inhibition by enhancing HRI expression (Alvarez-Castelao *et al.,* 2020).

On a side note, the notion of ISR 'exhaustion' has also been recently appreciated where translational-demanding cell types (in this study being pancreatic β cells as their cell model) are susceptible to ATF4-mediated transcriptome decay when faced with frequent ER stress insults (Chen *et al.,* 2022). Further independent studies on the sensitivity of different cell types to continuous rounds of stress would be extremely relevant in disease context. Nonetheless, the data presented in this chapter provides evidence of glial-specific recurrent ISR episodes when exposed to different ISR-triggering stressors.

4.4.3. eIF2Bδ localisation is remodelled in a temporal manner during cellular stress and VWMD-mimicking conditions.

The ISR-induced movement of eIF2Bδ to small bodies implies that compositional remodelling of eIF2B bodies may play a functional role during the ISR. Key questions remain to be addressed: is eIF2Bδ redistribution of small bodies observed in other cell types? And is this stress-induced feature of eIF2B localisation specific to the acute ISR? Accordingly, the data in this chapter demonstrates that eIF2Bδ localisation is increased to small eIF2B bodies during acute Tg and SA treatments in all three cell types (**Figure 4.9.** and **Figure 4.10.**), thus a general cellular feature of the acute ISR programme. At 24h of Tg treatment, this re-localisation of eIF2Bδ remains at levels observed in unstressed levels in all cell types (**Figure 4.9.**). This suggests that eIF2Bδ remodelling of small eIF2B bodies occurred pre-24h of Tg treatment, hence transient and may not be necessary upon the chronic ISR. Guan *et al* recently provided evidence that recovery of eIF2B activity is not required upon transition to a chronically activated ISR and may be alternatively mediated via eIF3 (Guan *et al.,* 2017). Although the activity of eIF2B bodies were not characterised in this chapter (further discussed in Chapter 5), it strengthens the notion that eIF2B localisation may play an additional role in the adaption from acute to chronic ISR acts.

Interestingly, an acute SA treatment to following chronically ER stressed cells displayed cell-type specific features of eIF2Bδ distribution to small eIF2B bodies (**Figure 4.10.**). Indeed, increased eIF2Bδ composition is observed in small bodies in astrocytic and oligodendrocytic cells, whilst neuronal cells remain largely unaffected. Moreover, this compositional remodelling of small bodies is again accompanied by increased levels of eIF2α-P in glial cells, suggesting a crossover between both cellular inputs (further discussed in 4.4.5). taken together these data suggest that eIF2Bδ remodelling of small eIF2B bodies are an integrative component of the acute ISR and may facilitate the transition to chronic stress, which requires further examination. Moreover, these data may provide more insightful evidence towards the VWMD glial-sensitive pathology. The second acute stress treatment to chronically stressed cells aimed to provide a cell-based platform to recapitulate VWMD. Here, glial cells are observed to selectively trigger a novel acute ISR, which includes eIF2Bδ redistribution of small

bodies, while neuronal cells redirect alternative mechanisms (as discussed in 4.4.2.). It is therefore an attractive possibility and suggests that eIF2B localisation during specific stress(es) could provide a better understanding of the relationship between mutational landscape and disease severity (Hamilton *et al.,* 2018).

4.4.4. Insights into potential cell-type specific eIF2B subcomplex arrangements during cellular stress.

It was previously reported that eIF2Bδ localisation is increased in small eIF2B bodies upon induction of the acute ISR, in astrocytic cells (Hodgson *et al.,* 2019). These data entail that, given the predominantly catalytic composition of astrocytic small bodies, the localisation of a novel subcomplex containing the ε, γ and δ subunits (eIF2B(γδε)) resides at these foci upon ISR activation. This eIF2B subcomplex failed to be identified by native mass spectrometry (MS) (Wortham *et al.,* 2014), arguably because it was not analysed during ISR stimulation. However, its existence is not discarded given that application of high collision energy to disrupt the eIF2B(βδγε) tetramer led to the dissociation of eIF2Bβ but not eIF2Bδ from the complex (Wortham *et al.,* 2014), suggesting that eIF2Bδ can interact with the eIF2B(γε) dimer in the absence of eIF2Bβ. Native MS analysis of eIF2B complexes during cellular stress could provide further insight into the identification of an eIF2B(γδε) sub-complex. The data in this chapter recapitulated the stress-induced eIF2Bδ phenotype observed by (Hodgson *et al.,* 2019) in astrocytic cells, which now has been expanded to neuronal and oligodendrocytic cells (**Figure 4.9.**). For the latter, an increased eIF2Bδ localisation strengthens the existence of an eIF2B(γδε) sub-complex given its compositional make-up of small eIF2B bodies being like astrocytic cells. However, the fact that neuronal cells follow this trend is rather intriguing. In chapter 3 of this thesis, the basal regulatory composition (including eIF2Bδ) of neuronal small eIF2B bodies is increased when compared to glial cells (**Figure 3.5.**), hence potentially containing a wider variety of eIF2B sub-complexes (dimers, tetramers and decamers); whilst glial cells predominantly harbour catalytic eIF2B(γε) dimers. Given the increased basal eIF2Bδ make-up of neuronal small bodies, it led to the theory that these bodies were primed for stress. Strikingly, eIF2Bδ localisation of neuronal small bodies is further

increased upon acute ISR stimulation (**Figure 4.9.** and **Figure 4.10.**). An intriguing question is whether selectively enhancing eIF2Bδ composition then signals the assembly of eIF2B(γδε), given that is not identified in unstressed cells (Wortham *et al.,* 2014), and/or whether the already elevated regulatory composition of neuronal small bodies is not indicative of tetramer and/or decamer localising at these foci? Further studies with pulldown assays and size-exclusion chromatography would be instrumental to decipher the validity of these models. It is also noteworthy that it cannot be ruled out whether eIF2Bδ redistribution is accompanied with increased eIF2Bα and eIF2Bβ localisation to neuronal small bodies as it was not quantified in this study. If these other subunits are present, then this suggests that decameric eIF2B predominantly resides at both small and large eIF2B bodies thus providing a pool of stress-sensitive sub-complexes for more robust repression of GEF activity at these sites. These hypothetical models will be tested on Chapter 5.

Another key question that remains unaddressed is the kinetics of eIF2B(γδε) sub-complex formation. It remains unknown whether eIF2B(γδε) is firstly formed and then assembled as small eIF2B bodies, or the existence of eIF2Bδ movement to pre-assembled small eIF2B bodies. To answer these questions future experiments could focus on live cell imaging using GFP-tagged eIF2Bδ to track its assembly and/or movement alongside tagged eIF2Bε to mark ε-containing small bodies. However, the data presented here strengthens the assembly model given that the number of neuronal small eIF2B bodies significantly increases during the acute ISR and at a lower magnitude in astrocytes and oligodendrocytes (**Figure 4.8.**).

4.4.5. Remodelling of eIF2Bδ localisation involves non-ISR mechanisms.

The data in this chapter and previous studies (Hodgson *et al.,* 2019) shows that eIF2Bδ localisation to small eIF2B bodies during the ISR correlates with increased levels of eIF2α-P. However, from data presented in this chapter these two events may be mutually exclusive to a certain degree (**Figure 4.11.**). When cells were treated with PERKi in the presence of ER stress, inhibition of eIF2α-P did not fully prevent eIF2Bδ redistribution to small eIF2B bodies and these changes were cell-specific. ISR stressors have obvious adversities by triggering multiple pathways that can influence our observations. Tg in addition to activating the ISR can also induce ROS-related mechanisms at least in liver and neuronal cells (Li & Hu, 2015; Wink *et al.,* 2017). Recently, "stress-free" virtual activation of eIF2α sensors is sufficient to prompt the acute-to-chronic temporal phases of the ISR (Batjargal *et al.,* 2022); nonetheless, a faultless ISR may rely on other cascade of mechanisms within specific time windows, which would not be recapitulated with "stress-free" approaches. The crossover between the ISR and the non-ISR branches of the unfolded protein response (XBP1 splicing, ATF6) occurs, where the ISR regulates non-ISR transcriptional programs and signalling magnitude (Majumder *et al.,* 2012; Teske *et al.,* 2011). Underlying UPR-mediated feedback control of the ISR has been vastly unappreciated. More importantly, given that ER stress-induced eIF2Bδ remodelling exists upon PERK inhibition (yet at a lower level), it is plausible to speculate that other pathways could serve as an activator of eIF2B body remodelling, further enhanced and/or maintained by eIF2α-P. This is consistent with previous observations that eIF2Bδ remodelling can occur in the absence eIF2α-P (Hodgson *et al.,* 2019). It is a complicated question to answer whether the ISR can, or even should, act single-handedly which warrants further investigation.

This stress-free increase of eIF2Bδ to small bodies is due to direct interaction of ISRIB molecule to eIF2Bδ (Hodgson *et al.,* 2019). ISIRB's binding site lies in the interfaces between eIF2Bβ and eIF2Bδ of opposing tetramers, serving as molecular stapler to promote decameric formation (Zyryanova *et al.,* 2018). ISRIB also seems able to individually target eIF2Bδ and no other eIF2B subunits (Sidrauski *et al.,* 2015b) which suggests that eIF2Bδ remodelling of small bodies may involve eIF2B-interacting molecules. Indeed, natural sugar metabolites bind to eIF2Bα_2 dimers and promote eIF2B decameric formation (Hao *et al.,* 2021).

More recently, viral proteins counteract ISR-induced translational shutdown by binding to host eIF2B via the interface between eIF2Bβ and eIF2Bδ subunits, hence competing with phospho-eIF2α due to overlapping binding sites (Kashiwagi *et al.,* 2019; Rabouw *et al.,* 2020). In yeast, YBR159W, an ER-anchored keto-acyl reductase involved in synthesis of fatty acids, physically interacts with the eIF2B subunits Gcd6p (eIF2Bε) and Gcd7p (eIF2Bβ) (Browne *et al.,* 2013). Interestingly, YBR159W knockdown phenocopied the effects of some Gcn3p/eIF2Bα mutants by inducing “microfoci” of eIF2B, as well as disrupted lipid membranes (Browne *et al.,* 2013; Norris *et al.,* 2021). Although the relationship between localisation of translation initiation factors and lipidic membranes has been established (Willett *et al.,* 2011), it further suggests that membrane-anchored proteins regulate eIF2B body dynamics by direct contact with specific eIF2B subunits. Understanding the mechanism(s) and/or molecules that drive eIF2Bδ redistribution are still unknown and warrant further investigation.

4.4.6. Final observations.

The results shown in this chapter demonstrate that eIF2B localisation is differentially impacted during the acute and chronic phases of the ISR. At the hub of these stress-induced localisation changes is eIF2Bδ redistribution of small eIF2B bodies, which may play a key role during the acute ISR and be less required upon a chronic ISR. Here it was also reported a glial specific ability to reset an acute ISR programme while undergoing chronic ER stress, whereas neuronal cells trigger eIF2α-independent mechanisms to control bulk translation. This subsequent acute ISR programme involves elevated eIF2α-P accompanied by enhanced eIF2Bδ composition to small eIF2B bodies in glial cell types. Moreover, remodelling of eIF2Bδ composition of small bodies is partially eIF2α-independent, hence involving other pathways and/or molecules.

Taken together, the regulatory composition of small eIF2B bodies is selectively targeted during cellular stress and leads to cell-type specific differences under certain stress stimulation (**Figure 4.12.**). The data collated and discussed in this chapter provides insights into the attractive concept of a cell-type specific activity of the ISR, here with focus on the localisation dynamics of eIF2B. For the next chapter, the functional relevance of these changes to eIF2B bodies and impact of ISR-targeting drugs will be addressed.

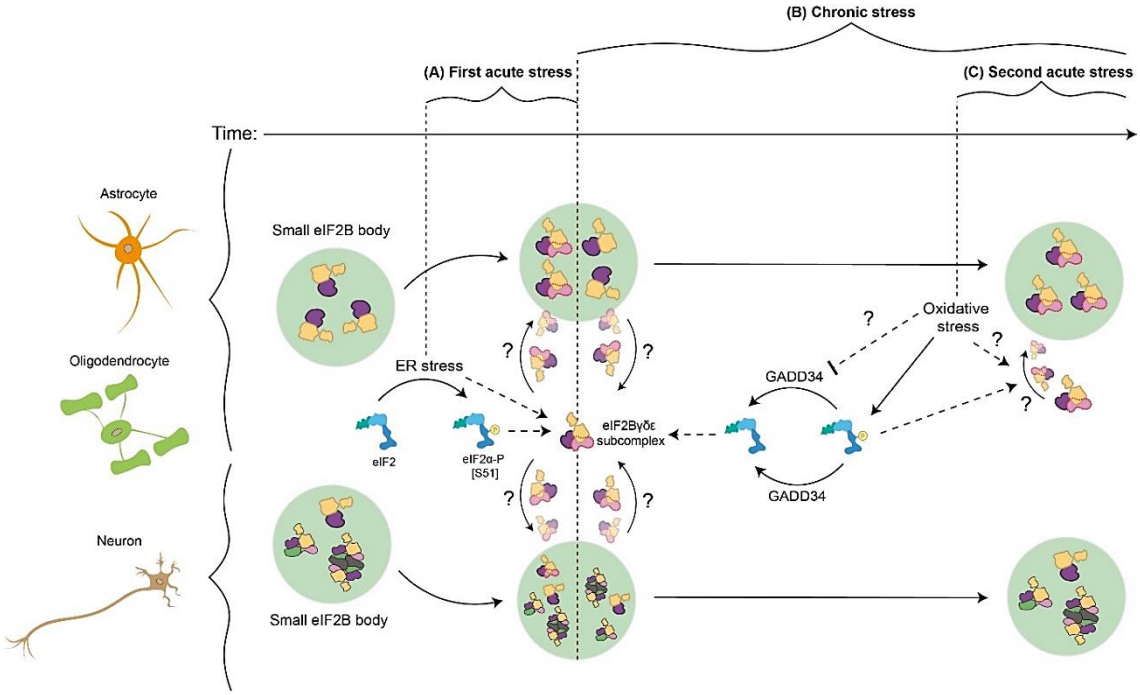

Figure 4.12. The eIF2Bδ composition of small eIF2B bodies is remodelled in a stress- and cell-type specific manner.
(A) Short-term ER or oxidative stress induces eIF2α-P accompanied by increased eIF2Bδ composition to small eIF2B bodies across all three cell types, thus a general feature of the acute ISR. The kinetics of eIF2B(γδε) formation remains unknown.
(B) During sustained ER stress (chronic ISR), GADD34 expression promotes eIF2α dephosphorylation coupled with eIF2Bδ composition of small bodies being restored to basal levels across all cell types.
(C) A subsequent oxidative stress to chronically ER stressed cells led to cell-type specific differences. Levels of eIF2α-P were again elevated in glial cells alongside eIF2Bδ remodelling of small bodies, while in neuronal cells it remained largely unchanged.

Chapter 5. Impact of ISRIB and cellular stress on the cell-type specific functionality of eIF2B localisation.

5.1. Introduction.

ISRIB is a potent small molecule that mitigates the ISR by targeting and activating eIF2B. Structurally, ISRIB binds at a symmetrical interface between the -β and -δ subunits and bridges two eIF2B(βδγε) tetramers to promote decamer formation (Tsai *et al.,* 2018; Zyryanova *et al.,* 2018). This action of ISRIB restores eIF2B activity which reverses the effects of eIF2α-P by recovering repression of protein synthesis and antagonizes ATF4-dependent reprogramming of translation (Sidrauski *et al.,* 2013; Sidrauski *et al.,* 2015b; Sekine *et al.,* 2015; Zyryanova *et al.,* 2021). ISRIB has been shown to regulate eIF2B bodies in astrocytes (Hodgson *et al.,* 2019). Here, ISRIB was proposed to mimic the action of the acute ISR by increasing eIF2Bδ localisation and GEF activity of small eIF2B bodies in unstressed cells. This suggests that eIF2Bδ remodelling may be an additional mechanism of action of ISRIB, which remains poorly understood. In parallel, ISRIB reversed the inhibitory effects of eIF2α-P in the GEF activity of large bodies (containing all eIF2B subunits) (Hodgson *et al.,* 2019). Thus, ISRIB targets eIF2B bodies depending on their sensitivity to eIF2α-P.

As discussed previously, ISRIB is a promising neuroprotective therapeutic by ameliorating neuropathology and inflammation in several disorders associated with a chronic ISR (see Introduction 1.4.2.). ISRIB relieves VWMD pathology in mouse models (Abbink *et al.,* 2019) and biochemical studies show that VWMD mutations that destabilize decameric eIF2B can be rescued by ISRIB which results in increased GEF activity (Wong *et al.,* 2018). However, it remains unknown whether ISRIB's action also involves the regulation of eIF2B bodies upon chronic ISR.

5.2. Hypothesis and rationale.

The main scientific aim of this chapter is to explore the crosstalk between ISRIB and the ISR in the eIF2Bδ composition and GEF activity of eIF2B bodies across the three cell types. Several studies have demonstrated that ISRIB rescues global translation in a variety of cell types and disease models (see Introduction section 1.4.2.) having a ubiquitous effectiveness on the control of protein synthesis. Because eIF2B is ISRIB's target and ISRIB mimics the acute ISR, the hypothesis is that ISRIB regulates eIF2B bodies in the presence of acute ISR similarly between the cell types used in this study. The impact of chronic ISR on ISRIB's action of eIF2B bodies is not known and will be investigated in this chapter. To achieve this, the experimental objectives were as follows:

- To cross-compare the steady-state distribution of the eIF2Bδ subunit and GEF activity of eIF2B bodies between cell types upon ISRIB treatment by transient transfection, immunocytochemistry, and confocal imaging (including FRAP analysis).
- To examine the potential cell-type specific impact of cellular stress (acute and chronic ISR) on the GEF activity of eIF2B bodies by FRAP analysis.
- Investigate the impact of ISRIB on the eIF2Bδ composition and GEF activity during cellular stress by FRAP analysis.

5.3. Results.

5.3.1. ISRIB's action is long-term and reverses the restorative effect of chronic ISR in eIF2Bδ localisation of small eIF2B bodies in astrocytes.

Chapter 3 demonstrated that eIF2Bδ localisation of small eIF2B bodies is increased upon induction of the acute ISR (Tg 1h). This was also shown to be a general cellular feature as it was observed in all three cell types. Given that ISRIB is proposed to mimic the action of the acute ISR (Hodgson *et al.,* 2019), ISRIB would also regulate eIF2Bδ redistribution in all cell types used in this study. To test this hypothesis SH-SY5Y, U373 and MO3.13 cells transiently expressing eIF2Bε-mGFP were treated with ISRIB for 1h and immunostained with an anti-eIF2Bδ antibody (**Figure 5.1. A and B**). U373 cells recapitulated the data shown in (Hodgson *et al.,* 2019), and MO3.13 cells also exhibited an increase in the % small eIF2B bodies co-localising with eIF2Bδ foci signal when compared to drug vehicle-control cells (**Figure 5.1. C i**). Surprisingly, SH-SY5Y cells did not show changes in eIF2Bδ distribution in comparison to vehicle levels (**Figure 5.1. C i**). Thus, ISRIB does not impact eIF2Bδ localisation of small bodies in neuronal cells.

eIF2Bδ re-localisation to small bodies is a transient feature specific to the acute ISR, and transition to chronic ISR (Tg 24h) restores eIF2Bδ composition to basal levels in all cell types. To further test ISRIB's mimicry of cellular stress, it was hypothesized that a chronic exposure of ISRIB (24h) (**Figure 5.1. A**) would recapitulate the effect of chronic ISR thus also restoring eIF2Bδ composition of small bodies in comparison to its 1h treatment. ISRIB for 24h did not increase the % of small eIF2B bodies co-localising with eIF2Bδ in comparison to vehicle in SH-SY5Y and MO3.13 cells (**Figure 5.1. C i**). Unexpectedly for U373 cells, the ISRIB for 24h significantly elevated the % of small eIF2B bodies co-localising with eIF2Bδ in comparison to vehicle (**Figure 5.1. C i**). These data suggest that ISRIB selectively maintains the increased eIF2Bδ composition in small eIF2B bodies of astrocytes during prologued treatment.

Because ISRIB ameliorates a vast number of disorders commonly characterized by a chronic ISR (see Introduction), the next aim was to test whether pre-conditioning cells to Tg for 24h would impact on ISRIB's cell-specific targeting of small eIF2B bodies. To do so, cells were firstly treated with ISRIB in the last 1h

of a 24h exposure of Tg (**Figure 5.1. C**). Immunofluorescence analysis demonstrated that ISRIB did not increase % of small eIF2B bodies co-localising with eIF2Bδ in SH-SY5Y and MO3.13 cells (**Figure 5.1. C i**). However, U373 cells once more showed increased eIF2Bδ localisation to small bodies (**Figure 5.1. C i**). Furthermore, a co-treatment of Tg and ISRIB for 24h (**Figure 5.1. A**) only revealed a similar significant increase of eIF2Bδ localisation in small bodies of U373 cells (**Figure 5.1. C i**). Hence, the action of ISRIB is independent of the restorative effect of chronic ISR in astrocytes, while chronic ISR prevents the action of ISRIB in oligodendrocytes.

In contrast to small eIF2B bodies, large eIF2B bodies remained overall unaffected by ISRIB and chronic ISR treatment (**Figure 5.1. C ii**).

Collectively, these results provide evidence that (1) ISRIB's action on small eIF2B bodies is cell-specific during unstressed conditions, (2) ISRIB has a long-term action in small eIF2B bodies of astrocytes, and (3) this extended action is selectively maintained in astrocytes during chronic ISR.

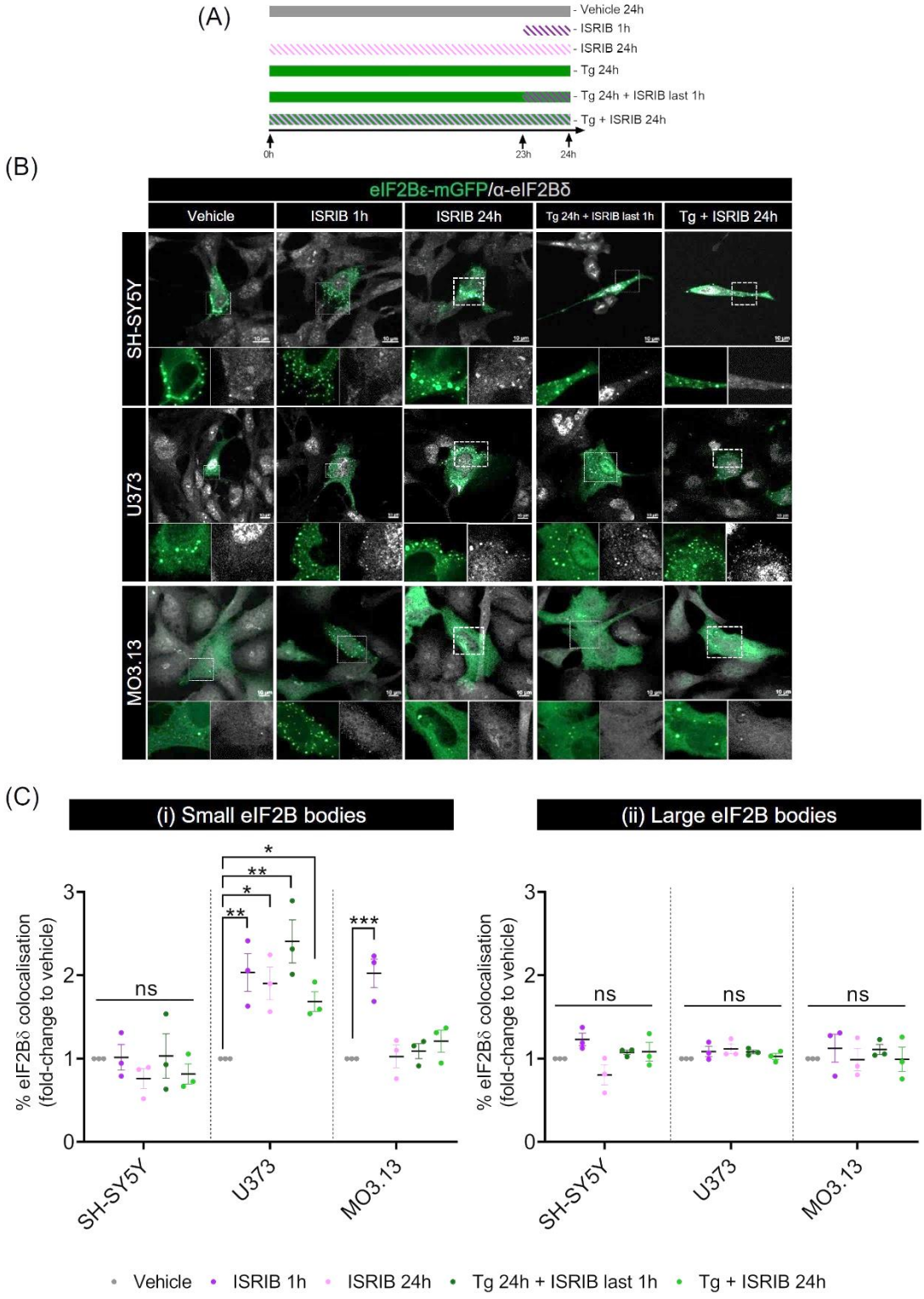
(A)
- Vehicle 24h
- ISRIB 1h
- ISRIB 24h
- Tg 24h
- Tg 24h + ISRIB last 1h
- Tg + ISRIB 24h
0h
23h
24h
(B)
eIF2Bε-mGFP/α-eIF2Bδ
Vehicle
ISRIB 1h
ISRIB 24h
Tg 24h + ISRIB last 1h
Tg + ISRIB 24h
SH-SY5Y
U373
MO3.13
(C)
(i) Small eIF2B bodies
(ii) Large eIF2B bodies
% eIF2Bδ colocalisation (fold-change to vehicle)
ns
*
**
***
SH-SY5Y
U373
MO3.13
Vehicle
ISRIB 1h
ISRIB 24h
Tg 24h + ISRIB last 1h
Tg + ISRIB 24h

Figure 5.1. ISRIB increases eIF2Bδ localisation of small eIF2B bodies in astrocytic and oligodendrocytic cells and chronic ER stress impacts eIF2Bδ redistribution in a cell-type manner.
(A) Time course of experimental setup.
(B) Representative images of SH-SY5Y, U373 and MO3.13 cells transiently transfected with eIF2Bε-mGFP and immunostained with an antibody against α-eIF2Bδ. Cells were treated with ISRIB (200nM) alone for 1h or added on the last hour of Tg (300nM) for 24h. DMSO for 24h was used as vehicle control. Scale bar: 10µm.
(C) Mean percentage of **(i)** small and **(ii)** large eIF2Bε-mGFP bodies displaying co-localisation with α-eIF2Bδ cytoplasmic foci was quantified manually and analysed in a population of 30 cells per replicate using one-way ANOVA followed by *post-hoc* Tukey's test for multiple comparisons. Data is presented as the fold-change relative to vehicle-treated cells. **p*=0.0239 (U373), ***p*= 0.0058 (U373); **p*=0.0015 (MO3.13).

5.3.2. Acute ISR and ISRIB impacts the shuttling of eIF2 through small eIF2B bodies in a cell-type manner.

ISRIB's mimicry of the acute ISR towards eIF2B localisation also resulted in increased GEF activity of small eIF2B bodies in astrocytes (Hodgson *et al.,* 2019). Whether this crossover effect of acute ISR and ISRIB in GEF activity was recapitulated in other cell types is not known. To test this, SH-SY5Y, U373 and MO3.13 cells were co-transfected with eIF2α-tGFP and eIF2Bε-RFP, treated with: (a) ISRIB alone for 1h, (b) Tg alone for 1h, or (c) co-treated with Tg and ISRIB for 1h and subjected to FRAP analysis (**Figure 5.2. A,** Appendix data).

ISRIB alone did not affect eIF2α-tGFP recovery of small eIF2B bodies in SH-SY5Y cells, while Tg slightly decreased eIF2α-tGFP recovery albeit with no statistical significance (p=0.0868) (Vehicle: 34.72% ± 2.09; ISRIB 1h: 31.47% ± 3.36; Tg 1h: 25.93% ± 2.49; Tg+ISRIB 1h: 29.79% ± 1.65) (**Figure 5.2. B i**).

In U373 cells, Tg alone, ISRIB alone or Tg in combination with ISRIB all significantly increased eIF2α-tGFP recovery of small eIF2B bodies, although the later displayed a significantly lower upregulation than ISRIB alone (Vehicle: 38.33% ± 2.30; ISRIB 1h: 59.40% ± 3.53; Tg 1h: 49.23% ± 1.85; Tg+ISRIB 1h: 48.11% ± 1.28) (**Figure 5.2. B i**). Additionally, the $t_{1/2}$ for eIF2α-tGFP recovery was slightly faster when treated with ISRIB alone, although with non-significant significance (p=0.2925) (Vehicle: 0.68 s ± 0.10; ISRIB 1h: 0.44 s ± 0.05; Tg 1h: 0.75 s ± 0.11; Tg+ISRIB 1h: 0.71 s ± 0.14) (**Figure 5.2. B ii**).

In contrast to the U373 cells, for MO3.13 cells no treatment showed any increase in eIF2α-tGFP recovery of small eIF2B bodies (Vehicle: 40.21% ± 1.73; ISRIB 1h: 41.42% ± 1.16; Tg 1h: 42.31% ± 3.17; Tg+ISRIB 1h: 36.85% ± 3.69) (**Figure 5.2. B i**).

Together these results suggest that ISRIB and acute ISR enhance eIF2 shuttling into small eIF2B bodies in astrocytes while acute ISR may inversely inhibit the movement of eIF2 in neuronal cells. In contrast, small bodies of oligodendrocytes are unregulatable by acute ER stress and ISRIB.

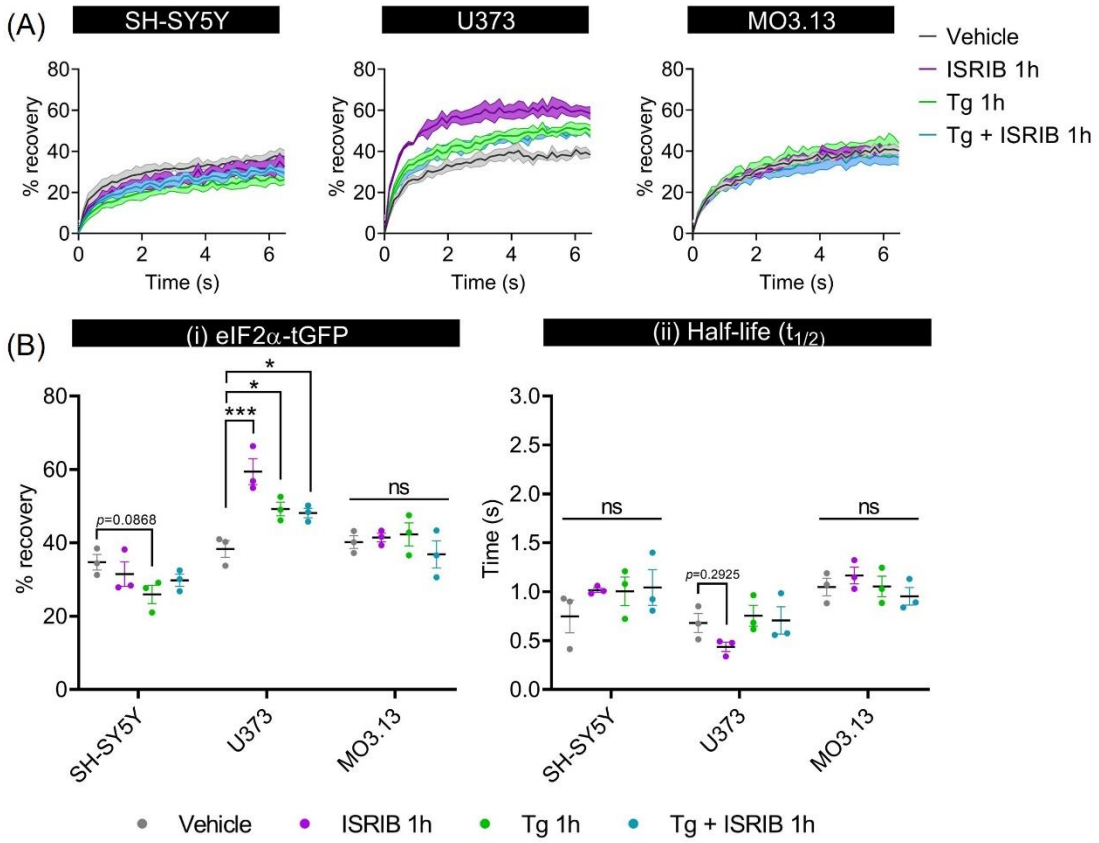

Figure 5.2. eIF2 shuttling is increased during acute ER stress and short-term ISRIB treatment in small eIF2B bodies of astrocytic cells.
SH-SY5Y, U373 and MO3.13 cells transiently co-transfected with eIF2α-tGFP and eIF2Bε-RFP. eIF2α-tGFP foci fluorescence was quantified to carry out fluorescence recovery after photobleaching (FRAP). eIF2Bε-RFP foci mark the eIF2B body. Cells were treated with ISRIB (200nM) alone for 1h, Tg (1μM) alone for 1h or Tg and ISRIB were co-treated for 1h. DMSO for 24h was used as vehicle control.
(A) Quantification of normalised FRAP curves for eIF2α-tGFP of 10-15 small eIF2Bε-RFP (<1μm^2) bodies of SH-SY5Y, U373 and MO3.13 cells. The data were graphed and shown as the mean and s.e.m. bands (*N=3*).
(B) (i) Mean percentage of eIF2α-tGFP recovery determined from normalised FRAP curves replicate using one-way ANOVA followed by *post-hoc* Tukey's test for multiple comparisons. U373: *** *p*=0.0006, **p*=0.0298 (Vehicle vs. Tg 1h), * *p*=0.0486 (Vehicle vs. Tg + ISRIB 1h). **(ii)** Quantification of the half time need for post-bleach full recovery of eIF2α-tGFP. Error bars: ± s.e.m. (*N*=3). ns: non-significant.

5.3.3. Acute ISR inhibits eIF2 shuttling through large eIF2B bodies which is reversed by ISRIB in a cell-type manner.

eIF2 shuttling is decreased in large eIF2B bodies of astrocytes upon the acute ISR and ISRIB reverses these inhibitory effects (Hodgson *et al.,* 2019). Applying the same rationale as described in 4.3.2., FRAP analysis was performed on large eIF2B bodies of SH-SY5Y, U373 and MO3.13 cells in the presence of (1) ISRIB alone for 1h, (2) Tg alone for 1h, or (3) co-treated with Tg and ISRIB for 1h (**Figure 5.3. A,** Appendix data).

In SH-SY5Y cells, ISRIB alone did not impact the recovery of eIF2α-tGFP however Tg treatment significantly decreased eIF2α-tGFP recovery and addition of ISRIB did not rescue this Tg-induced inhibitory effect (Vehicle: 45.42% ± 0.46; ISRIB 1h: 39.39% ± 4.18; Tg 1h: 32.68% ± 1.29; Tg+ISRIB 1h: 34.12% ± 2.95) (**Figure 5.3. B i**).

For U373 cells, ISRIB alone displayed non-significant changes to eIF2α-tGFP recovery while Tg treatment significantly decreased eIF2α-tGFP recovery, yet Tg-treated cells in the presence of ISRIB showed a significant rescue of eIF2α-tGFP recovery (Vehicle: 41.47% ± 1.73; ISRIB 1h: 43.16% ± 2.95; Tg 1h: 31.96% ± 0.93; Tg+ISRIB 1h: 40.32% ± 3.05) (**Figure 5.3. B i**). Moreover, Tg-treated large bodies showed significantly faster rate of recovery (measured by its half-life) in comparison to ISRIB-treated bodies (Vehicle: 0.830 s ± 0.035; ISRIB 1h: 0.714 s ± 0.052; Tg 1h: 1.065 s ± 0.138; Tg+ISRIB 1h: 0.829 s ± 0.002) (**Figure 5.3. B ii**). These results agree with the findings reported by (Hodgson *et al.,* 2019).

Finally, in MO3.13 cells, the % of eIF2α-tGFP remained largely unaffected with the various treatments of ISRIB and Tg (Vehicle: 28.00% ± 2.13; ISRIB 1h: 27.42% ± 1.20; Tg 1h: 30.12% ± 3.32; Tg+ISRIB 1h: 28.88% ± 2.19) (**Figure 5.3. B i**).

Taken together these data suggest that acute ISR inhibits eIF2 shuttling of large eIF2B bodies in neuronal cells and astrocytes although ISRIB is only able to reverse these inhibitory effects for the latter, while oligodendrocytes show no regulation by acute ISR and ISRIB.

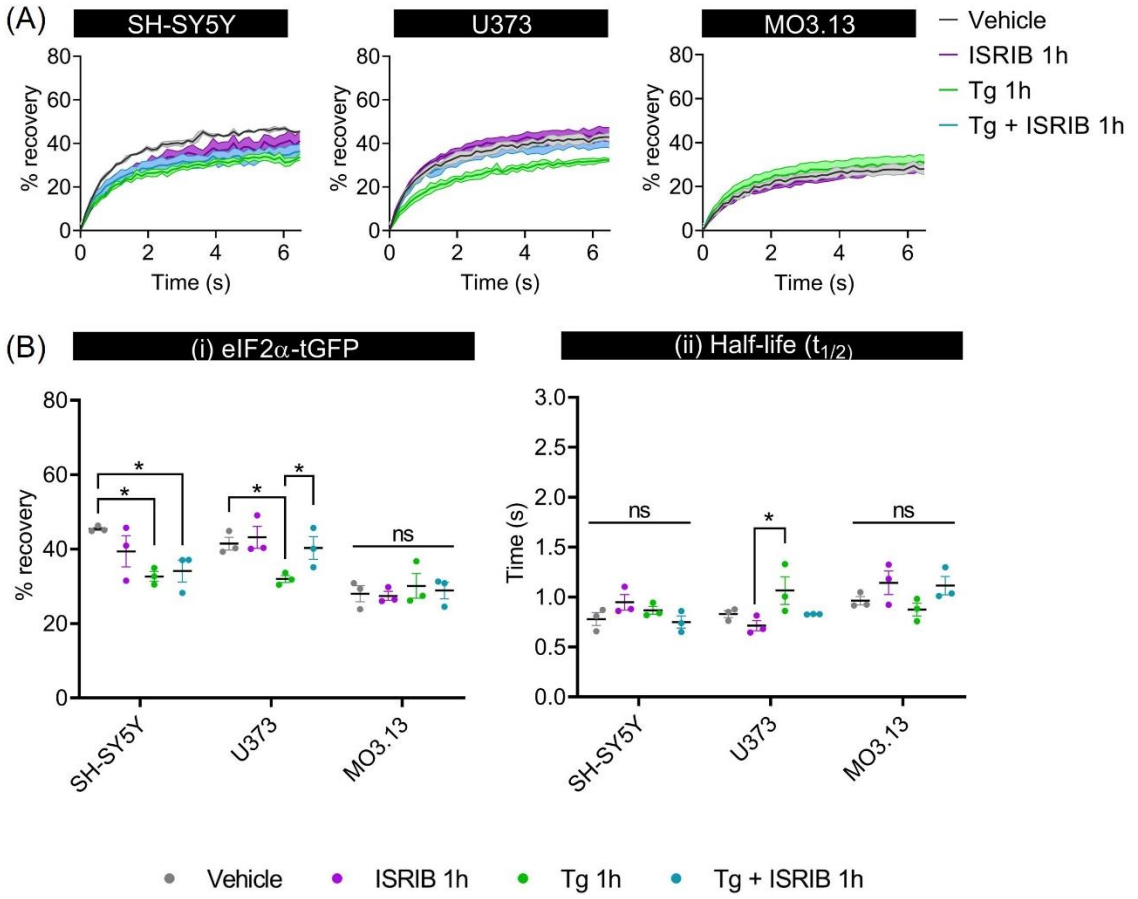

Figure 5.3. eIF2 shuttling is decreased during acute ER stress in large eIF2B bodies of neuronal and astrocytic cells while ISRIB reverses the effects of acute cellular stress in a cell-type manner.

SH-SY5Y, U373 and MO3.13 cells transiently co-transfected with eIF2α-tGFP and eIF2Bε-RFP. eIF2α-tGFP foci fluorescence was quantified to carry out fluorescence recovery after photobleaching (FRAP). eIF2Bε-RFP foci mark the eIF2B body. Cells were treated with ISRIB (200nM) alone for 1h, Tg (1μM) alone for 1h or Tg and ISRIB were co-treated for 1h. DMSO for 24h was used as vehicle control.

(A) Quantification of normalised FRAP curves for eIF2α-tGFP of 10-15 large eIF2Bε-RFP (≥1μm^2) bodies of SH-SY5Y, U373 and MO3.13 cells. The data were graphed and shown as the mean and s.e.m. bands (*N=3*).

(B) (i) Mean percentage of eIF2α-tGFP recovery determined from normalised FRAP curves replicate using one-way ANOVA followed by *post-hoc* Tukey's test for multiple comparisons (mean ± s.e.m, *N*=3). SH-SY5Y: **p*=0.0233 (Vehicle vs. Tg 1h), **p*=0.0409 (Vehicle vs. Tg + ISRIB 1h); U373: **p*=0.0480 (Vehicle vs. Tg 1h), **p*=0.0385 (Tg 1h vs. Tg + ISRIB 1h). **(ii)** Quantification of the half time need for post-bleach full recovery of eIF2α-tGFP (mean ± s.e.m, *N*=3). U373: *p= 0.0450 (ISRIB 1h vs. Tg 1h). ns: non-significant.

5.3.4. eIF2 shuttling through small eIF2B bodies is unaffected during chronic ISR while addition of ISRIB increases the movement of eIF2 in astrocytes.

Chapter 3 reported that the enhanced eIF2Bδ localisation of small eIF2B bodies induced by the acute ISR is reversed to its basal composition upon transition to chronic ISR (section 3.3.9). Therefore, the effect of chronic ISR coupled with short- and long-term co-treatment of ISRIB in small eIF2B bodies across the cell types was examined. To test this hypothesis, SH-SY5Y, U373 and MO3.13 were co-transfected with eIF2α-tGFP and eIF2Bε-RFP, treated with (1) ISRIB alone for 24h, (2) Tg alone for 24h, (3) Tg for 24h and ISRIB in the last 1h, or (4) co-treated with Tg and ISRIB for 24h; and then performed FRAP analysis (**Figure 5.4. A,** Appendix data,).

In SH-SY5Y and MO3.13 none of the treatments significantly impact the % or half-time of eIF2α-tGFP recovery of small eIF2B bodies (**Figure 5.4. B i and ii**).

In U373 cells, treatment of Tg for 24h did not affect the eIF2α-tGFP recovery in small eIF2B bodies in comparison to vehicle (Vehicle: 44.99% ± 2.83; Tg 24h: 41.42% ± 1.80) (**Figure 5.4. B i**). In all ISRIB treated samples, a significant increase of % recovery of eIF2α-tGFP was observed (ISRIB 24h: 59.79% ± 3.33; Tg 24h + ISRIB last 1h: 52.16% ± 2.05; Tg + ISRIB 24h: 61.97% ± 5.58) (**Figure 5.4. B i**). Overall, the half-life of eIF2α-tGFP displayed non-significant changes on the half-time of recovery (**Figure 5.4. B ii**). Hence, ISRIB selectively enhances the movement of eIF2 in astrocytes.

These results highlight that the action of ISRIB in the movement of eIF2 through of small eIF2B bodies is cell-specific and independent of the restorative effect of chronic ISR in astrocytes.

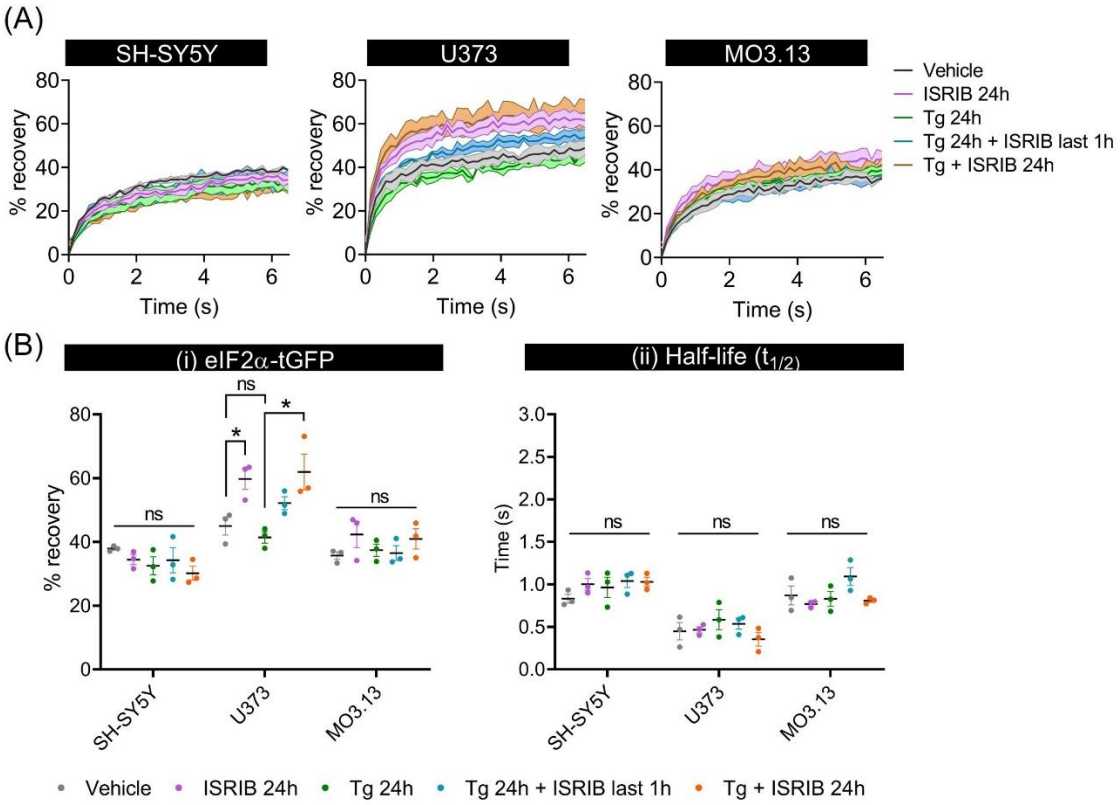

Figure 5.4. eIF2 shuttling through small eIF2B bodies is restored to basal levels during chronic ER stress however ISRIB further increases movement of eIF2 in astrocytic cells.
SH-SY5Y, U373 and MO3.13 cells transiently co-transfected with eIF2α-tGFP and eIF2Bε-RFP. eIF2α-tGFP foci fluorescence was quantified to carry out fluorescence recovery after photobleaching (FRAP). eIF2Bε-RFP foci mark the eIF2B body. Cells were treated with ISRIB (200nM) alone for 24h, Tg (300nM) alone for 24h, ISRIB added in the last hour of Tg for 24h and Tg and ISRIB were co-treated for 24h. DMSO for 24h was used as vehicle control.
(A) Quantification of normalised FRAP curves for eIF2α-tGFP of 10-15 small eIF2Bε-RFP (<1μm^2) bodies of SH-SY5Y, U373 and MO3.13 cells. The data were graphed and shown as the mean and s.e.m. bands (*N=3*).
(B) (i) Mean percentage of eIF2α-tGFP recovery determined from normalised FRAP curves replicate using one-way ANOVA followed by *post-hoc* Tukey's test for multiple comparisons. U373: **p*=0.0365 (Vehicle vs. ISRIB 24h), **p*=0.0174 (Tg 24h vs. Tg + ISRIB 24h). ns: non-significant. **(ii)** Quantification of the half time need for post-bleach full recovery of eIF2α-tGFP. Error bars: ± s.e.m. (*N*=3). ns: non-significant.

5.3.5. Chronic ISR and ISRIB impact eIF2 shuttling through large eIF2B bodies in a cell-type manner.

To investigate the impact of chronic ER stress coupled with ISRIB on the activity of large eIF2B bodies FRAP analysis of large eIF2B bodies was performed in SH-SY5Y, U373 and MO3.13 cells treated with the conditions previously described in section 5.3.8 (**Figure 5.5. A,** Appendix data).

In SH-SY5Y cells, ISRIB alone for 24h showed no significant effect on the % of eIF2α-tGFP recovery when compared to vehicle levels (Vehicle: 41.81% ± 1.67; ISRIB 24h: 38.76% ± 3.39) (**Figure 5.5. B i**). Tg alone for 24h modestly decreased the % of eIF2α-tGFP recovery compared to vehicle levels, while the presence of ISRIB in the last 1h or co-treated for 24h not only did not rescue this inhibitory effect of Tg but also showed a more significant reduction of eIF2 recovery (Tg 24h: 34.82% ± 4.66; Tg 24h + ISRIB last 1h: 25.84% ± 4.56; Tg + ISRIB 24h: 27.58% ± 1.39) (**Figure 5.5. B i**). In addition, the t1/2 of eIF2α-tGFP recovery reflected these changes in the % of recovery (**Figure 5.5. B ii**).

For U373 cells, the % of eIF2α-tGFP recovery remained largely like vehicle levels throughout all the conditions (Vehicle: 41.28% ± 3.99; ISRIB 24h: 45.43% ± 4.25; Tg 24h: 41.61% ± 2.38; Tg 24h + ISRIB last 1h: 42.49% ± 3.80; Tg+ISRIB 24h: 52.17% ± 8.17), and no significant differences in their $t_{1/2}$ recovery rates was observed either (**Figure 5.5. B i and ii**).

As for MO3.13 cells, the % of eIF2α-tGFP recovery remained largely similar to vehicle levels throughout all the conditions with the exception ISRIB for 24h where large eIF2B bodies showed a significant increase of eIF2α-tGFP recovery compared to the vehicle control (Vehicle: 23.70% ± 2.82; ISRIB 24h: 34.18% ± 1.85) (**Figure 5.5. B i**).

While there were some subtle changes of the % recovery of eIF2 in large eIF2B bodies during chronic ISR, the presence of ISRIB did not alter these changes. This suggests post-chronic ISR large bodies have recovered or maintained their GEF activity at levels similar to the vehicle and ISRIB doesn't seem to enhance or rescue this % recovery.

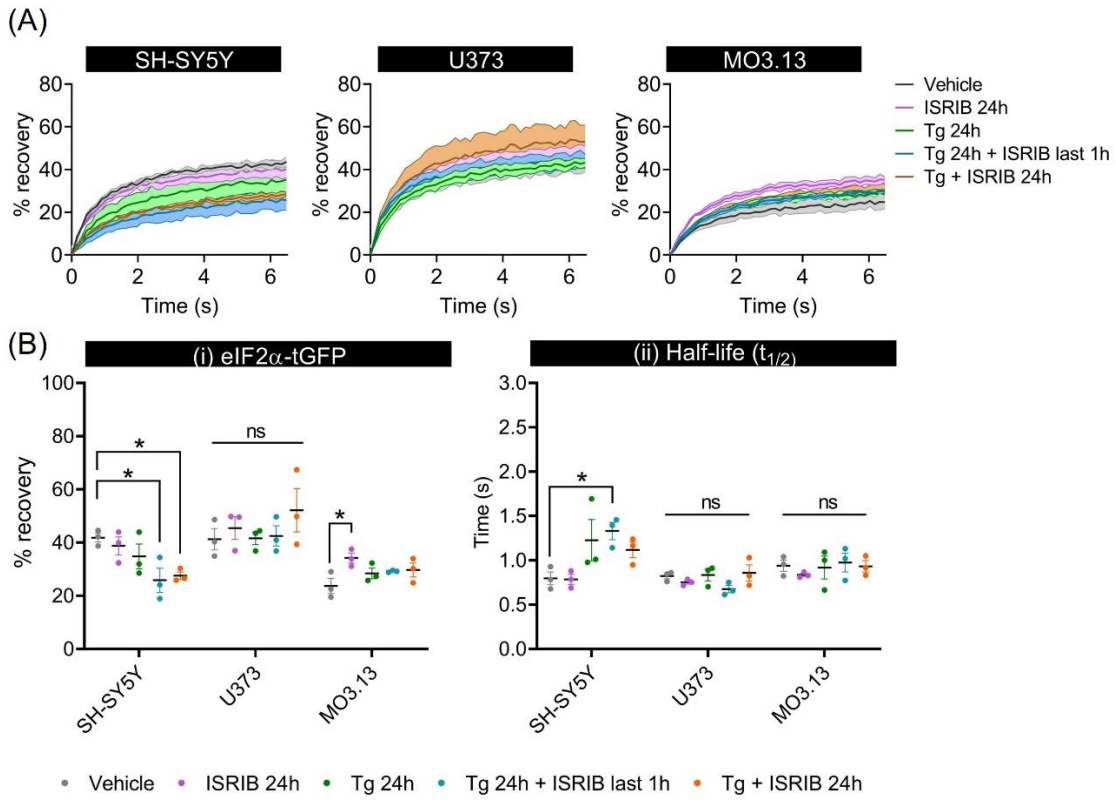

Figure 5.5. eIF2 shuttling in large eIF2B bodies is impacted in a cell-type specific manner in the presence of chronic ER stress and/or ISRIB.
SH-SY5Y, U373 and MO3.13 cells transiently co-transfected with eIF2α-tGFP and eIF2Bε-RFP. eIF2α-tGFP foci fluorescence was quantified to carry out fluorescence recovery after photobleaching (FRAP). eIF2Bε-RFP foci mark the eIF2B body. Cells were treated with ISRIB (200nM) alone for 24h, Tg (300nM) alone for 24h, ISRIB added in the last hour of Tg for 24h and Tg and ISRIB were co-treated for 24h. DMSO for 24h was used as vehicle control.
(A) Quantification of normalised FRAP curves for eIF2α-tGFP of 10-15 large eIF2Bε-RFP (≥1μm^2) bodies of SH-SY5Y, U373 and MO3.13 cells. The data were graphed and shown as the mean and s.e.m. bands (*N=3*).
(B) (i) Mean percentage of eIF2α-tGFP recovery determined from normalised FRAP curves. Statistical significance as indicated: **p*=0.0259 (SH-SY5Y: Vehicle vs. Tg 24h + ISRIB last 1h), **p*=0.0465 (SH-SY5Y: Vehicle vs. Tg + ISRIB 24h). ns: non-significant. **(ii)** Quantification of the half time need for post-bleach full recovery of eIF2α-tGFP. **p*=0.0426 (SH-SY5Y: Vehicle vs. Tg 24h + ISRIB last 1h). ns: non-significant. All error bars: ± s.e.m. (*N*=3).

5.3.6. Long-term ISRIB treatment rescues protein synthesis in astrocytes.

Having shown that ISRIB can differentially impact small and large eIF2B bodies during chronic stress, the relationship between the impact of ISRIB of eIF2B bodies and its overall effect on global translation was determined. To do so SH-SY5Y, U373 and MO3.13 cells were treated with Tg for 24h alone and then ISRIB was added either in the last 1h of treatment or co-treated with ISRIB for 24h. As controls, cells were treated with ISRIB alone for 1h and 24h. Cells were then subjected to puromycin incorporation assay to quantify levels of global protein synthesis (**Figure 5.6. A and B**).

Quantitation of the puromycin experiments revealed that ISRIB alone (1h and 24h) did not significantly affect basal translation levels in SH-SY5Y and MO3.13 cells (**Figure 5.6. C**). Unexpectedly, ISRIB for 24h mildly increased basal translation levels in U373 cells (p=0.0129) (**Figure 5.6. D**).

For all three cell types, exposure to Tg for 24h with the addition of ISRIB in the last 1h significantly increased levels of protein synthesis in comparison to ISRIB-untreated cells (**Figure 5.6. D**). Interestingly, when cells were exposed to a co-treatment of chronic ER stress and ISRIB for 24h non-significant changes in protein synthesis levels in SH-SY5Y and MO3.13 cells when compared to its respective ISRIB-untreated levels (**Figure 5.6. D**). This contrasted with the U373 cells where ISRIB significantly increased levels of protein synthesis when co-treated with chronic stress (**Figure 5.6. D**). These data show that long-term ISRIB treatment selectively rescues translation in astrocytes during chronic ISR.

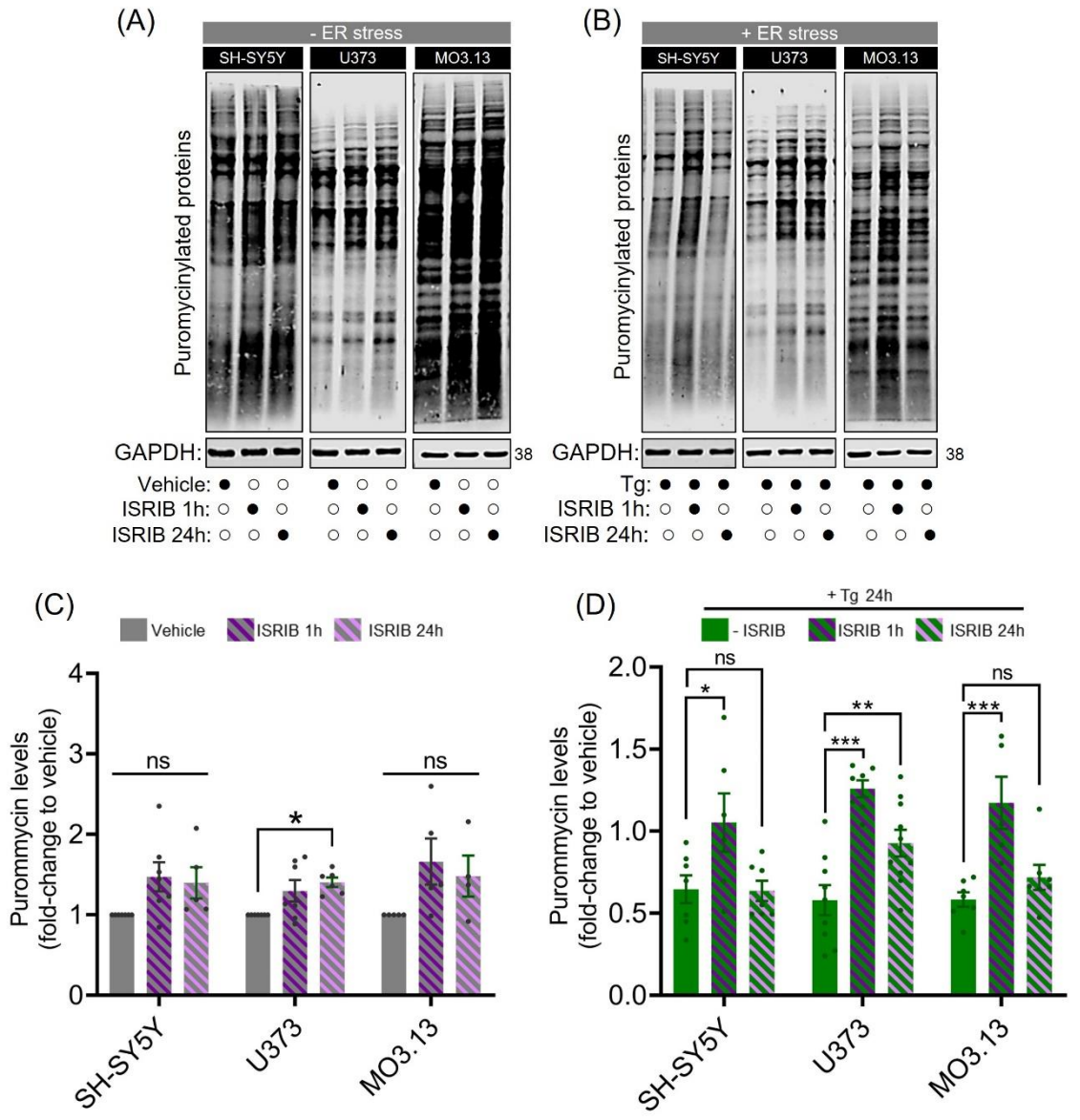

Figure 5.6. Translation is selectively restored in astrocytes in the presence of ISRIB for 24h during chronic ISR.
(A) Western blot analysis of SH-SY5Y, U373 and MO3.13 cells treated with ISRIB (200nM) alone for 1h or 24h and subjected to puromycin incorporation assay. GAPDH levels were used as loading control. DMSO for 24h was used as vehicle.
(B) Western blot analysis of SH-SY5Y, U373 and MO3.13 cells treated with Tg (300nM) alone for 24h, in the presence of ISRIB in the last 1h, or co-treated with ISRIB for 24h and subjected to puromycin incorporation assay. GAPDH levels were used as loading control. DMSO for 24h was used as vehicle.
(C,D) Quantification of mean intensity levels of puromycinylated proteins normalised against GAPDH levels and analysed using one-way ANOVA followed by *post-hoc* Tukey's test. Data is presented as fold-change levels of puromycin:GAPDH ratio in comparison to vehicle levels. All error bars: s.e.m. (N=4-10). *p=0.0129 (U373: Vehicle vs. ISRIB 24h), *p=0.0389 (SH-SY5Y: Tg 24h vs. Tg 24h + ISRIB last 1h), **p=0.0043 (U373: Tg 24h vs. Tg + ISRIB 24h), ***p<0.0001 (U373: Tg 24h vs. Tg 24h + ISRIB last 1h), ***p=0.0025 (MO3.13: Tg 24h vs. Tg 24h + ISRIB last 1h), ns: non-significant.

5.3.7. ISRIB remains active during long-term treatment.

ISRIB has a half-life of ~ 8 hours in mouse plasma and in the brain (Sidrauski *et al.,* 2013). Because ISRIB for 24h only showed significant impact on the eIF2Bδ composition and activity of small eIF2B bodies in U373 cells, whether this action of ISRIB was cell-specific and not due to its bioavailability was next examined.

SH-SY5Y, U373 and MO3.13 cells were pre-treated with ISRIB for 24h and further treated with Tg last 1h (**Figure 5.7. A i**) or SA for the last 30 minutes (**Figure 5.7. B i**). As control, cells were co-treated with Tg/SA and ISRIB for 1h or 30 minutes (**Figure 5.7. A i and B i**) to confirm the rescuing phenotype of short-term ISRIB treatment. Cells were subjected to puromycin incorporation assay to quantify levels of global protein synthesis (**Figure 5.7. A ii** and **B ii**). If ISRIB was still functional then ISRIB would ameliorate the impact of the stress on global protein synthesis.

Western blot analysis demonstrated that cells pre-treated with ISRIB showed significantly higher fold-change of global protein synthesis when challenged with Tg (**Figure 5.7. C**) or SA (**Figure 5.7. D**) in comparison to ISRIB-untreated cells. These results suggest that ISRIB remains active after 24h of treatment.

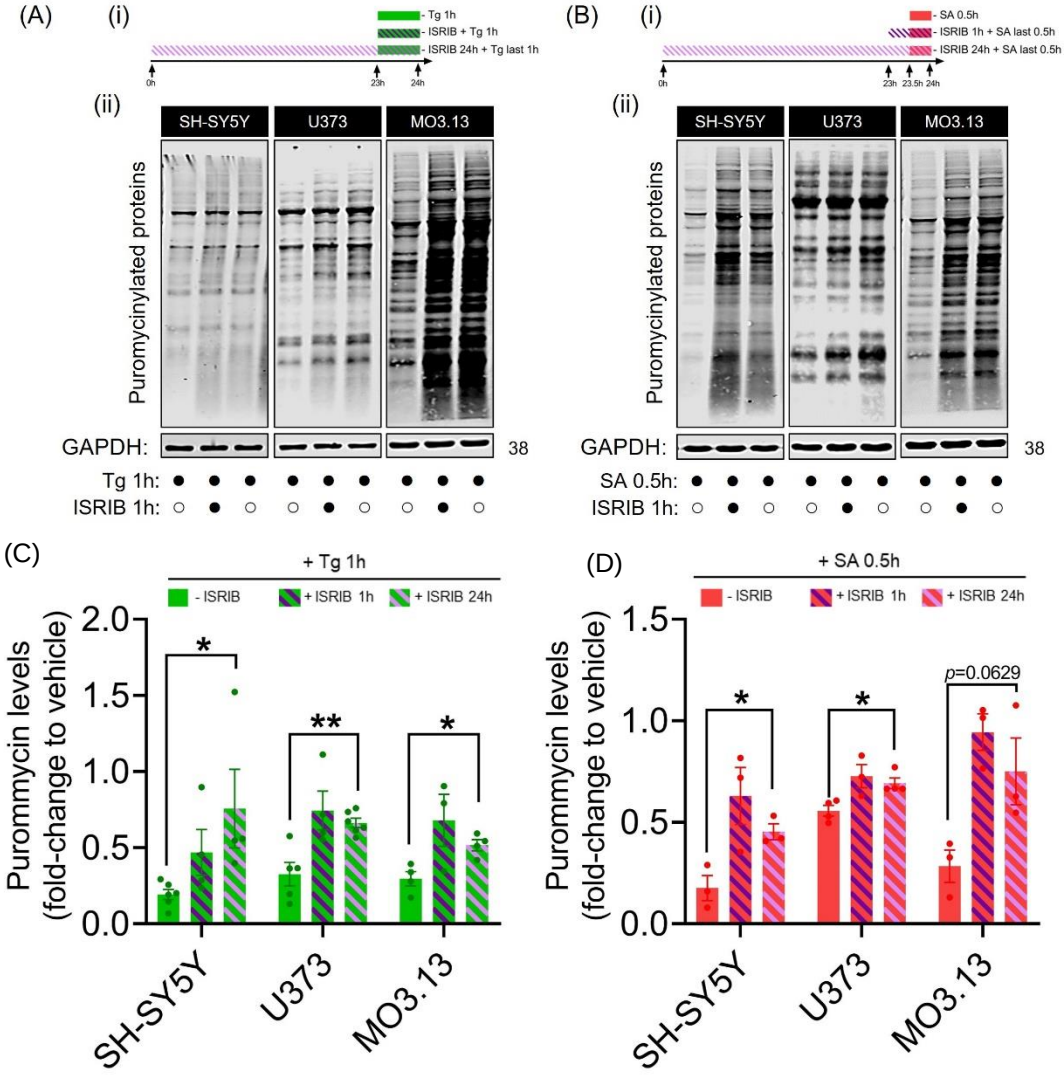

Figure 5.7. Pre-treatment of ISRIB for 24h is protective against subsequent acute ER stress and oxidative stress.
(A) (i) SH-SY5Y, U373 and MO3.13 cells treated with Tg alone for 1h, co-treated with ISRIB for 1h or added in the last 1h of a 24h treatment of ISRIB and **(ii)** subjected to puromycin incorporation assay and western blot analysis.
(B) (i) SH-SY5Y, U373 and MO3.13 cells treated with SA alone for 0.5h, co-treated with ISRIB for 1h or SA was added in the last 0.5h of a 1h treatment of ISRIB and **(ii)** subjected to puromycin incorporation assay and western blot analysis.
(C,D) Quantification of mean intensity levels of puromycinylated proteins normalised against GAPDH levels and analysed using unpaired Student *t*-test. Data is presented as fold-change levels of puromycin:GAPDH ratio in comparison to vehicle levels. All error bars: s.e.m. (*N*=3-6). **p*=0.0266 (SH-SY5Y: Tg 1h vs. ISRIB 24h + Tg 1h), ***p*=0.0018 (U373: Tg 1h vs. ISRIB 24h + Tg 1h), **p*=0.0103 (MO3.13: Tg 1h vs. ISRIB 24h + Tg 1h), **p*=0.0109 (SH-SY5Y: SA 0.5h vs. ISRIB 24h + SA 0.5h), **p*=0.0188 (U373: SA 0.5h vs. ISRIB 24h + SA 0.5h), ns: non-significant.

5.4. Discussion.

5.4.1. ISRIB predominantly targets the composition and activity of eIF2B bodies in astrocytes.

ISRIB has recently been shown to regulate eIF2B localisation by enhancing eIF2Bδ localisation in small bodies and increase the % recovery of eIF2 into small eIF2B bodies (Hodgson *et al.,* 2019). These findings led to a model whereby ISRIB may counteract stress-induced translation shutdown by providing a pool of GEF-enhanced and stress-insensitive eIF2B(γδε) sub-complexes localised to small bodies.

In this chapter, ISRIB-induced localisation of eIF2Bδ to small eIF2B bodies was specific to glial cells and not SH-SY5Y cells (**Figure 5.1.**). This was intriguing and may be related to early work presented in this thesis (see section 2.3.3.) showing increased basal level of eIF2Bδ in neuronal small bodies compared to the glial cells. Therefore, it is plausible that the impact that ISRIB has on eIF2Bδ redistribution may be linked to the composition and basal level of small bodies, which would follow in agreement to our observations that glial cell lines (both harbouring less eIF2Bδ) are then sensitive to ISRIB (**Figure 5.1.**).

Another possibility could be linked to the impact of ISRIB on eIF2Bδ's stability. Sidrauski and colleagues showed that ISRIB enhances the thermostability of eIF2Bδ but not the other subunits (Sidrauski *et al.,* 2015b). Although a recent study could not identify a correlation between *in vitro* thermostability and *in vivo* protein turnover (Collier *et al.,* 2020), this study focused on luminal lysosomal proteins and did not consider the additional impact of small molecules (Schreiber, 2019). Interestingly, the same group and others observed that the half-life of proteins varies between cell types (Collier *et al.,* 2020; Mathieson *et al.,* 2018; Rolfs *et al.,* 2021). Future research should be carried out to investigate the ISRIB-mediated turnover rates of eIF2Bδ between distinct cell types. It is also noteworthy that eIF2B subunits are stoichiometrically expressed to ensure efficient cycles of holocomplex formation (Wortham *et al.,* 2016). In this article, it was proposed that excessive eIF2Bδ is not assembled into eIF2B(βδγε) sub-complexes and are targeted for degradation (Wortham *et al.,* 2016). This study focused only on stead-state formation of eIF2B and did not examine the impact of ISR activation on eIF2B assembly. How ISRIB may affects the stoichiometric

levels of eIF2B subunits has, to the best of our knowledge, not yet been addressed.

It has previously been shown by several groups that increasing the expression of regulatory eIF2B subunits (α, β, δ) enhances eIF2B GEF activity (Dev *et al.,* 2010; Fabian *et al.,* 1997; Liu *et al.,* 2011; Williams *et al.,* 2001). Furthermore, Hodgson *et al* argued that ISRIB enhances GEF activity of small eIF2B bodies by increasing its eIF2Bδ composition as observed in U373 cells (Hodgson *et al.,* 2019). These studies were expanded in this thesis and show that the impact of ISRIB in mediating eIF2Bδ remodelling in small bodies cell-type specific (**Figure 5.1.**). This led us to the hypothesis that in the presence of ISRIB the GEF activity of small bodies would also be enhanced in a cell-type manner.

Surprisingly, a correlation between eIF2Bδ remodelling and GEF activity was not unanimously observed across the 3 cell lines tested (**Table 4.1.**). Despite eIF2Bδ being increased in small bodies of MO3.13 and U373 cells, only the small bodies for the latter exhibited increased shuttling of eIF2 (**Figure 5.2.**). These results suggest that enhancing basal activity of small bodies does not require increased eIF2Bδ as a general ISRIB-mediated feature, however it demonstrates a potential cell-specific relationship between eIF2Bδ remodelling and GEF activity of small eIF2B bodies as observed in U373 cells (**Table 4.1.**).

This cell-specific impact of ISRIB was further identified when cells were exposed to an acute Tg treatment in the presence or absence of ISRIB. Indeed, all conditions of Tg (observed in chapter 4) and ISRIB led to enhanced eIF2Bδ localisation to small bodies in U373 cells which, in parallel, displayed increased movement of eIF2 (**Figure 5.2.**). Altogether, these results demonstrate that astrocytic small eIF2B bodies are selectively remodelled during the acute ISR and ISRIB treatment, which may be at the hub of their GEF enhancement.

Chapter 3 argued that small bodies of SH-SY5Y cells may contain a higher variety of eIF2B sub-complexes. FRAP analysis data indeed point out that the movement of eIF2 is similarly inhibited in small and large eIF2B bodies in the presence of acute Tg (**Figure 5.2.** and **Figure 5.3.**) which suggests that different sized bodies may be functionally similar. As the catalytic eIF2B(γε) sub-complexes are unregulatable during cellular stress due to the lack of regulatory subunits (Liu *et al.,* 2011), it is therefore likely that small bodies in neuronal cells which already

have regulatory subunits would be targeted by stress. It would be important that future research utilises proteomic techniques to validate this cell-type specific sub-complex composition of eIF2B bodies.

ISRIB reverses the inhibitory effects of the acute ISR on large eIF2B bodies in astrocytes, hence potentially rescuing the pool of eIF2B subcomplexes untethered to phosphorylated eIF2α residing in large bodies (Hodgson *et al.,* 2019). Chapter 3 showed that large bodies of MO3.13 cells are largely depleted of eIF2Bβ, this suggests that the decameric eIF2B may not reside in large eIF2B bodies in MO3.13 cells. Therefore, the hypothesis that cellular stress would not impact the GEF activity of large bodies in this cell type was posed. Accordingly, acute Tg treatment did not decrease the shuttling of eIF2 to large bodies in MO3.13 cells (**Figure 5.3.**). In contrast the large eIF2B bodies of SH-SY5Y and U373 cells which contain all subunits of eIF2B (see chapter 3) showed decreased eIF2 shuttling through these eIF2B bodies during acute Tg treatment (**Figure 5.3.**). Rather surprisingly was the fact that ISRIB did not rescue this eIF2 shuttling in SH-SY5Y cells (**Figure 5.3.**). It has been shown that ISRIB cannot antagonize the ISR upon high levels of eIF2α-P (Rabouw *et al.,* 2019). Similarly, previous work from the Campbell group has shown that ISRIB fails to restore the activity of large bodies in the presence of high levels of eIF2α-P in U373 cells (Hodgson *et al.,* 2019). Since the acute ISR is upregulated in SH-SY5Y cells as previously demonstrated in chapter 3, it is plausible to speculate that the optimal threshold of eIF2α-P is surpassed upon acute Tg treatment rendering ISRIB ineffective. As such, a titration of lower dosages of Tg in the presence of ISRIB would be required to verify this hypothesis.

Table 5.1. Impact of ISRIB and cellular stress in eIF2Bδ composition and GEF activity of eIF2B bodies is cell-type specific.

	Cell line	Parameter	Treatments						
			ISRIB 1h	Tg 1h	Tg + ISRIB 1h	ISRIB 24h	Tg 24h	Tg 24h + ISRIB last 1h	Tg + ISRIB 24h
Small eIF2B bodies	SH-SY5Y	eIF2Bδ	No effect	Increased*	NA	No effect	Normalised	No effect	No effect
		eIF2 recovery	No effect	Decreased	Decreased	No effect	Decreased	Decreased	Decreased
	U373	eIF2Bδ	Increased	Increased*	NA	Increased	Normalised	Increased	Increased
		eIF2 recovery	Increased	Increased	Increased	Increased	Normalised	Increased	Increased
	MO3.13	eIF2Bδ	Increased	Increased*	NA	Normalised	Normalised	No effect	No effect
		eIF2 recovery	No effect	No effect	No effect	No effect	No effect	No effect	No effect
Large eIF2B bodies	SH-SY5Y	eIF2Bδ	No effect	No effect*	NA	No effect	No effect	No effect	No effect
		eIF2 recovery	No effect	Decreased	Decreased	No effect	Normalised	Decreased	Decreased
	U373	eIF2Bδ	No effect	No effect*	NA	No effect	No effect	No effect	No effect
		eIF2 recovery	No effect	Decreased	Normalised	No effect	No effect	No effect	No effect
	MO3.13	eIF2Bδ	No effect	No effect*	NA	No effect	No effect	No effect	No effect
		eIF2 recovery	No effect	No effect	No effect	Increased	No effect	No effect	No effect

NA, not analysed; *data from Chapter 3.

5.4.2. ISRIB has lasting effects on eIF2B bodies and translation in astrocytes.

A chronic Tg treatment did not interfere with ISRIB's ability of enhance eIF2Bδ localisation in U373 cells however it mitigated this mode of action of ISRIB in MO3.13 cells while exhibiting no effect in SH-SY5Y cells (**Figure 5.1.**). These findings demonstrate that ISRIB's mechanism of action involves cell-type specific regulation of eIF2Bδ localisation of small eIF2B bodies.

ISRIB reverses the inhibitory effects of eIF2α-P with restorative properties on global translation (see Introduction section 1.4.2.). In line with these reports, a 1h ISRIB treatment after chronic ISR rescued protein synthesis in all cell types (**Figure 5.6.**). Surprisingly, co-treating cells with Tg and ISRIB for 24h only showed a rescue phenotype in U373 cells (**Figure 5.6.**). ISRIB's bioavailability was sufficient at the 24h time point for all cell types by western blot analysis (**Figure 5.7.**). This indicates that ISRIB's action on eIF2B bodies is transient in neuronal and oligodendrocytes undergoing chronic ISR however it offers long-term rescue to astrocytes. Interestingly, in astrocytes short-term or co-treatment of ISRIB with chronic ISR also showed increased eIF2Bδ localisation (**Figure 5.1.**), thus ISRIB's effect on the eIF2Bδ composition of astrocytes is also long-lasting and independent of the action of chronic ISR in reversing eIF2Bδ redistribution. Moreover, these small eIF2B bodies were selectively targeted during co-treatment of ISRIB with chronic ISR as the same treatment did not affect large eIF2B bodies in both eIF2Bδ localisation and activity (**Figure 5.4.** and **Figure 5.5.**). Indeed, eIF2Bδ plays a key role in ISRIB's action of recovering translation explored here (Appendix data, **Figure A5**) and by others (Sidrauski *et al.,* 2015b). Now, a correlation between eIF2Bδ remodelling of small eIF2B bodies and translation rescue in astrocytes is highlighted as a potential cell-type specific mechanism of action of ISRIB.

This notion that ISRIB action on eIF2B bodies is prevalent in a cell-specific manner may be correlated to the poorly understood lasting effect of ISRIB described by some studies. Chou *et al.* elegantly reported that ISRIB counteracts elevated levels of eIF2α-P and improves cognition in mice models of traumatic brain injury (TBI) (Chou *et al.,* 2017). Interestingly, cognition was still improved weeks after ISRIB treatment ended (given its ~8h half-life in mouse plasma) with long-lasting rescue of dendritic spine degeneration yet remained unclear whether

ISRIB directly impacted neurons and/or other cell types (Chou *et al.,* 2017). Interestingly, astrocyte-derived signalling has been shown to guide spine formation (Chaudhuri *et al.,* 2020; Luarte *et al.,* 2020; Patel & Weaver, 2021) which then suggests, in combination with the data presented in this chapter, that ISRIB's action may involve enduring changes to the eIF2Bδ composition and activity of small eIF2B in astrocytes that further rescues neuronal function. Others have highlighted long-lasting amelioration of disease- and age-related neurological decline after a single ISRIB treatment (Hu *et al.,* 2022; Krukowski *et al.,* 2020; Oliveira *et al.,* 2021) yet the majority of these experimental setups were based on whole brain lysates hence impossible to discriminate the impact of ISRIB on a cell type basis. The possibility that these observations are influenced by the monocultured nature of these experiments at the cost of losing the *in vivo* context which is, of course, relevant to disease cannot be discarded (Klok *et al.,* 2018; Wisse *et al.,* 2018). Future work needs to be conducted in co-culture-based experiments to further the understanding of the cell-type specific action of ISRIB.

5.4.3. Insights of a cell-specific targeting of the ISR.

In this chapter demonstrated that ISRIB's mechanism of action involves cell-type specific regulation of the regulatory composition and activity of eIF2B bodies during unstressed and stressed conditions. Indeed, this provides a new platform for future research towards the notion of a cell-type specific targeting of eIF2B and action of ISRIB.

Interestingly, ISRIB has been recently shown to improve survival of ALS mutant SOD1-expressing hippocampal neurons by triggering cell-specific outputs (Bugallo *et al.,* 2020). In this study, ISRIB did not reduce neuronal ATF4 translation upon chronic ER stress as robustly as in ISRIB-treated glial cells. In fact, complete PERK inhibition repressed ATF4 translation as efficiently as ISRIB in mutSOD1-expressing glial cells but not in mutSOD1 neurons (Bugallo *et al.,* 2020), which implies that ISRIB may have limited inhibitory properties in neurons. However, ISRIB was still able to similarly rescue protein synthesis in both mutSOD1-expressing neurons and glia, hence relieving the neurotoxic translational repression imposed by PERK while maintaining translation of uORF-containing mRNAs (ATF4) in a cell-type manner (Bugallo *et al.,* 2020). ISRIB's

action may also be influenced by the cell-specific phosphorylation status of eIF2B subunits. Cagnetta and colleagues have shown that growth cue Semaphorin-3A (Sema3A) triggers eIF2α-P and locally dephosphorylates eIF2Bε (increasing GEF activity) to temporally uncouple eIF2B activity from eIF2α-P in axons of retinal ganglion cells (RGCs) (Cagnetta *et al.,* 2019). This dual stimulation of Sema3A revealed a subset of axonal proteins regulated by the Sema3A-eIF2α-P axis without global repression of translation as observed upon canonical stress (Cagnetta *et al.,* 2019). Another interesting possibility is neuronal-specific metabolites that either grant modest allosteric changes to eIF2B or occupy the pocket cavity where ISRIB binds (Tsai *et al.,* 2018; Hao *et al.,* 2021), which would constrain the magnitude of ISRIB's action. Altogether, pharmacological improvement of ISRIB formulation and/or localised delivery are warranted for further pre-clinical testing for ISR-related disorders.

Tissue-specific targeting of the ISR is also relevant to cognition. Recent studies suggest that normal cognition relies on eIF2α-dependent translation within specific neuronal subtypes. Learning tasks in mouse models reduced eIF2α-P levels in specific subsets of excitatory and inhibitory neurons (Sharma *et al.,* 2020). Similarly, selective manipulation of the PERK-eIF2α signalling cascade in dopaminergic neurons resulted in multiple cognitive failures (Longo *et al.,* 2021). Additionally, conflicting reports highlight the need to address the involvement of other cell types in cognitive decline. Growth factor BDNF has been shown to up-regulate ATF4 mRNA translation independently of eIF2α-P in hippocampal neurons (Liu *et al.,* 2018), whilst others report enhanced eIF2B activity upon BDNF treatment in similar cultured models (Takei *et al.,* 2001). It would be worthwhile to investigate how cell-specific eIF2B activation within different cell types such as microglia, astrocytes and oligodendrocytes are involved in cognitive decline.

5.4.4. Final observations.

ISRIB – a small molecule that stabilizes the eIF2B decamer and makes eIF2B insensitive to eIF2α-P – impacts the eIF2Bδ (thus regulatory) composition and GEF activity of eIF2B bodies in a cell-type manner. Here,a correlation was observed between enhanced eIF2Bδ localisation of small eIF2B bodies and increased movement of eIF2 through these bodies yet limited to astrocytes, suggesting that regulatory remodelling may only be functionally relevant on a cell type basis which warrants further examination.

Chapter 6. General discussion.

Over the past decade several publications have deepened the understanding of the structure and regulation of eIF2B. These accomplishments have congruently shown that eIF2B is a heterodecameric GEF protein assembled by its stoichiometrically regulated sub-complexes. eIF2B plays a key role in facilitating the initiation of translation while inhibition of eIF2B's GEF activity is the main regulatory event of the ISR. Recently, the Campbell group showed that eIF2B localises to cytoplasmic sites known as eIF2B bodies which are targeted not only by the action of the acute ISR but also ISR modulators.

ISR dysregulation is a hallmark of several human pathologies, mostly related to chronic activation of the ISR. More specifically, mutations in eIF2B are directly linked to VWMD, a neurological disorder that primarily affects glial cell types (astrocytes and oligodendrocytes). Whether eIF2B holds cell-type specific features is unknown. Thus, this thesis aimed to investigate potential cell-specific patterns of eIF2B localisation and correlation to the activity of the ISR.

6.1. eIF2B bodies are unique and regulated in a cell-specific manner.

Chapter 3 demonstrated that the prevalence, composition, and activity of eIF2B bodies is cell-type specific in a cohort of brain cells. In line with Hodgson *et al.,* (2019), two sub-populations of eIF2Bε-containing bodies based on size (small and large eIF2B bodies) were observed. While large eIF2B bodies (containing all subunits of eIF2B) were consistently present in all cell lines the smaller eIF2B bodies displayed some cell-specific disparities. These differences may reflect a cell-specific presence of eIF2B sub-complexes. Based on the co-localisation studies and FRAP analysis presented in this thesis, small eIF2B bodies are predominantly composed of catalytic subunits (γ,ε) as a general cellular feature, however tetramers and decamers also reside at these sites in neuronal cells albeit at a lower magnitude. During steady state, the rate of eIF2 shuttling in small bodies is similar between cell types, however the observed differences in subunit make-up is suggested to dictate their GEF activity during cellular stress and ISRIB (Hodgson *et al.,* 2019). Furthermore, the unexpected lack of eIF2Bβ in large eIF2B bodies in oligodendrocytes was reported which suggests lack of decameric eIF2B and may contribute to their decreased basal GEF activity.

Chapter 4 showed that the activity of the ISR is cell-type specific in a manner that correlates with compositional changes to eIF2B bodies. The eIF2Bδ composition of small eIF2B bodies is stimulated during the acute ISR across all cell types, however it is short-lived and not observed upon transition to a chronic ISR. Interestingly, chronically ER-stressed astrocytes and oligodendrocytes are able to reset their acute ISR when confronted with a subsequent oxidative stress. This also included eIF2Bδ remodelling of small eIF2B bodies. This cellular feature was not observed in neuronal cells, which suggests cell-specific sensitivity to restart the acute ISR and these cells may employ eIF2α-independent mechanisms to regulate protein synthesis.

In Chapter 5, the data presented in the previous chapters was further investigated using FRAP analysis to assess the functionality of eIF2B bodies during both acute and chronic ISR and in the presence of the eIF2B activator ISRIB. A cell-specific relationship between eIF2Bδ redistribution and eIF2 recovery was observed in astrocytic cells as illustrated in Figure 6.1. Indeed, in this cell line, ISRIB treatment has a dominant effect on increasing eIF2Bδ composition of small bodies, either alone or in combination with chronic ER stress, accompanied by an enhanced %

recovery of eIF2. This relationship is not recapitulated in the other cell types used in this study, which requires further *in vitro* studies to investigate the cell specific GEF activity of eIF2Bγδε subcomplexes.

Collectively, these results demonstrate that cells display cell-type specific localisation and regulation of eIF2B bodies. The existence of different eIF2B subcomplexes may allow unique rates of TC levels and adaptability to stress which overall might make translation more efficient and/or more easily regulated. More importantly, evidence of cell-type specific fine-tuning of eIF2B function and regulation, the core event of the ISR, was provided in this thesis; further emphasizing the need to tailor therapeutic interventions in a cell-type manner.

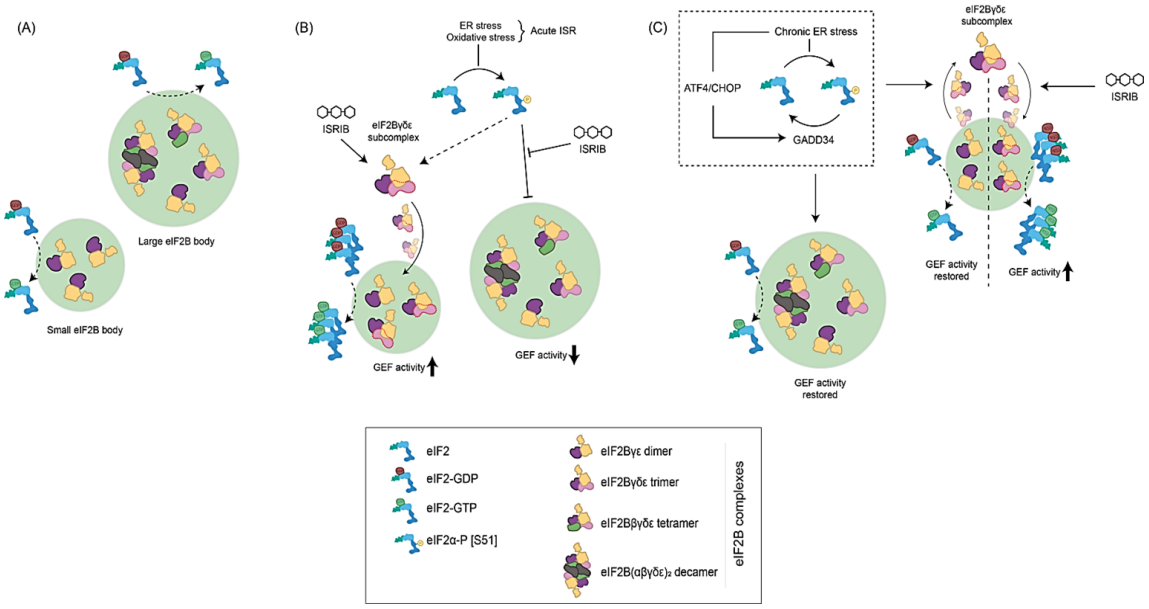

Figure 6.1. Working model for the impact of cellular stress and ISRIB in eIF2B bodies of astrocytes.
(A) eIF2B localises to small eIF2B bodies containing catalytic subcomplexes and larger eIF2B bodies containing a variety of regulatory subcomplexes (including decameric eIF2B).
(B) Upon activation of the acute ISR program, eIF2Bγδε subcomplexes are formed and localised to small eIF2B bodies which is suggested to have a regulatory role in eIF2B GEF activity; whilst large eIF2B bodies are negatively impacted.
(C) During transition to a chronic ISR, eIF2Bδ distribution in small bodies is reversed and GEF activity is restored to basal rates, whereas ISRIB treatment bypasses transient eIF2Bδ distribution by prompting extended eIF2Bγδε formation by direct interaction with eIF2Bδ.

6.2. eIF2Bδ as a therapeutic target.

The redistribution of eIF2Bδ to small eIF2B bodies upon induction of acute ISR occurs in all cell types while chronic ISR displays cell type disparities. This agrees with the model proposed by Hodgson *et al.,* 2019, and is now extended to neuronal cells and oligodendrocytes. Interestingly, a cell-specific ability of eIF2Bδ remodelling of small bodies was observed using a VWMD-mimicking stress treatment (chronic + acute ISR) in astrocytes and oligodendrocytes. Astrocytic dysfunction is the central pathomechanism of VWMD and cell-autonomous oligodendrocytic immaturation has also been reported (Bugiani *et al.,* 2018; Dooves *et al.,* 2016; Herrero *et al.,* 2019). Thus, these data highlight the first evidence of cell-specific eIF2B function wherein eIF2Bδ may be a crucial eIF2B subunit that contributes to the tissue-specific vulnerability of VWMD mutations. Furthermore, a novel mechanism of action of ISRIB is reported here, demonstrating that ISRIB regulates eIF2Bδ localisation and activity of eIF2B bodies in a cell-type manner.

Surprisingly, astrocytes are highly responsive to both the acute ISR and ISRIB given the observation of a correlation between increased eIF2Bδ and enhanced eIF2 shuttling in small eIF2B bodies but not in neuronal cells and oligodendrocytes. Moreover, this increase in the localisation of eIF2Bδ was sustained upon a longer treatment of ISRIB (24h) and restoration of translation was still observed in chronic ISR-induced astrocytes, while ISRIB only transiently restored translation in neurons and oligodendrocytes. Because the eIF2Bδ remodelling of small bodies is specific to the acute ISR, this thesis cautiously proposes that ISRIB can mimic a “prolonged” acute ISR effect by forming a stable pool of small eIF2B bodies containing ε-, γ-, and δ- subunits of enhanced GEF activity that restore translation during chronic ISR in astrocytes.

It is noteworthy that ISRIB’s cell-specific targeting of eIF2B bodies might be limited for personalised treatment for VWMD as its impact may be dependent on the specific causative mutation (notably eIF2Bβ and eIF2Bδ mutations that disrupt the binding pocket) (Abbink *et al.,* 2019; Slynko *et al.,* 2021). This highlights the need for new ISR modulators that can be appropriate for all VWMD patients is pivotal.

The protective role of a chronic ISR has been under intense investigation in the past years. Guanabenz and sephin 1 are inhibitors of PP1c-bound GADD34 which leads to sustained high levels of eIF2α-P in stressed cells. Both small molecules ameliorate VWMD pathology and are under clinical trials (Das *et al.,* 2015; van der Knaap *et al.,* 2022; Way *et al.,* 2015; Witkamp *et al.,* 2022) although the exact mechanism of action is still debatable (Crespillo-Casado *et al.,* 2017). Sephin 1 is also neuroprotective in OPCs of a multiple sclerosis mouse model by delaying translation recovery driven by prolonged eIF2α-P (Chen *et al.,* 2019). In line with these reports, the movement of eIF2Bδ is partially controlled by eIF2α-P was observed. Therefore, investigating whether these small drugs can manipulate the movement of eIF2Bδ would offer novel therapeutical avenues to ISR disorders beyond VWMD.

Interestingly, both ISRIB and estradiol valerate have been shown to delay ageing and confer thermal resistance by inhibiting the ISR in *C. elegans* (Derisbourg *et al.,* 2021). Although estradiol valerate was not initially identified in a ISR inhibition screening (possibly due to disparities of reporter assays used), another estradiol analogue (dibenzoylmethane, DBM) was detected (Halliday *et al.,* 2017). DBM is a curcumin-related molecule with anti-cancerogenic activity able to bind estrogen receptors (Jackson *et al.,* 2019; Lin *et al.,* 2006). DBM does not stabilize the eIF2B decamer however it increases eIF2Bδ localisation to small bodies (Hodgson *et al.,* 2019). Estradiol valerate and DBM do not bind to eIF2B like ISRIB and therefore must inhibit the ISR through different mechanisms. Further work is needed to determine the mechanism of action of these drugs.

6.3. How are mammalian eIF2B bodies formed?

Norris *et al.* observed that eIF2Bα is essential to maintain the integrity of eIF2B bodies in yeast which fits with the model presented by others that yeast eIF2B bodies are aggregates of eIF2B decamers (Norris *et al.,* 2021). Chapter 3 showed that, in mammalian cells, eIF2B subunits ε and γ form small eIF2B bodies, while the presence of regulatory subunit(s) may favour the coalescence of large eIF2B bodies (given the high average size of large eIF2B bodies in neuronal cells). The fact that eIF2B sub-complexes exist in different cells begs the question: what mediates this composition discrimination and how are eIF2B sub-complexes able to localise in a cell-type manner?

eIF2B bodies might share protein components and assembly processes to other membraneless organelles. Stress granules and P-bodies are functionally distinct entities yet rely on a fine balance between molecular motors dynein and kinesin to allow foci formation and dissolution upon stress (Loschi *et al.,* 2009). Recently, eIF2α kinase PKR was reported to form cytoplasmic foci upon poly I:C treatment (a PKR activator) that do not co-localise with eIF2α but rather act as storage sites of silenced PKR dimers to avoid exaggerated induction of eIF2α-P (Zappa *et al.,* 2022). Interestingly, these PKR bodies co-localise with P-body components Edc3 and Dcp1 but not canonical SG markers (Zappa *et al.,* 2022). Edc3 and Dcp1 are involved in mRNA decapping and degradation of P-bodies (Kedersha *et al.,* 2005), hence potentially weaponised to condensate dsRNA-bound PKR dimers to PKR bodies. Although the presence of P-body constituents might be inherently related to PKR's main function to sense dsRNA, it unveils a compositional crosstalk between membraneless organelles that could include eIF2B bodies.

This concentrated state is also well-known to occur via liquid-liquid phase separation (LLPS) (Wang *et al.,* 2021). LLPS is a process that condensates proteins and RNA-binding proteins into a state that resembles lipid droplets which includes (apart from SGs and P-bodies) centrosomes, Cajal bodies, paraspeckles, and DNA damage foci (*e.g*., 53BP1, γH2AX) (Brownsword & Locker, 2023). LLPS granules can be dynamically assembled, maintained, segregated, and fully dissolved, usually driven by environmental triggers (pH, temperature) or internal parameters (PTMs, protein concentration) (Wang *et al.,* 2021). Preliminary data presented in this thesis supports that eIF2B bodies also possess LLPS-like characteristics (Appendix data, **Figure A7**) and may be

assembled more rapidly than SGs (Moon & Parker, 2018a). In support of this, yeast eIF2B bodies can be formed under acidic pH conditions (Nüske *et al.,* 2020) and this thesis shows that eIF2B body formation is enhanced at different cell-specific magnitudes upon cellular stress. A key characteristic of LLPS granules is the presence of RNA (Roden & Gladfelter, 2021). RNA acts as a scaffold and subsequent crosslinker of RNA-binding proteins which is why the majority of LLPS granules are involved in RNA transcription, processing, and translation (Jain & Vale, 2017). Thus, it is important to investigate if eIF2B bodies contain RNA using RNA-FISH. Low sequence complexity, repeat motifs and disordered domains of proteins also drive LLPS granule formation (Martin & Mittag, 2018). Prime examples are TAR DNA-binding protein 43 (TDP-43) and Fused in Sarcoma (FUS). TDP-43 can self-assemble through its intrinsically disordered C-terminal domain while FUS contain a positively charged RGG domain that binds (negatively charged) RNA; and both are able to form irreversible inclusions linked to ALS pathology (Guerrero *et al.,* 2016). Interestingly, the HEAT domain of eIF2Bε is highly flexible and structurally exposed to accommodate eIF2 binding. However, the flexible nature of this region may act disordered-like and prompt self-assembly in a LLPS fashion, which is supported by structural studies that highlight eIF2Bε-eIF2Bε interactions to drive eIF2B body formation in yeast (Gordiyenko *et al.,* 2014; Marini *et al.,* 2020). Altogether, it is plausible to propose that eIF2B bodies carry LLPS-driven features (structural and/or compositional) that coordinate body formation which requires experimental validation.

6.4. Limitations and commentary of future research.

The localisation patterns of eIF2Bε-mGFP-containing bodies was investigated in three cell types. As proof-of-concept it was demonstrated that eIF2B bodies are cell-type specific when cross-compared between a neuronal, astrocytic and oligodendrocytic cell lines; however, this experimental model holds important limitations that need to be considered for proper interpretation of this study and future perspectives as listed below.

(1) *Transient transfection and protein localisation:* Short-term expression of proteins and fusion-proteins through transient transfections to study the subcellular distribution of proteins are widely used, although the major disadvantage is the magnitude of overexpression coupled with it (Gibson *et al.,* 2013). Assessing eIF2B localisation by transiently expressing a mGFP-fused ε-subunit may also be limited by the endogenous availability of other eIF2B subunits (Wortham *et al.,* 2014) and other interacting partners (Hanson *et al.,* 2022), hence potentially less affected by its overexpression. The fact that similar localisation patterns upon stable expression of eIF2Bε-mGFP is observed in U373 cells provides confidence to this model used here. Nonetheless, other changes that eIF2Bε overexpression may trigger cannot rule out such as the deregulated stoichiometric expression of eIF2Bγ. Cellular levels of eIF2Bγ are controlled by the expression of eIF2Bε to regulate assembly rates of eIF2Bγε dimers (Wortham *et al.,* 2014). Although no significant differences were observed in U373 cells (Hodgson, 2019), it is important to confirm that protein levels of eIF2B subunits are maintained upon transient transfection in all cell types. Another important consideration is whether the detection of eIF2B bodies is skewed between fixed and live cells. A recent report showed that PFA fixation changes LLPS behaviour by creating crosslinked-derived artifacts (Irgen-Gioro *et al.,* 2022), which may partially explain critical immunostaining drawbacks when alternatively using methanol in MO3.13 cells as a fixative (data not shown). Hence, to avoid misinterpretations or false-positive foci counting, a counterpart live-imaging when studying eIF2B bodies (and other LLPS granules) is recommended.

(2) *Cell models:* The nature of cell lines used in this study are another major drawback that needs to be considered. SH-SY5Y and U373, as neuroblastoma and astrocytoma cell lines (respectively), are cancer-derived and do not

recapitulate the metabolic burden of non-cancerous neurons and astrocytes (Ikari *et al.,* 2021; Vander Heiden & DeBerardinis, 2017) which might skew the observations reported in this thesis on the magnitude activity of the ISR and stress-induced effect on eIF2B bodies given the intimate link between cancer and the ISR (Licari *et al.,* 2021). This would fall in agreement with the observations that primary astrocytes have overall higher levels of eIF2α-P upon cellular stress though translation inhibition is like U373 cells. Furthermore, SH-SY5Y, despite being a dopaminergic neural cell line, it is cell-dividing and are not representative of a post-mitotic neuronal model (*e.g.,* able to repair DNA damage in mitosis through homologous recombination). To surpass these issues, future work should be conducted in iPSC-derived neural progenitor cells (NPCs) differentiated to neurons, astrocytes, and oligodendrocytes (Ladran *et al.,* 2013). Perhaps, even more importantly, is establishing a co-cultured system to confirm the findings reported in this study and offer clinical relevance to VWMD therapy. The experimental setup of this thesis aimed to unravel the individual contribution of cell types in eIF2B localisation and stress response profiles, however the cell-to-cell crosstalk is crucial for proper neuronal metabolism (*e.g.,* lactate deliverance from astrocytes), synaptic trafficking (*e.g.,* myelin coating of axons by oligodendrocytes) and are central of VWMD's cell-specific vulnerability (Klok *et al.,* 2018). Park *et al.* elegantly presented a microfluidic platform using tricultures of AD neurons, astrocytes, and microglia that mimicked microglial spatial recruitment and neuroinflammation markers that could not be observed in monocultures of the same cells (Park *et al.,* 2018). Interestingly, a 3D organoid with VWMD patient-derived iPSCs has been recently developed and fully recapitulated VWMD's main pathological hallmarks (GFAPδ expression, immature oligodendrocytes, sparse myelin) (Deng *et al.,* 2023), while cultured astrocytes from VWMD mutant eIF2Bε^{R191H} mice lose *in vivo* diseased phenotype (hypersensitive ISR) and instead behave like healthy astrocytes (Wisse *et al.,* 2018); altogether showing that future studies should devise and include co-cultured platforms to investigate VWMD pathomechanisms.

(3) *Co-localisation assay:* It is paramount to verify the presence of eIF2B sub-complexes in eIF2B bodies by proteomic analysis. This could involve isolation of eIF2B bodies by size exclusion chromatography and native co-IP of eIF2B subunits between different cell types to confirm the differential presence of eIF2B sub-complexes. In this thesis, co-localisation screening of α-, β-, δ-, and γ-

subunits to eIF2Bε-containing bodies was conducted by immunofluorescence analysis, which does not give direct evidence of eIF2B sub-complexes and relies on manual counting hence influenced by the user's criteria. Nonetheless, other quantitative methods such as Pearson's correlation coefficient were not suitable as it evaluates the intensity of the overlapping colour of multiple-channel fluorescence images and lacks sensitivity to measure individual foci signal (Dunn *et al.,* 2011). Alternative methods like FRET imaging analysis, which detects the physical contact between a donor- and acceptor-labelled fluorescent probes with ~0.09μm^2, is widely used to determine protein-protein interactions (Nouar *et al.,* 2013). However, employing FRET would likely result in false-negatives as the epitopes of eIF2Bα-γ subunits are at different distances and orientations to the mGFP-tag of eIF2Bε. However, combining FRET with object-based colocalization and pixel-intensity correlation using a novel *ImageJ* plug-in employs mathematical corrections by considering the aforementioned limitations (available on Github under: https://github.com/BHochreiter/ImageJ-FRET-and-coloc) (Lutz *et al.,* 2017), and could be used for future colocalization experiments.

6.5. Thesis conclusions.

The work presented in this thesis demonstrated that eIF2B localisation and its regulation during the activity of the ISR is cell-type specific. In mammalian cells, eIF2B bodies vary in size, eIF2B subunit composition and GEF activity in a cell type manner. eIF2Bδ composition of small eIF2B bodies is selectively remodelled during the acute ISR and may no longer be required during a chronic ISR. However, upon VWMD-mimicking stress, astrocytes and oligodendrocytes rely on the cellular ISR and eIF2Bδ remodelling while neurons alternatively trigger eIF2α-independent mechanisms. Furthermore, eIF2Bδ remodelling of small eIF2B bodies is suggested to be functionally relevant to astrocytes, the main culprit cell type in VWMD, and a potential key therapeutical target by ISR modulators. In conclusion, this thesis provides evidence that eIF2B bodies may contribute to the tissue sensitivity of VWMD and thus a key area of future research.

References.

Abbink, T. E. M., Wisse, L. E., Jaku, E., Thiecke, M. J., Voltolini-Gonzalez, D., Fritsen, H., Bobeldijk, S., Ter Braak, T. J., Polder, E., Postma, N. L., Bugiani, M., Struijs, E. A., Verheijen, M., Straat, N., van der Sluis, S., Thomas, A. A. M., Molenaar, D., & van der Knaap, M. S. (2019). Vanishing white matter: deregulated integrated stress response as therapy target. *Ann Clin Transl Neurol*, *6*(8), 1407-1422.

Abdel-Salam, G. M., Schaffer, A. E., Zaki, M. S., Dixon-Salazar, T., Mostafa, I. S., Afifi, H. H., & Gleeson, J. G. (2012). A homozygous IER3IP1 mutation causes microcephaly with simplified gyral pattern, epilepsy, and permanent neonatal diabetes syndrome (MEDS). *Am J Med Genet A*, *158a*(11), 2788-2796.

Abdulkarim, B., Nicolino, M., Igoillo-Esteve, M., Daures, M., Romero, S., Philippi, A., Senée, V., Lopes, M., Cunha, D. A., Harding, H. P., Derbois, C., Bendelac, N., Hattersley, A. T., Eizirik, D. L., Ron, D., Cnop, M., & Julier, C. (2015). A Missense Mutation in PPP1R15B Causes a Syndrome Including Diabetes, Short Stature, and Microcephaly. *Diabetes*, *64*(11), 3951-3962.

Aberg, K., Saetre, P., Jareborg, N., & Jazin, E. (2006). Human QKI, a potential regulator of mRNA expression of human oligodendrocyte-related genes involved in schizophrenia. *Proc Natl Acad Sci U S A*, *103*(19), 7482-7487.

Acker, M. G., Shin, B. S., Dever, T. E., & Lorsch, J. R. (2006). Interaction between eukaryotic initiation factors 1A and 5B is required for efficient ribosomal subunit joining. *J Biol Chem*, *281*(13), 8469-8475.

Acker, M. G., Shin, B. S., Nanda, J. S., Saini, A. K., Dever, T. E., & Lorsch, J. R. (2009). Kinetic analysis of late steps of eukaryotic translation initiation. *J Mol Biol*, *385*(2), 491-506.

Adomavicius, T., Guaita, M., Zhou, Y., Jennings, M. D., Latif, Z., Roseman, A. M., & Pavitt, G. D. (2019). The structural basis of translational control by eIF2 phosphorylation. *Nature Communications*, *10*(1), 2136-2133.

Alameda, L., Fournier, M., Khadimallah, I., Griffa, A., Cleusix, M., Jenni, R., Ferrari, C., Klauser, P., Baumann, P. S., Cuenod, M., Hagmann, P., Conus, P., & Do, K. Q. (2018). Redox dysregulation as a link between childhood trauma and psychopathological and neurocognitive profile in patients with early psychosis. *Proc Natl Acad Sci U S A*, *115*(49), 12495-12500.

Alamri, H., Al Mutairi, F., Alothman, J., Alothaim, A., Alfadhel, M., & Alfares, A. (2016). Diabetic ketoacidosis in vanishing white matter. *Clin Case Rep*, *4*(8), 717-720.

Alvarez-Castelao, B., Tom Dieck, S., Fusco, C. M., Donlin-Asp, P., Perez, J. D., & Schuman, E. M. (2020). The switch-like expression of heme-regulated kinase 1 mediates neuronal proteostasis following proteasome inhibition. *eLife*, *9*, e52714.

Andreou, A. Z., Harms, U., & Klostermeier, D. (2017). eIF4B stimulates eIF4A ATPase and unwinding activities by direct interaction through its 7-repeats region. *RNA Biol*, *14*(1), 113-123.

Antonellis, A., Ellsworth, R. E., Sambuughin, N., Puls, I., Abel, A., Lee-Lin, S. Q., Jordanova, A., Kremensky, I., Christodoulou, K., Middleton, L. T., Sivakumar, K., Ionasescu, V., Funalot, B., Vance, J. M., Goldfarb, L. G., Fischbeck, K. H., & Green, E. D. (2003). Glycyl tRNA synthetase mutations in Charcot-Marie-Tooth disease type 2D and distal spinal muscular atrophy type V. *Am J Hum Genet*, *72*(5), 1293-1299.

Arlt, A., & Schäfer, H. (2011). Role of the immediate early response 3 (IER3) gene in cellular stress response, inflammation and tumorigenesis. *Eur J Cell Biol*, *90*(6-7), 545-552.

Arnesen, T. (2011). Towards a functional understanding of protein N-terminal acetylation. *PLoS Biol*, *9*(5), e1001074.

Asano, K., Clayton, J., Shalev, A., & Hinnebusch, A. G. (2000). A multifactor complex of eukaryotic initiation factors, eIF1, eIF2, eIF3, eIF5, and initiator tRNA(Met) is an important translation initiation intermediate in vivo. *Genes Dev*, *14*(19), 2534-2546.

B'Chir, W., Maurin, A. C., Carraro, V., Averous, J., Jousse, C., Muranishi, Y., Parry, L., Stepien, G., Fafournoux, P., & Bruhat, A. (2013). The eIF2α/ATF4 pathway is essential for stress-induced autophagy gene expression. *Nucleic Acids Res*, *41*(16), 7683-7699.

Balachandran, S., & Barber, G. N. (2004). Defective translational control facilitates vesicular stomatitis virus oncolysis. *Cancer Cell*, *5*(1), 51-65.

Banerjee, R. (2012). Redox outside the box: linking extracellular redox remodeling with intracellular redox metabolism. *J Biol Chem*, *287*(7), 4397-4402.

Bartsch, D., Ghirardi, M., Skehel, P. A., Karl, K. A., Herder, S. P., Chen, M., Bailey, C. H., & Kandel, E. R. (1995). Aplysia CREB2 represses long-term facilitation: relief of repression converts transient facilitation into long-term functional and structural change. *Cell*, *83*(6), 979-992.

Batjargal, T., Zappa, F., Grant, R. J., Piscopio, R. A., Chialastri, A., Dey, S. S., Acosta-Alvear, D., & Wilson, M. Z. (2022). Optogenetic control of the integrated stress response reveals proportional encoding and the stress memory landscape. *bioRxiv*, 2022.2005.2024.493309.

Beilsten-Edmands, V., Gordiyenko, Y., Kung, J. C., Mohammed, S., Schmidt, C., & Robinson, C. V. (2015). eIF2 interactions with initiator tRNA and eIF2B are regulated by post-translational modifications and conformational dynamics. *Cell Discov*, *1*, 15020.

Berkovits, B. D., & Mayr, C. (2015). Alternative 3' UTRs act as scaffolds to regulate membrane protein localization. *Nature*, *522*(7556), 363–367

Berlanga, J. J., Ventoso, I., Harding, H. P., Deng, J., Ron, D., Sonenberg, N., Carrasco, L., & de Haro, C. (2006). Antiviral effect of the mammalian translation initiation factor 2alpha kinase GCN2 against RNA viruses. *EMBO J*, *25*(8), 1730-1740.

Bertsch, S., Lang, C. H., & Vary, T. C. (2011). Inhibition of glycogen synthase kinase 3[beta] activity with lithium in vitro attenuates sepsis-induced changes in muscle protein turnover. *Shock*, *35*(3), 266-274.

Bhat, M., Robichaud, N., Hulea, L., Sonenberg, N., Pelletier, J., & Topisirovic, I. (2015). Targeting the translation machinery in cancer. *Nat Rev Drug Discov*, *14*(4), 261-278.

Blazie, S. M., Takayanagi-Kiya, S., McCulloch, K. A., & Jin, Y. (2021). Eukaryotic initiation factor EIF-3.G augments mRNA translation efficiency to regulate neuronal activity. *eLife*, *10,* e68336.

Blümer, J., Rey, J., Dehmelt, L., Mazel, T., Wu, Y. W., Bastiaens, P., Goody, R. S., & Itzen, A. (2013). RabGEFs are a major determinant for specific Rab membrane targeting. *J Cell Biol*, *200*(3), 287-300.

Bogorad, A. M., Lin, K. Y., & Marintchev, A. (2017). Novel mechanisms of eIF2B action and regulation by eIF2α-P. *Nucleic Acids Res*, *45*(20), 11962-11979.

Bogorad, A. M., Xia, B., Sandor, D. G., Mamonov, A. B., Cafarella, T. R., Jehle, S., Vajda, S., Kozakov, D., & Marintchev, A. (2014). Insights into the architecture of the eIF2Balpha/beta/delta regulatory subcomplex. *Biochemistry*, *53*(21), 3432-3445.

Boltshauser, E., Barth, P. G., Troost, D., Martin, E., & Stallmach, T. (2002). "Vanishing white matter" and ovarian dysgenesis in an infant with cerebro-oculo-facio-skeletal phenotype. *Neuropediatrics*, *33*(2), 57-62.

Bond, S., Lopez-Lloreda, C., Gannon, P. J., Akay-Espinoza, C., & Jordan-Sciutto, K. L. (2020). The Integrated Stress Response and Phosphorylated Eukaryotic Initiation Factor 2α in Neurodegeneration. *J Neuropathol Exp Neurol*, *79*(2), 123-143.

Bos, J. L., Rehmann, H., & Wittinghofer, A. (2007). GEFs and GAPs: critical elements in the control of small G proteins. *Cell*, *129*(5), 865-877.

Boulay, A. C., Saubaméa, B., Adam, N., Chasseigneaux, S., Mazaré, N., Gilbert, A., Bahin, M., Bastianelli, L., Blugeon, C., Perrin, S., Pouch, J., Ducos, B., Le Crom, S., Genovesio, A., Chrétien, F., Declèves, X., Laplanche, J. L., & Cohen-Salmon, M. (2017). Translation in astrocyte distal processes sets molecular heterogeneity at the gliovascular interface. *Cell Discov*, *3*, 17005.

Brengues, M., & Parker, R. (2007). Accumulation of polyadenylated mRNA, Pab1p, eIF4E, and eIF4G with P-bodies in Saccharomyces cerevisiae. *Mol Biol Cell*, *18*(7), 2592-2602.

Briggs, D. I., Defensor, E., Memar Ardestani, P., Yi, B., Halpain, M., Seabrook, G., & Shamloo, M. (2017). Role of Endoplasmic Reticulum Stress in Learning and Memory Impairment and Alzheimer's Disease-Like Neuropathology in the PS19 and APP(Swe) Mouse Models of Tauopathy and Amyloidosis. *eNeuro*, *4*(4), ENEURO.0025-17.2017.

Browne, C. M., Samir, P., Fites, J. S., Villarreal, S. A., & Link, A. J. (2013). The yeast eukaryotic translation initiation factor 2B translation initiation complex interacts with the fatty acid synthesis enzyme YBR159W and endoplasmic reticulum membranes. *Mol Cell Biol*, *33*(5), 1041-1056.

Brownsword, M. J., & Locker, N. (2023). A little less aggregation a little more replication: Viral manipulation of stress granules. *Wiley Interdiscip Rev RNA*, *14*(1), e1741.

Bruck, W., Herms, J., Brockmann, K., Schulz-Schaeffer, W., & Hanefeld, F. (2001). Myelinopathia centralis diffusa (vanishing white matter disease): evidence of apoptotic oligodendrocyte degeneration in early lesion development. *Ann Neurol*, *50*(4), 532-536.

Bugallo, R., Marlin, E., Baltanás, A., Toledo, E., Ferrero, R., Vinueza-Gavilanes, R., Larrea, L., Arrasate, M., & Aragón, T. (2020). Fine tuning of the unfolded protein response by

ISRIB improves neuronal survival in a model of amyotrophic lateral sclerosis. *Cell Death Dis*, *11*(5), 397.

Bugiani, M., Boor, I., Powers, J. M., Scheper, G. C., & van der Knaap, M. S. (2010). Leukoencephalopathy with vanishing white matter: a review. *Journal of neuropathology and experimental neurology*, *69*(10), 987-996.

Bugiani, M., Boor, I., van Kollenburg, B., Postma, N., Polder, E., van Berkel, C., van Kesteren, R. E., Windrem, M. S., Hol, E. M., Scheper, G. C., Goldman, S. A., & van der Knaap, M. S. (2011). Defective glial maturation in vanishing white matter disease. *J Neuropathol Exp Neurol*, *70*(1), 69-82.

Bugiani, M., Postma, N., Polder, E., Dieleman, N., Scheffer, P. G., Sim, F. J., van der Knaap, M. S., & Boor, I. (2013). Hyaluronan accumulation and arrested oligodendrocyte progenitor maturation in vanishing white matter disease. *Brain*, *136*(Pt 1), 209-222.

Bugiani, M., Vuong, C., Breur, M., & van der Knaap, M. S. (2018). Vanishing white matter: a leukodystrophy due to astrocytic dysfunction. *Brain Pathol*, *28*(3), 408-421.

Burnett, B. J., Altman, R. B., Ferguson, A., Wasserman, M. R., Zhou, Z., & Blanchard, S. C. (2014). Direct evidence of an elongation factor-Tu/Ts·GTP·Aminoacyl-tRNA quaternary complex. *J Biol Chem*, *289*(34), 23917-23927.

Burnett, B. J., Altman, R. B., Ferrao, R., Alejo, J. L., Kaur, N., Kanji, J., & Blanchard, S. C. (2013). Elongation factor Ts directly facilitates the formation and disassembly of the Escherichia coli elongation factor Tu·GTP·aminoacyl-tRNA ternary complex. *J Biol Chem*, *288*(19), 13917-13928.

Bushong, E. A., Martone, M. E., Jones, Y. Z., & Ellisman, M. H. (2002). Protoplasmic astrocytes in CA1 stratum radiatum occupy separate anatomical domains. *J Neurosci*, *22*(1), 183-192.

Cabilly, Y., Barbi, M., Geva, M., Marom, L., Chetrit, D., Ehrlich, M., & Elroy-Stein, O. (2012). Poor Cerebral Inflammatory Response in eIF2B Knock-In Mice: Implications for the Aetiology of Vanishing White Matter Disease. *PLOS ONE*, *7*(10), e46715.

Cagnetta, R., Wong, H. H., Frese, C. K., Mallucci, G. R., Krijgsveld, J., & Holt, C. E. (2019). Noncanonical Modulation of the eIF2 Pathway Controls an Increase in Local Translation during Neural Wiring. *Mol Cell*, *73*(3), 474-489.e475.

Campbell, S. G., & Ashe, M. P. (2006). Localization of the translational guanine nucleotide exchange factor eIF2B: a common theme for GEFs? *Cell Cycle*, *5*(7), 678-680.

Campbell, S. G., Hoyle, N. P., & Ashe, M. P. (2005). Dynamic cycling of eIF2 through a large eIF2B-containing cytoplasmic body: implications for translation control. *J Cell Biol*, *170*(6), 925-934.

Carney, K. E., Milanese, M., van Nierop, P., Li, K. W., Oliet, S. H., Smit, A. B., Bonanno, G., & Verheijen, M. H. (2014). Proteomic analysis of gliosomes from mouse brain: identification and investigation of glial membrane proteins. *J Proteome Res*, *13*(12), 5918-5927.

Carpenter, M. D., Fischer, D. K., Zhang, S., Bond, A. M., Czarnecki, K. S., Woolf, M. T., Song, H., & Heller, E. A. (2022). Cell-type specific profiling of histone post-translational modifications in the adult mouse striatum. *Nat Commun*, *13*(1), 7720.

Charvet, C., Canonigo, A. J., Billadeau, D. D., & Altman, A. (2005). Membrane localization and function of Vav3 in T cells depend on its association with the adapter SLP-76. *J Biol Chem*, *280*(15), 15289-15299.

Chaudhuri, J., Chowdhury, D., & Maitra, U. (1999). Distinct functions of eukaryotic translation initiation factors eIF1A and eIF3 in the formation of the 40 S ribosomal preinitiation complex. *J Biol Chem*, *274*(25), 17975-17980.

Chaudhuri, A., Dasgheyb, R. M., DeVine, L. R., Bi, H., Cole, R. N., & Haughey, N. J. (2020). Stimulus-dependent modifications in astrocyte-derived extracellular vesicle cargo regulate neuronal excitability. *Glia*, *68*(1), 128-144. https://doi.org/10.1002/glia.23708

Chen, C.-W., Guan, B.-J., Alzahrani, M. R., Gao, Z., Gao, L., Bracey, S., Wu, J., Mbow, C. A., Jobava, R., Haataja, L., Zalavadia, A. H., Schaffer, A. E., Lee, H., LaFramboise, T., Bederman, I., Arvan, P., Mathews, C. E., Gerling, I. C., Kaestner, K. H., . . . Hatzoglou, M. (2022). Adaptation to chronic ER stress enforces pancreatic β-cell plasticity. *Nat Commun*, *13*(1), 4621.

Chen, Y., Podojil, J. R., Kunjamma, R. B., Jones, J., Weiner, M., Lin, W., Miller, S. D., & Popko, B. (2019). Sephin1, which prolongs the integrated stress response, is a promising therapeutic for multiple sclerosis. *Brain*, *142*(2), 344-361.

Cheng, H., Dufu, K., Lee, C. S., Hsu, J. L., Dias, A., & Reed, R. (2006). Human mRNA export machinery recruited to the 5' end of mRNA. *Cell*, *127*(7), 1389-1400.

Cheshire, J. L., Williams, B. R., & Baldwin, A. S., Jr. (1999). Involvement of double-stranded RNA-activated protein kinase in the synergistic activation of nuclear factor-kappaB by tumor necrosis factor-alpha and gamma-interferon in preneuronal cells. *J Biol Chem*, *274*(8), 4801-4806.

Chesnokova, E., Bal, N., & Kolosov, P. (2017). Kinases of eIF2a Switch Translation of mRNA Subset during Neuronal Plasticity. *Int J Mol Sci*, *18*(10).

Cheung, Y. N., Maag, D., Mitchell, S. F., Fekete, C. A., Algire, M. A., Takacs, J. E., Shirokikh, N., Pestova, T., Lorsch, J. R., & Hinnebusch, A. G. (2007). Dissociation of eIF1 from the 40S ribosomal subunit is a key step in start codon selection in vivo. *Genes Dev*, *21*(10), 1217-1230.

Chicurel, M. E., Terrian, D. M., & Potter, H. (1993). mRNA at the synapse: analysis of a synaptosomal preparation enriched in hippocampal dendritic spines. *J Neurosci*, *13*(9), 4054-4063.

Chou, A., Krukowski, K., Jopson, T., Zhu, P. J., Costa-Mattioli, M., Walter, P., & Rosi, S. (2017). Inhibition of the integrated stress response reverses cognitive deficits after traumatic brain injury. *Proc Natl Acad Sci U S A, 114*(31), E6420-E6426.

Choudhary, C., Kumar, C., Gnad, F., Nielsen, M. L., Rehman, M., Walther, T. C., Olsen, J. V., & Mann, M. (2009). Lysine acetylation targets protein complexes and co-regulates major cellular functions. *Science*, *325*(5942), 834-840.

Chung, K. T., Shen, Y., & Hendershot, L. M. (2002). BAP, a mammalian BiP-associated protein, is a nucleotide exchange factor that regulates the ATPase activity of BiP. *J Biol Chem*, *277*(49), 47557-47563.

Circir, A., Koksal Bicakci, G., Savas, B., Doken, D. N., Henden Ş, O., Can, T., Karaca, E., & Erson-Bensan, A. E. (2022). A C-term truncated EIF2Bγ protein encoded by an intronically polyadenylated isoform introduces unfavorable EIF2Bγ-EIF2γ interactions. *Proteins*, *90*(3), 889-897.

Collier, A. M., Nemtsova, Y., Kuber, N., Banach-Petrosky, W., Modak, A., Sleat, D. E., Nanda, V., & Lobel, P. (2020). Lysosomal protein thermal stability does not correlate with cellular half-life: global observations and a case study of tripeptidyl-peptidase 1. *Biochem J*, *477*(3), 727-745.

Condeelis, J., & Singer, R. H. (2005). How and why does beta-actin mRNA target? *Biol Cell*, *97*(1), 97-110.

Contestabile, A., Greco, B., Ghezzi, D., Tucci, V., Benfenati, F., & Gasparini, L. (2013). Lithium rescues synaptic plasticity and memory in Down syndrome mice. *J Clin Invest*, *123*(1), 348-361.

Coots, R. A., Liu, X. M., Mao, Y., Dong, L., Zhou, J., Wan, J., Zhang, X., & Qian, S. B. (2017). m(6)A Facilitates eIF4F-Independent mRNA Translation. *Mol Cell*, *68*(3), 504-514.e507.

Corbett A. H. (2018). Post-transcriptional regulation of gene expression and human disease. *Curr Opin Cell Biol.*, *52*, 96–104.

Costa-Mattioli, M., Gobert, D., Harding, H., Herdy, B., Azzi, M., Bruno, M., Bidinosti, M., Ben Mamou, C., Marcinkiewicz, E., Yoshida, M., Imataka, H., Cuello, A. C., Seidah, N., Sossin, W., Lacaille, J. C., Ron, D., Nader, K., & Sonenberg, N. (2005). Translational control of hippocampal synaptic plasticity and memory by the eIF2alpha kinase GCN2. *Nature*, *436*(7054), 1166-1173.

Costa-Mattioli, M., Gobert, D., Stern, E., Gamache, K., Colina, R., Cuello, C., Sossin, W., Kaufman, R., Pelletier, J., Rosenblum, K., Krnjević, K., Lacaille, J. C., Nader, K., & Sonenberg, N. (2007). eIF2alpha phosphorylation bidirectionally regulates the switch from short- to long-term synaptic plasticity and memory. *Cell*, *129*(1), 195-206.

Court, F. A., Hendriks, W. T., MacGillavry, H. D., Alvarez, J., & van Minnen, J. (2008). Schwann cell to axon transfer of ribosomes: toward a novel understanding of the role of glia in the nervous system. *J Neurosci*, *28*(43), 11024-11029.

Crespillo-Casado, A., Chambers, J. E., Fischer, P. M., Marciniak, S. J., & Ron, D. (2017). PPP1R15A-mediated dephosphorylation of eIF2α is unaffected by Sephin1 or Guanabenz. *eLife*, *6,* e26109.

Dang Do, A. N., Kimball, S. R., Cavener, D. R., & Jefferson, L. S. (2009). eIF2alpha kinases GCN2 and PERK modulate transcription and translation of distinct sets of mRNAs in mouse liver. *Physiol Genomics*, *38*(3), 328-341.

Das, I., Krzyzosiak, A., Schneider, K., Wrabetz, L., D'Antonio, M., Barry, N., Sigurdardottir, A., & Bertolotti, A. (2015). Preventing proteostasis diseases by selective inhibition of a phosphatase regulatory subunit. *Science*, *348*(6231), 239-242.

David, M., Petit, D., & Bertoglio, J. (2012). Cell cycle regulation of Rho signaling pathways. *Cell Cycle*, *11*(16), 3003-3010.

de Almeida, R. A., Fogli, A., Gaillard, M., Scheper, G. C., Boesflug-Tanguy, O., & Pavitt, G. D. (2013). A yeast purification system for human translation initiation factors eIF2 and eIF2Bepsilon and their use in the diagnosis of CACH/VWM disease. *PLOS ONE*, *8*(1), e53958.

De Franco, E., Caswell, R., Johnson, M. B., Wakeling, M. N., Zung, A., Dũng, V. C., Bích Ngọc, C. T., Goonetilleke, R., Vivanco Jury, M., El-Khateeb, M., Ellard, S., Flanagan, S. E., Ron, D., & Hattersley, A. T. (2020). De Novo Mutations in EIF2B1 Affecting eIF2 Signaling Cause Neonatal/Early-Onset Diabetes and Transient Hepatic Dysfunction. *Diabetes*, *69*(3), 477-483.

Delépine, M., Nicolino, M., Barrett, T., Golamaully, M., Lathrop, G. M., & Julier, C. (2000). EIF2AK3, encoding translation initiation factor 2-alpha kinase 3, is mutated in patients with Wolcott-Rallison syndrome. *Nat Genet*, *25*(4), 406-409.

Demeshkina, N., Jenner, L., Westhof, E., Yusupov, M., & Yusupova, G. (2012). A new understanding of the decoding principle on the ribosome. *Nature*, *484*(7393), 256-259.

Deng, J., Zhang, J., Gao, K., Zhou, L., Jiang, Y., Wang, J., & Wu, Y. (2023). Human-induced pluripotent stem cell-derived cerebral organoid of leukoencephalopathy with vanishing white matter. *CNS Neurosci Ther*, *29*(4), 1049-1066.

Dennis, M. D., Jefferson, L. S., & Kimball, S. R. (2012). Role of p70S6K1-mediated phosphorylation of eIF4B and PDCD4 proteins in the regulation of protein synthesis. *J Biol Chem*, *287*(51), 42890-42899.

Derisbourg, M. J., Wester, L. E., Baddi, R., & Denzel, M. S. (2021). Mutagenesis screen uncovers lifespan extension through integrated stress response inhibition without reduced mRNA translation. *Nat Commun*, *12*(1), 1678.

Dev, K., Qiu, H., Dong, J., Zhang, F., Barthlme, D., & Hinnebusch, A. G. (2010). The beta/Gcd7 subunit of eukaryotic translation initiation factor 2B (eIF2B), a guanine nucleotide exchange factor, is crucial for binding eIF2 in vivo. *Molecular and Cellular Biology*, *30*(21), 5218-5233.

Dever, T. E., Chen, J. J., Barber, G. N., Cigan, A. M., Feng, L., Donahue, T. F., London, I. M., Katze, M. G., & Hinnebusch, A. G. (1993). Mammalian eukaryotic initiation factor 2 alpha kinases functionally substitute for GCN2 protein kinase in the GCN4 translational control mechanism of yeast. *Proc Natl Acad Sci U S A*, *90*(10), 4616-4620.

Dever, T. E., Dinman, J. D., & Green, R. (2018). Translation Elongation and Recoding in Eukaryotes. *Cold Spring Harb Perspect Biol*, *10*(8), a032649.

Di Giammartino, D. C., Nishida, K., & Manley, J. L. (2011). Mechanisms and consequences of alternative polyadenylation. *Mol Cell*, *43*(6), 853-866.

Di Prisco, G. V., Huang, W., Buffington, S. A., Hsu, C. C., Bonnen, P. E., Placzek, A. N., Sidrauski, C., Krnjević, K., Kaufman, R. J., Walter, P., & Costa-Mattioli, M. (2014). Translational control of mGluR-dependent long-term depression and object-place learning by eIF2α. *Nat Neurosci*, *17*(8), 1073-1082.

Dietrich, J., Lacagnina, M., Gass, D., Richfield, E., Mayer-Pröschel, M., Noble, M., Torres, C., & Pröschel, C. (2005). EIF2B5 mutations compromise GFAP+ astrocyte generation in vanishing white matter leukodystrophy. *Nat Med*, *11*(3), 277-283.

Dmitriev, S. E., Terenin, I. M., Andreev, D. E., Ivanov, P. A., Dunaevsky, J. E., Merrick, W. C., & Shatsky, I. N. (2010). GTP-independent tRNA delivery to the ribosomal P-site by a novel eukaryotic translation factor. *J Biol Chem*, *285*(35), 26779-26787.

Dobrinskikh, E., Hennessy, C. E., Kurche, J. S., Kim, E., Estrella, A. M., Cardwell, J., Yang, I. V., & Schwartz, D. A. (2023). Epithelial Endoplasmic Reticulum Stress Enhances the Risk of Muc5b-associated Lung Fibrosis. *Am J Respir Cell Mol Biol*, *68*(1), 62-74.

Dolfi, S. C., Chan, L. L., Qiu, J., Tedeschi, P. M., Bertino, J. R., Hirshfield, K. M., Oltvai, Z. N., & Vazquez, A. (2013). The metabolic demands of cancer cells are coupled to their size and protein synthesis rates. *Cancer Metab*, *1*(1), 20.

Donnelly, C. J., Park, M., Spillane, M., Yoo, S., Pacheco, A., Gomes, C., Vuppalanchi, D., McDonald, M., Kim, H. H., Merianda, T. T., Gallo, G., & Twiss, J. L. (2013). Axonally synthesized beta-actin and GAP-43 proteins support distinct modes of axonal growth. *J Neurosci*, *33*(8), 3311-3322.

Donnelly, N., Gorman, A. M., Gupta, S., & Samali, A. (2013). The eIF2alpha kinases: their structures and functions. *Cellular and molecular life sciences : CMLS*, *70*(19), 3493-3511.

Dooves, S., Bugiani, M., Postma, N. L., Polder, E., Land, N., Horan, S. T., van Deijk, A.-L. F., van de Kreeke, A., Jacobs, G., Vuong, C., Klooster, J., Kamermans, M., Wortel, J., Loos, M., Wisse, L. E., Scheper, G. C., Abbink, T. E. M., Heine, V. M., & van der Knaap, M. S. (2016). Astrocytes are central in the pathomechanisms of vanishing white matter. *J Clin Invest*, *126*(4), 1512-1524.

Dooves, S., Bugiani, M., Wisse, L. E., Abbink, T. E. M., van der Knaap, M. S., & Heine, V. M. (2018). Bergmann glia translocation: a new disease marker for vanishing white matter identifies therapeutic effects of Guanabenz treatment. *Neuropathol Appl Neurobiol*, *44*(4), 391-403.

Dörrbaum, A. R., Kochen, L., Langer, J. D., & Schuman, E. M. (2018). Local and global influences on protein turnover in neurons and glia. *eLife*, *7,* e34202.

Draptchinskaia, N., Gustavsson, P., Andersson, B., Pettersson, M., Willig, T. N., Dianzani, I., Ball, S., Tchernia, G., Klar, J., Matsson, H., Tentler, D., Mohandas, N., Carlsson, B., & Dahl, N. (1999). The gene encoding ribosomal protein S19 is mutated in Diamond-Blackfan anaemia. *Nat Genet*, *21*(2), 169-175.

Droppelmann, C. A., Campos-Melo, D., Volkening, K., & Strong, M. J. (2014). The emerging role of guanine nucleotide exchange factors in ALS and other neurodegenerative diseases. *Front Cell Neurosci*, *8*, 282.

Dudka, W., Hoser, G., Mondal, S. S., Turos-Korgul, L., Swatler, J., Kusio-Kobialka, M., Wołczyk, M., Klejman, A., Brewinska-Olchowik, M., Kominek, A., Wiech, M., Machnicki, M. M., Seferynska, I., Stoklosa, T., & Piwocka, K. (2022). Targeting integrated stress response with ISRIB combined with imatinib treatment attenuates RAS/RAF/MAPK and STAT5 signaling and eradicates chronic myeloid leukemia cells. *BMC Cancer*, *22*(1), 1254.

Dunn, K. W., Kamocka, M. M., & McDonald, J. H. (2011). A practical guide to evaluating colocalization in biological microscopy. *Am J Physiol Cell Physiol*, *300*(4), C723-742.

Elsby, R., Heiber, J. F., Reid, P., Kimball, S. R., Pavitt, G. D., & Barber, G. N. (2011). The alpha subunit of eukaryotic initiation factor 2B (eIF2B) is required for eIF2-mediated translational suppression of vesicular stomatitis virus. *J Virol*, *85*(19), 9716-9725.

Eom, T., Antar, L. N., Singer, R. H., & Bassell, G. J. (2003). Localization of a beta-actin messenger ribonucleoprotein complex with zipcode-binding protein modulates the density of dendritic filopodia and filopodial synapses. *J Neurosci*, *23*(32), 10433-10444.

Erickson, F. L., & Hannig, E. M. (1996). Ligand interactions with eukaryotic translation initiation factor 2: role of the gamma-subunit. *EMBO J, 15*(22), 6311-6320.

Erzberger, J. P., Stengel, F., Pellarin, R., Zhang, S., Schaefer, T., Aylett, C. H. S., Cimermančič, P., Boehringer, D., Sali, A., Aebersold, R., & Ban, N. (2014). Molecular architecture of the 40S·eIF1·eIF3 translation initiation complex. *Cell*, *158*(5), 1123-1135.

Evans, J. C., Robinson, C. M., Shi, M., & Webb, D. J. (2015). The Guanine Nucleotide Exchange Factor (GEF) Asef2 Promotes Dendritic Spine Formation via Rac Activation and Spinophilin-dependent Targeting. *J Biol Chem*, *290*(16), 10295-10308.

Eyman, M., Cefaliello, C., Ferrara, E., De Stefano, R., Lavina, Z. S., Crispino, M., Squillace, A., van Minnen, J., Kaplan, B. B., & Giuditta, A. (2007). Local synthesis of axonal and presynaptic RNA in squid model systems. *Eur J Neurosci*, *25*(2), 341-350.

Fabian, J. R., Kimball, S. R., Heinzinger, N. K., & Jefferson, L. S. (1997). Subunit assembly and guanine nucleotide exchange activity of eukaryotic initiation factor-2B expressed in Sf9 cells. *J Biol Chem*, *272*(19), 12359-12365.

Feoktistova, K., Tuvshintogs, E., Do, A., & Fraser, C. S. (2013). Human eIF4E promotes mRNA restructuring by stimulating eIF4A helicase activity. *Proc Natl Acad Sci U S A*, *110*(33), 13339-13344.

Fijalkowska, D., Verbruggen, S., Ndah, E., Jonckheere, V., Menschaert, G., & Van Damme, P. (2017). eIF1 modulates the recognition of suboptimal translation initiation sites and steers gene expression via uORFs. *Nucleic Acids Res*, *45*(13), 7997-8013.

Fogli, A., Wong, K., Eymard-Pierre, E., Wenger, J., Bouffard, J.-P., Goldin, E., Black, D. N., Boespflug-Tanguy, O., & Schiffmann, R. (2002). Cree leukoencephalopathy and CACH/VWM disease are allelic at the EIF2B5 locus. *Ann Neurol*, *52*(4), 506-510.

Foster, J. B., Zhao, F., Wang, X., Xu, Z., Lin, K., Askwith, C. C., Hodgetts, K. J., & Lin, C. G. (2018). Pyridazine-derivatives Enhance Structural and Functional Plasticity of Tripartite Synapse Via Activation of Local Translation in Astrocytic Processes. *Neuroscience*, *388*, 224-238.

Francalanci, P., Eymard-Pierre, E., Dionisi-Vici, C., Boldrini, R., Piemonte, F., Virgili, R., Fariello, G., Bosman, C., Santorelli, F. M., Boespflug-Tanguy, O., & Bertini, E. (2001). Fatal infantile leukodystrophy: a severe variant of CACH/VWM syndrome, allelic to chromosome 3q27. *Neurology*, *57*(2), 265-270.

Franzmann, T. M., Jahnel, M., Pozniakovsky, A., Mahamid, J., Holehouse, A. S., Nüske, E., Richter, D., Baumeister, W., Grill, S. W., Pappu, R. V., Hyman, A. A., & Alberti, S. (2018). Phase separation of a yeast prion protein promotes cellular fitness. *Science*, *359*(6371), eaao5654.

Fritz, R. D., & Pertz, O. (2016). The dynamics of spatio-temporal Rho GTPase signaling: formation of signaling patterns. *F1000Res*, *5,* F1000 Faculty Rev-749.

Gallagher, J. W., Kubica, N., Kimball, S. R., & Jefferson, L. S. (2008). Reduced eukaryotic initiation factor 2Bepsilon-subunit expression suppresses the transformed phenotype of cells overexpressing the protein. *Cancer Res*, *68*(21), 8752-8760.

Galluzzi, L., Brenner, C., Morselli, E., Touat, Z., & Kroemer, G. (2008). Viral control of mitochondrial apoptosis. *PLoS Pathog*, *4*(5), e1000018.

García, M. A., Meurs, E. F., & Esteban, M. (2007). The dsRNA protein kinase PKR: virus and cell control. *Biochimie*, *89*(6-7), 799-811.

Gat-Viks, I., Geiger, T., Barbi, M., Raini, G., & Elroy-Stein, O. (2015). Proteomics-level analysis of myelin formation and regeneration in a mouse model for Vanishing White Matter disease. *J Neurochem*, *134*(3), 513-526.

Geva, M., Cabilly, Y., Assaf, Y., Mindroul, N., Marom, L., Raini, G., Pinchasi, D., & Elroy-Stein, O. (2010). A mouse model for eukaryotic translation initiation factor 2B-leucodystrophy reveals abnormal development of brain white matter. *Brain*, *133*(Pt 8), 2448-2461.

Ghaddar, N., Wang, S., Woodvine, B., Krishnamoorthy, J., van Hoef, V., Darini, C., Kazimierczak, U., Ah-Son, N., Popper, H., Johnson, M., Officer, L., Teodósio, A., Broggini, M., Mann, K. K., Hatzoglou, M., Topisirovic, I., Larsson, O., Le Quesne, J., & Koromilas, A. E. (2021). The integrated stress response is tumorigenic and constitutes a therapeutic liability in KRAS-driven lung cancer. *Nat Commun*, *12*(1), 4651.

Gibson, T. J., Seiler, M., & Veitia, R. A. (2013). The transience of transient overexpression. *Nat Methods*, *10*(8), 715-721.

Gilligan, M., Welsh, G. I., Flynn, A., Bujalska, I., Diggle, T. A., Denton, R. M., Proud, C. G., & Docherty, K. (1996). Glucose stimulates the activity of the guanine nucleotide-exchange factor eIF-2B in isolated rat islets of Langerhans. *J Biol Chem*, *271*(4), 2121-2125.

Gingras, A. C., Raught, B., & Sonenberg, N. (1999). eIF4 initiation factors: effectors of mRNA recruitment to ribosomes and regulators of translation. *Annu Rev Biochem*, *68*, 913-963.

Goh, K. C., deVeer, M. J., & Williams, B. R. (2000). The protein kinase PKR is required for p38 MAPK activation and the innate immune response to bacterial endotoxin. *EMBO J*, *19*(16), 4292-4297.

Golovko, A., Kojukhov, A., Guan, B. J., Morpurgo, B., Merrick, W. C., Mazumder, B., Hatzoglou, M., & Komar, A. A. (2016). The eIF2A knockout mouse. *Cell Cycle*, *15*(22), 3115-3120.

Gomez, E., & Pavitt, G. D. (2000). Identification of domains and residues within the epsilon subunit of eukaryotic translation initiation factor 2B (eIF2Bepsilon) required for guanine nucleotide exchange reveals a novel activation function promoted by eIF2B complex formation. *Mol Cell Biol*, *20*(11), 3965-3976.

Gordiyenko, Y., Llacer, J. L., & Ramakrishnan, V. (2019). Structural basis for the inhibition of translation through eIF2alpha phosphorylation. *Nat Commun*, *10*(1), 2640-2641.

Gordiyenko, Y., Schmidt, C., Jennings, M. D., Matak-Vinkovic, D., Pavitt, G. D., & Robinson, C. V. (2014). eIF2B is a decameric guanine nucleotide exchange factor with a γ2ε2 tetrameric core. *Nat Commun*, *5*, 3902.

Gracias, N. G., Shirkey-Son, N. J., & Hengst, U. (2014). Local translation of TC10 is required for membrane expansion during axon outgrowth. *Nat Communs*, *5*, 3506.

Gromadski, K. B., Schümmer, T., Strømgaard, A., Knudsen, C. R., Kinzy, T. G., & Rodnina, M. V. (2007). Kinetics of the interactions between yeast elongation factors 1A and 1Balpha, guanine nucleotides, and aminoacyl-tRNA. *J Biol Chem*, *282*(49), 35629-35637.

Gromadski, K. B., Wieden, H. J., & Rodnina, M. V. (2002). Kinetic mechanism of elongation factor Ts-catalyzed nucleotide exchange in elongation factor Tu. *Biochemistry*, *41*(1), 162-169.

Gross, M., Rubino, M. S., & Starn, T. K. (1988). Regulation of protein synthesis in rabbit reticulocyte lysate. Glucose 6-phosphate is required to maintain the activity of eukaryotic initiation factor (eIF)-2B by a mechanism that is independent of the phosphorylation of eIF-2 alpha. *J Biol Chem*, *263*(25), 12486-12492.

Grousl, T., Ivanov, P., Frýdlová, I., Vasicová, P., Janda, F., Vojtová, J., Malínská, K., Malcová, I., Nováková, L., Janosková, D., Valásek, L., & Hasek, J. (2009). Robust heat shock induces eIF2alpha-phosphorylation-independent assembly of stress granules containing eIF3 and 40S ribosomal subunits in budding yeast, Saccharomyces cerevisiae. *J Cell Sci*, *122*(Pt 12), 2078-2088.

Guan, B.-J., Krokowski, D., Majumder, M., Schmotzer, C. L., Kimball, S. R., Merrick, W. C., Koromilas, A. E., & Hatzoglou, M. (2014). Translational control during endoplasmic

reticulum stress beyond phosphorylation of the translation initiation factor eIF2α. *J Biol Chem*, *289*(18), 12593-12611.

Guan, B. J., van Hoef, V., Jobava, R., Elroy-Stein, O., Valasek, L. S., Cargnello, M., Gao, X. H., Krokowski, D., Merrick, W. C., Kimball, S. R., Komar, A. A., Koromilas, A. E., Wynshaw-Boris, A., Topisirovic, I., Larsson, O., & Hatzoglou, M. (2017). A Unique ISR Program Determines Cellular Responses to Chronic Stress. *Mol Cell*, *68*(5), 885-900.e886.

Guerrero, E. N., Wang, H., Mitra, J., Hegde, P. M., Stowell, S. E., Liachko, N. F., Kraemer, B. C., Garruto, R. M., Rao, K. S., & Hegde, M. L. (2016). TDP-43/FUS in motor neuron disease: Complexity and challenges. *Prog Neurobiol*, *145-146*, 78-97.

Guo, L., Chi, Y., Xue, J., Ma, L., Shao, Z., & Wu, J. (2017). Phosphorylated eIF2α predicts disease-free survival in triple-negative breast cancer patients. *Sci Rep*, *7*, 44674.

Guthrie, L. N., Abiraman, K., Plyler, E. S., Sprenkle, N. T., Gibson, S. A., McFarland, B. C., Rajbhandari, R., Rowse, A. L., Benveniste, E. N., & Meares, G. P. (2016). Attenuation of PKR-like ER Kinase (PERK) Signaling Selectively Controls Endoplasmic Reticulum Stress-induced Inflammation Without Compromising Immunological Responses. *J Biol Chem*, *291*(30), 15830-15840.

Halbeisen, R. E., Galgano, A., Scherrer, T., & Gerber, A. P. (2008). Post-transcriptional gene regulation: from genome-wide studies to principles. *Cel Mol Life Sci: CMLS, 65*(5), 798–813.

Halliday, M., Hughes, D., & Mallucci, G. R. (2017). Fine-tuning PERK signaling for neuroprotection. *J Neurochem*, *142*(6), 812-826.

Halliday, M., Radford, H., Sekine, Y., Moreno, J., Verity, N., le Quesne, J., Ortori, C. A., Barrett, D. A., Fromont, C., Fischer, P. M., Harding, H. P., Ron, D., & Mallucci, G. R. (2015). Partial restoration of protein synthesis rates by the small molecule ISRIB prevents neurodegeneration without pancreatic toxicity. *Cell Death Dis*, *6(3)*, e1672.

Hamilton, E. M. C., Van, D. L., Vermeulen, G., Gerver, J. A. M., Lourenço, C. M., Naidu, S., Mierzewska, H., Gemke, R. J. B. J., De Vet, H. C. W., Uitdehaag, B. M. J., Lissenberg-Witte, B. I., & Van, D. K. (2018). Natural History of Vanishing White Matter. *Annals of Neurology*, *84*(2), 274-288.

Han, A. P., Yu, C., Lu, L., Fujiwara, Y., Browne, C., Chin, G., Fleming, M., Leboulch, P., Orkin, S. H., & Chen, J. J. (2001). Heme-regulated eIF2alpha kinase (HRI) is required for translational regulation and survival of erythroid precursors in iron deficiency. *EMBO J*, *20*(23), 6909-6918.

Han, J., Back, S. H., Hur, J., Lin, Y. H., Gildersleeve, R., Shan, J., Yuan, C. L., Krokowski, D., Wang, S., Hatzoglou, M., Kilberg, M. S., Sartor, M. A., & Kaufman, R. J. (2013). ER-stress-induced transcriptional regulation increases protein synthesis leading to cell death. *Nat Cell Biol*, *15*(5), 481-490.

Hannig, E. M., Cigan, A. M., Freeman, B. A., & Kinzy, T. G. (1993). GCD11, a negative regulator of GCN4 expression, encodes the gamma subunit of eIF-2 in Saccharomyces cerevisiae. *Mol Cell Biol*, *13*(1), 506-520.

Hannig, E. M., & Hinnebusch, A. G. (1988). Molecular analysis of GCN3, a translational activator of GCN4: evidence for posttranslational control of GCN3 regulatory function. *Mol Cell Biol*, *8*(11), 4808-4820.

Hanson, F. M., Hodgson, R. E., de Oliveira, M. I. R., Allen, K. E., & Campbell, S. G. (2022). Regulation and function of eIF2B in neurological and metabolic disorders. *Biosci Rep*, *42*(6), BSR20211699.

Hao, Q., Heo, J. M., Nocek, B. P., Hicks, K. G., Stoll, V. S., Remarcik, C., Hackett, S., LeBon, L., Jain, R., Eaton, D., Rutter, J., Wong, Y. L., & Sidrauski, C. (2021). Sugar phosphate activation of the stress sensor eIF2B. *Nat Commun*, *12*(1), 3440.

Harada, K., Kamiya, T., & Tsuboi, T. (2016). Gliotransmitter Release from Astrocytes: Functional, Developmental, and Pathological Implications in the Brain. *Front Neurosci*, *9*, 499.

Harding, H. P., Novoa, I., Zhang, Y., Zeng, H., Wek, R., Schapira, M., & Ron, D. (2000). Regulated translation initiation controls stress-induced gene expression in mammalian cells. *Mol Cell*, *6*(5), 1099-1108.

Hellen, C. U. T. (2018). Translation Termination and Ribosome Recycling in Eukaryotes. *Cold Spring Harb Perspect Biol*, *10*(10), a032656.

Herrero, M., Daw, M., Atzmon, A., & Elroy-Stein, O. (2021). The Energy Status of Astrocytes Is the Achilles' Heel of eIF2B-Leukodystrophy. *Cells*, *10*(8), 1858.

Herrero, M., Mandelboum, S., & Elroy-Stein, O. (2019). eIF2B Mutations Cause Mitochondrial Malfunction in Oligodendrocytes. *Neuromolecular Med*, *21*(3), 303-313.

Hinnebusch, A. G. (2014). The scanning mechanism of eukaryotic translation initiation. *Annu Rev Biochem*, *83*, 779-812.

Hinnebusch, A. G., & Lorsch, J. R. (2012). The mechanism of eukaryotic translation initiation: new insights and challenges. *Cold Spring Harb Perspect Biol*, *4*(10), a011544.

Hodgson, R. E., Varanda, B. A., Ashe, M. P., Allen, K. E., & Campbell, S. G. (2019). Cellular eIF2B subunit localization: implications for the integrated stress response and its control by small molecule drugs. *Mol Biol Cell*, *30*(8), 942-958.

Holt, C. E., Martin, K. C., & Schuman, E. M. (2019). Local translation in neurons: visualization and function. *Nat Struct Mol Biol*, *26*(7), 557-566.

Hoyle, N. P., Castelli, L. M., Campbell, S. G., Holmes, L. E., & Ashe, M. P. (2007). Stress-dependent relocalization of translationally primed mRNPs to cytoplasmic granules that are kinetically and spatially distinct from P-bodies. *J Cell Biol*, *179*(1), 65-74.

Hu, H., Kahrizi, K., Musante, L., Fattahi, Z., Herwig, R., Hosseini, M., Oppitz, C., Abedini, S. S., Suckow, V., Larti, F., Beheshtian, M., Lipkowitz, B., Akhtarkhavari, T., Mehvari, S., Otto, S., Mohseni, M., Arzhangi, S., Jamali, P., Mojahedi, F., . . . Najmabadi, H. (2019). Genetics of intellectual disability in consanguineous families. *Mol Psychiatry*, *24*(7), 1027-1039.

Hu, Z., Yu, P., Zhang, Y., Yang, Y., Zhu, M., Qin, S., Xu, J.-T., Duan, D., Wu, Y., Wang, D., Rowan, M. J., & Hu, N.-W. (2022). Inhibition of the ISR abrogates mGluR5-dependent long-term depression and spatial memory deficits in a rat model of Alzheimer's disease. *Transl Psychiatry*, *12*(1), 96.

Huang, H. K., Yoon, H., Hannig, E. M., & Donahue, T. F. (1997). GTP hydrolysis controls stringent selection of the AUG start codon during translation initiation in Saccharomyces cerevisiae. *Genes Dev*, *11*(18), 2396-2413.

Huber, K. M., Kayser, M. S., & Bear, M. F. (2000). Role for rapid dendritic protein synthesis in hippocampal mGluR-dependent long-term depression. *Science*, *288*(5469), 1254-1257.

Hunkeler, M., Hagmann, A., Stuttfeld, E., Chami, M., Guri, Y., Stahlberg, H., & Maier, T. (2018). Structural basis for regulation of human acetyl-CoA carboxylase. *Nature*, *558*(7710), 470-474.

Huttelmaier, S., Zenklusen, D., Lederer, M., Dictenberg, J., Lorenz, M., Meng, X., Bassell, G. J., Condeelis, J., & Singer, R. H. (2005). Spatial regulation of beta-actin translation by Src-dependent phosphorylation of ZBP1. *Nature*, *438*(7067), 512-515.

Huyghe, A., Horzinski, L., Henaut, A., Gaillard, M., Bertini, E., Schiffmann, R., Rodriguez, D., Dantal, Y., Boespflug-Tanguy, O., & Fogli, A. (2012). Developmental splicing deregulation in leukodystrophies related to EIF2B mutations. *PLOS ONE*, *7*(6), e38264.

Ikari, R., Mukaisho, K. I., Kageyama, S., Nagasawa, M., Kubota, S., Nakayama, T., Murakami, S., Taniura, N., Tanaka, H., Kushima, R. P., & Kawauchi, A. (2021). Differences in the Central Energy Metabolism of Cancer Cells between Conventional 2D and Novel 3D Culture Systems. *Int J Mol Sci*, *22*(4), 1805.

Irgen-Gioro, S., Yoshida, S., Walling, V., & Chong, S. (2022). Fixation can change the appearance of phase separation in living cells. *eLife*, *11,* e79903.

Izumi, Y., & Zorumski, C. F. (2020). Inhibitors of cellular stress overcome acute effects of ethanol on hippocampal plasticity and learning. *Neurobiol Dis*, *141*, 104875.

Jackson, K. M., Frazier, M. C., Mancia, M. D., & Shaw, R. N. (2019). Chapter 1 - Recent advances in the licorice root constituent dibenzoylmethane as a potential therapeutic option for cancer. In R. Atta ur (Ed.), *Studies in Natural Products Chemistry* (Vol. 63, pp. 1-19). Elsevier.

Jackson, R. J., Hellen, C. U., & Pestova, T. V. (2010). The mechanism of eukaryotic translation initiation and principles of its regulation. *Nature reviews: Mol Cell Biol*, *11*(2), 113-127.

Jain, A., & Vale, R. D. (2017). RNA phase transitions in repeat expansion disorders. *Nature*, *546*(7657), 243-247.

Jennings, M. D., Kershaw, C. J., Adomavicius, T., & Pavitt, G. D. (2017). Fail-safe control of translation initiation by dissociation of eIF2α phosphorylated ternary complexes. *eLife*, *6,* e24542.

Jennings, M. D., & Pavitt, G. D. (2010). eIF5 has GDI activity necessary for translational control by eIF2 phosphorylation. *Nature*, *465*(7296), 378-381.

Jennings, M. D., Zhou, Y., Mohammad-Qureshi, S. S., Bennett, D., & Pavitt, G. D. (2013). eIF2B promotes eIF5 dissociation from eIF2*GDP to facilitate guanine nucleotide exchange for translation initiation. *Genes Dev*, *27*(24), 2696-2707.

Jewer, M., Lee, L., Leibovitch, M., Zhang, G., Liu, J., Findlay, S. D., Vincent, K. M., Tandoc, K., Dieters-Castator, D., Quail, D. F., Dutta, I., Coatham, M., Xu, Z., Puri, A., Guan,

B. J., Hatzoglou, M., Brumwell, A., Uniacke, J., Patsis, C., . . . Postovit, L. M. (2020). Translational control of breast cancer plasticity. *Nat Commun*, *11*(1), 2498.

Jiang, H. Y., & Wek, R. C. (2005). GCN2 phosphorylation of eIF2alpha activates NF-kappaB in response to UV irradiation. *Biochem J*, *385*(Pt 2), 371-380.

Jiang, Z., Belforte, J. E., Lu, Y., Yabe, Y., Pickel, J., Smith, C. B., Je, H. S., Lu, B., & Nakazawa, K. (2010). eIF2alpha Phosphorylation-dependent translation in CA1 pyramidal cells impairs hippocampal memory consolidation without affecting general translation. *J Neurosci*, *30*(7), 2582-2594.

Johnson, E. C., & Kang, J. (2016). A small molecule targeting protein translation does not rescue spatial learning and memory deficits in the hAPP-J20 mouse model of Alzheimer's disease. *PeerJ*, *4*, e2565.

Jousse, C., Oyadomari, S., Novoa, I., Lu, P., Zhang, Y., Harding, H. P., & Ron, D. (2003). Inhibition of a constitutive translation initiation factor 2alpha phosphatase, CReP, promotes survival of stressed cells. *J Cell Biol*, *163*(4), 767-775.

Jung, H., Yoon, B. C., & Holt, C. E. (2012). Axonal mRNA localization and local protein synthesis in nervous system assembly, maintenance and repair. *Nat Rev Neurosci*, *13*(5), 308-324.

Kamphuis, W., Mamber, C., Moeton, M., Kooijman, L., Sluijs, J. A., Jansen, A. H., Verveer, M., de Groot, L. R., Smith, V. D., Rangarajan, S., Rodriguez, J. J., Orre, M., & Hol, E. M. (2012). GFAP isoforms in adult mouse brain with a focus on neurogenic astrocytes and reactive astrogliosis in mouse models of Alzheimer disease. *PLOS ONE*, *7*(8), e42823.

Kantor, L., Harding, H. P., Ron, D., Schiffmann, R., Kaneski, C. R., Kimball, S. R., & Elroy-Stein, O. (2005). Heightened stress response in primary fibroblasts expressing mutant eIF2B genes from CACH/VWM leukodystrophy patients. *Hum Genet*, *118*(1), 99-106.

Kapp, L. D., & Lorsch, J. R. (2004). The molecular mechanics of eukaryotic translation. *Annu Rev Biochem*, *73*, 657-704.

Karpinski, B. A., Morle, G. D., Huggenvik, J., Uhler, M. D., & Leiden, J. M. (1992). Molecular cloning of human CREB-2: an ATF/CREB transcription factor that can negatively regulate transcription from the cAMP response element. *Proc Natl Acad Sci U S A*, *89*(11), 4820-4824.

Kashiwagi, K., Ito, T., & Yokoyama, S. (2017). Crystal structure of eIF2B and insights into eIF2-eIF2B interactions. *FEBS J*, *284*(6), 868-874.

Kashiwagi, K., Takahashi, M., Nishimoto, M., Hiyama, T. B., Higo, T., Umehara, T., Sakamoto, K., Ito, T., & Yokoyama, S. (2016). Crystal structure of eukaryotic translation initiation factor 2B. *Nature*, *531*(7592), 122-125.

Kashiwagi, K., Yokoyama, T., Nishimoto, M., Takahashi, M., Sakamoto, A., Yonemochi, M., Shirouzu, M., & Ito, T. (2019). Structural basis for eIF2B inhibition in integrated stress response. *Science*, *364*(6439), 495-499.

Kaspar, S., Oertlin, C., Szczepanowska, K., Kukat, A., Senft, K., Lucas, C., Brodesser, S., Hatzoglou, M., Larsson, O., Topisirovic, I., & Trifunovic, A. (2021). Adaptation to mitochondrial stress requires CHOP-directed tuning of ISR. *Sci Adv*, *7*(22), eabf0971.

Kastan, J. P., Dobrikova, E. Y., Bryant, J. D., & Gromeier, M. (2020). CReP mediates selective translation initiation at the endoplasmic reticulum. *Sci Adv*, *6*(23), eaba0745.

Kedersha, N., Stoecklin, G., Ayodele, M., Yacono, P., Lykke-Andersen, J., Fritzler, M. J., Scheuner, D., Kaufman, R. J., Golan, D. E., & Anderson, P. (2005). Stress granules and processing bodies are dynamically linked sites of mRNP remodeling. *J Cell Biol*, *169*(6), 871-884.

Keefe, M. D., Soderholm, H. E., Shih, H. Y., Stevenson, T. J., Glaittli, K. A., Bowles, D. M., Scholl, E., Colby, S., Merchant, S., Hsu, E. W., & Bonkowsky, J. L. (2020). Vanishing white matter disease expression of truncated EIF2B5 activates induced stress response. *eLife*, *9*, e56319

Kelemen, O., Convertini, P., Zhang, Z., Wen, Y., Shen, M., Falaleeva, M., & Stamm, S. (2013). Function of alternative splicing. *Gene, 514*(1), 1–30.

Kenner, L. R., Anand, A. A., Nguyen, H. C., Myasnikov, A. G., Klose, C. J., McGeever, L. A., Tsai, J. C., Miller-Vedam, L. E., Walter, P., & Frost, A. (2019). eIF2B-catalyzed nucleotide exchange and phosphoregulation by the integrated stress response. *Science*, *364*(6439), 491-495.

Kernohan, K. D., Tétreault, M., Liwak-Muir, U., Geraghty, M. T., Qin, W., Venkateswaran, S., Davila, J., Holcik, M., Majewski, J., Richer, J., & Boycott, K. M. (2015). Homozygous mutation in the eukaryotic translation initiation factor 2alpha phosphatase gene, PPP1R15B, is associated with severe microcephaly, short stature and intellectual disability. *Hum Mol Genet*, *24*(22), 6293-6300.

Kershaw, C. J., Jennings, M. D., Cortopassi, F., Guaita, M., Al-Ghafli, H., & Pavitt, G. D. (2021). GTP binding to translation factor eIF2B stimulates its guanine nucleotide exchange activity. *iScience*, *24*(12), 103454.

Kida, S. (2012). A Functional Role for CREB as a Positive Regulator of Memory Formation and LTP. *Exp Neurobiol*, *21*(4), 136-140.

Kim, E., Kim, J. H., Seo, K., Hong, K. Y., An, S. W. A., Kwon, J., Lee, S. V., & Jang, S. K. (2018). eIF2A, an initiator tRNA carrier refractory to eIF2α kinases, functions synergistically with eIF5B. *Cell Mol Life Sci*, *75*(23), 4287-4300.

Kim, J. H., Park, S. M., Park, J. H., Keum, S. J., & Jang, S. K. (2011). eIF2A mediates translation of hepatitis C viral mRNA under stress conditions. *EMBO J*, *30*(12), 2454-2464.

Kimball, S. R., Horetsky, R. L., & Jefferson, L. S. (1998). Implication of eIF2B rather than eIF4E in the regulation of global protein synthesis by amino acids in L6 myoblasts. *J Biol Chem*, *273*(47), 30945-30953.

Klein, P., Kallenberger, S. M., Roth, H., Roth, K., Ly-Hartig, T. B. N., Magg, V., Aleš, J., Talemi, S. R., Qiang, Y., Wolf, S., Oleksiuk, O., Kurilov, R., Di Ventura, B., Bartenschlager, R., Eils, R., Rohr, K., Hamprecht, F. A., Höfer, T., Fackler, O. T., . . . Ruggieri, A. (2022). Temporal control of the integrated stress response by a stochastic molecular switch. *Sci Adv*, *8*(12), eabk2022.

Klok, M. D., Bugiani, M., de Vries, S. I., Gerritsen, W., Breur, M., van, d. S., Heine, V. M., Kole, M. H. P., Baron, W., & van der Knaap, M. S. (2018). Axonal abnormalities in vanishing white matter. *Ann Clin Transl Neurol*, *5*(4), 429–444.

Kojima, E., Takeuchi, A., Haneda, M., Yagi, A., Hasegawa, T., Yamaki, K., Takeda, K., Akira, S., Shimokata, K., & Isobe, K. (2003). The function of GADD34 is a recovery from a shutoff of protein synthesis induced by ER stress: elucidation by GADD34-deficient mice. *FASEB J*, *17*(11), 1573-1575.

Kole, A. J., Annis, R. P., & Deshmukh, M. (2013). Mature neurons: equipped for survival. *Cell Death Dis*, *4*(6), e689.

Komiyama, N. H., Watabe, A. M., Carlisle, H. J., Porter, K., Charlesworth, P., Monti, J., Strathdee, D. J., O'Carroll, C. M., Martin, S. J., Morris, R. G., O'Dell, T. J., & Grant, S. G. (2002). SynGAP regulates ERK/MAPK signaling, synaptic plasticity, and learning in the complex with postsynaptic density 95 and NMDA receptor. *J Neurosci*, *22*(22), 9721-9732.

Krichevsky, A. M., & Kosik, K. S. (2001). Neuronal RNA granules: a link between RNA localization and stimulation-dependent translation. *Neuron*, *32*(4), 683-696.

Krishnamoorthy, T., Pavitt, G. D., Zhang, F., Dever, T. E., & Hinnebusch, A. G. (2001). Tight binding of the phosphorylated alpha subunit of initiation factor 2 (eIF2alpha) to the regulatory subunits of guanine nucleotide exchange factor eIF2B is required for inhibition of translation initiation. *Mol Cell Biol*, *21*(15), 5018-5030.

Krukowski, K., Nolan, A., Frias, E. S., Boone, M., Ureta, G., Grue, K., Paladini, M. S., Elizarraras, E., Delgado, L., Bernales, S., Walter, P., & Rosi, S. (2020). Small molecule cognitive enhancer reverses age-related memory decline in mice. *eLife*, *9*, e62048.

Kuhle, B., Eulig, N. K., & Ficner, R. (2015). Architecture of the eIF2B regulatory subcomplex and its implications for the regulation of guanine nucleotide exchange on eIF2. *Nucleic Acids Res*, *43*(20), 9994-10014.

Kwon, O. S., An, S., Kim, E., Yu, J., Hong, K. Y., Lee, J. S., & Jang, S. K. (2017). An mRNA-specific tRNAi carrier eIF2A plays a pivotal role in cell proliferation under stress conditions: stress-resistant translation of c-Src mRNA is mediated by eIF2A. *Nucleic Acids Res*, *45*(1), 296-310.

Lacerda, R., Menezes, J., & Romão, L. (2017). More than just scanning: the importance of cap-independent mRNA translation initiation for cellular stress response and cancer. *Cell Mol Life Sci*, *74*(9), 1659-1680.

Ladiges, W. C., Knoblaugh, S. E., Morton, J. F., Korth, M. J., Sopher, B. L., Baskin, C. R., MacAuley, A., Goodman, A. G., LeBoeuf, R. C., & Katze, M. G. (2005). Pancreatic beta-cell failure and diabetes in mice with a deletion mutation of the endoplasmic reticulum molecular chaperone gene P58IPK. *Diabetes*, *54*(4), 1074-1081.

Ladran, I., Tran, N., Topol, A., & Brennand, K. J. (2013). Neural stem and progenitor cells in health and disease. *Wiley Interdiscip Rev Syst Biol Med*, *5*(6), 701-715.

Lee, A. S., Kranzusch, P. J., & Cate, J. H. (2015). eIF3 targets cell-proliferation messenger RNAs for translational activation or repression. *Nature*, *522*(7554), 111-114.

Lee, A. S., Kranzusch, P. J., Doudna, J. A., & Cate, J. H. (2016). eIF3d is an mRNA cap-binding protein that is required for specialized translation initiation. *Nature*, *536*(7614), 96-99.

Leegwater, P. A., Vermeulen, G., Könst, A. A., Naidu, S., Mulders, J., Visser, A., Kersbergen, P., Mobach, D., Fonds, D., van Berkel, C. G., Lemmers, R. J., Frants, R. R., Oudejans, C. B., Schutgens, R. B., Pronk, J. C., & van der Knaap, M. S. (2001). Subunits of the translation initiation factor eIF2B are mutant in leukoencephalopathy with vanishing white matter. *Nat Genet*, *29*(4), 383-388.

Leferink, P. S., Breeuwsma, N., Bugiani, M., van der Knaap, M. S., & Heine, V. M. (2018). Affected astrocytes in the spinal cord of the leukodystrophy vanishing white matter. *Glia*, *66*(4), 862-873.

Li, L., & Hu, G. (2015). Pink1 protects cortical neurons from thapsigargin-induced oxidative stress and neuronal apoptosis. *Biosci Rep*, *35*(1), e00174.

Li, W., Wang, X., Van Der Knaap, M. S., & Proud, C. G. (2004). Mutations linked to leukoencephalopathy with vanishing white matter impair the function of the eukaryotic initiation factor 2B complex in diverse ways. *Mol Cell Biol*, *24*(8), 3295-3306.

Li, X. B., Gu, J. D., & Zhou, Q. H. (2015). Review of aerobic glycolysis and its key enzymes - new targets for lung cancer therapy. *Thorac cancer*, *6*(1), 17-24.

Liberman, N., Gandin, V., Svitkin, Y. V., David, M., Virgili, G., Jaramillo, M., Holcik, M., Nagar, B., Kimchi, A., & Sonenberg, N. (2015). DAP5 associates with eIF2β and eIF4AI to promote Internal Ribosome Entry Site driven translation. *Nucleic Acids Res*, *43*(7), 3764-3775.

Licari, E., Sánchez-Del-Campo, L., & Falletta, P. (2021). The two faces of the Integrated Stress Response in cancer progression and therapeutic strategies. *Int J Biochem Cell Biol*, *139*, 106059.

Lin, C. C., Tsai, Y. L., Huang, M. T., Lu, Y. P., Ho, C. T., Tseng, S. F., & Teng, S. C. (2006). Inhibition of estradiol-induced mammary proliferation by dibenzoylmethane through the E2-ER-ERE-dependent pathway. *Carcinogenesis*, *27*(1), 131-136.

Lin, K. Y., Nag, N., Pestova, T. V., & Marintchev, A. (2018). Human eIF5 and eIF1A Compete for Binding to eIF5B. *Biochemistry*, *57*(40), 5910–5920.

Liu, J., Amar, F., Corona, C., So, R. W. L., Andrews, S. J., Nagy, P. L., Shelanski, M. L., & Greene, L. A. (2018). Brain-Derived Neurotrophic Factor Elevates Activating Transcription Factor 4 (ATF4) in Neurons and Promotes ATF4-Dependent Induction of Sesn2. *Front Mol Neurosci*, *11*, 62.

Liu, R., van der Lei, H. D., Wang, X., Wortham, N. C., Tang, H., van Berkel, C. G., Mufunde, T. A., Huang, W., van der Knaap, M. S., Scheper, G. C., & Proud, C. G. (2011). Severity of vanishing white matter disease does not correlate with deficits in eIF2B activity or the integrity of eIF2B complexes. *Hum Mutat*, *32*(9), 1036-1045.

Liu, Y., Han, S. S., Wu, Y., Tuohy, T. M., Xue, H., Cai, J., Back, S. A., Sherman, L. S., Fischer, I., & Rao, M. S. (2004). CD44 expression identifies astrocyte-restricted precursor cells. *Dev Biol*, *276*(1), 31-46.

Llácer, J. L., Hussain, T., Saini, A. K., Nanda, J. S., Kaur, S., Gordiyenko, Y., Kumar, R., Hinnebusch, A. G., Lorsch, J. R., & Ramakrishnan, V. (2018). Translational initiation factor eIF5 replaces eIF1 on the 40S ribosomal subunit to promote start-codon recognition. *eLife*, *7,* e39273

Longchamp, A., Mirabella, T., Arduini, A., MacArthur, M. R., Das, A., Treviño-Villarreal, J. H., Hine, C., Ben-Sahra, I., Knudsen, N. H., Brace, L. E., Reynolds, J., Mejia, P., Tao, M., Sharma, G., Wang, R., Corpataux, J. M., Haefliger, J. A., Ahn, K. H., Lee, C. H., . . . Mitchell, J. R. (2018). Amino Acid Restriction Triggers Angiogenesis via GCN2/ATF4 Regulation of VEGF and H(2)S Production. *Cell*, *173*(1), 117-129.e114.

Longo, F., Mancini, M., Ibraheem, P. L., Aryal, S., Mesini, C., Patel, J. C., Penhos, E., Rahman, N., Mamcarz, M., Santini, E., Rice, M. E., & Klann, E. (2021). Cell-type-specific disruption of PERK-eIF2α signaling in dopaminergic neurons alters motor and cognitive function. *Mol Psychiatry*, *26*(11), 6427-6450.

Loschi, M., Leishman, C. C., Berardone, N., & Boccaccio, G. L. (2009). Dynein and kinesin regulate stress-granule and P-body dynamics. *J Cell Sci*, *122*(Pt 21), 3973-3982.

Loveland, A. B., Demo, G., Grigorieff, N., & Korostelev, A. A. (2017). Ensemble cryo-EM elucidates the mechanism of translation fidelity. *Nature*, *546*(7656), 113-117.

Low, L. K., & Cheng, H. J. (2006). Axon pruning: an essential step underlying the developmental plasticity of neuronal connections. *Philos Trans R Soc Lond B Biol Sci*, *361*(1473), 1531-1544.

Lu, L., Han, A. P., & Chen, J. J. (2001). Translation initiation control by heme-regulated eukaryotic initiation factor 2alpha kinase in erythroid cells under cytoplasmic stresses. *Mol Cell Biol*, *21*(23), 7971-7980.

Lu, P. D., Jousse, C., Marciniak, S. J., Zhang, Y., Novoa, I., Scheuner, D., Kaufman, R. J., Ron, D., & Harding, H. P. (2004). Cytoprotection by pre-emptive conditional phosphorylation of translation initiation factor 2. *EMBO J*, *23*(1), 169-179.

Lu, Y. N., Kavianpour, S., Zhang, T., Zhang, X., Nguyen, D., Thombre, R., He, L., & Wang, J. (2021). MARK2 phosphorylates eIF2α in response to proteotoxic stress. *PLoS Biol*, *19*(3), e3001096.

Luarte, A., Henzi, R., Fernández, A., Gaete, D., Cisternas, P., Pizarro, M., Batiz, L. F., Villalobos, I., Masalleras, M., Vergara, R., Varas-Godoy, M., Abarzua-Catalan, L., Herrera-Molina, R., Lafourcade, C., & Wyneken, U. (2020). Astrocyte-Derived Small Extracellular Vesicles Regulate Dendritic Complexity through miR-26a-5p Activity. *Cells*, *9*(4), 930.

Lutz, M. I., Schwaiger, C., Hochreiter, B., Kovacs, G. G., & Schmid, J. A. (2017). Novel approach for accurate tissue-based protein colocalization and proximity microscopy. *Sci Rep*, *7*(1), 2668.

Ma, T., Trinh, M. A., Wexler, A. J., Bourbon, C., Gatti, E., Pierre, P., Cavener, D. R., & Klann, E. (2013). Suppression of eIF2α kinases alleviates Alzheimer's disease-related plasticity and memory deficits. *Nat Neurosci*, *16*(9), 1299-1305.

Maag, D., Algire, M. A., & Lorsch, J. R. (2006). Communication between eukaryotic translation initiation factors 5 and 1A within the ribosomal pre-initiation complex plays a role in start site selection. *J Mol Biol*, *356*(3), 724-737.

Maag, D., & Lorsch, J. R. (2003). Communication between eukaryotic translation initiation factors 1 and 1A on the yeast small ribosomal subunit. *J Mol Biol*, *330*(5), 917-924.

Majumdar, R., Bandyopadhyay, A., & Maitra, U. (2003). Mammalian translation initiation factor eIF1 functions with eIF1A and eIF3 in the formation of a stable 40 S preinitiation complex. *J Biol Chem*, *278*(8), 6580-6587.

Majumder, M., Huang, C., Snider, M. D., Komar, A. A., Tanaka, J., Kaufman, R. J., Krokowski, D., & Hatzoglou, M. (2012). A novel feedback loop regulates the response to endoplasmic reticulum stress via the cooperation of cytoplasmic splicing and mRNA translation. *Mol Cell Biol*, *32*(5), 992-1003.

Man, J. H. K., van Gelder, C., Breur, M., Okkes, D., Molenaar, D., van der Sluis, S., Abbink, T., Altelaar, M., van der Knaap, M. S., & Bugiani, M. (2022). Cortical Pathology in Vanishing White Matter. *Cells*, *11*(22), 3581.

Marciniak, S. J., Yun, C. Y., Oyadomari, S., Novoa, I., Zhang, Y., Jungreis, R., Nagata, K., Harding, H. P., & Ron, D. (2004). CHOP induces death by promoting protein synthesis and oxidation in the stressed endoplasmic reticulum. *Genes Dev*, *18*(24), 3066-3077.

Marini, G., Nüske, E., Leng, W., Alberti, S., & Pigino, G. (2020). Reorganization of budding yeast cytoplasm upon energy depletion. *Mol Biol Cell*, *31*(12), 1232-1245.

Martin, E. W., & Mittag, T. (2018). Relationship of Sequence and Phase Separation in Protein Low-Complexity Regions. *Biochemistry*, *57*(17), 2478-2487.

Martin, L., Kimball, S. R., & Gardner, L. B. (2010). Regulation of the unfolded protein response by eif2Bdelta isoforms. *J Biol Chem*, *285*(42), 31944-31953.

Mason, J. T., & O'Leary, T. J. (1991). Effects of formaldehyde fixation on protein secondary structure: a calorimetric and infrared spectroscopic investigation. *J Histochem Cytochem*, *39*(2), 225-229.

Masuda, S., Das, R., Cheng, H., Hurt, E., Dorman, N., & Reed, R. (2005). Recruitment of the human TREX complex to mRNA during splicing. *Genes Dev, 19*(13), 1512–1517.

Mathieson, T., Franken, H., Kosinski, J., Kurzawa, N., Zinn, N., Sweetman, G., Poeckel, D., Ratnu, V. S., Schramm, M., Becher, I., Steidel, M., Noh, K. M., Bergamini, G., Beck, M., Bantscheff, M., & Savitski, M. M. (2018). Systematic analysis of protein turnover in primary cells. *Nat Commun*, *9*(1), 689.

Matsukawa, T., Wang, X., Liu, R., Wortham, N. C., Onuki, Y., Kubota, A., Hida, A., Kowa, H., Fukuda, Y., Ishiura, H., Mitsui, J., Takahashi, Y., Aoki, S., Takizawa, S., Shimizu, J., Goto, J., Proud, C. G., & Tsuji, S. (2011). Adult-onset leukoencephalopathies with vanishing white matter with novel missense mutations in EIF2B2, EIF2B3, and EIF2B5. *Neurogenetics*, *12*(3), 259-261.

Mazaré, N., Oudart, M., & Cohen-Salmon, M. (2021). Local translation in perisynaptic and perivascular astrocytic processes - a means to ensure astrocyte molecular and functional polarity? *J Cell Sci*, *134*(2), jcs251629.

McCullough, K. D., Martindale, J. L., Klotz, L. O., Aw, T. Y., & Holbrook, N. J. (2001). Gadd153 sensitizes cells to endoplasmic reticulum stress by down-regulating Bcl2 and perturbing the cellular redox state. *Mol Cell Biol*, *21*(4), 1249-1259.

McEwen, E., Kedersha, N., Song, B., Scheuner, D., Gilks, N., Han, A., Chen, J.-J., Anderson, P., & Kaufman, R. J. (2005). Heme-regulated inhibitor kinase-mediated phosphorylation of eukaryotic translation initiation factor 2 inhibits translation, induces stress granule formation, and mediates survival upon arsenite exposure. *J Biol Chem*, *280*(17), 16925-16933.

McManus, E. J., Sakamoto, K., Armit, L. J., Ronaldson, L., Shpiro, N., Marquez, R., & Alessi, D. R. (2005). Role that phosphorylation of GSK3 plays in insulin and Wnt signalling defined by knockin analysis. *EMBO J*, *24*(8), 1571-1583.

Mendoza, M. B., Gutierrez, S., Ortiz, R., Moreno, D. F., Dermit, M., Dodel, M., Rebollo, E., Bosch, M., Mardakheh, F. K., & Gallego, C. (2021). The elongation factor eEF1A2 controls translation and actin dynamics in dendritic spines. *Sci Signal*, *14*(691), eabf5594.

Merrick, W. C., & Pavitt, G. D. (2018). Protein Synthesis Initiation in Eukaryotic Cells. *Cold Spring Harb Perspect Biol*, *10*(12), ea033092.

Meyer, K. D., Patil, D. P., Zhou, J., Zinoviev, A., Skabkin, M. A., Elemento, O., Pestova, T. V., Qian, S. B., & Jaffrey, S. R. (2015). 5' UTR m(6)A Promotes Cap-Independent Translation. *Cell*, *163*(4), 999-1010.

Molenaar, J. J., Domingo-Fernandez, R., Ebus, M. E., Lindner, S., Koster, J., Drabek, K., Mestdagh, P., van Sluis, P., Valentijn, L. J., van Nes, J., Broekmans, M., Haneveld, F., Volckmann, R., Bray, I., Heukamp, L., Sprussel, A., Thor, T., Kieckbusch, K., Klein-Hitpass, L., . . . Schulte, J. H. (2012). LIN28B induces neuroblastoma and enhances MYCN levels via let-7 suppression. *Nat Gen*, *44*(11), 1199-1206.

Monin, A., Fournier, M., Baumann, P. S., Cuénod, M., & Do, K. Q. (2016). Chapter 28 - Role of Redox Dysregulation in White Matter Anomalies Associated with Schizophrenia. *Handbook of Behav Neurosci*, *23*, 481-500.

Montani, D., Girerd, B., Jaïs, X., Levy, M., Amar, D., Savale, L., Dorfmüller, P., Seferian, A., Lau, E. M., Eyries, M., Le Pavec, J., Parent, F., Bonnet, D., Soubrier, F., Fadel, E., Sitbon, O., Simonneau, G., & Humbert, M. (2017). Clinical phenotypes and outcomes of heritable and sporadic pulmonary veno-occlusive disease: a population-based study. *Lancet Respir Med*, *5*(2), 125-134.

Moon, S. L., & Parker, R. (2018a). Analysis of eIF2B bodies and their relationships with stress granules and P-bodies. *Sci Rep*, *8*(1), 12264.

Moon, S. L., & Parker, R. (2018b). EIF2B2 mutations in vanishing white matter disease hypersuppress translation and delay recovery during the integrated stress response. *RNA*, *24*(6), 841-852.

Moqtaderi, Z., Geisberg, J. V., & Struhl, K. (2014). Secondary structures involving the poly(A) tail and other 3' sequences are major determinants of mRNA isoform stability in yeast. *Microb Cell, 1*(4), 137–139.

Moretti, J., Chastagner, P., Gastaldello, S., Heuss, S. F., Dirac, A. M., Bernards, R., Masucci, M. G., Israël, A., & Brou, C. (2010). The translation initiation factor 3f (eIF3f) exhibits a deubiquitinase activity regulating Notch activation. *PLoS Biol*, *8*(11), e1000545.

Morita, M., Gravel, S. P., Chénard, V., Sikström, K., Zheng, L., Alain, T., Gandin, V., Avizonis, D., Arguello, M., Zakaria, C., McLaughlan, S., Nouet, Y., Pause, A., Pollak, M., Gottlieb, E., Larsson, O., St-Pierre, J., Topisirovic, I., & Sonenberg, N. (2013). mTORC1 controls mitochondrial activity and biogenesis through 4E-BP-dependent translational regulation. *Cell Metab*, *18*(5), 698-711.

Nakamura, A., Fujihashi, M., Aono, R., Sato, T., Nishiba, Y., Yoshida, S., Yano, A., Atomi, H., Imanaka, T., & Miki, K. (2012). Dynamic, ligand-dependent conformational change triggers reaction of ribose-1,5-bisphosphate isomerase from Thermococcus kodakarensis KOD1. *J Biol Chem*, *287*(25), 20784-20796.

Naveau, M., Lazennec-Schurdevin, C., Panvert, M., Dubiez, E., Mechulam, Y., & Schmitt, E. (2013). Roles of yeast eIF2alpha and eIF2beta subunits in the binding of the initiator methionyl-tRNA. *Nucleic Acids Res*, *41*(2), 1047-1057.

Nern, A., & Arkowitz, R. A. (2000). G proteins mediate changes in cell shape by stabilizing the axis of polarity. *Mol Cell*, *5*(5), 853-864.

Noree, C., Sato, B. K., Broyer, R. M., & Wilhelm, J. E. (2010). Identification of novel filament-forming proteins in Saccharomyces cerevisiae and Drosophila melanogaster. *J Cell Biol*, *190*(4), 541-551.

Norris, K., Hodgson, R. E., Dornelles, T., Allen, K. E., Abell, B. M., Ashe, M. P., & Campbell, S. G. (2021). Mutational analysis of the alpha subunit of eIF2B provides insights into the role of eIF2B bodies in translational control and VWM disease. *J Biol Chem*, *296*, 100207.

Nouar, R., Devred, F., Breuzard, G., & Peyrot, V. (2013). FRET and FRAP imaging: approaches to characterise tau and stathmin interactions with microtubules in cells. *Biol Cell*, *105*(4), 149-161.

Nüske, E., Marini, G., Richter, D., Leng, W., Bogdanova, A., Franzmann, T. M., Pigino, G., & Alberti, S. (2020). Filament formation by the translation factor eIF2B regulates protein synthesis in starved cells. *Biol Open*, *9*(7), bio046391.

O'Connor, T., Sadleir, K. R., Maus, E., Velliquette, R. A., Zhao, J., Cole, S. L., Eimer, W. A., Hitt, B., Bembinster, L. A., Lammich, S., Lichtenthaler, S. F., Hébert, S. S., De Strooper, B., Haass, C., Bennett, D. A., & Vassar, R. (2008). Phosphorylation of the translation initiation factor eIF2alpha increases BACE1 levels and promotes amyloidogenesis. *Neuron*, *60*(6), 988-1009.

Oliveira, M. M., & Klann, E. (2021). eIF2-dependent translation initiation: Memory consolidation and disruption in Alzheimer's disease. *Semin Cell Dev Biol, 125,* 101–109.

Oliveira, M. M., Lourenco, M. V., Longo, F., Kasica, N. P., Yang, W., Ureta, G., Ferreira, D. D. P., Mendonça, P. H. J., Bernales, S., Ma, T., De Felice, F. G., Klann, E., & Ferreira, S. T. (2021). Correction of eIF2-dependent defects in brain protein synthesis, synaptic plasticity, and memory in mouse models of Alzheimer's disease. *Sci Signal*, *14*(668), eabc5429.

Ong, S. E., Blagoev, B., Kratchmarova, I., Kristensen, D. B., Steen, H., Pandey, A., & Mann, M. (2002). Stable isotope labeling by amino acids in cell culture, SILAC, as a simple and accurate approach to expression proteomics. *Mol Cell Proteomics*, *1*(5), 376-386.

Onuki, R., Bando, Y., Suyama, E., Katayama, T., Kawasaki, H., Baba, T., Tohyama, M., & Taira, K. (2004). An RNA-dependent protein kinase is involved in tunicamycin-induced apoptosis and Alzheimer's disease. *EMBO Jj*, *23*(4), 959-968.

Osmani, N., Peglion, F., Chavrier, P., & Etienne-Manneville, S. (2010). Cdc42 localization and cell polarity depend on membrane traffic. *J Cell Biol*, *191*(7), 1261-1269.

Oyadomari, S., Takeda, K., Takiguchi, M., Gotoh, T., Matsumoto, M., Wada, I., Akira, S., Araki, E., & Mori, M. (2001). Nitric oxide-induced apoptosis in pancreatic beta cells is mediated by the endoplasmic reticulum stress pathway. *Proc Natl Acad Sci U S A*, *98*(19), 10845-10850.

Ozgen, H., Baron, W., Hoekstra, D., & Kahya, N. (2016). Oligodendroglial membrane dynamics in relation to myelin biogenesis. *Cellular and molecular life sciences : CMLS*, *73*(17), 3291-3310.

Pakos-Zebrucka, K., Koryga, I., Mnich, K., Ljujic, M., Samali, A., & Gorman, A. M. (2016). The integrated stress response. *EMBO Rep*, *17*(10), 1374-1395.

Pal, J. K., Chen, J. J., & London, I. M. (1991). Tissue distribution and immunoreactivity of heme-regulated eIF-2 alpha kinase determined by monoclonal antibodies. *Biochemistry*, *30*(9), 2555-2562.

Palam, L. R., Gore, J., Craven, K. E., Wilson, J. L., & Korc, M. (2015). Integrated stress response is critical for gemcitabine resistance in pancreatic ductal adenocarcinoma. *Cell Death Dis*, *6*(10), e1913.

Parasuraman, P., Mulligan, P., Walker, J. A., Li, B., Boukhali, M., Haas, W., & Bernards, A. (2017). Interaction of p190A RhoGAP with eIF3A and Other Translation Preinitiation Factors Suggests a Role in Protein Biosynthesis. *J Biol Chem*, *292*(7), 2679-2689.

Park, C. K., & Horton, N. C. (2019). Structures, functions, and mechanisms of filament forming enzymes: a renaissance of enzyme filamentation. *Biophys Rev*, *11*(6), 927-994.

Park, J., Wetzel, I., Marriott, I., Dréau, D., D'Avanzo, C., Kim, D. Y., Tanzi, R. E., & Cho, H. (2018). A 3D human triculture system modeling neurodegeneration and neuroinflammation in Alzheimer's disease. *Nat Neurosci*, *21*(7), 941-951.

Passmore, L. A., Schmeing, T. M., Maag, D., Applefield, D. J., Acker, M. G., Algire, M. A., Lorsch, J. R., & Ramakrishnan, V. (2007). The eukaryotic translation initiation factors eIF1 and eIF1A induce an open conformation of the 40S ribosome. *Mol Cell*, *26*(1), 41-50.

Patay, Z. (2005). Diffusion-weighted MR imaging in leukodystrophies. *Eur Radiol*, *15*(11), 2284-2303.

Patel, M. R., & Weaver, A. M. (2021). Astrocyte-derived small extracellular vesicles promote synapse formation via fibulin-2-mediated TGF-β signaling. *Cell Rep*, *34*(10), 108829.

Patel, V. L., Mitra, S., Harris, R., Buxbaum, A. R., Lionnet, T., Brenowitz, M., Girvin, M., Levy, M., Almo, S. C., Singer, R. H., & Chao, J. A. (2012). Spatial arrangement of an RNA zipcode identifies mRNAs under post-transcriptional control. *Genes Dev, 26*(1)*,* 43–53.

Paulin, F. E., Campbell, L. E., O'Brien, K., Loughlin, J., & Proud, C. G. (2001). Eukaryotic translation initiation factor 5 (eIF5) acts as a classical GTPase-activator protein. *Curr Biol*, *11*(1), 55-59.

Pavitt, G. D. (2005). eIF2B, a mediator of general and gene-specific translational control. *Biochem Soc Trans*, *33*(Pt 6), 1487-1492.

Pavitt, G. D., Ramaiah, K. V., Kimball, S. R., & Hinnebusch, A. G. (1998). eIF2 independently binds two distinct eIF2B subcomplexes that catalyze and regulate guanine-nucleotide exchange. *Genes Dev*, *12*(4), 514-526.

Pavitt, G. D., Yang, W., & Hinnebusch, A. G. (1997). Homologous segments in three subunits of the guanine nucleotide exchange factor eIF2B mediate translational regulation by phosphorylation of eIF2. *Mol Cell Biol*, *17*(3), 1298-1313.

Pelletier, J., Graff, J., Ruggero, D., & Sonenberg, N. (2015). Targeting the eIF4F translation initiation complex: a critical nexus for cancer development. *Cancer Res*, *75*(2), 250-263.

Pelletier, J., & Sonenberg, N. (1988). Internal initiation of translation of eukaryotic mRNA directed by a sequence derived from poliovirus RNA. *Nature*, *334*(6180), 320-325.

Peng, Y., & Croce, C. M. (2016). The role of MicroRNAs in human cancer. *Signal Transduct Target Ther*, *1*, 15004.

Perng, M. D., Wen, S. F., Gibbon, T., Middeldorp, J., Sluijs, J., Hol, E. M., & Quinlan, R. A. (2008). Glial fibrillary acidic protein filaments can tolerate the incorporation of assembly-compromised GFAP-delta, but with consequences for filament organization and alphaB-crystallin association. *Mol Cell Biol*, *19*(10), 4521-4533.

Petrovska, I., Nüske, E., Munder, M. C., Kulasegaran, G., Malinovska, L., Kroschwald, S., Richter, D., Fahmy, K., Gibson, K., Verbavatz, J.-M., & Alberti, S. (2014). Filament formation by metabolic enzymes is a specific adaptation to an advanced state of cellular starvation. *eLife*, *3*, e02409.

Piccirillo, C. A., Bjur, E., Topisirovic, I., Sonenberg, N., & Larsson, O. (2014). Translational control of immune responses: from transcripts to translatomes. *Nat Immunol*, *15*(6), 503-511.

Pietra, G. G., Capron, F., Stewart, S., Leone, O., Humbert, M., Robbins, I. M., Reid, L. M., & Tuder, R. M. (2004). Pathologic assessment of vasculopathies in pulmonary hypertension. *J Am Coll Cardiol*, *43*(12 Suppl S), 25S-32S.

Pizzinga, M., Bates, C., Lui, J., Forte, G., Morales-Polanco, F., Linney, E., Knotkova, B., Wilson, B., Solari, C. A., Berchowitz, L. E., Portela, P., & Ashe, M. P. (2019). Translation factor mRNA granules direct protein synthetic capacity to regions of polarized growth. *J Cell Biol*, *218*(5), 1564-1581.

Placzek, A. N., Prisco, G. V., Khatiwada, S., Sgritta, M., Huang, W., Krnjević, K., Kaufman, R. J., Dani, J. A., Walter, P., & Costa-Mattioli, M. (2016). eIF2α-mediated translational control regulates the persistence of cocaine-induced LTP in midbrain dopamine neurons. *eLife*, *5,* e17517.

Polley, S., Lyumkis, D., & Horton, N. C. (2019). Mechanism of Filamentation-Induced Allosteric Activation of the SgrAI Endonuclease. *Structure*, *27*(10), 1497-1507.e3.

Poulton, C. J., Schot, R., Kia, S. K., Jones, M., Verheijen, F. W., Venselaar, H., de Wit, M. C., de Graaff, E., Bertoli-Avella, A. M., & Mancini, G. M. (2011). Microcephaly with simplified gyration, epilepsy, and infantile diabetes linked to inappropriate apoptosis of neural progenitors. *Am J Hum Genet*, *89*(2), 265-276.

Price, N. T., Mellor, H., Craddock, B. L., Flowers, K. M., Kimball, S. R., Wilmer, T., Jefferson, L. S., & Proud, C. G. (1996). eIF2B, the guanine nucleotide-exchange factor for eukaryotic initiation factor 2. Sequence conservation between the alpha, beta and delta subunits of eIF2B from mammals and yeast. *Biochem J*, *318(Pt 2)*, 637-643.

Rabouw, H. H., Langereis, M. A., Anand, A. A., Visser, L. J., de Groot, R. J., Walter, P., & van Kuppeveld, F. J. M. (2019). Small molecule ISRIB suppresses the integrated stress response within a defined window of activation. *Proc Natl Acad Sci U S A*, *116*(6), 2097-2102.

Rabouw, H. H., Visser, L. J., Passchier, T. C., Langereis, M. A., Liu, F., Giansanti, P., van Vliet, A. L. W., Dekker, J. G., van der Grein, S. G., Saucedo, J. G., Anand, A. A., Trellet, M. E., Bonvin, A., Walter, P., Heck, A. J. R., de Groot, R. J., & van Kuppeveld, F. J. M. (2020). Inhibition of the integrated stress response by viral proteins that block p-eIF2-eIF2B association. *Nat Microbiol*, *5*(11), 1361-1373.

Raini, G., Sharet, R., Herrero, M., Atzmon, A., Shenoy, A., Geiger, T., & Elroy-Stein, O. (2017). Mutant eIF2B leads to impaired mitochondrial oxidative phosphorylation in vanishing white matter disease. *J Neurochem*, *141*(5), 694-707.

Ramanathan, A., Robb, G. B., & Chan, S. H. (2016). mRNA capping: biological functions and applications. *Nucleic Acids Res*, *44*(16), 7511–7526.

Ramos-Fernández, E., Tajes, M., Ill-Raga, G., Vargas, L., Busquets-García, A., Bosch-Morató, M., Guivernau, B., Valls-Comamala, V., Gomis, M., Grau, C., Fandos, C., Rosen, M. D., Rabinowitz, M. H., Inestrosa, N., Maldonado, R., Altafaj, X., Ozaita, A., Alvarez, A., Vicente, R., . . . Muñoz, F. J. (2016). Glutamatergic stimulation induces GluN2B translation by the nitric oxide-Heme-Regulated eIF2α kinase in cortical neurons. *Oncotarget*, *7*(37), 58876-58892.

Rangaraju, V., Tom Dieck, S., & Schuman, E. M. (2017). Local translation in neuronal compartments: how local is local? *EMBO Rep*, *18*(5), 693-711.

Reinhard, N. R., van Helden, S. F., Anthony, E. C., Yin, T., Wu, Y. I., Goedhart, J., Gadella, T. W., & Hordijk, P. L. (2016). Spatiotemporal analysis of RhoA/B/C activation in primary human endothelial cells. *Sci Rep*, *6*, 25502.

Rittiner, J. E., Caffall, Z. F., Hernández-Martinez, R., Sanderson, S. M., Pearson, J. L., Tsukayama, K. K., Liu, A. Y., Xiao, C., Tracy, S., Shipman, M. K., Hickey, P., Johnson, J., Scott, B., Stacy, M., Saunders-Pullman, R., Bressman, S., Simonyan, K., Sharma, N., Ozelius, L. J., . . . Calakos, N. (2016). Functional Genomic Analyses of Mendelian and Sporadic Disease Identify Impaired eIF2α Signaling as a Generalizable Mechanism for Dystonia. *Neuron*, *92*(6), 1238-1251.

Rode, S., Ohm, H., Anhäuser, L., Wagner, M., Rosing, M., Deng, X., Sin, O., Leidel, S. A., Storkebaum, E., Rentmeister, A., Zhu, S., & Rumpf, S. (2018). Differential Requirement for Translation Initiation Factor Pathways during Ecdysone-Dependent Neuronal Remodeling in Drosophila. *Cell Rep*, *24*(9), 2287-2299.e2284.

Roden, C., & Gladfelter, A. S. (2021). RNA contributions to the form and function of biomolecular condensates. *Nat Rev Mol Cell Biol*, *22*(3), 183-195.

Rodriguez, D., Gelot, A., della Gaspera, B., Robain, O., Ponsot, G., Sarlieve, L. L., Ghandour, S., Pompidou, A., Dautigny, A., Aubourg, P., & Pham-Dinh, D. (1999). Increased density of oligodendrocytes in childhood ataxia with diffuse central hypomyelination (CACH) syndrome: neuropathological and biochemical study of two cases. *Acta Neuropathol*, *97*(5), 469-480.

Rolfs, Z., Frey, B. L., Shi, X., Kawai, Y., Smith, L. M., & Welham, N. V. (2021). An atlas of protein turnover rates in mouse tissues. *Nat Commun*, *12*(1), 6778.

Rosenberg, T., Gal-Ben-Ari, S., Dieterich, D. C., Kreutz, M. R., Ziv, N. E., Gundelfinger, E. D., & Rosenblum, K. (2014). The roles of protein expression in synaptic plasticity and memory consolidation. *Front Mol Neurosci*, *7*, 86.

Ross, J. A., Dungen, K. V., Bressler, K. R., Fredriksen, M., Khandige Sharma, D., Balasingam, N., & Thakor, N. (2019). Eukaryotic initiation factor 5B (eIF5B) provides a critical cell survival switch to glioblastoma cells via regulation of apoptosis. *Cell Death Dis*, *10*(2), 57.

Rutkowski, D. T., Arnold, S. M., Miller, C. N., Wu, J., Li, J., Gunnison, K. M., Mori, K., Sadighi Akha, A. A., Raden, D., & Kaufman, R. J. (2006). Adaptation to ER stress is mediated by differential stabilities of pro-survival and pro-apoptotic mRNAs and proteins. *PLoS Biol*, *4*(11), e374.

Ruvolo, P. P., Gao, F., Blalock, W. L., Deng, X., & May, W. S. (2001). Ceramide regulates protein synthesis by a novel mechanism involving the cellular PKR activator RAX. *J Biol Chem*, *276*(15), 11754-11758.

Sahoo, P. K., Smith, D. S., Perrone-Bizzozero, N., & Twiss, J. L. (2018). Axonal mRNA transport and translation at a glance. *J Cell Sci*, *131*(8), jcs196808.

Sakers, K., Lake, A. M., Khazanchi, R., Ouwenga, R., Vasek, M. J., Dani, A., & Dougherty, J. D. (2017). Astrocytes locally translate transcripts in their peripheral processes. *Proc Natl Acad Sci U S A*, *114*(19), E3830-E3838.

Sanz, M. A., González Almela, E., & Carrasco, L. (2017). Translation of Sindbis Subgenomic mRNA is Independent of eIF2, eIF2A and eIF2D. *Sci Rep*, *7*, 43876.

Schanzenbächer, C. T., Sambandan, S., Langer, J. D., & Schuman, E. M. (2016). Nascent Proteome Remodeling following Homeostatic Scaling at Hippocampal Synapses. *Neuron*, *92*(2), 358-371.

Scheper, G. C., van der Knaap, M. S., & Proud, C. G. (2007). Translation matters: protein synthesis defects in inherited disease. *Nat Rev Genet*, *8*(9), 711-723.

Schewe, D. M., & Aguirre-Ghiso, J. A. (2009). Inhibition of eIF2alpha dephosphorylation maximizes bortezomib efficiency and eliminates quiescent multiple myeloma cells surviving proteasome inhibitor therapy. *Cancer Res*, *69*(4), 1545-1552.

Schiffmann, R., Moller, J. R., Trapp, B. D., Shih, H. H., Farrer, R. G., Katz, D. A., Alger, J. R., Parker, C. C., Hauer, P. E., & Kaneski, C. R. (1994). Childhood ataxia with diffuse central nervous system hypomyelination. *Ann Neurol*, *35*(3), 331-340.

Schmitt, E., Naveau, M., & Mechulam, Y. (2010). Eukaryotic and archaeal translation initiation factor 2: a heterotrimeric tRNA carrier. *FEBS Lett*, *584*(2), 405-412.

Schmitt, E., Panvert, M., Lazennec-Schurdevin, C., Coureux, P. D., Perez, J., Thompson, A., & Mechulam, Y. (2012). Structure of the ternary initiation complex aIF2-GDPNP-methionylated initiator tRNA. *Nat Struct Mol Biol*, *19*(4), 450-454.

Schoof, M., Wang, L., Cogan, J. Z., Lawrence, R. E., Boone, M., Wuerth, J. D., Frost, A., & Walter, P. (2021). Viral evasion of the integrated stress response through antagonism of eIF2-P binding to eIF2B. *Nat Commun*, *12*(1), 1-12.

Schreiber, S. L. (2019). A Chemical Biology View of Bioactive Small Molecules and a Binder-Based Approach to Connect Biology to Precision Medicines. *Isr J Chem*, *59*(1-2), 52-59.

Schuster, S. L., & Hsieh, A. C. (2019). The Untranslated Regions of mRNAs in Cancer. *Trends Cancer, 5*(4), 245–262.

Sekine, Y., Zyryanova, A., Crespillo-Casado, A., Amin-Wetzel, N., Harding, H. P., & Ron, D. (2016). Paradoxical Sensitivity to an Integrated Stress Response Blocking Mutation in Vanishing White Matter Cells. *PLoS ONE*, *11*(11), e0166278.

Sekine, Y., Zyryanova, A., Crespillo-Casado, A., Fischer, P. M., Harding, H. P., & Ron, D. (2015). Mutations in a translation initiation factor identify the target of a memory-enhancing compound. *Science*, *348*(6238), 1027–1030.

Senderek, J., Krieger, M., Stendel, C., Bergmann, C., Moser, M., Breitbach-Faller, N., Rudnik-Schöneborn, S., Blaschek, A., Wolf, N. I., Harting, I., North, K., Smith, J., Muntoni, F., Brockington, M., Quijano-Roy, S., Renault, F., Herrmann, R., Hendershot, L. M., Schröder, J. M., . . . Zerres, K. (2005). Mutations in SIL1 cause Marinesco-Sjögren syndrome, a cerebellar ataxia with cataract and myopathy. *Nat Genet*, *37*(12), 1312-1314.

Shankar, G. M., Li, S., Mehta, T. H., Garcia-Munoz, A., Shepardson, N. E., Smith, I., Brett, F. M., Farrell, M. A., Rowan, M. J., Lemere, C. A., Regan, C. M., Walsh, D. M., Sabatini, B. L., & Selkoe, D. J. (2008). Amyloid-beta protein dimers isolated directly from Alzheimer's brains impair synaptic plasticity and memory. *Nat Med*, *14*(8), 837-842.

Shao, S., Murray, J., Brown, A., Taunton, J., Ramakrishnan, V., & Hegde, R. S. (2016). Decoding Mammalian Ribosome-mRNA States by Translational GTPase Complexes. *Cell*, *167*(5), 1229-1240.e1215.

Sharma, V., Sood, R., Khlaifia, A., Eslamizade, M. J., Hung, T.-Y., Lou, D., Asgarihafshejani, A., Lalzar, M., Kiniry, S. J., Stokes, M. P., Cohen, N., Nelson, A. J., Abell, K., Possemato, A. P., Gal-Ben-Ari, S., Truong, V. T., Wang, P., Yiannakas, A., Saffarzadeh, F., . . . Sonenberg, N. (2020). eIF2α controls memory consolidation via excitatory and somatostatin neurons. *Nature*, *586*(7829), 412-416.

Shavit, E., Michaelson, D. M., & Chapman, J. (2011). Anatomical localization of protease-activated receptor-1 and protease-mediated neuroglial crosstalk on peri-synaptic astrocytic endfeet. *J Neurochem*, *119*(3), 460-473.

Shelkovnikova, T. A., Dimasi, P., Kukharsky, M. S., An, H., Quintiero, A., Schirmer, C., Buée, L., Galas, M.-C., & Buchman, V. L. (2017). Chronically stressed or stress-preconditioned neurons fail to maintain stress granule assembly. *Cell Death Dis*, *8*(5), e2788.

Shen, Q. J., Kassim, H., Huang, Y., Li, H., Zhang, J., Li, G., Wang, P. Y., Yan, J., Ye, F., & Liu, J. L. (2016). Filamentation of Metabolic Enzymes in Saccharomyces cerevisiae. *J Genet Genomics*, *43*(6), 393-404.

Shen, X., Yang, Y., Liu, W., Sun, M., Jiang, J., Zong, H., & Gu, J. (2004). Identification of the p28 subunit of eukaryotic initiation factor 3(eIF3k) as a new interaction partner of cyclin D3. *FEBS Lett*, *573*(1-3), 139-146.

Shi, Y., Yang, Y., Hoang, B., Bardeleben, C., Holmes, B., Gera, J., & Lichtenstein, A. (2016). Therapeutic potential of targeting IRES-dependent c-myc translation in multiple myeloma cells during ER stress. *Oncogene*, *35*(8), 1015-1024.

Shigeoka, T., Jung, H., Jung, J., Turner-Bridger, B., Ohk, J., Lin, J. Q., Amieux, P. S., & Holt, C. E. (2016). Dynamic Axonal Translation in Developing and Mature Visual Circuits. *Cell*, *166*(1), 181-192.

Shigeoka, T., Koppers, M., Wong, H. H., Lin, J. Q., Cagnetta, R., Dwivedy, A., de Freitas Nascimento, J., van Tartwijk, F. W., Ströhl, F., Cioni, J. M., Schaeffer, J., Carrington, M., Kaminski, C. F., Jung, H., Harris, W. A., & Holt, C. E. (2019). On-Site Ribosome Remodeling by Locally Synthesized Ribosomal Proteins in Axons. *Cell Rep*, *29*(11), 3605-3619.e3610.

Shimada, S., Shimojima, K., Sangu, N., Hoshino, A., Hachiya, Y., Ohto, T., Hashi, Y., Nishida, K., Mitani, M., Kinjo, S., Tsurusaki, Y., Matsumoto, N., Morimoto, M., & Yamamoto, T. (2015). Mutations in the genes encoding eukaryotic translation initiation factor 2B in Japanese patients with vanishing white matter disease. *Brain Dev*, *37*(10), 960-966.

Sidrauski, C., Acosta-Alvear, D., Khoutorsky, A., Vedantham, P., Hearn, B. R., Li, H., Gamache, K., Gallagher, C. M., Ang, K. K. H., Wilson, C., Okreglak, V., Ashkenazi, A., Hann, B., Nader, K., Arkin, M. R., Renslo, A. R., Sonenberg, N., & Walter, P. (2013). Pharmacological brake-release of mRNA translation enhances cognitive memory. *eLife*, *2*, e00498.

Sidrauski, C., McGeachy, A. M., Ingolia, N. T., & Walter, P. (2015a). The small molecule ISRIB reverses the effects of eIF2α-P on translation and stress granule assembly. *eLife*, *4,* e05033

Sidrauski, C., Tsai, J. C., Kampmann, M., Hearn, B. R., Vedantham, P., Jaishankar, P., Sokabe, M., Mendez, A. S., Newton, B. W., Tang, E. L., Verschueren, E., Johnson, J. R., Krogan, N. J., Fraser, C. S., Weissman, J. S., Renslo, A. R., & Walter, P. (2015b). Pharmacological dimerization and activation of the exchange factor eIF2B antagonizes the integrated stress response. *eLife*, *4*, e07314.

Simonetti, A., Brito Querido, J., Myasnikov, A. G., Mancera-Martinez, E., Renaud, A., Kuhn, L., & Hashem, Y. (2016). eIF3 Peripheral Subunits Rearrangement after mRNA Binding and Start-Codon Recognition. *Mol Cell*, *63*(2), 206-217.

Singh, G., Pratt, G., Yeo, G. W., & Moore, M. J. (2015). The Clothes Make the mRNA: Past and Present Trends in mRNP Fashion. *Annu Rev Biochem*, *84*, 325–354.

Skopkova, M., Hennig, F., Shin, B. S., Turner, C. E., Stanikova, D., Brennerova, K., Stanik, J., Fischer, U., Henden, L., Müller, U., Steinberger, D., Leshinsky-Silver, E., Bottani, A., Kurdiova, T., Ukropec, J., Nyitrayova, O., Kolnikova, M., Klimes, I., Borck, G., . . . Kalscheuer, V. M. (2017). EIF2S3 Mutations Associated with Severe X-Linked Intellectual Disability Syndrome MEHMO. *Hum Mutat*, *38*(4), 409-425.

Slynko, I., Nguyen, S., Hamilton, E. M. C., Wisse, L. E., de Esch, I. J. P., de Graaf, C., Bruning, J. B., Proud, C. G., Abbink, T. E. M., & van der Knaap, M. S. (2021). Vanishing white matter: Eukaryotic initiation factor 2B model and the impact of missense mutations. *Mol Genet Genomic Med*, *9*(3), e1593.

Smart, F. M., Edelman, G. M., & Vanderklish, P. W. (2003). BDNF induces translocation of initiation factor 4E to mRNA granules: evidence for a role of synaptic microfilaments and integrins. *Proc Natl Acad Sci U S A*, *100*(24), 14403-14408.

Smith, H. L., Freeman, O. J., Butcher, A. J., Holmqvist, S., Humoud, I., Schätzl, T., Hughes, D. T., Verity, N. C., Swinden, D. P., Hayes, J., de Weerd, L., Rowitch, D. H., Franklin, R. J. M., & Mallucci, G. R. (2020). Astrocyte Unfolded Protein Response Induces a Specific Reactivity State that Causes Non-Cell-Autonomous Neuronal Degeneration. *Neuron*, *105*(5), 855-866.e855.

Sokabe, M., Fraser, C. S., & Hershey, J. W. (2012). The human translation initiation multi-factor complex promotes methionyl-tRNAi binding to the 40S ribosomal subunit. *Nucleic Acids Res*, *40*(2), 905-913.

Sonenberg, N., & Hinnebusch, A. G. (2009). Regulation of translation initiation in eukaryotes: mechanisms and biological targets. *Cell*, *136*(4), 731-745.

Starck, S. R., Tsai, J. C., Chen, K., Shodiya, M., Wang, L., Yahiro, K., Martins-Green, M., Shastri, N., & Walter, P. (2016). Translation from the 5' untranslated region shapes the integrated stress response. *Science*, *351*(6272), aad3867.

Stellingwerff, M. D., Al-Saady, M. L., van de Brug, T., Barkhof, F., Pouwels, P. J. W., & van der Knaap, M. S. (2021). MRI Natural History of the Leukodystrophy Vanishing White Matter. *Radiology*, *300*(3), 671-680.

Stellingwerff, M. D., van de Wiel, M. A., & van der Knaap, M. S. (2022). Radiological correlates of episodes of acute decline in the leukodystrophy vanishing white matter. *Neuroradiology, 65*(4), 855-863.

Stern-Ginossar, N., Thompson, S. R., Mathews, M. B., & Mohr, I. (2019). Translational Control in Virus-Infected Cells. *Cold Spring Harb Perspect Biol*, *11*(3), a033001.

Sun, D., & Jakobs, T. C. (2012). Structural remodeling of astrocytes in the injured CNS. *Neuroscientist*, *18*(6), 567-588.

Sutton, M. A., & Schuman, E. M. (2006). Dendritic protein synthesis, synaptic plasticity, and memory. *Cell*, *127*(1), 49-58.

Synofzik, M., Haack, T. B., Kopajtich, R., Gorza, M., Rapaport, D., Greiner, M., Schönfeld, C., Freiberg, C., Schorr, S., Holl, R. W., Gonzalez, M. A., Fritsche, A., Fallier-Becker,

P., Zimmermann, R., Strom, T. M., Meitinger, T., Züchner, S., Schüle, R., Schöls, L., & Prokisch, H. (2014). Absence of BiP co-chaperone DNAJC3 causes diabetes mellitus and multisystemic neurodegeneration. *Am J Hum Genet*, *95*(6), 689-697.

Tahmasebi, S., Khoutorsky, A., Mathews, M. B., & Sonenberg, N. (2018). Translation deregulation in human disease. *Nat Rev Mol Cell Biol*, *19*(12), 791-807.

Takei, N., Kawamura, M., Hara, K., Yonezawa, K., & Nawa, H. (2001). Brain-derived neurotrophic factor enhances neuronal translation by activating multiple initiation processes: comparison with the effects of insulin. *J Biol Chem*, *276*(46), 42818-42825.

Taylor, E. J., Campbell, S. G., Griffiths, C. D., Reid, P. J., Slaven, J. W., Harrison, R. J., Sims, P. F., Pavitt, G. D., Delneri, D., & Ashe, M. P. (2010). Fusel alcohols regulate translation initiation by inhibiting eIF2B to reduce ternary complex in a mechanism that may involve altering the integrity and dynamics of the eIF2B body. *Mol Biol Cell*, *21*(13), 2202-2216.

Taylor, R. W., Pyle, A., Griffin, H., Blakely, E. L., Duff, J., He, L., Smertenko, T., Alston, C. L., Neeve, V. C., Best, A., Yarham, J. W., Kirschner, J., Schara, U., Talim, B., Topaloglu, H., Baric, I., Holinski-Feder, E., Abicht, A., Czermin, B., . . . Chinnery, P. F. (2014). Use of whole-exome sequencing to determine the genetic basis of multiple mitochondrial respiratory chain complex deficiencies. *JAMA*, *312*(1), 68-77.

Terenzio, M., Koley, S., Samra, N., Rishal, I., Zhao, Q., Sahoo, P. K., Urisman, A., Marvaldi, L., Oses-Prieto, J. A., Forester, C., Gomes, C., Kalinski, A. L., Di Pizio, A., Doron-Mandel, E., Perry, R. B.-T., Koppel, I., Twiss, J. L., Burlingame, A. L., & Fainzilber, M. (2018). Locally translated mTOR controls axonal local translation in nerve injury. *Science*, *359*(6382), 1416-1421.

Teske, B. F., Fusakio, M. E., Zhou, D., Shan, J., McClintick, J. N., Kilberg, M. S., & Wek, R. C. (2013). CHOP induces activating transcription factor 5 (ATF5) to trigger apoptosis in response to perturbations in protein homeostasis. *Mol Biol Cell*, *24*(15), 2477-2490.

Teske, B. F., Wek, S. A., Bunpo, P., Cundiff, J. K., McClintick, J. N., Anthony, T. G., & Wek, R. C. (2011). The eIF2 kinase PERK and the integrated stress response facilitate activation of ATF6 during endoplasmic reticulum stress. *Mol Biol Cell*, *22*(22), 4390-4405.

Thakor, N., and Holcik, M. (2012). IRES-mediated translation of cellular messenger RNA operates in eIF2alpha-independent manner during stress. *Nucleic Acids Res*, *40*, 541–552

Thakor, N., Smith, M. D., Roberts, L., Faye, M. D., Patel, H., Wieden, H. J., Cate, J. H. D., & Holcik, M. (2017). Cellular mRNA recruits the ribosome via eIF3-PABP bridge to initiate internal translation. *RNA Biol*, *14*(5), 553-567.

Thoma, C., Bergamini, G., Galy, B., Hundsdoerfer, P., & Hentze, M. W. (2004). Enhancement of IRES-mediated translation of the c-myc and BiP mRNAs by the poly(A) tail is independent of intact eIF4G and PABP. *Mol Cell*, *15*(6), 925-935.

Thomas, V. N., Weiss, E. L., & Brace, J. L. (2018). Asymmetric secretion in budding yeast reinforces daughter cell identity. *bioRxiv*, 483388.

Thompson, L., Depledge, D. P., Burgess, H. M., & Mohr, I. (2022). An eIF3d-dependent switch regulates HCMV replication by remodeling the infected cell translation landscape to mimic chronic ER stress. *Cell Rep*, *39*(5), 110767.

Thompson, R. C., & Stone, P. J. (1977). Proofreading of the codon-anticodon interaction on ribosomes. *Proc Natl Acad Sci U S A*, *74*(1), 198-202.

Thoreen, C. C. (2017). The molecular basis of mTORC1-regulated translation. *Biochem Soc Trans*, *45*(1), 213-221.

Toyama, Brandon H., Savas, Jeffrey N., Park, Sung K., Harris, Michael S., Ingolia, Nicholas T., Yates, John R., & Hetzer, Martin W. (2013). Identification of Long-Lived Proteins Reveals Exceptional Stability of Essential Cellular Structures. *Cell*, *154*(5), 971-982.

Troiano, N. W., Ciovacco, W. A., & Kacena, M. A. (2009). The Effects of Fixation and Dehydration on the Histological Quality of Undecalcified Murine Bone Specimens Embedded in Methylmethacrylate. *J Histotech*, *32*(1), 27-31.

Tsai, J. C., Miller-Vedam, L. E., Anand, A. A., Jaishankar, P., Nguyen, H. C., Renslo, A. R., Frost, A., & Walter, P. (2018). Structure of the nucleotide exchange factor eIF2B reveals mechanism of memory-enhancing molecule. *Science*, *359*(6383), eaaq0939.

Turner-Bridger, B., Jakobs, M., Muresan, L., Wong, H. H., Franze, K., Harris, W. A., & Holt, C. E. (2018). Single-molecule analysis of endogenous beta-actin mRNA trafficking reveals a mechanism for compartmentalized mRNA localization in axons. *Proc Natl Acad Sci U S A*, *115*(41), E9697-E9706.

Ulc, A., Gottschling, C., Schäfer, I., Wegrzyn, D., van Leeuwen, S., Luft, V., Reinhard, J., & Faissner, A. (2017). Involvement of the guanine nucleotide exchange factor Vav3 in central nervous system development and plasticity. *Biol Chem*, *398*(5-6), 663-675.

Vaklavas, C., Grizzle, W. E., Choi, H., Meng, Z., Zinn, K. R., Shrestha, K., & Blume, S. W. (2016). IRES inhibition induces terminal differentiation and synchronized death in triple-negative breast cancer and glioblastoma cells. *Tumour Biol*, *37*(10), 13247-13264.

van der Knaap, M. S., Barth, P. G., Gabreels, F. J., Franzoni, E., Begeer, J. H., Stroink, H., Rotteveel, J. J., & Valk, J. (1997). A new leukoencephalopathy with vanishing white matter. *Neurology*, *48*(4), 845-855.

van der Knaap, M. S., Bonkowsky, J. L., Vanderver, A., Schiffmann, R., Krägeloh-Mann, I., Bertini, E., Bernard, G., Fatemi, S. A., Wolf, N. I., Saunier-Vivar, E., Rauner, R., Dekker, H., van Bokhoven, P., van de Ven, P., & Leferink, P. S. (2022). Therapy Trial Design in Vanishing White Matter: An Expert Consortium Opinion. *Neurol Genet*, *8*(2), e657.

van der Knaap, M. S., Breiter, S. N., Naidu, S., Hart, A. A., & Valk, J. (1999). Defining and Categorizing Leukoencephalopathies of Unknown Origin: MR Imaging Approach. *Radiology*, *213*(1), 121-133.

van der Knaap, M. S., & Bugiani, M. (2017). Leukodystrophies: a proposed classification system based on pathological changes and pathogenetic mechanisms. *Acta Neuropathol*, *134*(3), 351-382.

van der Knaap, M. S., Kamphorst, W., Barth, P. G., Kraaijeveld, C. L., Gut, E., & Valk, J. (1998). Phenotypic variation in leukoencephalopathy with vanishing white matter. *Neurology*, *51*(2), 540-547.

van der Knaap, M. S., Leegwater, P. A., Könst, A. A., Visser, A., Naidu, S., Oudejans, C. B., Schutgens, R. B., & Pronk, J. C. (2002). Mutations in each of the five subunits of translation initiation factor eIF2B can cause leukoencephalopathy with vanishing white matter. *Ann Neurol*, *51*(2), 264-270.

van der Knaap, M. S., Pronk, J. C., & Scheper, G. C. (2006). Vanishing white matter disease. *Lancet Neurol*, *5*(5), 413-423.

van der Knaap, M. S., van Berkel, C. G. M., Herms, J., van Coster, R., Baethmann, M., Naidu, S., Boltshauser, E., Willemsen, M. A. A. P., Plecko, B., Hoffmann, G. F., Proud, C. G., Scheper, G. C., & Pronk, J. C. (2003). eIF2B-Related Disorders: Antenatal Onset and Involvement of Multiple Organs. *Am J Hum Genet*, *73*(5), 1199-1207.

van der Lei, H. D., van Berkel, C. G., van Wieringen, W. N., Brenner, C., Feigenbaum, A., Mercimek-Mahmutoglu, S., Philippart, M., Tatli, B., Wassmer, E., Scheper, G. C., & van der Knaap, M. S. (2010). Genotype-phenotype correlation in vanishing white matter disease. *Neurology*, *75*(17), 1555-1559.

van Haren, K., van der Voorn, J. P., Peterson, D. R., van der Knaap, M. S., & Powers, J. M. (2004). The life and death of oligodendrocytes in vanishing white matter disease. *J Neuropathol Exp Neurol*, *63*(6), 618-630.

van Kollenburg, B., van Dijk, J., Garbern, J., Thomas, A. A., Scheper, G. C., Powers, J. M., & van der Knaap, M. S. (2006). Glia-specific activation of all pathways of the unfolded protein response in vanishing white matter disease. *J Neuropathol Exp Neurol*, *65*(7), 707-715.

Vander Heiden, M. G., & DeBerardinis, R. J. (2017). Understanding the Intersections between Metabolism and Cancer Biology. *Cell*, *168*(4), 657-669.

Varone, E., Decio, A., Barbera, M. C., Bolis, M., Di Rito, L., Pisati, F., Giavazzi, R., & Zito, E. (2022). Endoplasmic reticulum oxidoreductin 1-alpha deficiency and activation of protein translation synergistically impair breast tumour resilience. *Br J Pharmacol*, *179*(23), 5180-5195.

Vasudevan, D., Neuman, S. D., Yang, A., Lough, L., Brown, B., Bashirullah, A., Cardozo, T., & Ryoo, H. D. (2020). Translational induction of ATF4 during integrated stress response requires noncanonical initiation factors eIF2D and DENR. *Nat Commun*, *11*(1), 4677.

Vattem, K. M., & Wek, R. C. (2004). Reinitiation involving upstream ORFs regulates ATF4 mRNA translation in mammalian cells. *Proc Natl Acad Sci U S A*, *101*(31), 11269-11274.

Ventura, M., Mateo, F., Serratosa, J., Salaet, I., Carujo, S., Bachs, O., & Pujol, M. J. (2010). Nuclear translocation of glyceraldehyde-3-phosphate dehydrogenase is regulated by acetylation. *Int J Biochem Cell Biol*, *42*(10), 1672-1680.

Vermeulen, G., Seidl, R., Mercimek-Mahmutoglu, S., Rotteveel, J. J., Scheper, G. C., & van der Knaap, M. S. (2005). Fright is a provoking factor in vanishing white matter disease. *Annals of Neurology*, *57*(4), 560-563.

Walker, B. A., Ji, S. J., & Jaffrey, S. R. (2012). Intra-axonal translation of RhoA promotes axon growth inhibition by CSPG. *J Neurosci*, *32*(41), 14442-14447.

Wang, B., Zhang, L., Dai, T., Qin, Z., Lu, H., Zhang, L., & Zhou, F. (2021). Liquid-liquid phase separation in human health and diseases. *Signal Transduct Target Ther*, *6*(1), 290.

Wang, X., Wortham, N. C., Liu, R., & Proud, C. G. (2012). Identification of residues that underpin interactions within the eukaryotic initiation factor (eIF2) 2B complex. *J Biol Chem*, *287*(11), 8263-8274.

Watanabe, S., Markov, N. S., Lu, Z., Piseaux Aillon, R., Soberanes, S., Runyan, C. E., Ren, Z., Grant, R. A., Maciel, M., Abdala-Valencia, H., Politanska, Y., Nam, K., Sichizya, L., Kihshen, H. G., Joshi, N., McQuattie-Pimentel, A. C., Gruner, K. A., Jain, M., Sznajder, J. I., . . . Misharin, A. V. (2021). Resetting proteostasis with ISRIB promotes epithelial differentiation to attenuate pulmonary fibrosis. *Proc Natl Acad Sci U S A*, *118*(20), e2101100118.

Way, S. W., Podojil, J. R., Clayton, B. L., Zaremba, A., Collins, T. L., Kunjamma, R. B., Robinson, A. P., Brugarolas, P., Miller, R. H., Miller, S. D., & Popko, B. (2015). Pharmaceutical integrated stress response enhancement protects oligodendrocytes and provides a potential multiple sclerosis therapeutic. *Nat Commun*, *6*, 6532.

Webb, B. L., & Proud, C. G. (1997). Eukaryotic initiation factor 2B (eIF2B). *Int J Biochem Cell Biol*, *29*(10), 1127-1131.

Wegrzyn, D., Zokol, J., & Faissner, A. (2022). Vav3-Deficient Astrocytes Enhance the Dendritic Development of Hippocampal Neurons in an Indirect Co-culture System. *Front Cell Neurosci*, *15*, 817277.

Weingarten-Gabbay, S., Elias-Kirma, S., Nir, R., Gritsenko, A. A., Stern-Ginossar, N., Yakhini, Z., Weinberger, A., & Segal, E. (2016). Comparative genetics. Systematic discovery of cap-independent translation sequences in human and viral genomes. *Science*, *351*(6270), aad4939.

Welsh, G. I., Miller, C. M., Loughlin, A. J., Price, N. T., & Proud, C. G. (1998). Regulation of eukaryotic initiation factor eIF2B: glycogen synthase kinase-3 phosphorylates a conserved serine which undergoes dephosphorylation in response to insulin. *FEBS Lett*, *421*(2), 125-130.

Wilczynska, A., Aigueperse, C., Kress, M., Dautry, F., & Weil, D. (2005). The translational regulator CPEB1 provides a link between dcp1 bodies and stress granules. *J Cell Sci*, *118*(Pt 5), 981-992.

Wilkinson, B., Li, J., & Coba, M. P. (2017). Synaptic GAP and GEF Complexes Cluster Proteins Essential for GTP Signaling. *Sci Rep*, *7*(1), 5272.

Willett, M., Brocard, M., Davide, A., & Morley, S. J. (2011). Translation initiation factors and active sites of protein synthesis co-localize at the leading edge of migrating fibroblasts. *Biochem J*, *438*(1), 217-227.

Williams, D. D., Pavitt, G. D., & Proud, C. G. (2001). Characterization of the initiation factor eIF2B and its regulation in Drosophila melanogaster. *J Biol Chem*, *276*(6), 3733-3742.

Wink, S., Hiemstra, S., Herpers, B., & van de Water, B. (2017). High-content imaging-based BAC-GFP toxicity pathway reporters to assess chemical adversity liabilities. *Arch Toxicol*, *91*(3), 1367-1383.

Wisse, L. E., Ter Braak, T. J., van de Beek, M. C., van Berkel, C. G. M., Wortel, J., Heine, V. M., Proud, C. G., van der Knaap, M. S., & Abbink, T. E. M. (2018). Adult mouse eIF2Bε Arg191His astrocytes display a normal integrated stress response in vitro. *Sci Rep*, *8*(1), 3773.

Witkamp, D., Oudejans, E., Hu, A. N. G. V., Hoogterp, L., Krzywańska, A. M., Žnidaršič, M., Marinus, K., de Veij Mestdagh, C. F., Bartelink, I., Bugiani, M., van der Knaap, M. S., & Abbink, T. E. M. (2022). Guanabenz ameliorates disease in vanishing white matter mice in contrast to sephin1. *Ann Clin Transl Neurol*, *9*(8), 1147-1162.

Wolzak, K., Nölle, A., Farina, M., Abbink, T. E., van der Knaap, M. S., Verhage, M., & Scheper, W. (2022). Neuron-specific translational control shift ensures proteostatic resilience during ER stress. *EMBO J*, *41*(16), e110501.

Wong, H. H., Lin, J. Q., Strohl, F., Roque, C. G., Cioni, J. M., Cagnetta, R., Turner-Bridger, B., Laine, R. F., Harris, W. A., Kaminski, C. F., & Holt, C. E. (2017). RNA Docking and Local Translation Regulate Site-Specific Axon Remodeling In Vivo. *Neuron*, *95*(4), 852-868.e858.

Wong, K., Armstrong, R. C., Gyure, K. A., Morrison, A. L., Rodriguez, D., Matalon, R., Johnson, A. B., Wollmann, R., Gilbert, E., Le, T. Q., Bradley, C. A., Crutchfield, K., & Schiffmann, R. (2000). Foamy cells with oligodendroglial phenotype in childhood

ataxia with diffuse central nervous system hypomyelination syndrome. *Acta Neuropathol*, *100*(6), 635-646.

Wong, Y. L., LeBon, L., Basso, A. M., Kohlhaas, K. L., Nikkel, A. L., Robb, H. M., Donnelly-Roberts, D. L., Prakash, J., Swensen, A. M., Rubinstein, N. D., Krishnan, S., McAllister, F. E., Haste, N. V., O'Brien, J. J., Roy, M., Ireland, A., Frost, J. M., Shi, L., Riedmaier, S., . . . Sidrauski, C. (2019). eIF2B activator prevents neurological defects caused by a chronic integrated stress response. *eLife*, *8*, e42940.

Wong, Y. L., LeBon, L., Edalji, R., Lim, H. B., Sun, C., & Sidrauski, C. (2018). The small molecule ISRIB rescues the stability and activity of Vanishing White Matter Disease eIF2B mutant complexes. *eLife*, *7*, e32733.

Wortham, N. C., Martinez, M., Gordiyenko, Y., Robinson, C. V., & Proud, C. G. (2014). Analysis of the subunit organization of the eIF2B complex reveals new insights into its structure and regulation. *FASEB J*, *28*(5), 2225-2237.

Wortham, N. C., & Proud, C. G. (2015). eIF2B: recent structural and functional insights into a key regulator of translation. *Biochem Soc Trans*, *43*(6), 1234-1240.

Wortham, N. C., Stewart, J. D., Harris, S., Coldwell, M. J., & Proud, C. G. (2016). Stoichiometry of the eIF2B complex is maintained by mutual stabilization of subunits. *Biochem J*, *473*(5), 571-580.

Xu, H., Bensalel, J., Capobianco, E., Lu, M. L., & Wei, J. (2022). Impaired Restoration of Global Protein Synthesis Contributes to Increased Vulnerability to Acute ER Stress Recovery in Huntington's Disease. *Cell Mol Neurobiol*, *42*(8), 2757-2771.

Yadav, V., Gao, X.-H., Willard, B., Hatzoglou, M., Banerjee, R., & Kabil, O. (2017). Hydrogen sulfide modulates eukaryotic translation initiation factor 2α (eIF2α) phosphorylation status in the integrated stress-response pathway. *J Biol Chem*, *292*(32), 13143-13153.

Yamaguchi, H., & Wang, H. G. (2004). CHOP is involved in endoplasmic reticulum stress-induced apoptosis by enhancing DR5 expression in human carcinoma cells. *J Biol Chem*, *279*(44), 45495-45502.

Yamamoto, H., Unbehaun, A., Loerke, J., Behrmann, E., Collier, M., Bürger, J., Mielke, T., & Spahn, C. M. (2014). Structure of the mammalian 80S initiation complex with initiation factor 5B on HCV-IRES RNA. *Nat Struct Mol Biol*, *21*(8), 721-727.

Yanagiya, A., Svitkin, Y. V., Shibata, S., Mikami, S., Imataka, H., & Sonenberg, N. (2009). Requirement of RNA binding of mammalian eukaryotic translation initiation factor 4GI (eIF4GI) for efficient interaction of eIF4E with the mRNA cap. *Mol Cell Biol*, *29*(6), 1661-1669.

Yang, R., Wek, S. A., & Wek, R. C. (2000). Glucose limitation induces GCN4 translation by activation of Gcn2 protein kinase. *Mol Cell Biol*, *20*(8), 2706-2717.

Ye, J., Kumanova, M., Hart, L. S., Sloane, K., Zhang, H., De Panis, D. N., Bobrovnikova-Marjon, E., Diehl, J. A., Ron, D., & Koumenis, C. (2010). The GCN2-ATF4 pathway is critical for tumour cell survival and proliferation in response to nutrient deprivation. *EMBO J*, *29*(12), 2082-2096.

Young-Baird, S. K., Lourenço, M. B., Elder, M. K., Klann, E., Liebau, S., & Dever, T. E. (2020). Suppression of MEHMO Syndrome Mutation in eIF2 by Small Molecule ISRIB. *Mol Cell*, *77*(4), 875-886.e877.

Zappa, F., Muniozguren, N. L., Wilson, M. Z., Costello, M. S., Ponce-Rojas, J. C., & Acosta-Alvear, D. (2022). Signaling by the integrated stress response kinase PKR is fine-tuned by dynamic clustering. *J Cell Biol*, *221*(7), e202111100.

Zhan, K., Narasimhan, J., & Wek, R. C. (2004). Differential activation of eIF2 kinases in response to cellular stresses in Schizosaccharomyces pombe. *Genetics*, *168*(4), 1867-1875.

Zhang, P., McGrath, B., Li, S., Frank, A., Zambito, F., Reinert, J., Gannon, M., Ma, K., McNaughton, K., & Cavener, D. R. (2002). The PERK eukaryotic initiation factor 2 alpha kinase is required for the development of the skeletal system, postnatal growth, and the function and viability of the pancreas. *Mol Cell Biol*, *22*(11), 3864-3874.

Zhang, W., Feng, D., Li, Y., Iida, K., McGrath, B., & Cavener, D. R. (2006). PERK EIF2AK3 control of pancreatic beta cell differentiation and proliferation is required for postnatal glucose homeostasis. *Cell Metab*, *4*(6), 491-497.

Zhao, B. S., Roundtree, I. A., & He, C. (2017). Post-transcriptional gene regulation by mRNA modifications. *Nat Rev Mol Cell Biol, 18*(1)*,* 31–42.

Zhou, F., Zhang, H., Kulkarni, S. D., Lorsch, J. R., & Hinnebusch, A. G. (2020). eIF1 discriminates against suboptimal initiation sites to prevent excessive uORF translation genome-wide. *RNA*, *26*(4), 419-438.

Zhou, J., Wan, J., Gao, X., Zhang, X., Jaffrey, S. R., & Qian, S. B. (2015). Dynamic m(6)A mRNA methylation directs translational control of heat shock response. *Nature*, *526*(7574), 591-594.

Zhou, L., Li, P., Chen, N., Dai, L. F., Gao, K., Liu, Y. N., Shen, L., Wang, J. M., Jiang, Y. W., & Wu, Y. (2019). Modeling vanishing white matter disease with patient-derived induced pluripotent stem cells reveals astrocytic dysfunction. *CNS Neurosci Ther*, *25*(6), 759-771.

Zhou, H., & Rigoutsos, I. (2014). MiR-103a-3p targets the 5' UTR of GPRC5A in pancreatic cells. *RNA, 20*(9), 1431–1439.

Zhu, P. J., Khatiwada, S., Cui, Y., Reineke, L. C., Dooling, S. W., Kim, J. J., Li, W., Walter, P., & Costa-Mattioli, M. (2019). Activation of the ISR mediates the behavioral and neurophysiological abnormalities in Down syndrome. *Science*, *366*(6467), 843-849.

Zivraj, K. H., Tung, Y. C., Piper, M., Gumy, L., Fawcett, J. W., Yeo, G. S., & Holt, C. E. (2010). Subcellular profiling reveals distinct and developmentally regulated repertoire of growth cone mRNAs. *J Neurosci*, *30*(46), 15464-15478.

Zoll, W. L., Horton, L. E., Komar, A. A., Hensold, J. O., & Merrick, W. C. (2002). Characterization of mammalian eIF2A and identification of the yeast homolog. *J Biol Chem*, *277*(40), 37079-37087.

Zyryanova, A. F., Kashiwagi, K., Rato, C., Harding, H. P., Crespillo-Casado, A., Perera, L. A., Sakamoto, A., Nishimoto, M., Yonemochi, M., Shirouzu, M., Ito, T., & Ron, D. (2021). ISRIB Blunts the Integrated Stress Response by Allosterically Antagonising the Inhibitory Effect of Phosphorylated eIF2 on eIF2B. *Mol Cell*, *81*(1), 88-103.e106.

Zyryanova, A. F., Weis, F., Faille, A., Alard, A. A., Crespillo-Casado, A., Sekine, Y., Harding, H. P., Allen, F., Parts, L., Fromont, C., Fischer, P. M., Warren, A. J., & Ron, D. (2018). Binding of ISRIB reveals a regulatory site in the nucleotide exchange factor eIF2B. *Science*, *359*(6383), 1533-1536.

Appendix.

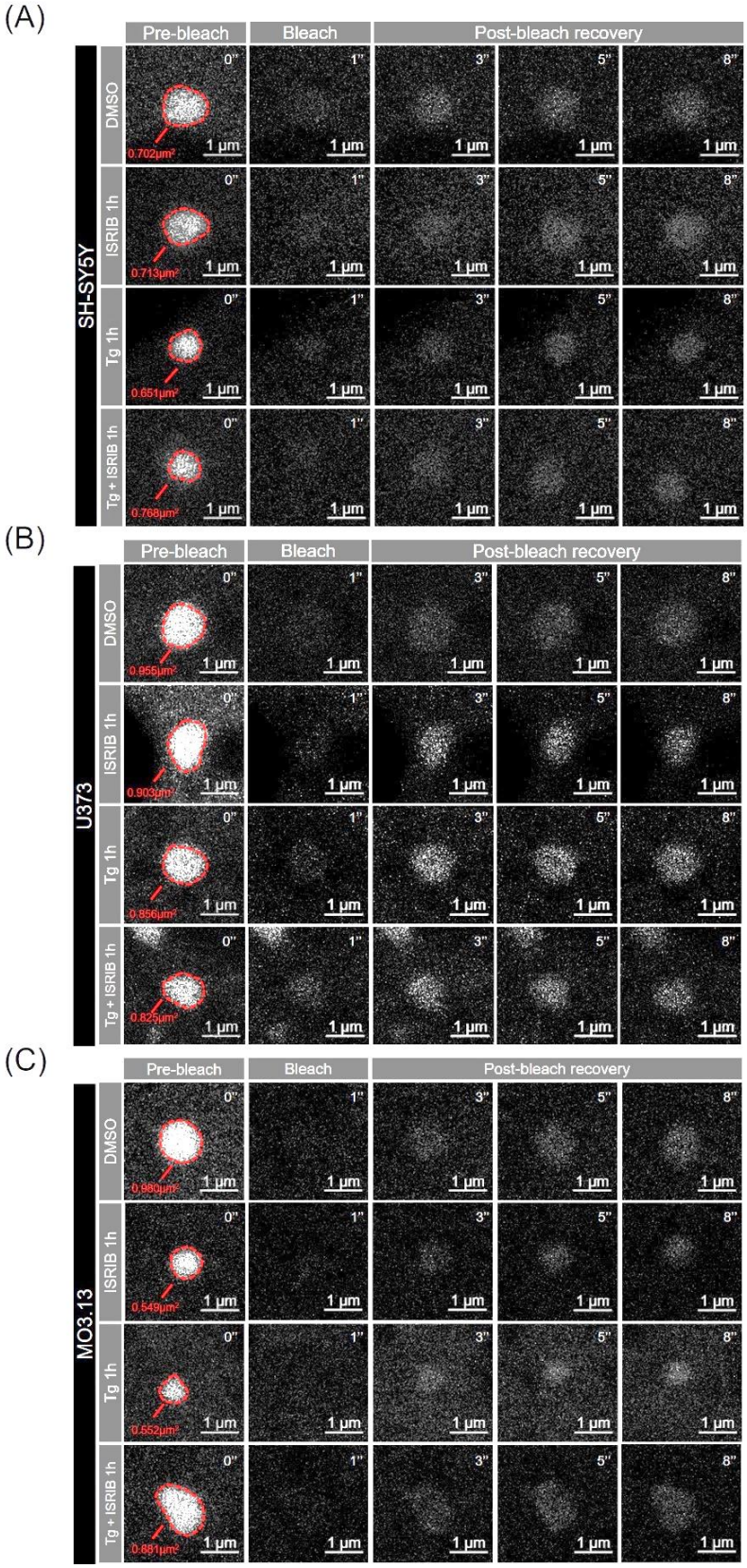

Figure A1. FRAP imaging of small eIF2B bodies upon acute ISR (ER stress) and ISRIB. Representative images of a single small eIF2B body (<1µm²) in **(A)** SH-SY5Y, **(B)** U373 and **(C)** MO3.13 cells. Single eIF2α-tGFP bodies were photobleached with a 488-nm laser beam and fluorescence recovery was monitored over a period of 8 s.

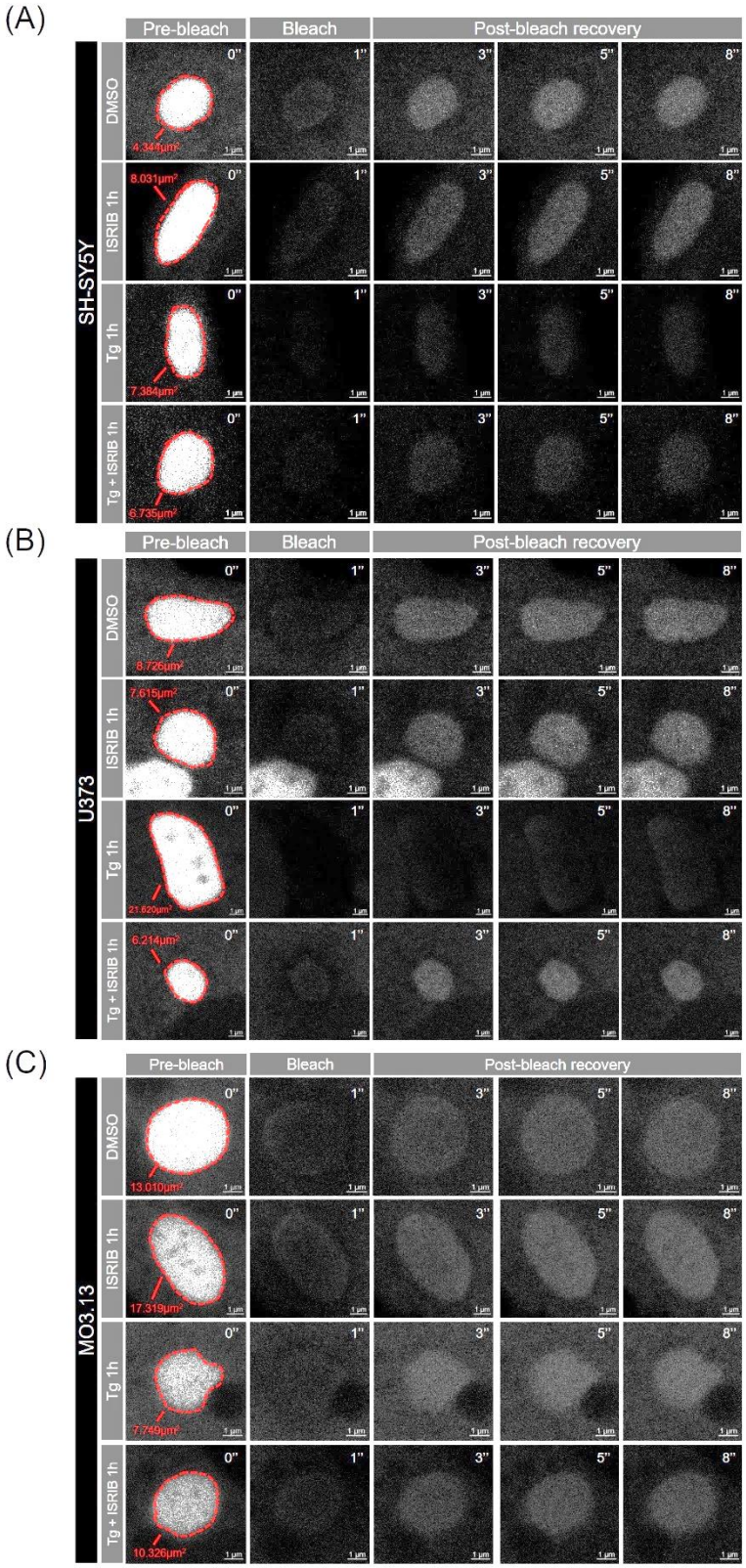

Figure A2. FRAP imaging of large eIF2B bodies upon acute ISR (ER stress) and ISRIB. Representative images of a single small eIF2B body (≥1µm²) in **(A)** SH-SY5Y, **(B)** U373 and **(C)** MO3.13 cells. Single eIF2α-tGFP bodies were photobleached with a 488-nm laser beam and fluorescence recovery was monitored over a period of 8 s.

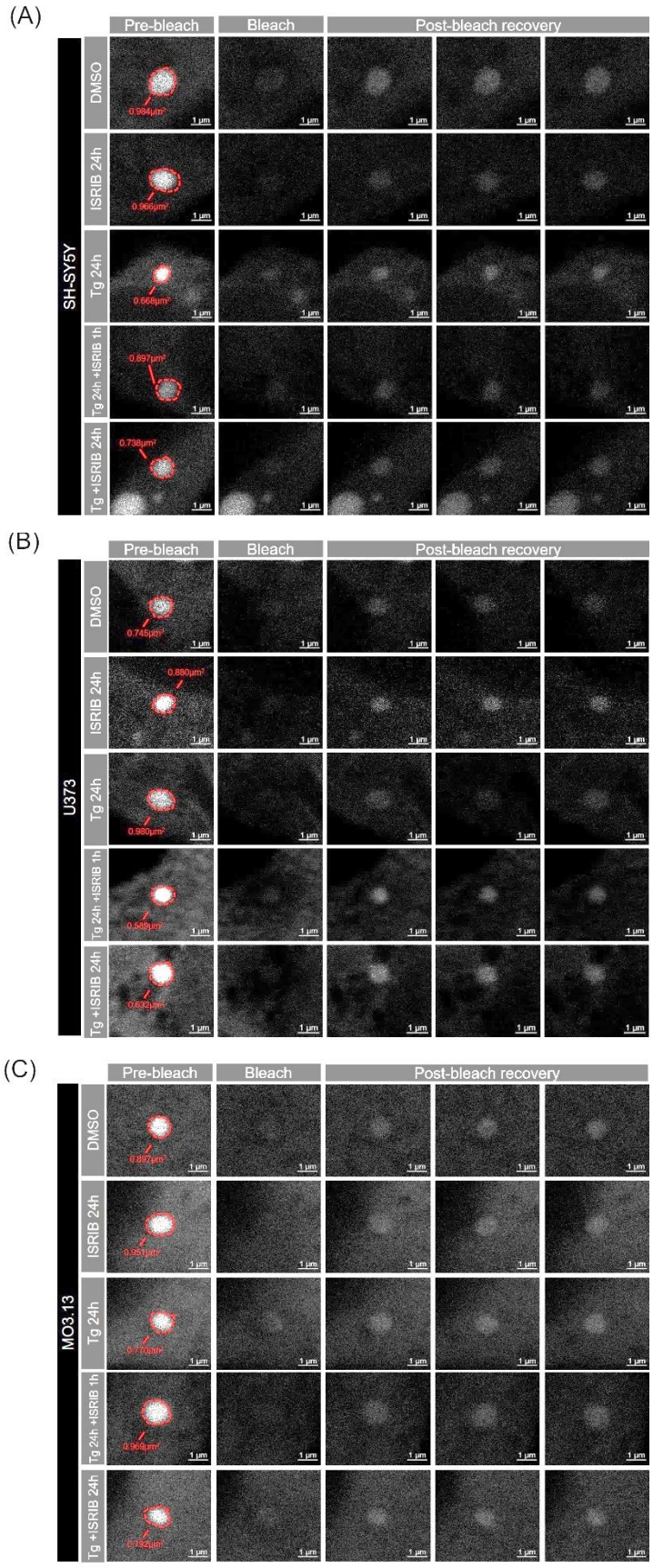

Figure A3. FRAP imaging of small eIF2B bodies upon chronic ISR (ER stress) and ISRIB. Representative images of a single small eIF2B body (<1μm^2) in **(A)** SH-SY5Y, **(B)** U373 and **(C)** MO3.13 cells. Single eIF2α-tGFP bodies were photobleached with a 488-nm laser beam and fluorescence recovery was monitored over a period of 8 s.

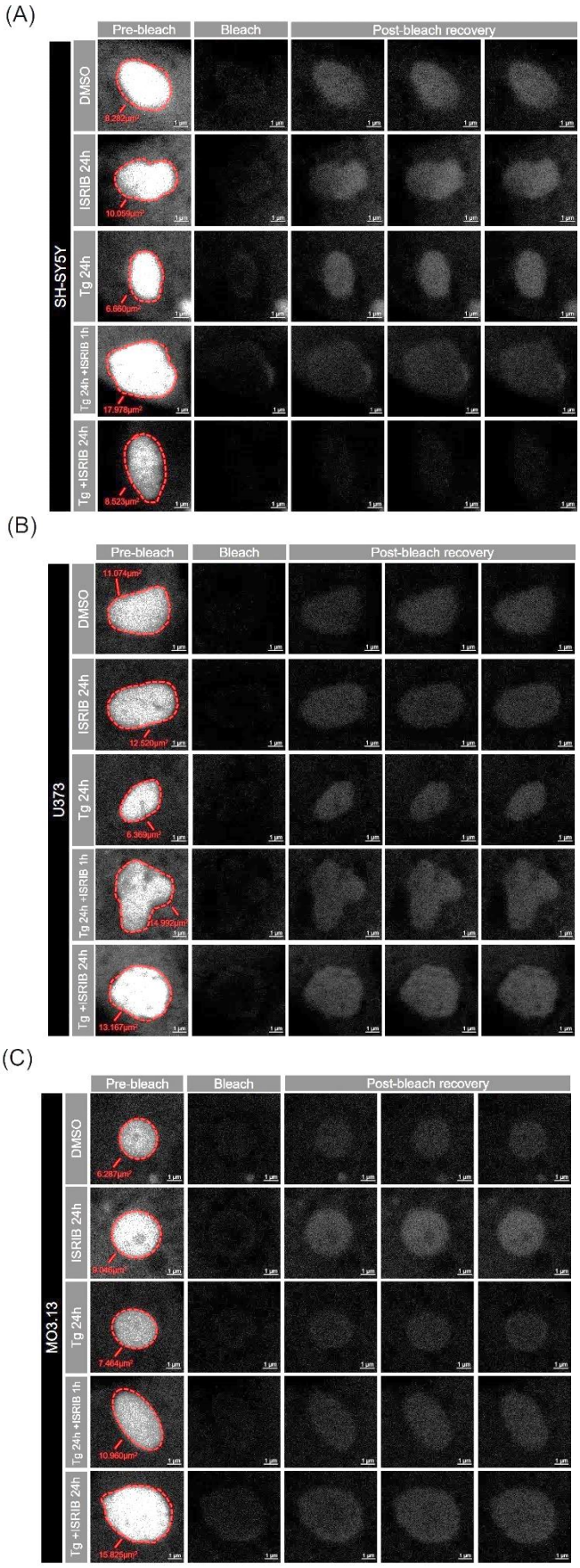

Figure A4. FRAP imaging of large eIF2B bodies upon chronic ISR (ER stress) and ISRIB. Representative images of a single small eIF2B body (≥1µm^2) in **(A)** SH-SY5Y, **(B)** U373 and **(C)** MO3.13 cells. Single eIF2α-tGFP bodies were photobleached with a 488-nm laser beam and fluorescence recovery was monitored over a period of 8 s.

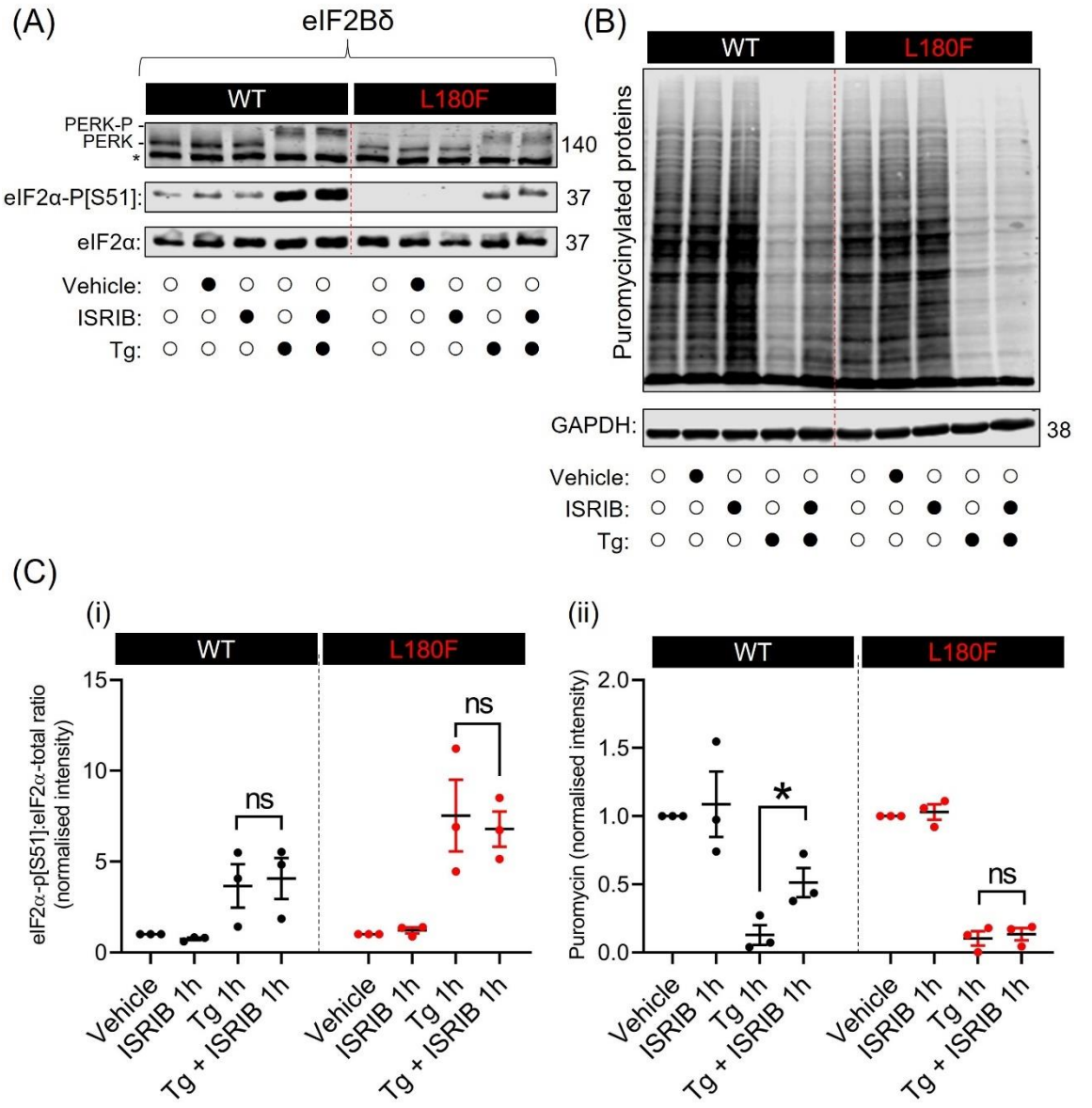

Figure A5. Global translation cannot be rescued by ISRIB in ISRIB-resistant eIF2Bδ$^{L180F/L180F}$ mutant cells. Wild-type (WT) and eIF2Bδ mutant (L180F) CHO cells were treated with Tg (1μM) alone for 1h, ISRIB (200nM) alone for 1h or co-treated with Tg and ISRIB for 1h.

(A) Western blot analysis of WT and L180F CHO cells immunoblotted against PERK (*low band*: unphosphorylated PERK, *upper band*: phosphorylated PERK), phosphorylated eIF2α (eIF2α-p[S51]) and total eIF2α. *non-specific band.

(B) Western blot analysis of WT and L180F CHO cells subjected to puromycin incorporation assay. GAPDH levels were used as loading control.

(C) Quantification of mean intensity levels of eIF2α-p[S51] normalised against total levels of eIF2α. **(ii)** Quantification of mean intensity levels of puromycinylated proteins normalised against GAPDH levels. Data was analysed using one-way ANOVA followed by *post-hoc* Tukey's test. All error bars: s.e.m. (*N*=3).

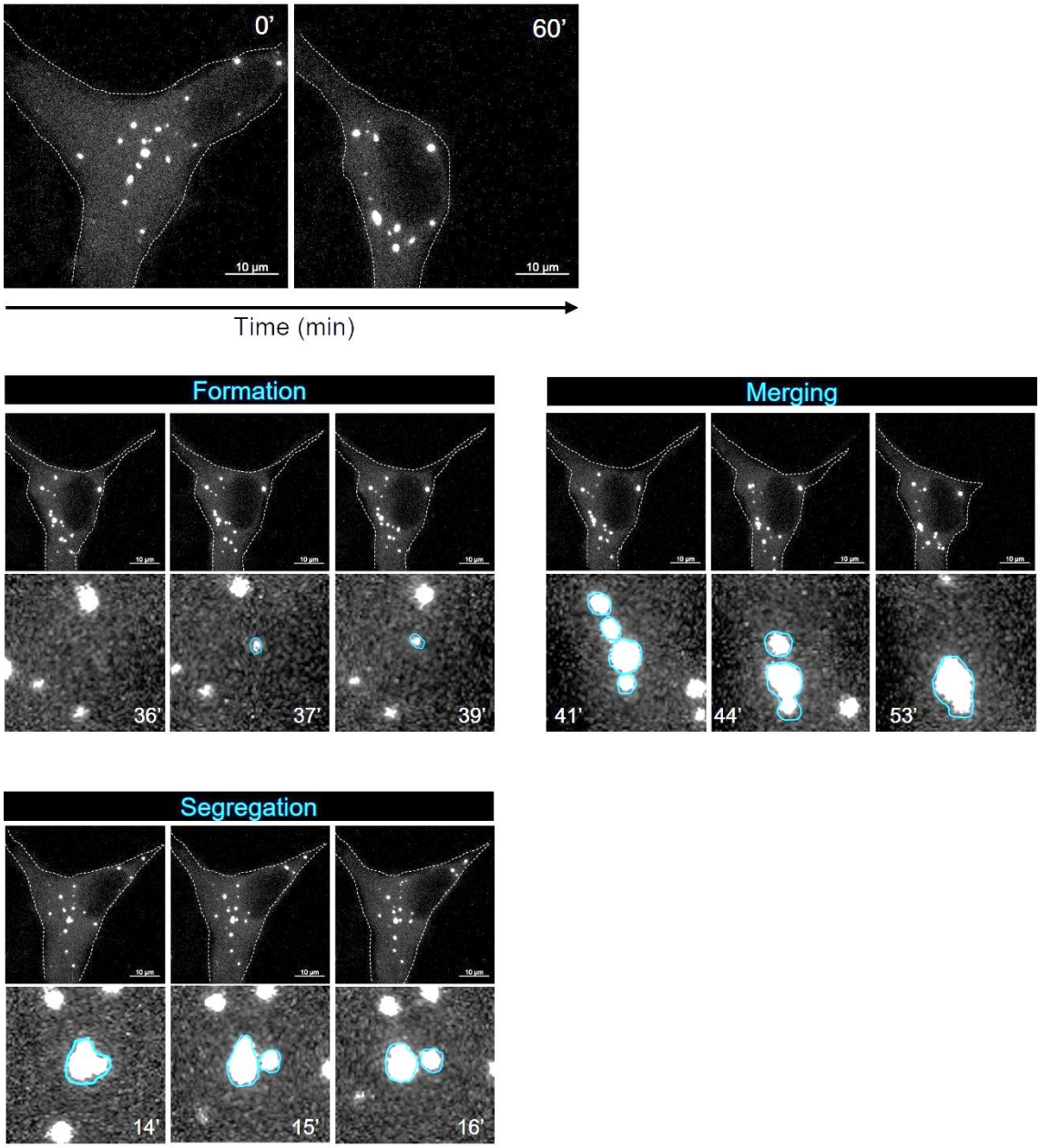

Figure A6. eIF2B bodies act as LLPS granules. (A) Representative live-images of a MO3.13 cell transfected with eIF2Bε-RFP and captured over 120 minutes. (B) Representative live-imaging time-lapse images showing formation, merging and segregation of eIF2Bε-RFP bodies. Scale bar: 10 µm.